MEASUREMENT OF ROTORDYNAMIC COEFFICIENTS FOR A HIGH SPEED FLEXURE-PIVOT TILTING-PAD BEARING (LOAD BETWEEN PAD) CONFIGURATION

A Thesis

by

ADNAN MAHMOUD AL-GHASEM

Submitted to the Office of Graduate Studies of
Texas A&M University
in partial fulfillment of the requirements for the degree of

MASTER OF SCIENCE

May 2004

Major Subject: Mechanical Engineering

MEASUREMENT OF ROTORDYNAMIC COEFFICIENTS FOR A HIGH SPEED FLEXURE-PIVOT TILTING-PAD BEARING (LOAD BETWEEN PAD) CONFIGURATION

A Thesis

by

ADNAN MAHMOUD AL-GHASEM

Submitted to Texas A&M University
in partial fulfillment of the requirements
for the degree of

MASTER OF SCIENCE

Approved as to style and content by:

Dara W. Childs (Chair of Committee)	Luis A. San Andrés (Member)
Hamid Toliyat (Member)	Dennis L. O'Neal (Head of Department)

May 2004

Major Subject: Mechanical Engineering

ABSTRACT

Measurement of Rotordynamic Coefficients for a High Speed
Flexure-Pivot Tilting-Pad Bearing (Load Between Pad) Configuration. (May 2004)
Adnan Mahmoud Al-Ghasem, B.Sc.; M.Sc., Jordan University of Science and Technology
Chair of Advisory Committee: Dr. Dara W. Childs

This thesis presents the dynamic and static forced performance of a flexure-pivot tilting-pad bearing load between pad (LBP) configuration for different rotor speeds and bearing unit loadings. The bearing has the following design parameters: 4 pads with pad arc angle 72^o and 50% pivot offset, pad axial length 0.0762 m (3 in), pad radial clearance 0.254 mm (0.010 in), bearing radial clearance 0.1905 mm (0.0075 in), preload 0.25 and shaft nominal diameter of 0.11684 m (4.600 in). The dynamic coefficients and the static performance parameters of the FPB have been compared with the theoretical predictions using the isothermal analysis from the rotordynamic software suite XLTRC^2-XLTFPBrg.

The bearing shows a small attitude angle, about 10^o, which indicates small cross-coupling stiffnesses. The pad temperatures increase in the circumferential direction of rotation with speed and load. The pads maximum temperature was measured near the trailing edge.

The dependency of the stiffness and damping coefficients on the excitation frequency has been studied. The frequency dependency in the dynamic coefficients was removed by introducing an added mass coefficient to the bearing model. The direct added mass coefficients were around 32 kg. The direct stiffness and damping coefficients increase with load, while increasing and decreasing with rotor speed, respectively. A small whirl frequency ratio (WFR) was found of about 0.15, and it decreases with load and increases with speed.

A comparison between the dynamic stiffnesses using a Reynolds equation and the bulk-flow Navier-Stokes models with the experimental dynamic stiffnesses shows that the Reynolds model (even for laminar flows) is not adequate, and that the bulk-flow model should be used for rotordynamic coefficients prediction. The bulk-flow model in general predicts well the static performance parameters and the direct dynamic coefficients, and underpredicts the cross-coupled coefficients (overpredicts the stability).

DEDICATION

To my family:

Parents, ***wife***, ***brothers*** and ***sisters***

And especially to my son ***Mahmoud*** and daughter ***Salma***

ACKNOWLEDGMENTS

"*Thanks to Allah for guidance and success*"

I would like to express my deepest thanks and appreciation to Dr. Dara W. Childs for his supervision, direction and continuous support through my graduate research and studies. His kindness and understanding overwhelmed me. His profound knowledge in turbomachinery helped me to overcome obstacles in my research and to understand many aspects in turbomachinery.

My sincere thanks go also to Dr. San Andres for his valuable recommendations and input regarding the use of XLTFPBrg code, as well as for serving on my committee. I would like also to thank Dr. Hamid Toliyat for his help in serving as a committee member.

A special thanks to Turbomachinery Research Consortium (TRC) for funding and to KMC bearings for providing the flexure-pivot bearing.

I also thank my coworkers and friends at the Turbomachinery Laboratory for their support and understanding.

Finally, I am indebted to Jordan University of Science and Technology for everything, beginning with my B.Sc. degree and ending with supporting my studies at Texas A&M University.

TABLE OF CONTENTS

Page

ABSTRACT iii

DEDICATION iv

ACKNOWLEDGMENTS v

TABLE OF CONTENTS vi

LIST OF FIGURES viii

LIST OF TABLES xi

NOMENCLATURE xiii

INTRODUCTION 1

LITERATURE REVIEW 5

TEST RIG DESCRIPTION 9

- Main Test Section 9
- Shaker System 10
- Static Loader 11
- Instrumentation 11
- Flexure-Pivot Bearing Geometry 12

EXPERIMENTAL PROCEDURES 14

- Procedure for Finding the Bearing Center 14
- Static Tests Procedure 15
- Dynamic Tests Procedure 15
- Static Parameters Identification Procedure 16
  - Sommerfeld Number 16
  - Eccentricity Ratio and Attitude Angle 17
  - Estimated Frictional Power Loss 17
- Dynamic Parameters Identification Procedure 18

EXPERIMENTAL RESULTS AND PREDICTIONS 20

- XLTRC^2-XLTFPBrg Code 20
- Static Test Results 26
  - Eccentricity Ratio and Attitude Angle 27
  - Power Losses 32
  - Oil and Pads Temperatures 33
- Dynamic Results 45
  - Identifying Rotordynamic Coefficients 45
    - Stiffness and Added Mass Coefficients 46
    - Damping Coefficients 46
  - Uncertainty Calculations 47
  - Baseline Dynamic Stiffness 49

Page

Dynamic Stiffness Comparison 51
Results 55
Stiffness Coefficients 55
Damping Coefficients 59
Added-Mass Coefficients 62
Whirl Frequency Ratio (WFR) 66
SUMMARY AND CONCLUSION 69
REFERENCES 72
APPENDIX 75
VITA 115

LIST OF FIGURES

Page

Figure 1. Tilting-pad bearings; (a) rocker-pivot, (b) flexure-pivot 2
Figure 2. Pad – shaft assembly after [1] 2
Figure 3. Main test section of the test rig 9
Figure 4. Shaker-stinger configuration (NDE side) 10
Figure 5. Static loader assembly (NDE side) 11
Figure 6. Thermocouples location on the FPB 12
Figure 7. Bearing-stator assembly 13
Figure 8. Schematic for finding the bearing center 14
Figure 9. Dynamic force coefficients in fluid film bearings 19
Figure 10. Input screen of the XLTFPBrg software 21
Figure 11. Output screen of the XLTFPBrg software 21
Figure 12. Coordinate systems for: (a) test rig, and (b) theory 22
Figure 13. Effects of using different thermal analysis on direct: (a) stiffness (b) damping and (c) added mass coefficients 25
Figure 14. Effects of using different bearing clearance on direct: (a) stiffness (b) damping and (c) added mass coefficients 26
Figure 15. Experimental and theoretical loci plot of FPB centerline for different rotor speeds: (a) 4000 rpm, (b) 6000 rpm, (c) 8000 rpm, (d) 10000 rpm and (e) 12000 rpm. 28
Figure 16. Experimental and theoretical (bulk-flow) average loci plot of FPB centerline for different rotor speeds. 29
Figure 17. Attitude angle versus applied static load for different rotor speeds: (a) theoretical (bulk-flow) and (b) experimental 29
Figure 18. Experimental and theoretical (bulk-flow) attitude angle versus eccentricity for different rotor speeds. 30
Figure 19. Experimental and theoretical (bulk-flow) attitude angle versus Sommerfeld number for different applied static loads. 31
Figure 20. Experimental and theoretical (bulk-flow) attitude angle versus Sommerfeld number for different rotor speeds. 31
Figure 21. Experimental and theoretical (bulk-flow) eccentricity ratio versus Sommerfeld number 31
Figure 22. Experimental and theoretical power losses versus rotor speeds for different static loads: (a) 0.01 kN, (b) 3.1 kN, (c) 9.24 kN and (d) 6.16 kN. 32

Page

Figure 23. Experimental and theoretical power losses versus: (a) rotor speeds for different static loads and (b) static loads for different rotor speeds. 33

Figure 24. Inlet and outlet oil temperatures versus applied static loads for: (a) 4000 rpm, (b) 6000 rpm, (c) 8000 rpm, (d) 10000 rpm, and (e) 12000 rpm. 35

Figure 25. Inlet and outlet oil temperatures versus rotor speeds for different static loads: (a) 0 kN, (b) 1.6 kN, (c) 3.1 kN, (d) 4.6 kN, (e) 6.2 kN, and (f) 9.2 kN..... 36

Figure 26. Pads temperatures versus applied static load at 4000 rpm for different thermocouple locations: (a) pad 1A, (b) pad 2A, (c) pad 3A, (d) pad 4A, and (e) pad 4B. 38

Figure 27. Pads temperatures versus applied static load at 6000 rpm for different thermocouple locations: (a) pad 1A, (b) pad 2A, (c) pad 3A, (d) pad 4A, and (e) pad 4B. 39

Figure 28. Pads temperatures versus applied static load at 8000 rpm for different thermocouple locations: (a) pad 1A, (b) pad 2A, (c) pad 3A, (d) pad 4A, and (e) pad 4B. 40

Figure 29. Pads temperatures versus applied static load at 10000 rpm for different thermocouple locations: (a) pad 1A, (b) pad 2A, (c) pad 3A, (d) pad 4A, and (e) pad 4B. 41

Figure 30. Pads temperatures versus applied static load at 12000 rpm for different thermocouple locations: (a) pad 1A, (b) pad 2A, (c) pad 3A, (d) pad 4A, and (e) pad 4B. 42

Figure 31. Pads circumferential temperature profiles for different applied static loads at: (a) 4000 rpm, (b) 6000 rpm, (c) 8000 rpm, (d) 10000 rpm, and (e) 12000 rpm..... 43

Figure 32. Pads circumferential temperature profiles for speeds for different rotor speeds at: (a) 0 kN, (b) 1.6 kN, (c) 3.1 kN, (d) 4.6 kN, (e) 6.2 kN, and (f) 9.2 kN. 44

Figure 33. Experimental dynamic stiffnesses and their fit versus the excitation frequency at 12000 rpm and 1.4 kPa bearing unit loading..... 48

Figure 34. Predicted dynamic stiffnesses and their fit versus the excitation frequency at 12000 rpm and 1.4 kPa bearing unit loading 49

Figure 35. Baseline real dynamic stiffness parts versus excitation frequency for different stator mass: (a) direct, and (b) cross-coupled..... 50

Figure 36. Baseline imaginary dynamic stiffness parts versus excitation frequency for different stator mass: (a) direct, and (b) cross-coupled 50

Figure 37. Experimental and theoretical dynamic stiffnesses versus the excitation frequency at 4000 rpm and 1.4 kPa bearing unit loading..... 51

Figure 38. Experimental and theoretical dynamic stiffnesses versus the excitation frequency at 4000 rpm and 692.2 kPa bearing unit loading..... 52

Figure 39. Experimental and theoretical dynamic stiffnesses versus the excitation frequency at 12000 rpm and 1.4 kPa bearing unit loading..... 53

Figure 40. Experimental and theoretical dynamic stiffnesses versus the excitation frequency at 12000 rpm and 1038.2 kPa bearing unit loading..... 54

Page

Figure 41. Schematic representation of the cross-coupled force after Zeidan [7] 55

Figure 42. Stiffness coefficients in [MN/m] vs. static loads in [kN] for different rotor speeds: (a) 4000 rpm, (b) 6000 rpm, (c) 8000 rpm, (d) 10000 rpm, and (e) 12000 rpm. 56

Figure 43. Stiffness coefficients versus rotor speeds for different bearing unit loading: (a) 1.4 kPa, (b) 175.9 kPa, (c) 348.4 kPa, (d) 513.8 kPa, (e) 692.2 kPa, and (f) 1038.2 kPa. . 58

Figure 44. Non-dimensional stiffness coefficients versus Sommerfeld number: (a) direct, and (b) cross-coupled 59

Figure 45. Non-dimensional stiffness coefficients versus eccentricity ratio: (a) direct, and (b) cross-coupled 59

Figure 46. Damping coefficients in kN.s/m versus static loads in kN for different rotor speeds: (a) 4000 rpm, (b) 6000 rpm, (c) 8000 rpm, (d) 10000 rpm, and (e) 12000 rpm. 60

Figure 47. Damping coefficients versus rotor speeds for different bearing unit loading: (a) 1.4 kPa, (b) 175.9 kPa, (c) 348.4 kPa, (d) 513.8 kPa, (e) 692.2 kPa, and (f) 1038.2 kPa. . 61

Figure 48. Non-dimensional damping coefficients versus Sommerfeld number: (a) direct, and (b) cross-coupled 62

Figure 49. Non-dimensional damping coefficients versus eccentricity ratio: (a) direct, and (b) cross-coupled 62

Figure 50. Added-mass coefficients in [kg] versus static loads in [kN] for different rotor speeds:(a) 4000 rpm, (b) 6000 rpm, (c) 8000 rpm, (d) 10000 rpm, and (e) 12000 rpm. 63

Figure 51. Added-mass coefficients versus rotor speeds for different bearing unit loading: (a) 1.4 kPa, (b) 175.9 kPa, (c) 348.4 kPa, (d) 513.8 kPa, (e) 692.2 kPa, and (f) 1038.2 kPa 64

Figure 52. Non-dimensional added-mass coefficients versus Sommerfeld number: (a) direct, and (b) cross-coupled. 65

Figure 53. Non-dimensional added-mass coefficients versus eccentricity ratio: (a) direct, and (b) cross-coupled 65

Figure 54. Experimental WFR versus rotor speed for different bearing unit loading, with and without fluid inertial effects 67

Figure 55. Experimental WFR versus rotor speed for different bearing unit loading, with fluid inertial effects 68

Figure 56. Experimental and theoretical WFR versus rotor speed at 1.4 kPa and 175.9 kPa bearing units loading 68

Figure 57. Thermocouples location on each pad, drive end (DE) side. 80

LIST OF TABLES

Page

Table 1. Flexure-pivot bearing design parameters 13
Table 2. Nominal test matrix for static tests 15
Table 3. Nominal test matrix for dynamic tests 16
Table 4. Actual test bearing unit loading 16
Table 5. Maximum Reynolds number for different rotor speeds 20
Table 6. "Thermal analysis options" - XLTFPBrg help file 24
Table 7. Average pads temperature at 5% for different rotor speed 24
Table 8. Static performance parameters and measurement data 76
Table 9. Pads temperatures 78
Table 10. Thermocouples number and location on each pad 80
Table 11. Experimental stiffness coefficients and their uncertainties, and the coefficient of determination (R^2) value. 81
Table 12. Theoretical stiffness coefficients and the coefficient of determination (R^2) value 82
Table 13. Experimental damping coefficients and their uncertainties and the coefficient of determination (R^2) value. 83
Table 14. Theoretical damping coefficients and the coefficient of determination (R^2) value. 84
Table 15. Experimental and theoretical added-mass coefficients and experimental uncertainties 85
Table 16. Experimental dynamic stiffnesses at 4000 rpm and 1.4 kPa bearing unit loading 86
Table 17. Experimental dynamic stiffnesses at 4000 rpm and 175.9 kPa bearing unit loading 87
Table 18. Experimental dynamic stiffnesses at 4000 rpm and 348.4 kPa bearing unit loading 88
Table 19. Experimental dynamic stiffnesses at 4000 rpm and 513.8 kPa bearing unit loading 89
Table 20. Experimental dynamic stiffnesses at 4000 rpm and 692.2 kPa bearing unit loading 90
Table 21. Experimental dynamic stiffnesses at 6000 rpm and 1.4 kPa bearing unit loading 91
Table 22. Experimental dynamic stiffnesses at 6000 rpm and 175.9 kPa bearing unit loading 92
Table 23. Experimental dynamic stiffnesses at 6000 rpm and 348.4 kPa bearing unit loading 93
Table 24. Experimental dynamic stiffnesses at 6000 rpm and 513.8 kPa bearing unit loading 94
Table 25. Experimental dynamic stiffnesses at 6000 rpm and 692.2 kPa bearing unit loading 95
Table 26. Experimental dynamic stiffnesses at 6000 rpm and 1038.2 kPa bearing unit loading 96
Table 27. Experimental dynamic stiffnesses at 8000 rpm and 1.4 kPa bearing unit loading 97
Table 28. Experimental dynamic stiffnesses at 8000 rpm and 175.9 kPa bearing unit loading 98

Page

Table 29. Experimental dynamic stiffnesses at 8000 rpm and 348.4 kPa bearing unit loading ... 99
Table 30. Experimental dynamic stiffnesses at 8000 rpm and 513.8 kPa bearing unit loading . 100
Table 31. Experimental dynamic stiffnesses at 8000 rpm and 692.2 kPa bearing unit loading . 101
Table 32. Experimental dynamic stiffnesses at 8000 rpm and 1038.2 kPa bearing unit loading 102
Table 33. Experimental dynamic stiffnesses at 10000 rpm and 1.4 kPa bearing unit loading ... 103
Table 34. Experimental dynamic stiffnesses at 10000 rpm and 175.9 kPa bearing unit loading 104
Table 35. Experimental dynamic stiffnesses at 10000 rpm and 348.4 kPa bearing unit loading 105
Table 36. Experimental dynamic stiffnesses at 10000 rpm and 513.8 kPa bearing unit loading 106
Table 37. Experimental dynamic stiffnesses at 10000 rpm and 692.2 kPa bearing unit loading 107
Table 38: Experimental dynamic stiffnesses at 10000 rpm and 1038.2 kPa bearing unit loading ... 108
Table 39. Experimental dynamic stiffnesses at 12000 rpm and 1.4 kPa bearing unit loading ... 109
Table 40. Experimental dynamic stiffnesses at 12000 rpm and 175.9 kPa bearing unit loading 110
Table 41. Experimental dynamic stiffnesses at 12000 rpm and 348.4 kPa bearing unit loading 111
Table 42. Experimental dynamic stiffnesses at 12000 rpm and 513.8 kPa bearing unit loading 112
Table 43. Experimental dynamic stiffnesses at 12000 rpm and 692.2 kPa bearing unit loading 113
Table 44. Experimental dynamic stiffnesses at 12000 rpm and 1038.2 kPa bearing unit loading ... 114

NOMENCLATURE

a_x, a_y	Measured stator acceleration in the x and y directions, respectively [m/s^2]
A_x, A_y	Fourier transformation of a_x and a_y, respectively
A_{ij}	Intercept coefficient of the fitting line for the real dynamic stiffness in [MN/m]
ΔA_{ij}	Uncertainty in the A_{ij} coefficient [MN/m]
B_{ij}	Slope coefficient of the fitting line for the real and imaginary dynamic stiffness parts in [kg] and [kN.s/m], respectively.
ΔB_{ij}	Uncertainty in the B_{ij} coefficient
c_{ij}	Dimensionless damping coefficient = C_{ij} $(C_p\ \omega/W)$
C_b	Radial bearing clearance [m]
C_p	Radial pad clearance [m]
C_P	Oil specific heat [J/(kg.K^o)]
C_{ij}	Damping coefficient [kN.s/m]
D	Inside bearing diameter [m]
D_x, D_y	Fourier transformation of Δx and Δy, respectively
e_{xDE}, e_{xNDE}	Bearing displacement in the x direction at the DE and NDE sides, respectively [m]
e_{yDE}, e_{yNDE}	Bearing displacement in the y direction at the DE and NDE sides, respectively [m]
e_x, e_y	Average bearing displacement in the x and y directions, respectively [m]
f_{bx}, f_{by}	Bearing reaction force in the x and y directions, respectively [N]
f_x, f_y	Measured excitation force in the x and y directions, respectively [N]
F_x, F_y	Fourier transformation of f_x and f_y, respectively.
h_{ij}	Dynamic stiffness vector of one out of 10 tests [MN/m]
H_{ij}	Average dynamic stiffness vector for the 10 tests [MN/m]
$\overline{H}_{ij}$	Average of H_{ij} over the dynamic stiffness vector length n [MN/m]
$\hat{H}_{ij}$	Predicted dynamic stiffness vector [MN/m]
i, j	Subscripts representing x and y
$\boldsymbol{j}$	$\sqrt{-1}$
k_{ij}	Dimensionless stiffness coefficient = K_{ij} (C_p/W)
K_{ij}	Stiffness coefficient [MN/m]

L	Pad length [m]
m_{ij}	Dimensionless added mass coefficient = $M_{ij}\ (C_p\ \omega^2/W)$
M_{ij}	Added mass coefficient [kg]
M_s	Stator mass [kg]
n	Dynamic stiffness vector length
N	Rotor speed [Hz]
p	Bearing unit loading = $W/(LD)$ [kPa]
P	Power loss [W]
$\dot{Q}$	Oil volumetric flowrate [m^3/s]
R_b	Bearing radius [m]
R_p	Pad radius [m]
R_s	Shaft radius [m]
S	Sommerfeld number = $\mu\ N\ L\ D\ (D/2C_p)^2/W$
S_{ij}	Standard deviation of h_{ij} about H_{ij} [MN/m]
T_{oDE}, T_{oNDE}	Oil outlet temperature at the DE and NDE sides, respectively [K^o]
T_o	Average oil outlets temperature [K^o]
T_{in}	Oil inlet temperature [K^o]
$T_{average}$	Average oil inlet and outlets temperature [K^o]
U_{ij}	Uncertainty in dynamic stiffness (H_{ij}) [MN/m]
W	Applied static load in the positive y-direction [N]
Δx, Δy	Measured relative displacement between the rotor and the bearing in the x and y directions, respectively [m]
x, y	Displacement direction

Greek symbols

ρ	Oil density [kg/m^3]
μ	Oil viscosity [Pa.s]
ε_0	Eccentricity ratio = $(e_x^2 + e_y^2)^{0.5}/C_p$
ϕ	Attitude angle = $tan^{-1}(e_y/e_x)\ 180/\pi$ [degree]
θ_{pad}	Angle of the pad arc [degree]
θ_{pivot}	Angle of the pivot position in the direction of rotation [degree]

ω	Rotor speed [rpm]
Ω	Excitation frequency [Hz]
ω_s	Onest speed of instability [rpm]
χ	Independent variable used for fitting the real and the imaginary dynamic stiffness terms and equal to Ω and Ω^2, respectively.

Abbreviations

DE	Drive end
NDE	Non-drive end
EDM	Electrical discharge machining
FPB	Flexure-pivot bearing
EXP	Experiment
LBP	Load between pads
LOP	Load on pad
TH	Theory (bulk-flow unless mentioned otherwise)
TPJB	Tilting-pad journal bearing
Im( )	Imaginary part ( )
Re( )	Real part ( )
rpm	Revolution per minute
WFR	Whirl frequency ratio

INTRODUCTION

The significant role of rotordynamics takes place by ensuring the safe and reliable operation of rotating machines. Many turbomachines operate above the first critical speed, and in many cases just below the second critical speed. This fact leads to the importance of gaining an insight into the rotordynamic behavior of these machines through combined experimental testing and numerical modeling. Bearings are one of the most important elements in a machine; in most cases, they are the key for stable machines.

Bearings can be classified into two major types: rolling and sliding bearings. Bearings have been used a long time to reduce friction and wear and to carry the load applied to the shaft. Ball bearings are one type of rolling bearings, and have been used for this purpose and are still being used until this day for low to moderate speeds with light loads. On the other hand, fluid film bearings are used for medium to high speeds with heavy load applications. They are of a sliding type bearing. The basic types of full fluid film bearings are: hydrostatic, hydrodynamic or hybrid (a combination of the former two). To develop hydrodynamic pressure force in a fluid film bearing, three factors are required: relative motion between the sliding surfaces, converging geometry, and viscous fluid. On the other hand, hydrostatic fluid film bearing require external pressure and some type of flow restrictor, regardless of the former three factors.

Two types of hydrodynamic bearing geometries are used in rotating machinery: fixed geometry bearings (plain journal, lemon bore, three lobes, canted bore, etc.) and tilting-pad journal bearings (TPJB). The tilting-pad radial bearings (load between pad and load on pad configurations) are the most universally applied design for high-speed rotors because of their superior stability characteristics for machines requiring the maximum rotordynamic stability, due to the fact that the cross-coupled stiffness coefficients terms K_{xy} , K_{yx} are effectively removed by the free movement of the pads about a pivot. There are different types of pivots (rocker shown in figure 1(a), flexure-pivot shown in figure 1(b), spherical, etc.).

This thesis follows the style and format of the ASME Journal of Tribology.

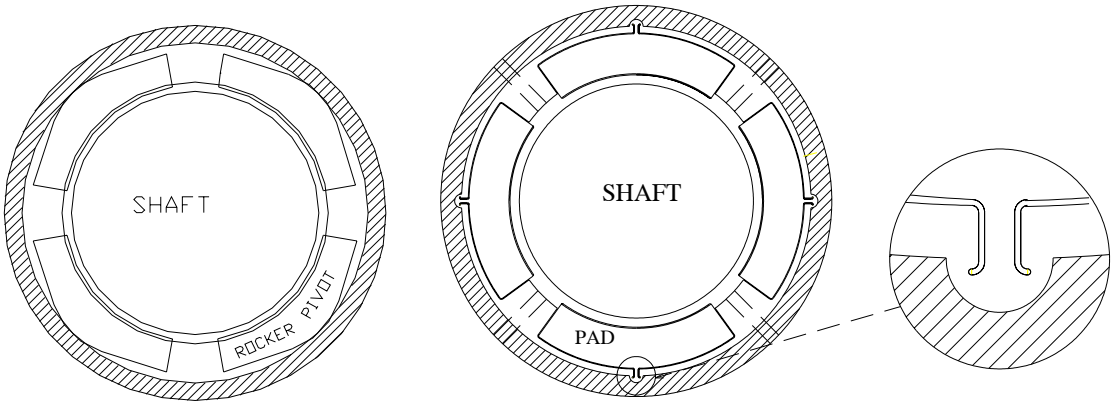

(a) (b)

Figure 1. Tilting-pad bearings; (a) rocker-pivot, (b) flexure-pivot

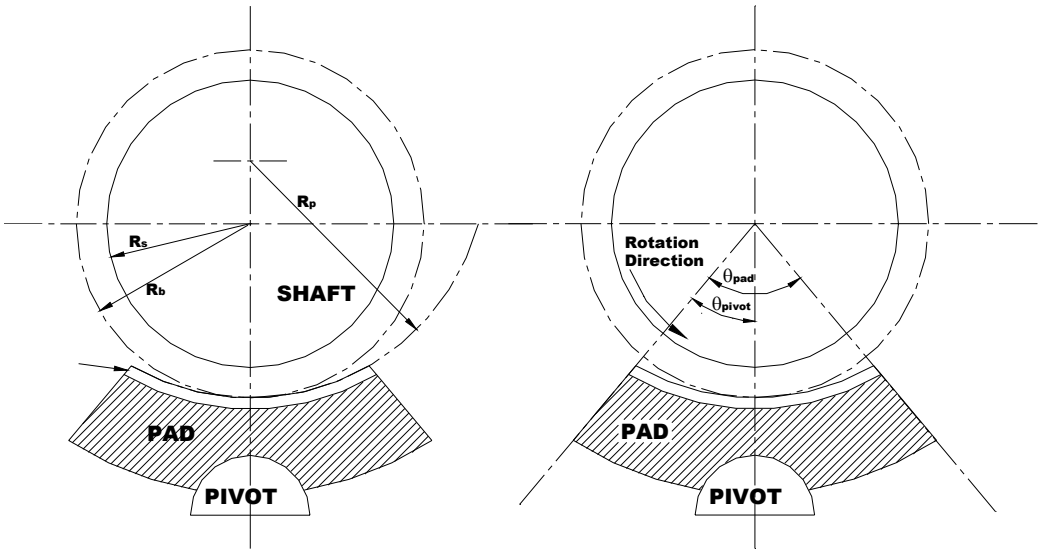

Figure 2. Pad – shaft assembly after [1]

Figure 2 shows some of the following important geometrical parameters in TPJBs:

(a) Pivot structural design (spherical, cylindrical, rocker, and flexure).

(b) Pad preload which is the amount of convergence and divergence that is built on the pad geometry, and defined as $1-\frac{C_b}{C_p}$.Where $C_b = R_b - R_s$ is the bearing clearance, and $C_p = R_p - R_s$ is the pad clearance.

(c) Pivot offset defined as $\frac{\theta_{pivot}}{\theta_{pad}}$.

(d) Number of Pads.

(e) Pad arc length θ_{pad}.

(f) Thin Babbitt layer, applied to the pad surface to protect the shaft.

As seen in Figure 2 the pad can pivot in all directions if the pivot is spherical and about one axis if the pivot is a cylindrical or rocker type. Therefore the spherical-pivot design is preferred in most cases since it tolerates shaft misalignment. The stiffness and the load capacity of a bearing depend on pad preload; a positive preload can be developed by boring the arcs of the pads to a larger radius than the bearing radius. Zero preload means the pads are concentric with the shaft, and a shaft eccentricity is needed to create a converging geometry. Pad preloads are normally between 0 and 0.5. Pad offset is a measure of how far along the pad arc the pivot is located in the direction of shaft rotation. A 0.5 offset means that the pivot is positioned in the middle of the pad arc. Offset value greater than 0.5 will increase the minimum film thickness and the load capacity. Pivot offsets are normally between 0.5 and 0.7 [1].

The scientific appreciation of hydrodynamics in lubrication started at the end of the 18th century when Reynolds [2] published his paper which presented the basic theory behind modern hydrodynamic lubrication. Zeidan and Paquette [3] discuss the limitations and problems associated with high speed and highly loaded hydrodynamic bearings of different types. Nicholas [4] discusses the basic design of a tilting-pad journal bearing (TPJB) in terms of operating load, speed and metal temperature limits. He also discusses the effects of TPJB geometric properties on the rotordynamics of the bearings and addresses the advantage and disadvantages of not preloading the pads.

Figure 1(b) shows the flexible-pivot bearing (FPB). The pads are supported by a beam element "web". The web is designed to have a sufficient radial stiffness to support the pad and the load of the shaft in the radial direction, and at the same time allows the pads to tilt to achieve high stability (low cross-coupling stiffnesses). Armentrout and Paquette [5] introduced a new one-piece journal bearing design, the flexure-pivot bearing (FPB), that offers many of the beneficial rotordynamic advantages of tilting-pad journal bearings (TPJBs). FPB consists of centrally-pivoted pads machined from a solid blank through an electrical discharge machining (EDM) process. Performance data for a FPB in terms of stability were presented by [5] for a high

speed turbo-compressor. Kepple et al. [6] reported that the first FPB set was installed in 1994. They discuss the disadvantages of tilting bad bearing (pivot wear, complexity in design, production, installation and maintenance) and compare it to a new bearing design “flexure-pivot bearing (FPB)” which have stability characteristic similar to tilting-pad bearings. Zeidan [7] discusses the cross-coupling characteristics that are present in all rotating machinery operating in fluid film bearings and its dramatic effect on stability. Then, he describes some problems and drawbacks in the widely used tilting-pad bearings mentioned earlier, and discusses the FPB to address these problems. Chen et al. [8] address the beneficial uses of optimized-design FPB and compare it to a conventional bearing in a high-speed integrally-geared compressor, in terms of lowering the frictional losses and having a wider operating temperature range. DeChoudhury et al. [9] studied the effects of replacing a five shoe tilting-pad journal bearing and taper-land thrust bearing system with a new radial and thrust bearing flexible pad type system in a high speed centrifugal compressor. Their tests show a lower oil temperature rise and reduced frictional power loss.

LITERATURE REVIEW

Many test studies have been conducted to determine the performance of the tilting-pad journal bearings (TPJB) under static and dynamic loads for their importance in the design stage. Fu and Parkins [10] develop a simple computer code (using one iteration loop for the oil film temperature) to analysis TPJB under static load. They study the effects of applying a static load on pad flutter, tilt angle, oil film thickness, and maximum oil film temperature and eccentricity ratio for each pad.

Walton and San Andrés [11] performed static tests on a four-pad FPB load between pad configuration (radial clearance of 0.14 mm (0.0055 in), axial length of 40 mm (1.5745 in), offset of 0.5, null preload and *L/D* ratio of 0.31). They reported measurements of bearing eccentricities and pad temperature and compared the results obtained to predictions. The maximum rotational speed was 4500 rpm, and the maximum static load applied was 1400 N. They found that the maximum defect temperature was on the trailing edge of the loaded pad as expected, and that there was a negligible cross coupling displacement for all test conditions. In addition, they predicted the power loss from a thermal analysis, showing good agreement with numerical prediction. San Andrés and Jackson [12] performed similar tests as in [11] for the same bearing for load on pad (LOP) configuration with larger radial clearance of 0.2032 mm (0.008 in). They conclude the same as in [11] except that the attitude angle was higher, about 30°, because the rotational web stiffness had more effect on the attitude angle as the bearing clearance increases.

DeChoudhury and Barth [13] conducted tests to measure the oil film temperatures distribution for a 5 shoe tilting-pad journal bearings and compared it to the discharge oil temperature. Their results show that the film temperatures are much higher and more sensitive to load and speed changes than the discharge oil temperature. On the other hand, the discharge oil temperature is more sensitive than the oil film temperatures to the oil flow-rate changes.

Edney and Mellinger [14] introduce a new TPB design based on the concept of directed lubrication (supplying cool oil directly into the oil film to minimize the effects of the hot oil carryover) and compared it to a conventional flooded style design by conducting experimental tests over a range of shaft speeds 4000-16000 rpm at relatively light load. They measure the pads temperatures, oil flow rate, oil inlet and exit temperatures. Then they compare the effects of pad material, bearing clearance and oil flow rates on the pads temperatures and power losses.

Harangozo et al. [15] compare the effects of different lubrication methods (flooded, directed and leading edge) on the performance of a 4-shoe tilting-pad journal bearing (LBP configuration) in terms of reducing pad temperatures and power losses, over a range of shaft speeds up to 7000 rpm and loads up to 22 kN. They found that the leading edge lubrication method is preferable on the other methods in most cases.

Stiffness, damping and added mass coefficients are very important in initial rotordynamic designs. These coefficients are typically expressed in terms of two dimensional matrices and used in the following linearized force-displacement bearing model.

$$-\begin{bmatrix} f_{bx} \\ f_{by} \end{bmatrix} = \begin{bmatrix} K_{xx} & K_{xy} \\ K_{yx} & K_{yy} \end{bmatrix} \begin{bmatrix} \Delta x \\ \Delta y \end{bmatrix} + \begin{bmatrix} C_{xx} & C_{xy} \\ C_{yy} & C_{yy} \end{bmatrix} \begin{bmatrix} \Delta \dot{x} \\ \Delta \dot{y} \end{bmatrix} + \begin{bmatrix} M_{xx} & M_{xy} \\ M_{yx} & M_{yy} \end{bmatrix} \begin{bmatrix} \Delta \ddot{x} \\ \Delta \ddot{y} \end{bmatrix}$$

In performing a stability analysis of high-speed machinery running on tilting-pad bearings, one would ask if the rotordynamic coefficients should be calculated at the synchronous precession (running speed) frequency or at the rotor's natural frequency. Lund [16] discusses how to calculate these coefficients at the running speed (synchronous precession frequency) for a tilting-pad journal bearing, considering the pads' inertia. The stability analysis was presented by Lund [17] in 1965. He demonstrates how to calculate the whirl frequency ratio (WFR) for an elastic rotor supported by journal bearings.

Nicholas et al. [18] analyzed a 5-shoe TPB using the finite element approach and the pad-assembly method to obtain stiffness and damping coefficients at the running speed frequency for different offsets, preloads, *L/D* ratios, and load configurations (LOP, LBP). They concluded that increasing the bearing preload will increase bearing stiffness and eliminate the stiffness asymmetry at high Sommerfeld numbers. Similar but less dramatic effects were obtained for increasing the bearing offset. Small difference between LOP and LBP configurations was seen at high Sommerfeld numbers. Rough [19] combined the pad translation and rotation effects with the pad assembly technique to obtain bearing properties for rotordynamics calculations. Brockwell et al. [20] tested a 5-shoe TPB (LBP configuration) to investigate the dynamic coefficients. Measurements were conducted for various testing conditions. The maximum shaft speed and static load were 3600 rpm and 4.5 kN, respectively. They compared their results with predictions, taking into account the thermal and elastic effects in the bearings, pivot support flexibility and the shaft flexibility and found that the comparison was satisfactory. Negligible cross-coupled stiffness coefficients were reported.

Parkins and Horner [21] measured the stiffness coefficients, pad temperature, eccentricity and attitude angle for a high speed tilting-pad bearing (LOP/LBP configurations) over a range of loads and rotational speeds. They reported negative attitude angles. Good agreement between the measured and predicted bearing temperature and direct stiffness coefficients was found. The cross-coupling stiffness coefficients were under predicted. Chen [22] presents a general method for calculating the dynamic coefficients of flexible-pad journal bearings. The flexibility of the support web (translations and rotation) and the mass/inertia of the pad are included in his analysis

The majority of the analysis was based on solving the Reynolds equation; which is a simplified form of the Navier-Stokes equations neglecting the temporal and convective fluid inertia terms, especially for laminar flows. Reinhardt and Lund [23] show the significance of fluid inertia (added-mass coefficients) on a journal bearing operating in a laminar flow regime.

San Andrés [24] presented an analysis of flexure-pivot tilting-pad hybrid bearings operating in the turbulent flow regime, using bulk-flow transport equations (mass-continuity, momentum, and energy equations). His predictions using liquid oxygen as a lubricant show the advantages of using this type of bearings in a cryogenic turbopump. A reduction in whirl frequency ratio was produced, without degrading the static load performance or having a reduction in direct stiffness and damping coefficients.

Parsell et al. [25] obtained a set of equations to calculate the reduced dynamic coefficients for a tilting-pad bearing in terms of the complete dynamic coefficients, including pad degrees of freedom at the stability threshold. They showed that the frequency of the excitation force is one of the important parameters affecting the dynamic characteristics of high speed bearings. They concluded that the stiffness coefficients of a preloaded 5-shoe tilting-pad bearing decrease slightly with an increase of excitation frequency, while the damping coefficients increase slightly. Barrett et al. [26] continued the previous work by including the real parts of the system eigenvalues. Their results were presented using a 5-shoe tilting-pad bearing (LBP configuration) with negligible pad inertia effects. They conclude that rotor stability calculations using synchronously reduced coefficients (ignoring real parts of the system eigenvalues) would overestimate the stability of the system for small preloads with high Sommerfeld numbers. Ha and Yang [27] measured the effects of excitation frequency on the stiffness and damping coefficients of a 5-shoe tilting-pad bearing (LOP configuration). The maximum rotational speed used in that test was 3600 rpm. They conclude the same as in [25].

The central rotordynamic issue concerning tilting-pad bearings in general, and flexure-pivot pad bearing (FPB) in particular, is: are the rotordynamic coefficients of a FPB frequency dependent or not? Because of the importance of this question, this work provides an in-depth knowledge regarding the dependence of rotordynamic coefficients on excitation frequency. Static and dynamic tests were performed to investigate this relationship for the FPB (LBP configuration). The results of these tests were compared with predictions obtained from classical lubrication and bulk-flow models.

TEST RIG DESCRIPTION

Main Test Section

The test rig described by Kaul [28] for oil seals has been used with some modification. Figure 3 show the main test section of the test rig that was used to study the static and dynamic performance of the flexure-pivot tilting-pad bearing.

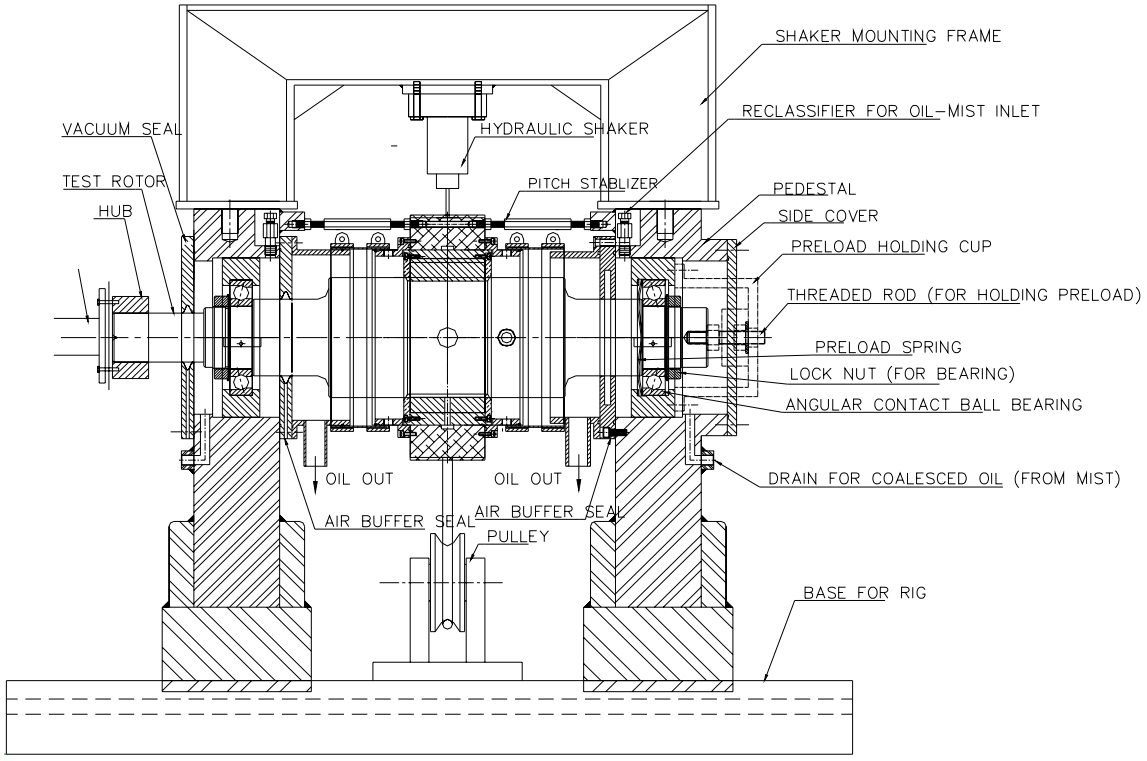

Figure 3. Main test section of the test rig

The test rig consists of the following two major components: (1) the base which is fabricated from welded mild steel plates to support the main test section and the air drive turbine, (2) two pedestals spaced approximately 381 mm (15 in) apart to support the test rotor. An air turbine that can deliver approximately 65 kW (90 hp) was used to drive the rotor up to a maximum speed of 17,000 rpm (283.3 Hz) through a high-speed flexible-disc coupling. The test

rotor has a diameter of 0.1168095 m (4.5988 in). The rotor is supported on two ball bearings. They are lubricated through an oil-mist system.

A stator is used to hold the flexure-pivot tilting-pad bearing and all the associated instrumentation such as thermocouples, pressure probes, accelerometers, etc. The static and dynamic loads applied to the stator come, respectively, from a pneumatic loader and two hydraulic shakers. Six pitch stabilizers were used to hold the stator axially. These pitch stabilizers are also used to angularly align the shaft with the rotor.

Shaker System

Two orthogonally mounted hydraulic shaker heads are attached to the stator middle section via elastic stingers. Stingers isolate the test structure from the dynamics of the shakers structure. The stator-shaker-stinger arrangement is shown in Figure 4. The *x*-direction shaker can excite the stator with dynamic loads up to 4.45 kN (1000 lbf) in tension and compression, while the *y*-direction shaker can excite the stator with dynamic loads up to 4.45 kN (1000 lbf) in tension and 11.1 kN (2500 lbf) in compression. Both shakers can excite at frequencies up to 1000 Hz.

The load applied to the stator is measured with load cells located between the stingers and the shaker frame. Although, the shakers can provide static and dynamic loads, they were configured to provide dynamic loads exclusively for the present study.

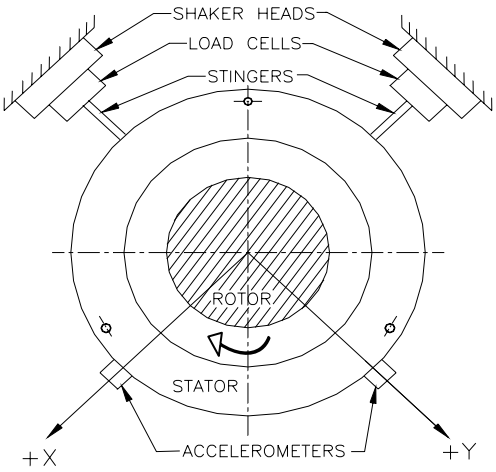

Figure 4. Shaker-stinger configuration (NDE side)

Static Loader

Figure 5 shows the static loader assembled with the test rig. A pneumatic loader is used to apply a static load to the stator in the positive *y*-direction. The static loader cable is connected to the stator assembly through a yoke and a spring system to assure that the load is applied exclusively in one direction. The rated maximum available load is a bout 22.2 kN (5000 lbf). The piston is driven by air at a supply pressure of 827.4 kPa (120 psi). The applied load is measured with a load cell attached to the static loader cable.

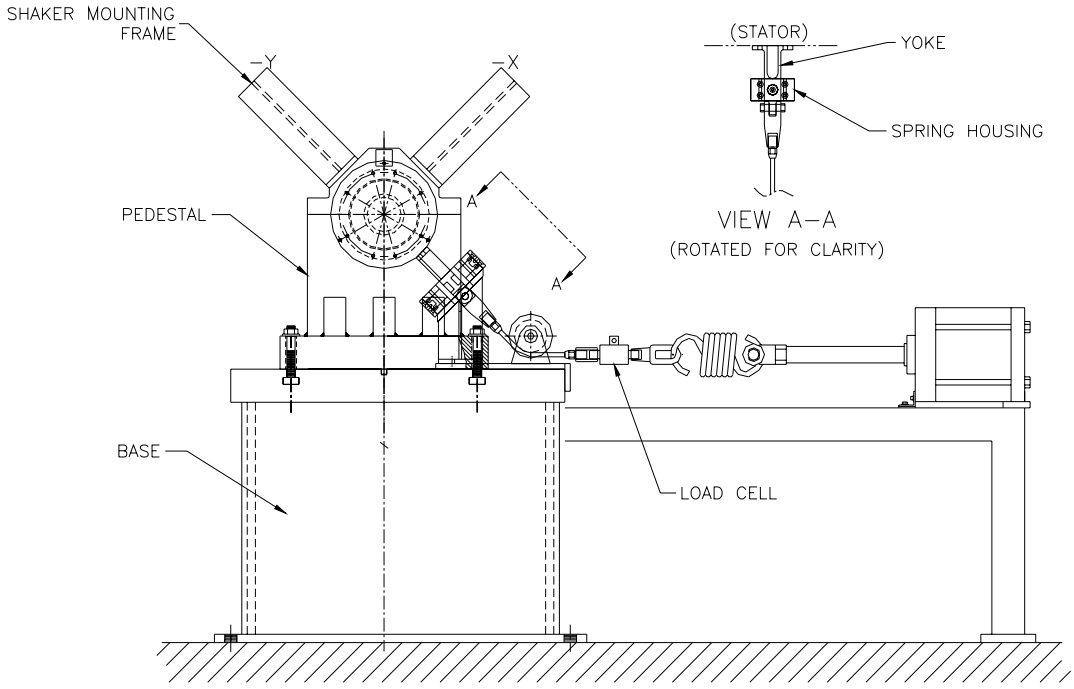

Figure 5. Static loader assembly (NDE side)

Instrumentation

Six high-sensitivity proximity probes, located in the stator end caps on the exit sides of the FPB, record the relative motion of the stator with respect to the rotor for the *x* and *y* directions of excitation force. Two radial proximity probes were installed in the end cap at the non-drive end (NDE) side. In addition, four probes were installed in the end cap at the drive end

(DE) side to measure the pitch and yaw of the stator. Two of the probes installed in the end cap at the DE side were used to provide a feedback to the shakers' control system.

Piezoelectric accelerometers measure the stator absolute acceleration in the *x* and *y* directions. Static pressure and temperature probes were installed at the stator oil-inlet chamber and at both end caps at the exits of the FPB. Figure 6 shows the location of the 19 thermocouple fixed to the pads in the circumferential direction.

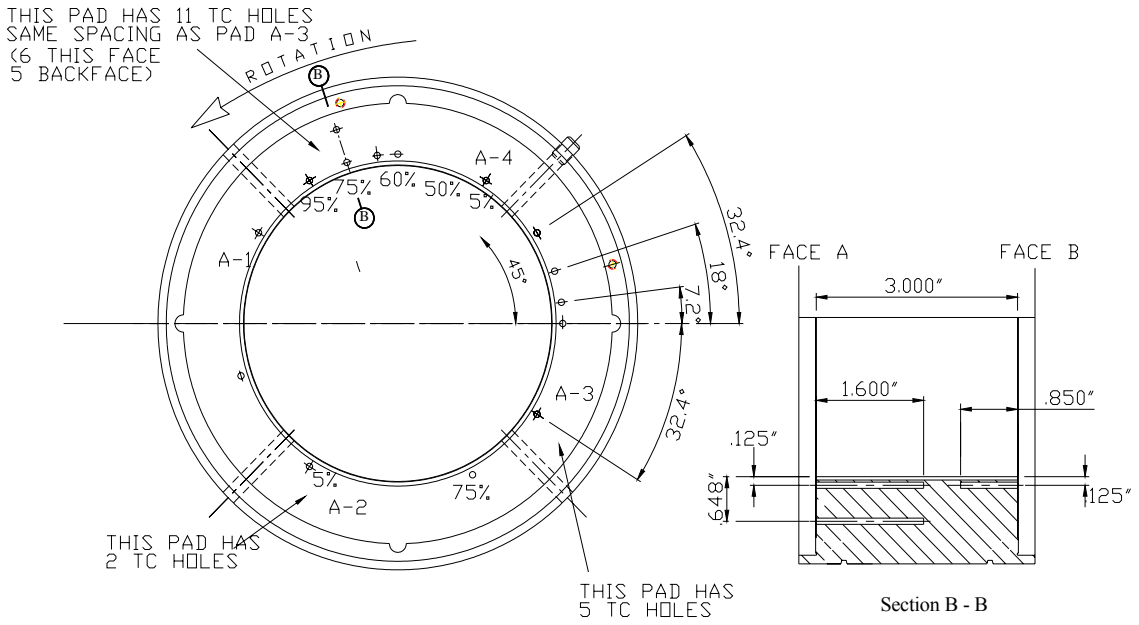

Figure 6. Thermocouples location on the FPB

Flexure-Pivot Bearing Geometry

Figure 7 shows the FPB - stator assembly consisting of the bearing, stator and two end caps. The FPB design parameters and the type of the oil used are shown in Table 1.

Table 1. Flexure-pivot bearing design parameters

Number of pads	4
Configuration	LBP
Pad arc angle	72°
Pivot offset	50%
Rotor diameter	116.8095 ± 0.0051 mm (4.5988 ± 0.0002 in)
Pad axial length	76.2 ± 0.0254 mm (3 ± 0.001 in)
Radial pad clearance(C_p)	0.254 ± 0.0127 mm (0.010 ± 0.0005 in)
Radial bearing clearance(C_b)	0.1905 ± 0.0127 mm (0.0075 ± 0.0005 in)
Preload	0.25
Pad rotational stiffness	1694.8 N.m/rad (15000 lb.in/rad)
Pad polar inertia	7.448×10^{-5} kg.m^2(6.59×10^{-4} lbm.s^2.in)
Pad mass	1.226 kg (2.70 lbm)
Web thickness	2.1251 mm (0.0837 in)
Web height	7.4379 mm (0.2928 in)
Lubricant type	ISO VG32

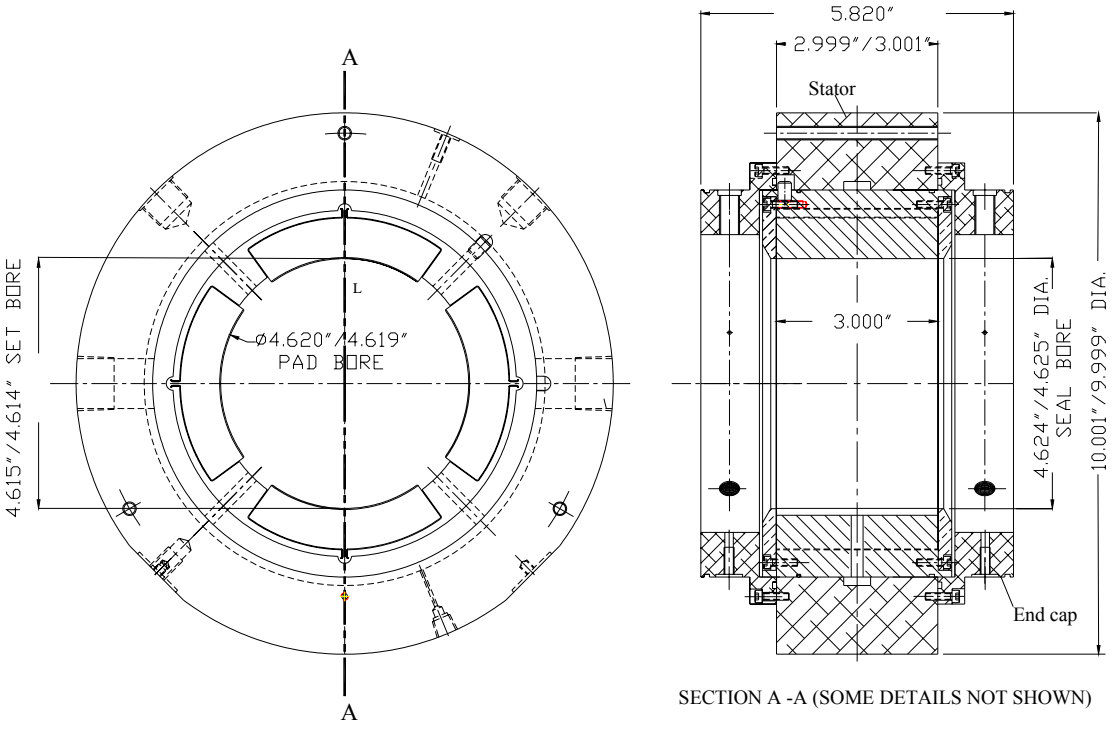

Figure 7. Bearing-stator assembly

EXPERIMENTAL PROCEDURES

The following procedures were followed to test the flexure-pivot bearing and to identify its static and dynamic parameters determining its performance.

Procedure for Finding the Bearing Center

Figure 8 shows a graphical representation of the procedure used for centering the bearing using the bump test, according to the following steps:

Step 1: By moving the bearing using the hydraulic shakers from an initial position along an axis that is oriented at 45^{o} from the *x*-axis, until the corresponding pad or edge hits the rotor, then moving it in the opposite direction until it hits again. Then the middle point between these two hits is the initial center of the bearing.

Step 2: Moving the bearing in a perpendicular direction to the first axis and by following the same procedure, we find the middle point in that direction.

Step 3: If the middle point found in step 2 is in the same location as the middle point found in step 1 the bearing center is defined; otherwise, first and second steps are repeated.

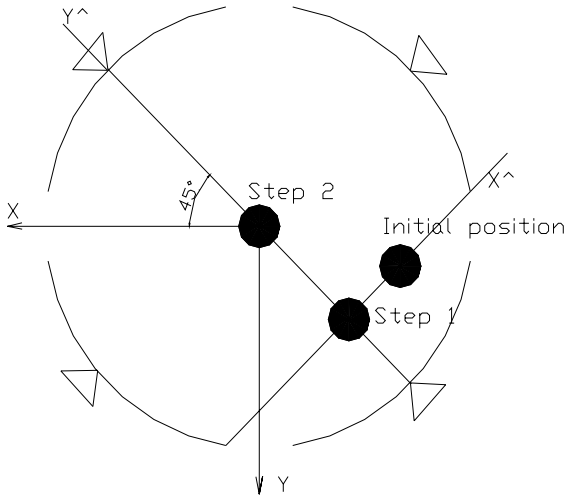

Figure 8. Schematic for finding the bearing center

After the bearing have been centered, the diametral clearance is measured along the *X*^ and the *Y*^ axes (Figure 8) and found to be 330.2 μm and 431.8 μm (13 mils and 17 mils), respectively.

These different clearances in the *X*^ and *Y*^ directions suggests that the bearing was "crushed" at some stage of the assembly process.

Static Tests Procedure

Static tests have been performed for the five rotational speeds of Table 2 at a constant oil flow rate 53 lit/min (14 gpm). The oil flowrate was selected to make sure that the FPB does not starve (remains fully flooded). Air is supplied to the drive turbine to reach the nominal speed required with a maximum variation of ±100 rpm. Then the stator was centered with respect to the rotor using the shakers.

Table 2. Nominal test matrix for static tests

Flowrate [LPM] / Speed [RPM]	53
4000	*
6000	*
8000	*
10000	*
12000	*

Once a steady-state condition is achieved, the following sets of data were taken and are provided in the Appendix, Tables 8 and 9:

(a) Stator position in the *x* and *y* directions at the DE plane and the NDE plane.

(b) Oil mass flowrate measured upstream of the test section.

(c) Oil inlet and outlet temperatures.

(d) Static load applied by the pneumatic loader.

(e) Pads temperature distributions (see Figure 6 for locations).

The load is increased in steps until reaching (if possible) 1034.2 kPa (150 psi) as shown in Table 3. The cited sets of data were recorded at each test condition.

Dynamic Tests Procedure

Dynamic tests were performed by shaking the stator in the *x* and *y* directions, independently, for every point in the test matrix shown in Table 3. The excitation of the shakers was a pseudo-random waveform type with frequencies from 20 to 320 Hz in 10 *Hz* increment. The magnitude of the excitation force was controlled such that the FPB will have a linear

behavior during testing. In general, the motion of the stator has been kept between 10 and 20 μm (0.4 - 0.8 mils) during excitation, which is about 5 - 10% of the bearing clearance.

Table 3. Nominal test matrix for dynamic tests

Bearing unit loading (*kPa*) / Rotor speed [*rpm*]	0	172.4	344.7	517.1	689.5	1034.2
4000	*	*	*	*	*	N/A
6000	*	*	*	*	*	*
8000	*	*	*	*	*	*
10000	*	*	*	*	*	*
12000	*	*	*	*	*	*

Table 4. Actual test bearing unit loading

Bearing Unit Loading (kPa) = *W/(L D)*	1.4	175.9	348.4	513.8	692.2	1038.2
Load (kN)	0.01	1.57	3.10	4.57	6.16	9.24

One set of the dynamic stiffness coefficients is obtained as the average of 32 separate shake tests, which are averaged in the frequency domain using a pseudo-random waveform. To estimate the variability of dynamic data, 10 consecutive tests (each including 32 separate shake tests) were conducted. During these tests, the operating conditions (load and speed) were held approximately constant. The following sets of data were recorded at each of the test conditions shown in Table 3 in the time domain for the duration of shaking in each direction (0.1 sec):

(a) Excitation force component vector.

(b) Stator acceleration vector component.

(c) Stator position in the *x* and *y* directions at the NDE plane.

Static Parameters Identification Procedure

The static performance of the FPB is determined through the following parameters

Sommerfeld Number

The Sommerfeld number is defined by

$$S = \frac{\mu_{T_{average}} N L D}{W}\left(\frac{D}{2C_p}\right)^2, \qquad (1)$$

where $\mu_{T_{average}}$ is the oil viscosity at the average of oil inlet and outlet temperatures in Pa.s, N is the rotor speed in Hz. L is the pad length , D is the inside bearing diameter , W is the applied static load in N, and C_p is the pad radial clearance.

Eccentricity Ratio and Attitude Angle

The eccentricity ratio and the attitude angle, respectively, are defined by

$$\varepsilon_0 = \sqrt{(e_x^2 + e_y^2)/C_p} \tag{2}$$

$$\phi = \frac{180}{\pi}\tan^{-1}\left[\frac{e_y}{e_x}\right], \tag{3}$$

where ε_0 is the eccentricity ratio, ϕ is the attitude angle in degree, e_x and e_y are the average[1] bearing displacement in the x and y directions, respectively.

Estimated Frictional Power Loss

The estimated frictional power loss is defined by

$$P = \dot{Q}\left[(\rho C_P)_{T_o} T_o - (\rho C_P)_{T_{in}} T_{in}\right], \tag{4}$$

where $\dot{Q}$ is the oil volumetric flowrate in m^3/s, ρ and C_P, are the oil density in kg/m^3 and specific heat in J/(kg.^{o}K), respectively. T_o is the average[1] oil outlet temperature and T_{in} is the oil inlet temperature in ^0K.

The viscosity, specific heat and density for the oil type (ISO VG32) used in the above equations was calculated according to Equations (5, 6 and 7), respectively. (Based on XLTRC[2] built-in data).

$$\mu = 0.045336\, e^{-0.0300686(T-294.2611)} \quad \text{(Pa.}s\text{)} \tag{5}$$

$$C_P = 3.6273T + 811.75 \quad \text{(J/(kg.}^o\text{K))} \tag{6}$$

$$\rho = -0.6616T + 1064 \quad \text{(kg/m}^3\text{)}, \tag{7}$$

where T in ^0K.

The static parameters are shown in the Appendix Table 8.

[1] The average between the DE and the NDE measurements.

Dynamic Parameters Identification Procedure

This section details the rotordynamic parameter identification procedure and has been adapted from Childs and Hale [29] and repeated here for clarification purposes. The Stator assembly is excited by hydraulic shakers in two orthogonal planes *(x*, *y*). The equations of motion for the stator can be written as:

$$M_s\begin{bmatrix} a_x \\ a_y \end{bmatrix} = \begin{bmatrix} f_x \\ f_y \end{bmatrix} - \begin{bmatrix} f_{bx} \\ f_{by} \end{bmatrix}, \tag{8}$$

where a_x and a_y are the measured components of the stator's acceleration f_x, f_y are the measured excitation force component, f_{bx}, f_{by} are the bearing reaction force components, and M_s is the stator mass. The *x* and *y* subscripts in these equations identify the *x* and *y* directions.

The test apparatus is used to measure rotordynamic coefficients for a bearing using a linearized force-displacement model for bearing given by

$$-\begin{bmatrix} f_{bx} \\ f_{by} \end{bmatrix} = \begin{bmatrix} K_{xx} & K_{xy} \\ K_{yx} & K_{yy} \end{bmatrix}\begin{bmatrix} \Delta x \\ \Delta y \end{bmatrix} + \begin{bmatrix} C_{xx} & C_{xy} \\ C_{yy} & C_{yy} \end{bmatrix}\begin{bmatrix} \Delta \dot{x} \\ \Delta \dot{y} \end{bmatrix} + \begin{bmatrix} M_{xx} & M_{xy} \\ M_{yx} & M_{yy} \end{bmatrix}\begin{bmatrix} \Delta \ddot{x} \\ \Delta \ddot{y} \end{bmatrix}, \tag{9}$$

where $\Delta x, \Delta y$ are defined as the relative motion between the rotor and the stator. The subscripts (*xx, yy*) and (*xy, yx*) refers to the direct and cross-coupled terms, respectively. Figure 9 show a representation for the stiffness and damping coefficients. Substituting Eq. (9) into Eq. (8) and rearranging gives

$$\begin{bmatrix} f_x - M_s a_x \\ f_y - M_s a_y \end{bmatrix} = -\begin{bmatrix} K_{xx} & K_{xy} \\ K_{yx} & K_{yy} \end{bmatrix}\begin{bmatrix} \Delta x \\ \Delta y \end{bmatrix} - \begin{bmatrix} C_{xx} & C_{xy} \\ C_{yy} & C_{yy} \end{bmatrix}\begin{bmatrix} \Delta \dot{x} \\ \Delta \dot{y} \end{bmatrix} - \begin{bmatrix} M_{xx} & M_{xy} \\ M_{yx} & M_{yy} \end{bmatrix}\begin{bmatrix} \Delta \ddot{x} \\ \Delta \ddot{y} \end{bmatrix} \tag{10}$$

The left hand vector of Eq. (10) is a known function of time (measured). On the right hand side, $\Delta x(t)$ and $\Delta y(t)$ are also measured functions of time. The rotordynamic coefficients are determined in the frequency domain via the Fast Fourier Transform $\mathfrak{F}$, which yields

$$\begin{bmatrix} F_x - M_s A_x \\ F_y - M_s A_y \end{bmatrix} = -\begin{bmatrix} H_{xx} & H_{xy} \\ H_{yx} & H_{yy} \end{bmatrix}\begin{bmatrix} D_x \\ D_y \end{bmatrix} \tag{11}$$

where $F_k = \mathfrak{F}(f_k)$, $A_k = \mathfrak{F}(a_k)$, $D_k = \mathfrak{F}(\Delta k)$.

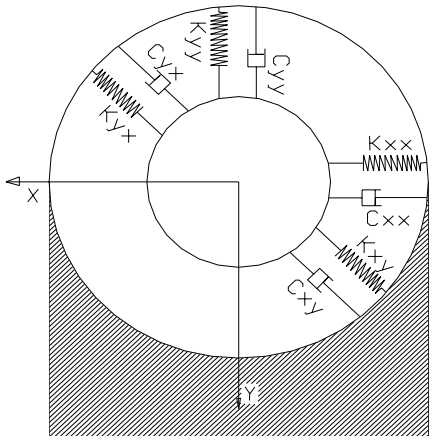

Figure 9. Dynamic force coefficients in fluid film bearings

The elements of the frequency response function H in Eq. (11) are related to the coefficients defined in Eq. (10) by Eq. (12)

$$H_{ij} = K_{ij} - M_{ij}\Omega^2 + \boldsymbol{j}(\Omega C_{ij}) \tag{12}$$

Where i, j are subscripts representing x and y, Ω is the excitation frequency and $\boldsymbol{j} = \sqrt{-1}$. Equation (11) provides two equations in the four unknowns H_{xx} , H_{xy} ,H_{yx} H_{yy} .To provide four independent equations, alternate shakes about an eccentric rotor position were conducted on the stator in orthogonal directions (x and y) yielding four equations and four unknowns, given by

$$\begin{bmatrix} F_{xx} - M_s A_{xx} & F_{xy} - M_s A_{xy} \\ F_{yx} - M_s A_{yx} & F_{yy} - M_s A_{yy} \end{bmatrix} = -\begin{bmatrix} H_{xx} & H_{xy} \\ H_{yx} & H_{yy} \end{bmatrix}\begin{bmatrix} D_{xx} & D_{xy} \\ D_{yx} & D_{yy} \end{bmatrix} \tag{13}$$

After solving Eq. (13) for the complex dynamic-stiffness matrix H, the rotordynamic coefficients can be identified according to Eq. (12) using a least-square fit as explained in the experimental dynamic results.

EXPERIMENTAL RESULTS AND PREDICTIONS

Experimental and prediction results are both presented in this chapter, and a comparison between the two is made. This chapter is divided into three main sections. The first section talks about the theory behind XLTFPBrg software and discuss the entries that have the most remarkable effects on the performance of the FPB under study. The second and third sections discuss the static and dynamic performance of the FPB, respectively.

XLTRC^2-XLTFPBrg Code

The XLTRC^2-XLTFPBrg software based on San Andrés [30] was used to predict the static and dynamic performance of the FPB. This model is based on the bulk-flow governing equations (mass conservation, axial and circumferential momentum, and energy equations) for laminar and turbulent flow in the thin fluid film lands of the bearing. Fluid inertia effects (temporal and convective terms) can be accounted for using this software. Table 5 shows the calculated Reynolds number for different rotor speeds. The highest Reynolds number calculated in these experiments was less than 350 at 12,000 rpm, which indicates operating in the laminar flow regime. When ignoring the fluid inertia (in most laminar flows), the Reynolds equation model is used.

Perturbation analysis is carried out around an equilibrium static position for the journal displacement in the x and y directions, in addition to the pad rotational angle. The results of the perturbation analysis are zeroth and first order flow equations. By solving these equations numerically the flow field is determined leading to the rotordynamic coefficients. San Andrés [28] discusses in detail the bulk-flow analysis of FPB.

Table 5. Maximum Reynolds number for different rotor speeds

Rotor Speed (rpm)	4000	6000	8000	10000	12000
Max. Reynolds Number ($\rho\, C_p\, \omega\, R_s/\mu$)	119	179	240	294	344

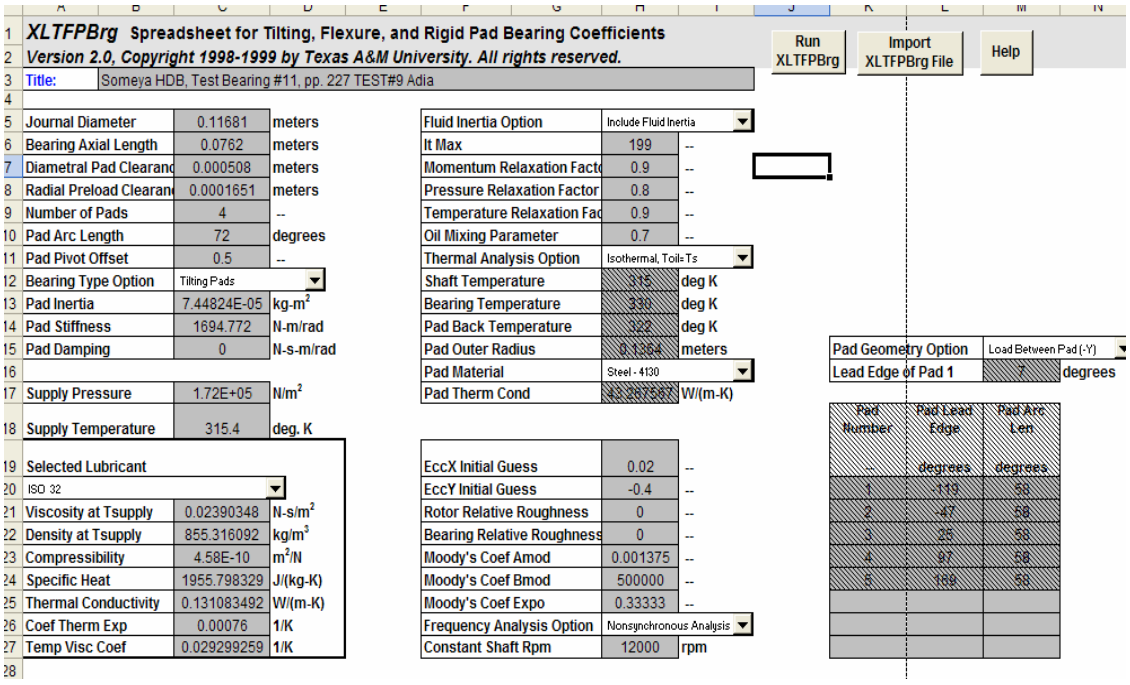

XLTFPBrg Spreadsheet for Tilting, Flexure, and Rigid Pad Bearing Coefficients

Version 2.0, Copyright 1998-1999 by Texas A&M University. All rights reserved.

Run XLTFPBrg | Import XLTFPBrg File | Help

Title: Someya HDB, Test Bearing #11, pp. 227 TEST#9 Adia

Journal Diameter	0.11681	meters	
Bearing Axial Length	0.0762	meters	
Diametral Pad Clearanc	0.000508	meters	
Radial Preload Clearanc	0.0001651	meters	
Number of Pads	4	--	
Pad Arc Length	72	degrees	
Pad Pivot Offset	0.5	--	
Bearing Type Option	Tilting Pads		
Pad Inertia	7.44824E-05	kg-m^2	
Pad Stiffness	1694.772	N-m/rad	
Pad Damping	0	N-s-m/rad	
Supply Pressure	1.72E+05	N/m^2	
Supply Temperature	315.4	deg. K	
Selected Lubricant			
ISO 32			
Viscosity at Tsupply	0.02390348	N-s/m^2	
Density at Tsupply	855.316092	kg/m^3	
Compressibility	4.58E-10	m^2/N	
Specific Heat	1955.798329	J/(kg-K)	
Thermal Conductivity	0.131083492	W/(m-K)	
Coef Therm Exp	0.00076	1/K	
Temp Visc Coef	0.029299259	1/K	

Fluid Inertia Option	Include Fluid Inertia	
It Max	199	--
Momentum Relaxation Facto	0.9	--
Pressure Relaxation Factor	0.8	--
Temperature Relaxation Fac	0.9	--
Oil Mixing Parameter	0.7	--
Thermal Analysis Option	Isothermal, Toil=Ts	
Shaft Temperature	315	deg K
Bearing Temperature	330	deg K
Pad Back Temperature	322	deg K
Pad Outer Radius	0.1364	meters
Pad Material	Steel - 4130	
Pad Therm Cond	42.267587	W/(m-K)
EccX Initial Guess	0.02	--
EccY Initial Guess	-0.4	--
Rotor Relative Roughness	0	--
Bearing Relative Roughness	0	--
Moody's Coef Amod	0.001375	--
Moody's Coef Bmod	500000	--
Moody's Coef Expo	0.33333	--
Frequency Analysis Option	Nonsynchronous Analysis	
Constant Shaft Rpm	12000	rpm

Pad Geometry Option	Load Between Pad (-Y)
Lead Edge of Pad 1	7 degrees

Pad Number	Pad Lead Edge (degrees)	Pad Arc Len (degrees)
1	119	58
2	-47	58
3	25	58
4	97	58
5	169	58

Figure 10. Input screen of the XLTFPBrg software

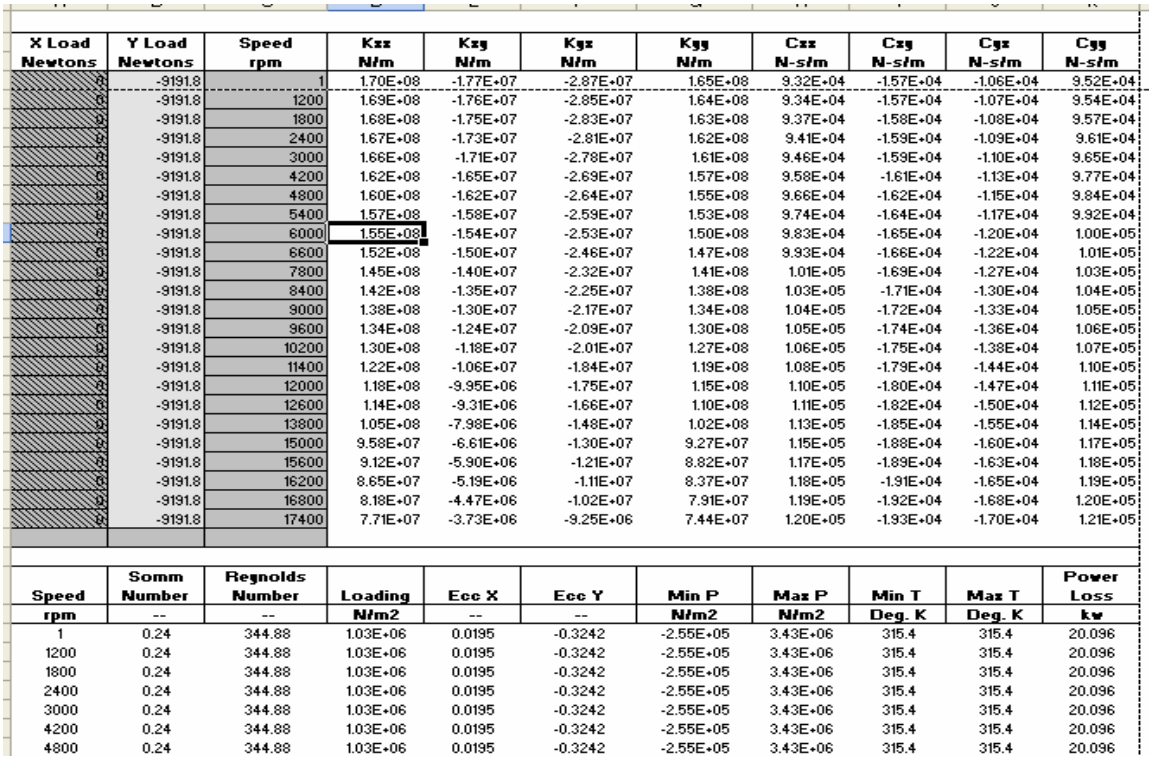

X Load Newtons	Y Load Newtons	Speed rpm	Kzz N/m	Kzy N/m	Kyz N/m	Kyy N/m	Czz N-s/m	Czy N-s/m	Cyz N-s/m	Cyy N-s/m
0	-9191.8	1	1.70E+08	-1.77E+07	-2.87E+07	1.65E+08	9.32E+04	-1.57E+04	-1.06E+04	9.52E+04
0	-9191.8	1200	1.69E+08	-1.76E+07	-2.85E+07	1.64E+08	9.34E+04	-1.57E+04	-1.07E+04	9.54E+04
0	-9191.8	1800	1.68E+08	-1.75E+07	-2.83E+07	1.63E+08	9.37E+04	-1.58E+04	-1.08E+04	9.57E+04
0	-9191.8	2400	1.67E+08	-1.73E+07	-2.81E+07	1.62E+08	9.41E+04	-1.59E+04	-1.09E+04	9.61E+04
0	-9191.8	3000	1.66E+08	-1.71E+07	-2.78E+07	1.61E+08	9.46E+04	-1.59E+04	-1.10E+04	9.65E+04
0	-9191.8	4200	1.62E+08	-1.65E+07	-2.69E+07	1.57E+08	9.58E+04	-1.61E+04	-1.13E+04	9.77E+04
0	-9191.8	4800	1.60E+08	-1.62E+07	-2.64E+07	1.55E+08	9.66E+04	-1.62E+04	-1.15E+04	9.84E+04
0	-9191.8	5400	1.57E+08	-1.58E+07	-2.59E+07	1.53E+08	9.74E+04	-1.64E+04	-1.17E+04	9.92E+04
0	-9191.8	6000	1.55E+08	-1.54E+07	-2.53E+07	1.50E+08	9.83E+04	-1.65E+04	-1.20E+04	1.00E+05
0	-9191.8	6600	1.52E+08	-1.50E+07	-2.46E+07	1.47E+08	9.93E+04	-1.66E+04	-1.22E+04	1.01E+05
0	-9191.8	7800	1.45E+08	-1.40E+07	-2.32E+07	1.41E+08	1.01E+05	-1.69E+04	-1.27E+04	1.03E+05
0	-9191.8	8400	1.42E+08	-1.35E+07	-2.25E+07	1.38E+08	1.03E+05	-1.71E+04	-1.30E+04	1.04E+05
0	-9191.8	9000	1.38E+08	-1.30E+07	-2.17E+07	1.34E+08	1.04E+05	-1.72E+04	-1.33E+04	1.05E+05
0	-9191.8	9600	1.34E+08	-1.24E+07	-2.09E+07	1.30E+08	1.05E+05	-1.74E+04	-1.36E+04	1.06E+05
0	-9191.8	10200	1.30E+08	-1.18E+07	-2.01E+07	1.27E+08	1.06E+05	-1.75E+04	-1.38E+04	1.07E+05
0	-9191.8	11400	1.22E+08	-1.06E+07	-1.84E+07	1.19E+08	1.08E+05	-1.79E+04	-1.44E+04	1.10E+05
0	-9191.8	12000	1.18E+08	-9.95E+06	-1.75E+07	1.15E+08	1.10E+05	-1.80E+04	-1.47E+04	1.11E+05
0	-9191.8	12600	1.14E+08	-9.31E+06	-1.66E+07	1.10E+08	1.11E+05	-1.82E+04	-1.50E+04	1.12E+05
0	-9191.8	13800	1.05E+08	-7.98E+06	-1.48E+07	1.02E+08	1.13E+05	-1.85E+04	-1.55E+04	1.14E+05
0	-9191.8	15000	9.58E+07	-6.61E+06	-1.30E+07	9.27E+07	1.15E+05	-1.88E+04	-1.60E+04	1.17E+05
0	-9191.8	15600	9.12E+07	-5.90E+06	-1.21E+07	8.82E+07	1.17E+05	-1.89E+04	-1.63E+04	1.18E+05
0	-9191.8	16200	8.65E+07	-5.19E+06	-1.11E+07	8.37E+07	1.18E+05	-1.91E+04	-1.65E+04	1.19E+05
0	-9191.8	16800	8.18E+07	-4.47E+06	-1.02E+07	7.91E+07	1.19E+05	-1.92E+04	-1.68E+04	1.20E+05
0	-9191.8	17400	7.71E+07	-3.73E+06	-9.25E+06	7.44E+07	1.20E+05	-1.93E+04	-1.70E+04	1.21E+05

Speed rpm	Somm Number --	Reynolds Number --	Loading N/m2	Ecc X --	Ecc Y --	Min P N/m2	Max P N/m2	Min T Deg. K	Max T Deg. K	Power Loss kw
1	0.24	344.88	1.03E+06	0.0195	-0.3242	-2.55E+05	3.43E+06	315.4	315.4	20.096
1200	0.24	344.88	1.03E+06	0.0195	-0.3242	-2.55E+05	3.43E+06	315.4	315.4	20.096
1800	0.24	344.88	1.03E+06	0.0195	-0.3242	-2.55E+05	3.43E+06	315.4	315.4	20.096
2400	0.24	344.88	1.03E+06	0.0195	-0.3242	-2.55E+05	3.43E+06	315.4	315.4	20.096
3000	0.24	344.88	1.03E+06	0.0195	-0.3242	-2.55E+05	3.43E+06	315.4	315.4	20.096
4200	0.24	344.88	1.03E+06	0.0195	-0.3242	-2.55E+05	3.43E+06	315.4	315.4	20.096
4800	0.24	344.88	1.03E+06	0.0195	-0.3242	-2.55E+05	3.43E+06	315.4	315.4	20.096

Figure 11. Output screen of the XLTFPBrg software

Figure 10 and Figure 11 show the input and output data screens for the XLTFPBrg program, respectively. All the entries seen in Figure 10 remains unchanged for all tests conditions except for the following entries:

(a) Supply temperature entry (inlet oil temperature)

(b) EccX and EccY initial guesses, pressure and temperature relaxation factors entries (for faster convergence)

(c) Constant shaft speed entry (rotor speed)

(d) Y-Load entry (applied static load)

Looking from the DE side, the coordinate system describing the test rig is shown in Figure 12(a).The coordinate system for the XLTRC^2 –XLTFPBrg code used to predict the performance and the rotordynamic coefficients is shown in Figure 12(b).

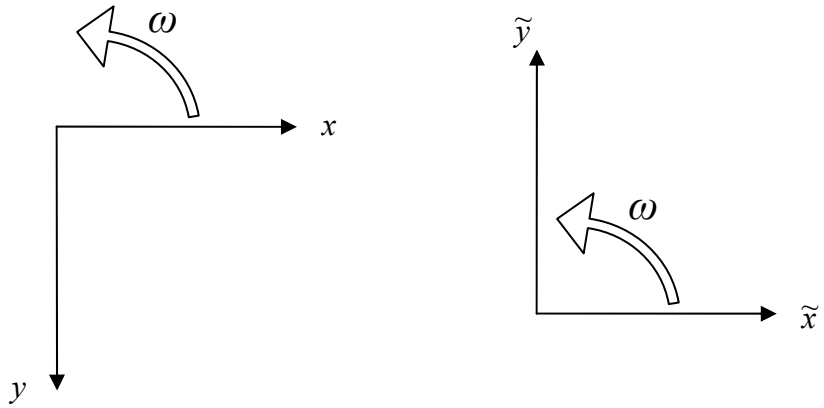

(a) (b)

Figure 12. Coordinate systems for: (a) test rig, and (b) theory

The reaction force of the FPB can be written either using Eq. (14) in the test rig coordinate system or using Eq. (15) in the XLTRC^2 code coordinate system.

$$-\begin{bmatrix} f_{bx} \\ f_{by} \end{bmatrix} = \begin{bmatrix} K_{xx} & K_{xy} \\ K_{yx} & K_{yy} \end{bmatrix} \begin{bmatrix} \Delta x \\ \Delta y \end{bmatrix} + \begin{bmatrix} C_{xx} & C_{xy} \\ C_{yx} & C_{yy} \end{bmatrix} \begin{bmatrix} \Delta \dot{x} \\ \Delta \dot{y} \end{bmatrix} + \begin{bmatrix} M_{xx} & M_{xy} \\ M_{yx} & M_{yy} \end{bmatrix} \begin{bmatrix} \Delta \ddot{x} \\ \Delta \ddot{y} \end{bmatrix} \tag{14}$$

$$-\begin{bmatrix} \tilde{f}_{bx} \\ \tilde{f}_{by} \end{bmatrix} = \begin{bmatrix} \tilde{K}_{xx} & \tilde{K}_{xy} \\ \tilde{K}_{yx} & \tilde{K}_{yy} \end{bmatrix} \begin{bmatrix} \Delta \tilde{x} \\ \Delta \tilde{y} \end{bmatrix} + \begin{bmatrix} \tilde{C}_{xx} & \tilde{C}_{xy} \\ \tilde{C}_{yx} & \tilde{C}_{yy} \end{bmatrix} \begin{bmatrix} \Delta \dot{\tilde{x}} \\ \Delta \dot{\tilde{y}} \end{bmatrix} + \begin{bmatrix} \tilde{M}_{xx} & \tilde{M}_{xy} \\ \tilde{M}_{yx} & \tilde{M}_{yy} \end{bmatrix} \begin{bmatrix} \Delta \ddot{\tilde{x}} \\ \Delta \ddot{\tilde{y}} \end{bmatrix} \tag{15}$$

where,

$$\begin{bmatrix} f_{bx} \\ f_{by} \end{bmatrix} = \begin{bmatrix} \widetilde{f}_{bx} \\ -\widetilde{f}_{by} \end{bmatrix}, \tag{16}$$

$$\begin{bmatrix} x \\ y \end{bmatrix} = \begin{bmatrix} 1 & 0 \\ 0 & -1 \end{bmatrix} \begin{bmatrix} \widetilde{x} \\ \widetilde{y} \end{bmatrix} \tag{17}$$

Transforming the code-coordinate system to the test-rig-coordinate system can be done by substituting Eqs. (16 and 17) into Eq. (14) giving

$$\begin{bmatrix} \widetilde{f}_{bx} \\ \widetilde{f}_{by} \end{bmatrix} = \begin{bmatrix} K_{xx} & -K_{xy} \\ -K_{yx} & K_{yy} \end{bmatrix} \begin{bmatrix} \Delta\widetilde{x} \\ \Delta\widetilde{y} \end{bmatrix} + \begin{bmatrix} C_{xx} & -C_{xy} \\ -C_{yx} & C_{yy} \end{bmatrix} \begin{bmatrix} \Delta\dot{\widetilde{x}} \\ \Delta\dot{\widetilde{y}} \end{bmatrix} + \begin{bmatrix} M_{xx} & -M_{xy} \\ -M_{yx} & M_{yy} \end{bmatrix} \begin{bmatrix} \Delta\ddot{\widetilde{x}} \\ \Delta\ddot{\widetilde{y}} \end{bmatrix}. \tag{18}$$

Comparing Eq. (18) with Eq. (15), the following results are obtained.

$$\begin{aligned} &K_{xx} = K_{\widetilde{x}\widetilde{x}},\ K_{yy} = K_{\widetilde{y}\widetilde{y}},\ K_{xy} = -K_{\widetilde{x}\widetilde{y}},\ K_{yx} = -K_{\widetilde{y}\widetilde{x}} \\ &C_{xx} = C_{\widetilde{x}\widetilde{x}},\ C_{yy} = C_{\widetilde{y}\widetilde{y}},\ C_{xy} = -C_{\widetilde{x}\widetilde{y}},\ C_{yx} = -C_{\widetilde{y}\widetilde{x}} \\ &M_{xx} = M_{\widetilde{x}\widetilde{x}},\ M_{yy} = M_{\widetilde{y}\widetilde{y}},\ M_{xy} = -M_{\widetilde{x}\widetilde{y}},\ M_{yx} = -M_{\widetilde{y}\widetilde{x}} \end{aligned} \tag{19}$$

For comparison purposes the outputs of the XLTFPBrg code seen in Figure 11 were transformed to the test-rig-coordinate system using Eq. (19).

The following two frequency analysis options available to calculate the rotordynamic coefficients (K_{ij}, C_{ij}):

(a) Synchronous analysis: the stiffness and damping coefficients are calculated at a whirl frequency equal to the shaft running speed (frequency independent coefficients).

(b) Non-synchronous analysis: the stiffness and damping coefficients are calculated at different whirl frequencies starting from approximately zero frequency (very small) up to, normally 2 times the shaft running speed. (frequency dependent coefficients).

"For the Nonsynchronous option, the shaft speed is taken from the Constant Shaft rpm input cell, and the whirl frequency is taken from the Speed column. For this type of analysis, only *K* and *C* will change with whirl speed, all the other output parameters like Reynolds number, pad temperature and pressure will be the same for each whirl speed since the shaft speed is constant." taken from XLTFPBrg help file.

The energy equation is used in the analysis through choosing one of the available thermal analysis options shown in Table 6.

Table 6. "Thermal analysis options" - XLTFPBrg help file

Option	**Description(**subscripts: J=journal, b=bearing, s=supply)
1) Adiabatic, QJ=Qb=0	Adiabatic Solid Surfaces (Qb=QJ=0)
2) Isothermal, TJ=Const, Tb=Const	Isothermal journal & bearing: TJ ; Tb
3) Isothermal, Toil=TS	Isothermal (Barotropic) fluid film (T=Ts everywhere)
4) QJ=0, Tb=Const	Adiabatic journal (QJ=0) & Isothermal bearing (Tb)
5) TJ=Const, Qb=0	Isothermal journal(TJ) & Adiabatic bearing (Qb=0)
6) QJ=0, TPB=Const	Adiabatic journal (QJ=0) & Radial heat flow on bearing pad
7) TJ=Const, TPB=Const	Isothermal journal (TJ) & Radial heat flow on bearing pad with outer temperature (TPB).

To study the effect of excitation frequency on the rotordynamic coefficients, the Non-synchronous analysis option was used. From the available experimental data, we can choose one of the following thermal analysis options. Option 1(adiabatic) or option 3(Isothermal). Neither of these options matches the actual test condition. The adiabatic option considers no heat transfer through the shaft and bearing, but we observed during testing a hot stator. On the other hand, the isothermal option considers the oil temperature to be constant everywhere and equal to the supply temperature, but we measured an increase in the oil outlets temperatures and in the circumferential pads temperatures.

A comparison between the direct coefficients obtained using the adiabatic and the isothermal options with the experimental results are shown in Figure 13. Clearly, the predictions using the isothermal model agree more closely with the experimental results. Therefore option 3 in Table 6 was used as the thermal analysis option (Isothermal, $T_{oil} = T_{supply}$). The average of all pads temperature at 5% of the pad arc length in the direction of rotation was taken as the supply oil temperature and is given in Table 7 over the applied static load range for each running speed

Table 7. Average pads temperature at 5% for different rotor speed

Rotor Speed (*rpm*)	4000	6000	8000	10000	12000
Average Pads Temp. at 5% (C)	39.45	39.55	41.15	41.75	42.25

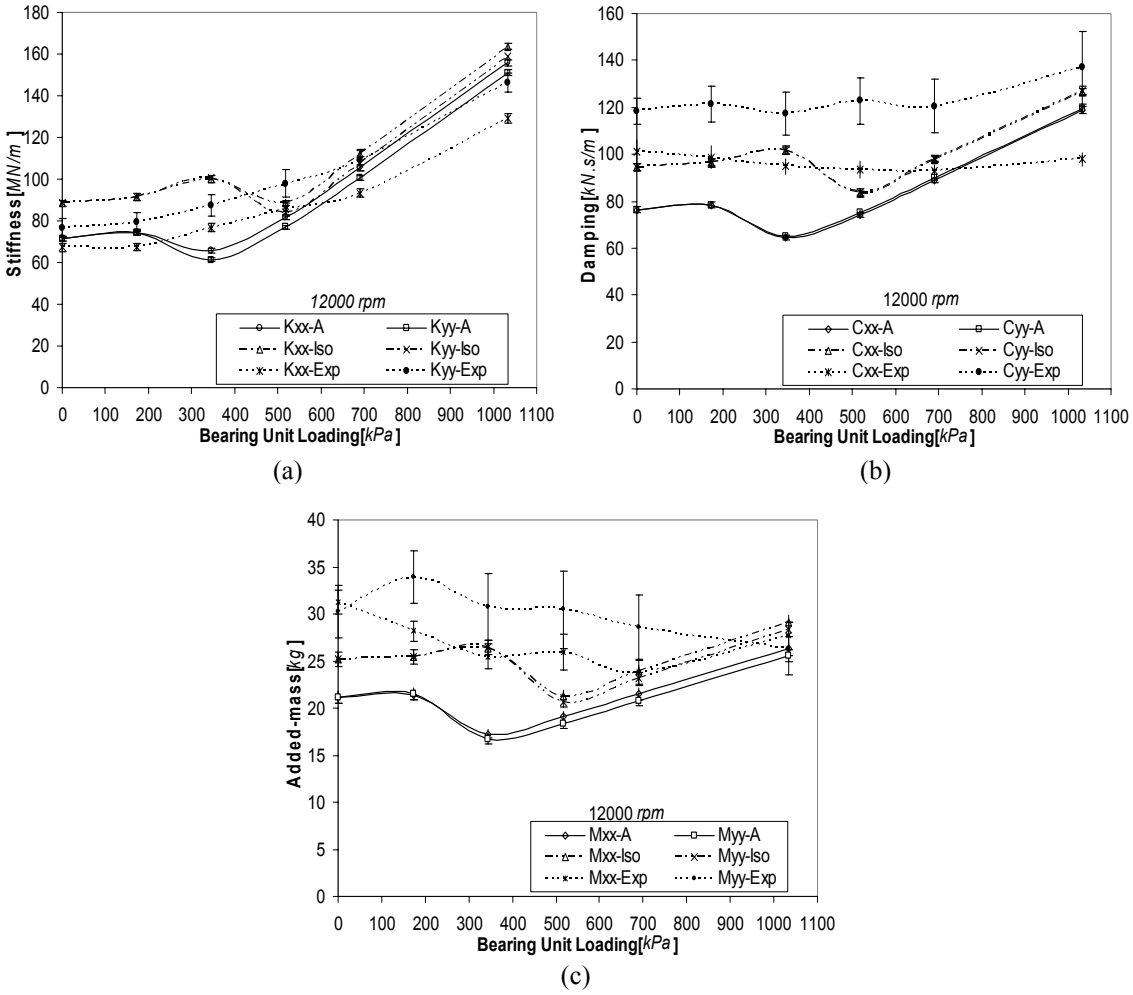

Figure 13. Effects of using different thermal analysis on direct: (a) stiffness (b) damping and (c) added mass coefficients

The nominal radial bearing clearance is 190.5 μm (7.5 mils). While, the minimum measured radial bearing clearance using the bump test was 165.1 μm (6.5 mils). As seen in Figure 14, changing the clearance has a dramatic effect on the predicted rotordynamic coefficients. Decreasing the bearing clearance from 190.5 μm (7.5 mils) to 165.1 μm (6.5 mils) with constant pad radial clearance of 254 μm (10 mils) will result in an increase up to 30% in the rotordynamic coefficients, especially at low bearing unit loading. In addition, we see that using 165.1 μm (6.5 mils) bearing clearance gives good agreement with the experimental results. In conclusion, non-synchronous isothermal analysis with a radial bearing clearance of 165.1 μm (6.5 mils) will be used in predicting the performance of the FPB using the XLTFPBrg software.

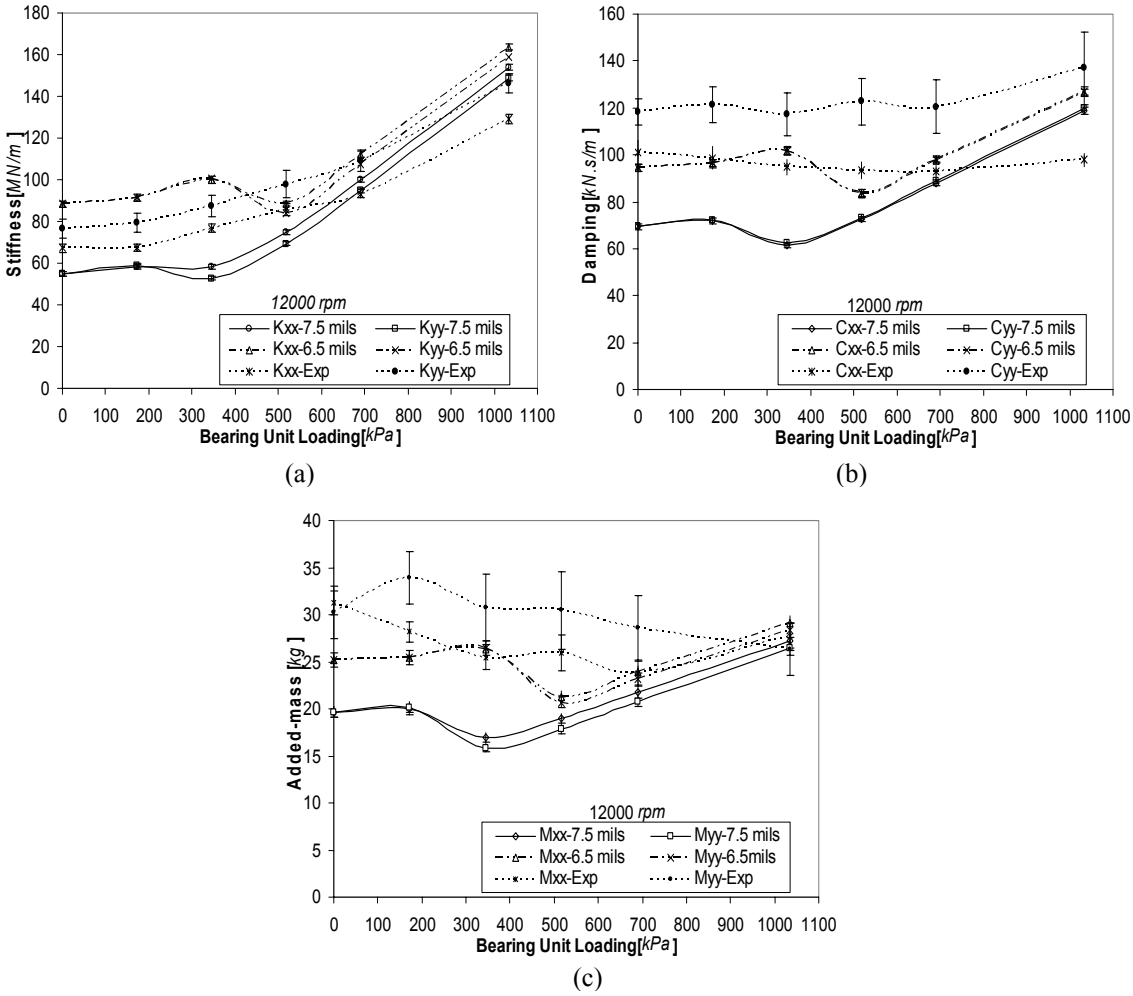

Figure 14. Effects of using different bearing clearance on direct: (a) stiffness (b) damping and (c) added mass coefficients

Static Test Results

The static results are discussed below in the following three sections: (1) eccentricity ratio and attitude angle, (2) power losses, and (3) oil and pads temperatures. Tables 8 and 9 in the Appendix show the measured static data and the calculated static performance parameters.

Eccentricity Ratio and Attitude Angle

A good idea of the dynamic performance of the FPB can be obtained from studying the stator load-displacement locus plot. When applying a static load to the bearing in the positive *y* direction while the rotor rotates in a counter-clockwise direction, displacements of the stator in the positive *y* and *x* directions are expected. The magnitude of displacement in the *x* direction with respect to the displacement in the *y* direction is an indication of the magnitude of the cross coupled stiffness K_{yx}. This relative displacement can be expressed in terms of the attitude angle ϕ . The larger the attitude angle, the larger the cross-coupled stiffness coefficients (K_{yx} and K_{xy}). Another important realization from the locus plot is the static eccentricity ratio ε_0 , which is a relative indication of the magnitude of the direct stiffness coefficients (K_{yy} and K_{xx}) the larger ε_0 , the smaller the direct stiffness coefficients, for the same applied static load. To monitor pitching and yawing between the rotor and the bearing, the static experimental results were measured at both the drive end (DE) and the non-drive end (NDE) sides. For comparison purposes, the average measurement between the DE and the NDE will be used.

The coordinate system used in plotting Figures 15 and 16 are the coordinates of the bearing looking from the DE side. Figure 15 shows the experimental and theoretical loci plots for different rotor speeds. The maximum bearing unit loading reached at 4000 rpm was 689.5 kPa. For other rotor speeds a 1034.2 kPa bearing unit loading was reached. The operational eccentricity ratio ε_0 at high loads for almost all rotor speeds lies between 40-50% of the pad radial clearance. In addition, a small attitude angle around 10^o was seen at high loads. Good agreement between the theoretical predictions and the experimental results is seen up to $\varepsilon_0 \cong 0.2$. The theory under-predicts ϕ and ε_0 for eccentricity ratios greater than 0.2.

Figure 16 shows the experimental and theoretical locus plot of the average measurements for different rotor speeds. As seen, increasing the rotational speed will lead to lower ϕ and ε_0 values, because increasing ω increases the hydrodynamic lift forces in the fluid film. The theoretical predictions and experimental results show good agreement especially at low eccentricity ratio.

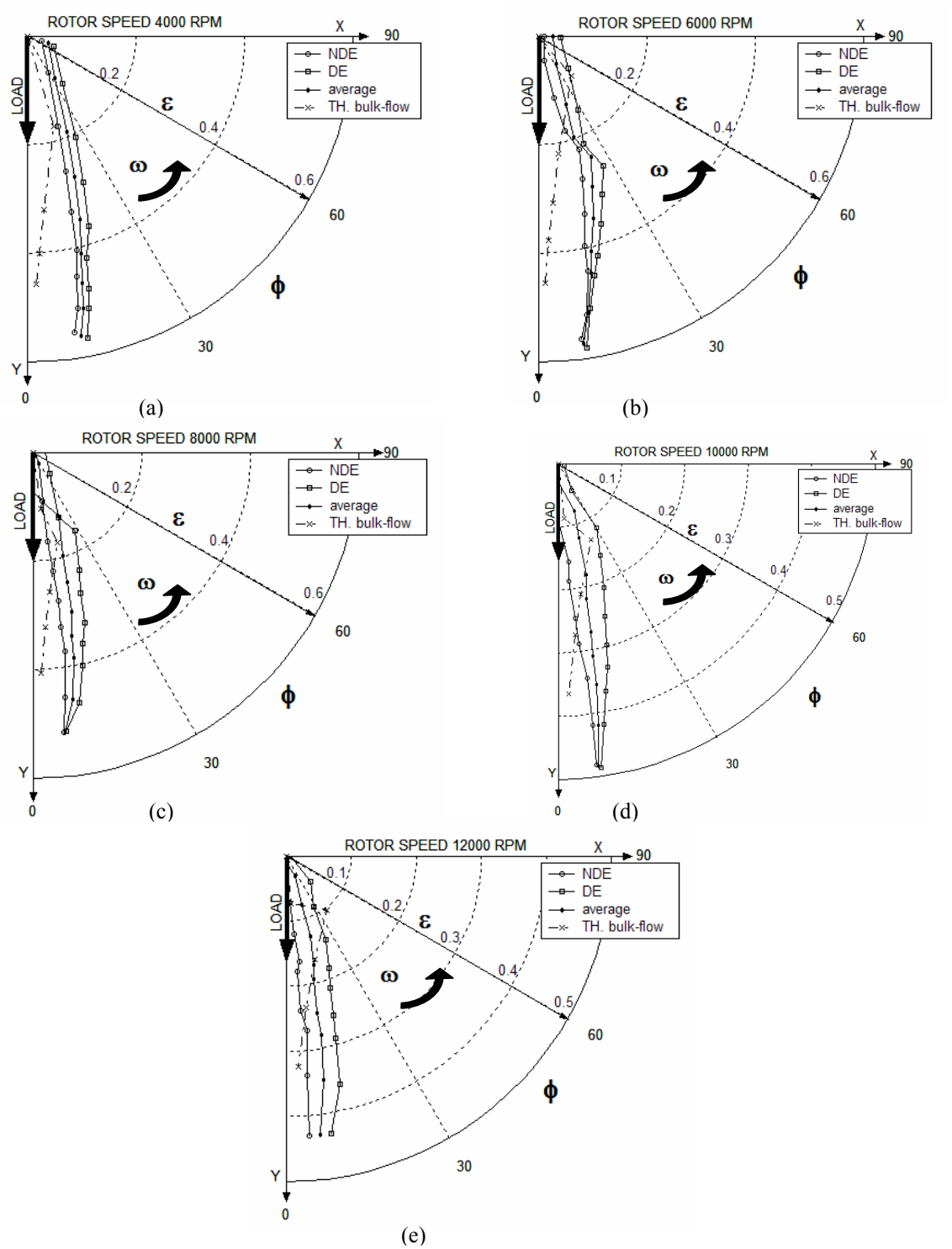

Figure 15. Experimental and theoretical loci plot of FPB centerline for different rotor speeds: (a) 4000 rpm, (b) 6000 rpm, (c) 8000 rpm, (d) 10000 rpm and (e) 12000 rpm

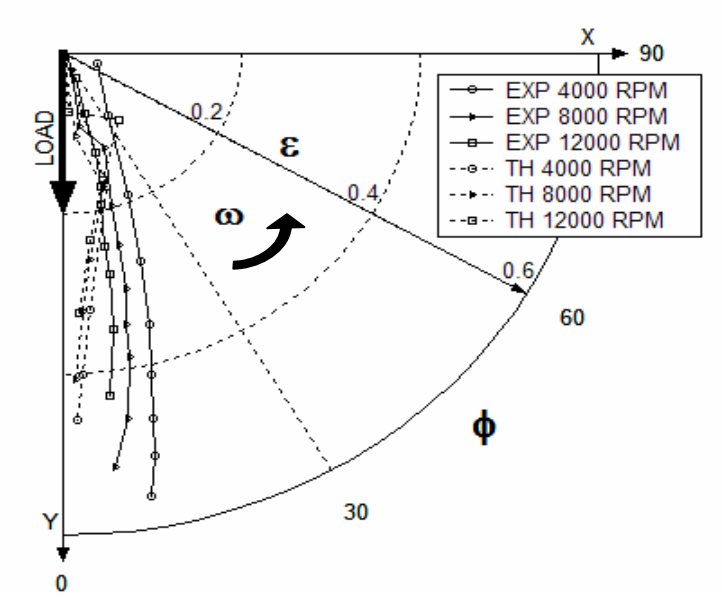

Figure 16. Experimental and theoretical (bulk-flow) average loci plot of FPB centerline for different rotor speeds

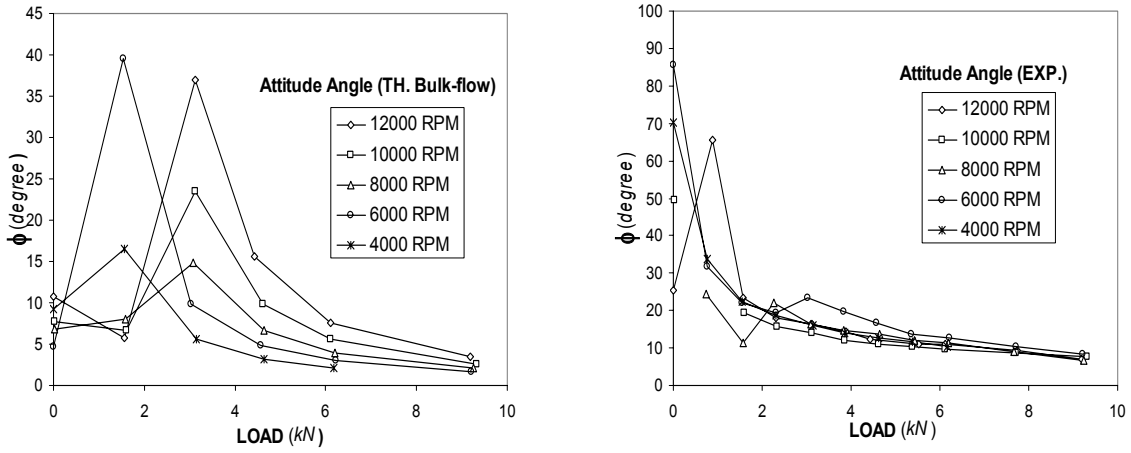

(a) (b)

Figure 17. Attitude angle versus applied static load for different rotor speeds: (a) theoretical (bulk-flow) and (b) experimental

The theoretical and experimental attitude angle ϕ versus the applied static load for different rotor speeds are shown in Figures 17a and 17b, respectively. The obvious pattern of the attitude angle is that it decreases with increasing the applied static load and approaches a constant value at high loads regardless of the operating speed. The experimental attitude angle is almost twice

the predicted one. The same observed pattern is seen in Figure 18 when plotting the attitude angle versus the eccentricity ratio, since high eccentricity ratios correspond to high loads. Additionally, the decrease in attitude angle with increasing speed is seen clearly. Taking into consideration that Sommerfeld number contains the combined effects of oil viscosity (oil temperature), rotational speed, and applied static load. High Sommerfeld numbers result from high oil viscosity (or low oil temperature), high rotational speed, and low applied static load. On the other hand, lower Sommerfeld numbers arise from low oil viscosity (or high oil temperature), low rotational speed and high applied static load.

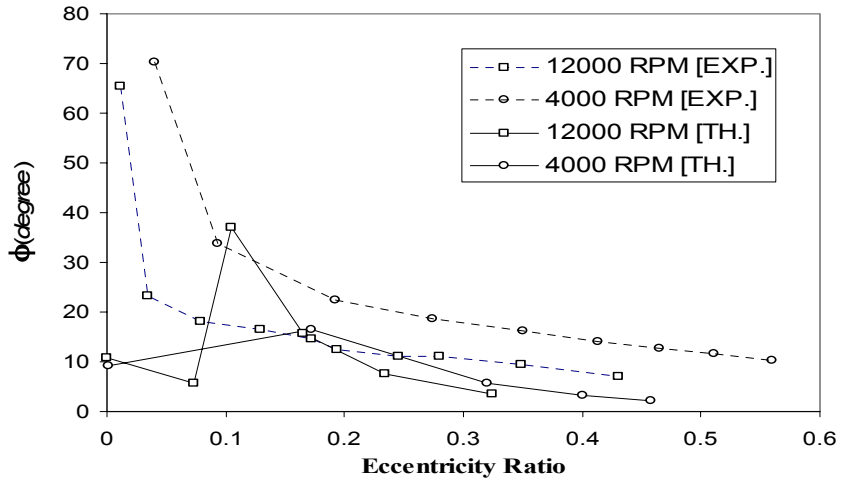

Figure 18. Experimental and theoretical (bulk-flow) attitude angle versus eccentricity for different rotor speeds

Figure 19 and Figure 20 demonstrate the variation of the attitude angle with Sommerfeld number. In Figure 19, for constant load lines, the attitude angle decreases with increasing rotor speed. On the other hand, the attitude angle for high loads is smaller than the attitude angle for low loads. Using constant speed lines, Figure 20 show the same behavior. In general, we can say that the attitude angle increases with increasing Sommerfeld number to a constant value around 25 degree, the theory under-predicts the attitude angle in most cases and capture the general trends of the attitude angle.

One of the most important operating design curves is the curve of eccentricity ratio versus Sommerfeld number shown in Figure 21. The eccentricity ratio decreases with increasing Sommerfeld Number. The theory under-predicts the eccentricity ratio for low Sommerfeld numbers by less than 20% and does a good job for high Sommerfeld numbers.

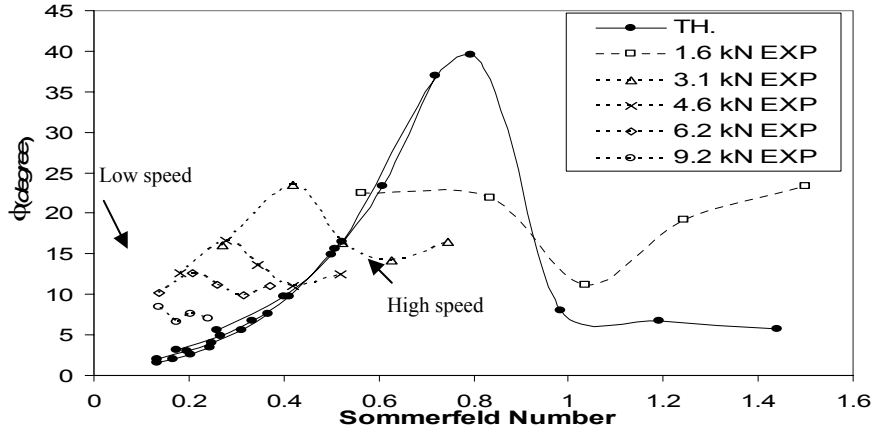

Figure 19. Experimental and theoretical (bulk-flow) attitude angle versus Sommerfeld number for different applied static loads

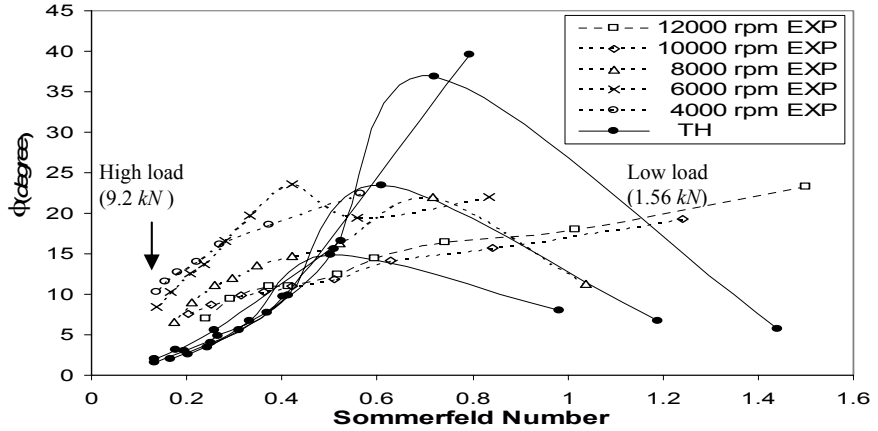

Figure 20. Experimental and theoretical (bulk-flow) attitude angle versus Sommerfeld number for different rotor speeds

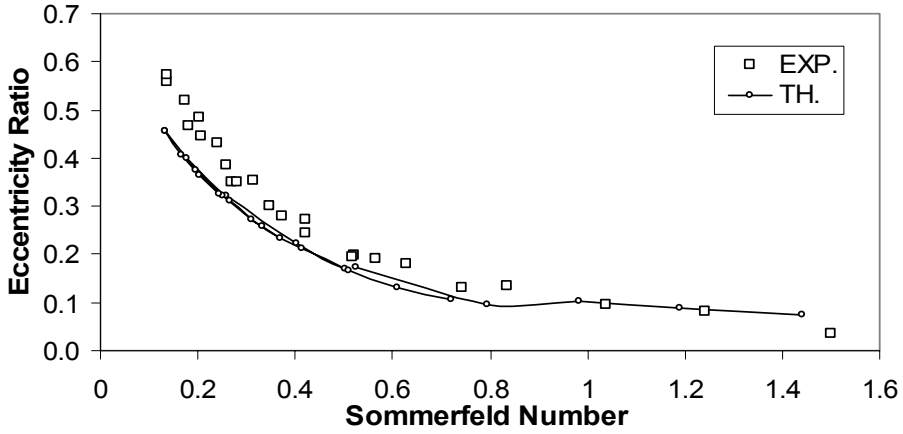

Figure 21. Experimental and theoretical (bulk-flow) eccentricity ratio versus Sommerfeld number

Power Losses

Power losses are very important in the design stage of any machine, to determine the minimum driver power required. The power losses of the FPB are mainly of frictional type. Frictional power loss arises due to shear stresses that are developed on the fluid film between the rotor and each pad when the rotor rotates. As a result, drag torques opposite to the direction of rotor rotation will be generated requiring an increase in the driving power.

Since the test rig was not equipped with a torque meter, the experimental power losses were calculated based on the measured rise in the oil temperature. This calculation was based on the assumption that the heat generated in the fluid film was totally carried by the lubricating oil. This assumption can be supported by the fact that we have a high flow-rate (53.3 lit/min) and a relatively small measured temperature rise at the oil exits. In addition, the measurement of heat transfer by conduction was not possible for technical issues (the temperatures of the stator surface and underneath the pads were not available).

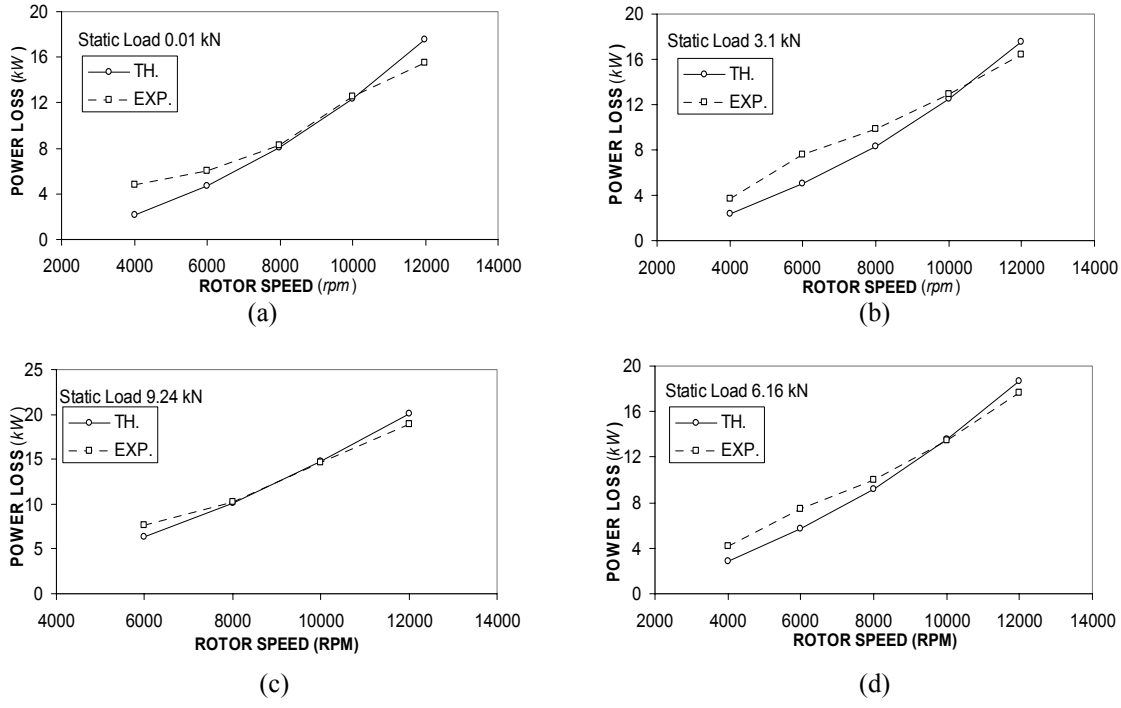

Figure 22. Experimental and theoretical power losses versus rotor speeds for different static loads: (a) 0.01 kN, (b) 3.1 kN, (c) 9.24 kN and (d) 6.16 kN

Figure 22 shows the experimental and predicted power losses versus rotor speed for different static loads. We know that drag power is proportional to oil viscosity and the square of the rotor speed, so higher speeds means higher power losses leading to increased oil outlet temperatures. In consequence, the oil viscosity will decrease; therefore, the power loss will also decrease until reaching a steady state. For that reason, the plot of power loss versus the rotational speed looks more like a straight line than a parabola. As seen in

Figure 22 (a, b, c and d) the power loss increases with increasing rotor speeds. The theoretical power loss agrees well with the experimental results.

Figure 23 (a and b) show that the power loss increase is more sensitive to increases in rotor speed than to increases in the applied static load.

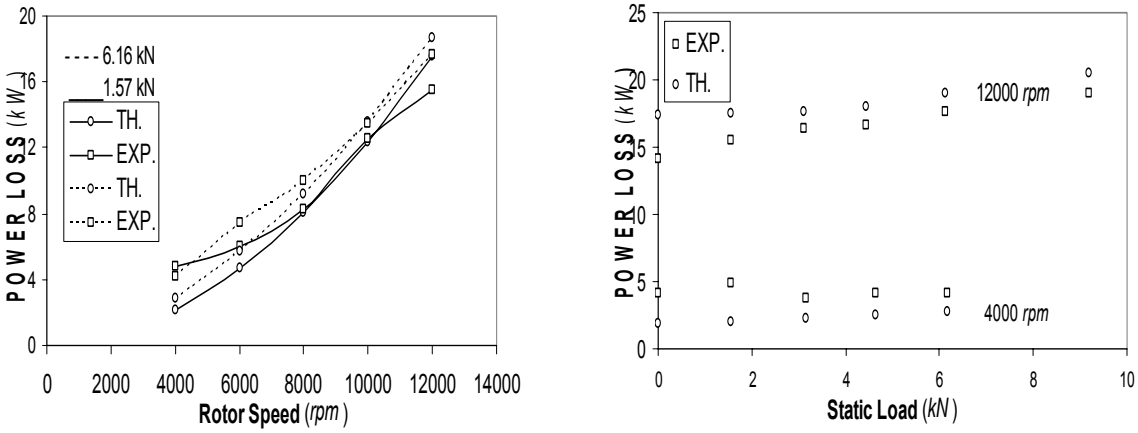

(a) (b)

Figure 23. Experimental and theoretical power losses versus: (a) rotor speeds for different static loads and (b) static loads for different rotor speeds

Oil and Pads Temperatures

Temperature is the best indication of bearing operating condition, from the following two perspectives:

(a) **Oil viscosity.** The oil viscosity versus temperature of most turbine oils takes the form, $\mu(T) = \mu_r \, e^{\alpha(T-T_r)}$, where T is oil temperature in C^o and μ_r is a reference oil viscosity at temperature (T_r) and α is a constant. The oil type used in this experiment was ISO VG32- Turbine oil and its viscosity is given by

$$\mu(T) = 0.04534\, e^{-0.03007(T-21.11)}, \qquad (20)$$

Equation (20) shows that the oil viscosity decreases exponentially with increasing oil temperature. Knowing that decreasing oil viscosity will produce a decrease in damping, oil temperature has a direct influence on the bearing characteristics.

(b) **Bearing clearance.** The increase in oil temperature will cause the external rotor and internal bearing surfaces to grow in the radial direction (thermal growth). Therefore, changing the bearing and pads clearances will lead to a change in bearing preload. Nicholas [4] discusses the effects of changing bearing preload and clearance on the rotordynamic coefficients. In general, for constant bearing preload, decreasing bearing clearance will be accompanied with an increase in direct damping and stiffness. On the other hand, increasing bearing preload will result in an increase in direct stiffness and a decrease in direct damping.

Figure 24 shows the inlet and outlets oil temperatures versus applied static load for different rotor speeds. The inlet oil temperature was maintained constant for all test condition around $37.8\ C^o$ with $\pm 1 C^o$ difference. Outlets oil temperatures were measured at both sides of the bearing; drive end (DE) and non-drive end (NDE). As we can see from Figure 24, the outlets oil temperatures are almost constant with the applied static load for any rotor speed. In addition, the DE outlet oil temperature is higher than the NDE oil outlet temperature by (3 to 4) C^o. That temperature difference can be explained as follows. Since the bearing outside diameter was larger than the inside diameter of the stator, the bearing stator was assembled through a shrink fit process. Therefore, the stator was heated and then the bearing was installed. During the cooling process of the bearing-stator, the DE side was probably crushed more than the NDE side due to any or all of the following factors:

(a) One of the oil seal between the bearing and the stator was partially displaced (confirmed after disassembly).

(b) Pitching between the bearing and the stator (could have happened during assembly).

(c) Stator and/or bearing surfaces machined dissimilarly.

The following facts support that the bearing was crushed:

(a) There was a difference in the oil flow-rate from each side of the bearing (visually confirmed).

(b) The measured bearing clearance shown in Figure 8 (pivot to pivot) along the X^ and the Y^ axes were found to be 13 and 17 mils, respectively.

(c) The oil outlets temperatures difference of (3 to 4 C^o **)** is constant for almost all operating conditions indicating that it results from the bearing geometry as seen in figures (24, 25).

(d) Pad #4 temperatures difference between the DE and the NDE sides as seen in figures (26, 27, 28, 29, 30, 31, and 32).

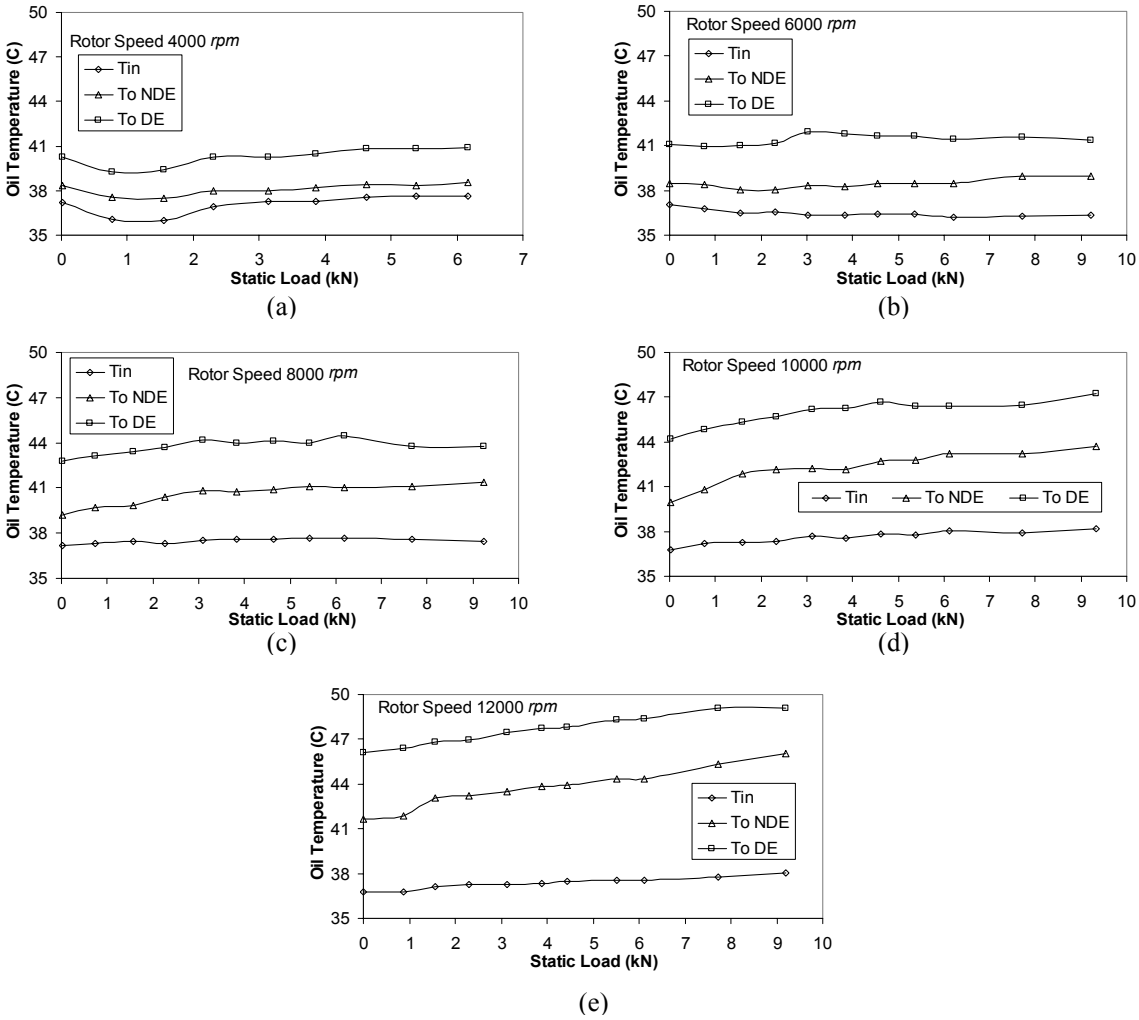

Figure 24. Inlet and outlet oil temperatures versus applied static loads for: (a) 4000 rpm, (b) 6000 rpm, (c) 8000 rpm, (d) 10000 rpm, and (e) 12000 rpm

Figure 25 shows the inlet and outlets oil temperatures versus rotor speed for different applied static loads. For any applied static load, the outlets oil temperatures are increasing with increasing rotor speed.

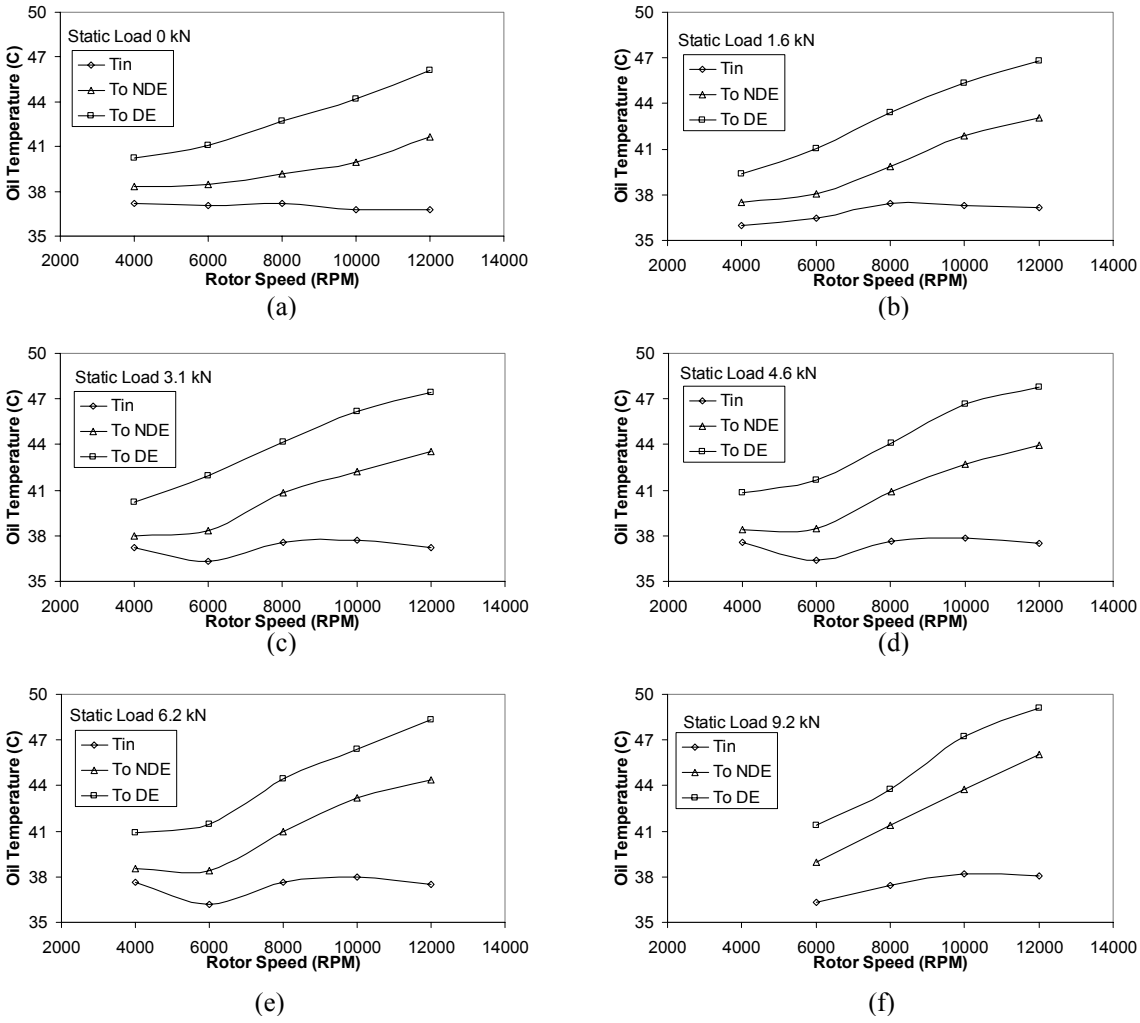

Figure 25. Inlet and outlet oil temperatures versus rotor speeds for different static loads: (a) 0 kN, (b) 1.6 kN, (c) 3.1 kN, (d) 4.6 kN, (e) 6.2 kN, and (f) 9.2 kN

After reaching the desired rotor speed, the bearing was centered, and then the static load increased, starting form 0 N in increments of about 750 N up to almost 9.25 kN. The static and dynamic tests for each condition were conducted at the same time. Since there were 10 dynamic tests for each operating condition, the temperatures were recorded at the last dynamic test after reaching a thermal equilibrium.

Figures 26, 27, 28, 29, and 30 show the 19 thermocouple temperatures that were embedded in the two sides of the bearing pads versus the applied static load for different rotor speeds. Each statically unloaded pad (#1 and #2) has two thermocouples placed on the DE side at 5% and 75% of pad arc length in the direction of rotation. Each statically loaded pad (#3 and #4) has five thermocouples placed on the DE side at 5%, 50%, 60%, 75% and 95% of pad arc length in the direction of rotation. In addition, pad #4 has also five thermocouples placed on the NDE side opposite to those in the DE side. As we can see from Figures 26, 27, 28, 29, and 30, the temperatures are in general increasing in the circumferential direction of each pad for any operating condition. Note that at the no load condition the 4 pads were initially preloaded.

The temperatures for statically loaded pads (#3, #4) increase with increasing static loads. On the other hand, the temperatures for statically unloaded pads (#1, #2) decrease at the trailing edge (75%) and increase at the leading edge (5%) with increasing applied load. Given that, by increasing the applied static load we are loading pads #3 and #4, and also unloading pads #1 and #2. The slight increase in temperature of pads #1 and #2 at the leading edge (5%) comes from the hot oil carry over from the trailing edge of the previous pad. The maximum temperature of pads #1, #2 and #3 were measured at 75% for all operating conditions. In contrast, the maximum temperature of pad #4 at high speeds (8000, 10000 and 12000 rpm) and at low speeds was measured at 95% and 75%, respectively, for almost all applied static loads. The difference between the location of the maximum temperature of pads #3 and #4 can be explained by good mixing at the trailing edge of pad 3, since the high fluid film pressure on pad #4 imposes a flow restriction. Therefore the fresh oil will reduce pad #3 temperature at the trailing edge (95%) through mixing with the hot oil. On the other hand, the fluid film pressure on pad #1 is much less than the pressure on pad #4; the fresh oil will have a small flow restriction. Therefore, the fresh oil will have a small effect on reducing pad #4 temperature at the trailing edge (95%). The gap between pad #3 and pad #4 works like a pocket that is always full of fresh oil. The measurement of pad #4 temperature at the leading edge (5%), which is around 40 C^o for all operating conditions support that claim. This can be easily seen in Figure 29 and Figure 30.

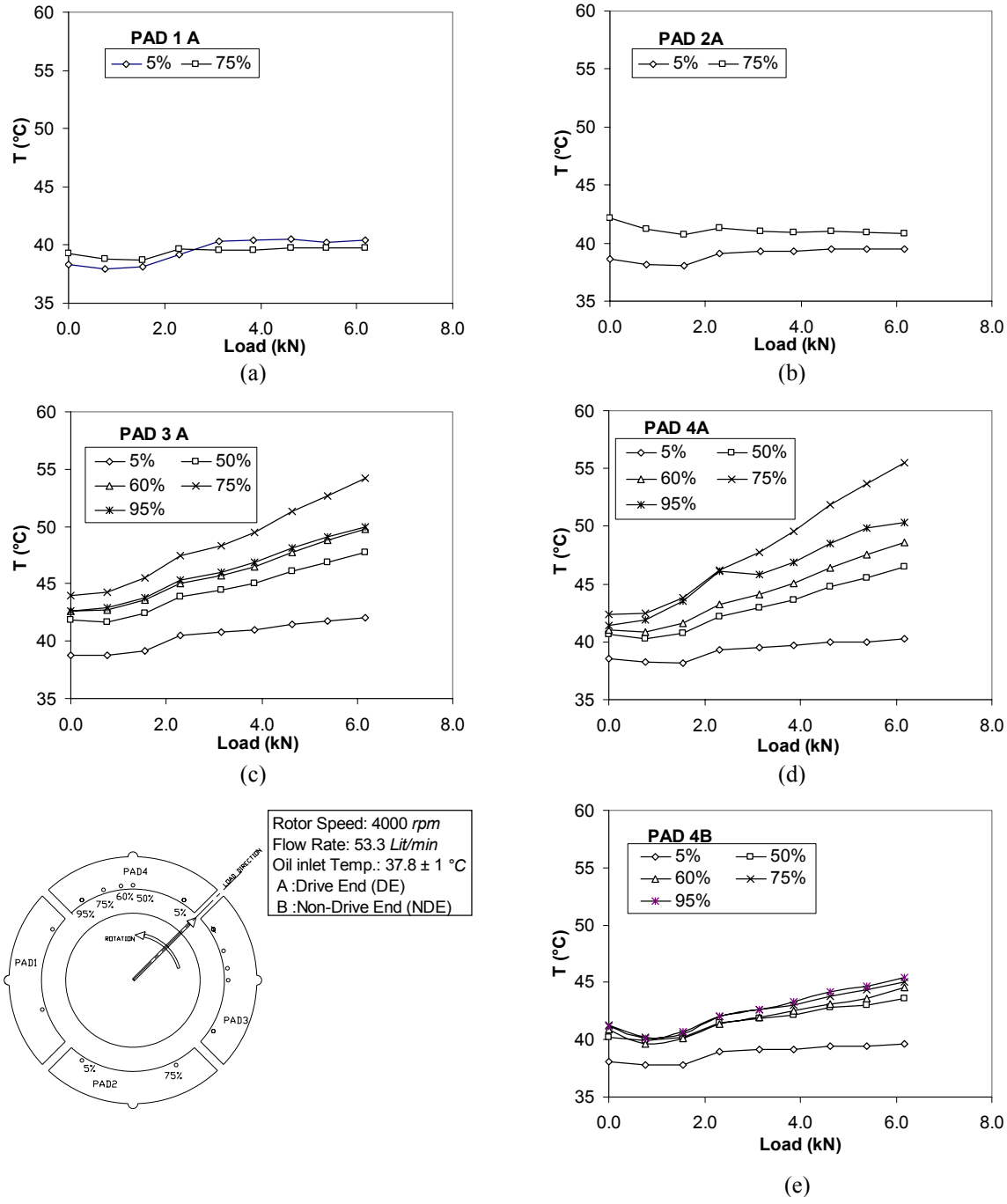

Figure 26. Pads temperatures versus applied static load at 4000 rpm for different thermocouple locations: (a) pad 1A, (b) pad 2A, (c) pad 3A, (d) pad 4A, and (e) pad 4B

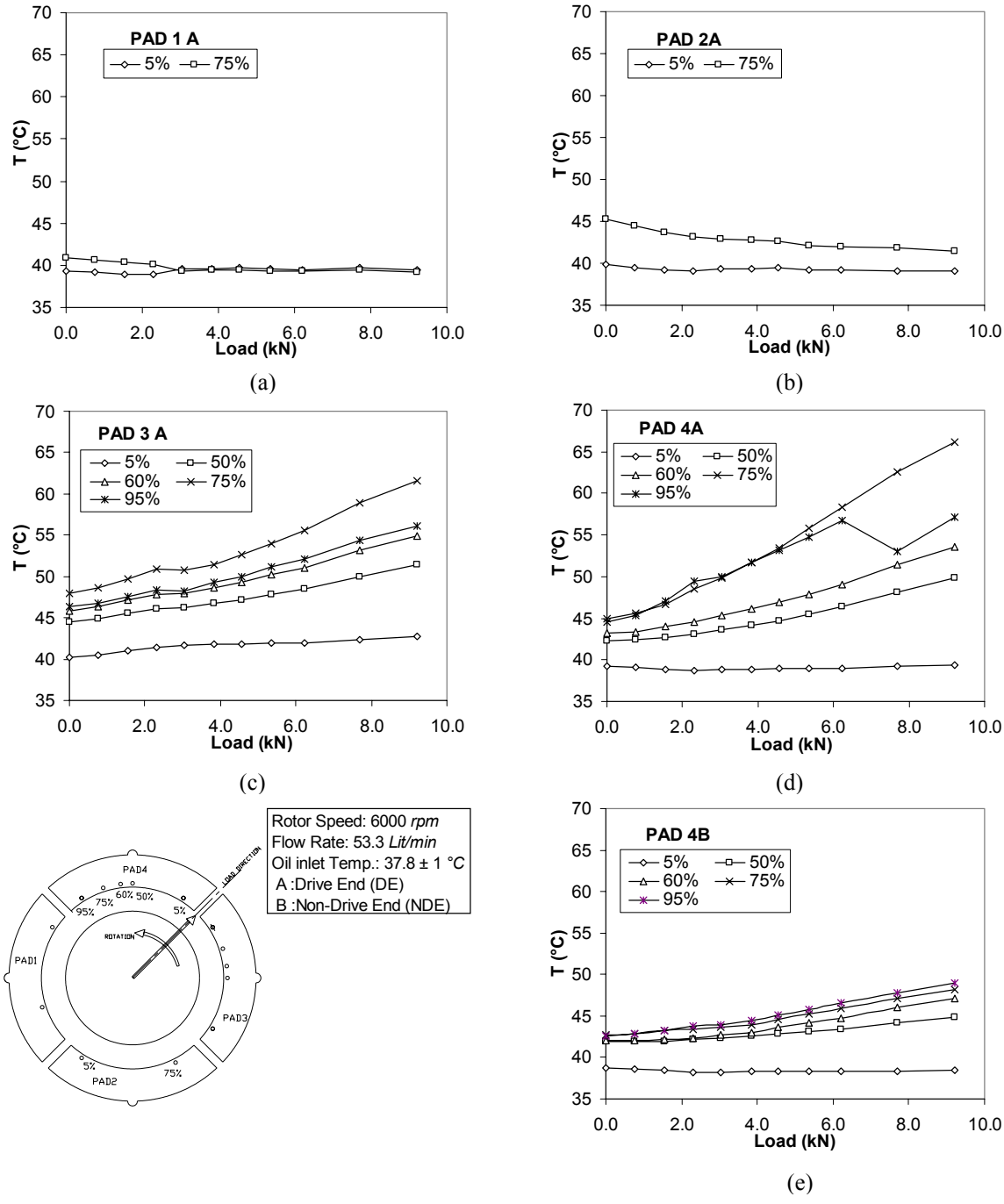

Figure 27. Pads temperatures versus applied static load at 6000 rpm for different thermocouple locations: (a) pad 1A, (b) pad 2A, (c) pad 3A, (d) pad 4A, and (e) pad 4B

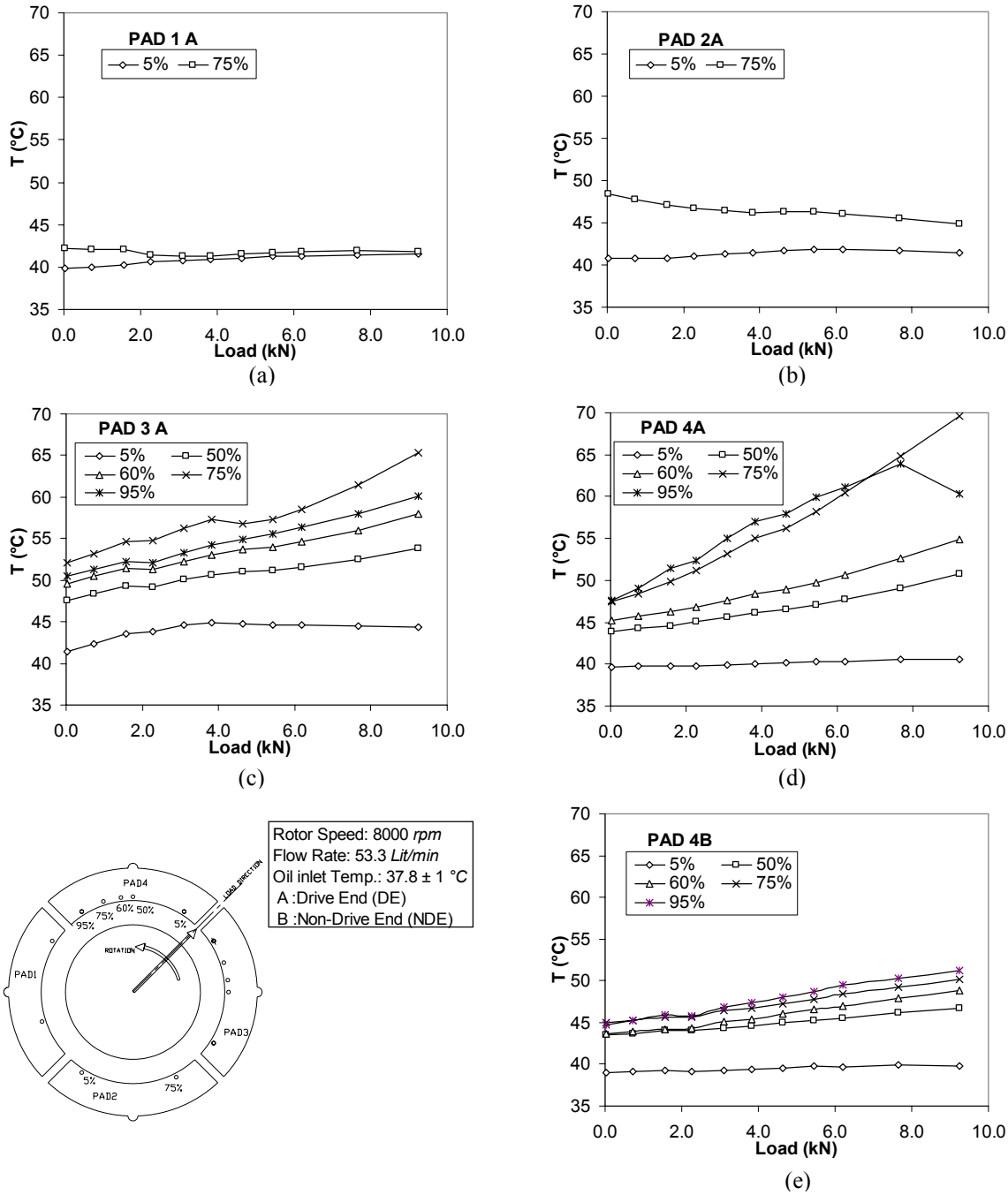

Figure 28. Pads temperatures versus applied static load at 8000 rpm for different thermocouple locations: (a) pad 1A, (b) pad 2A, (c) pad 3A, (d) pad 4A, and (e) pad 4B

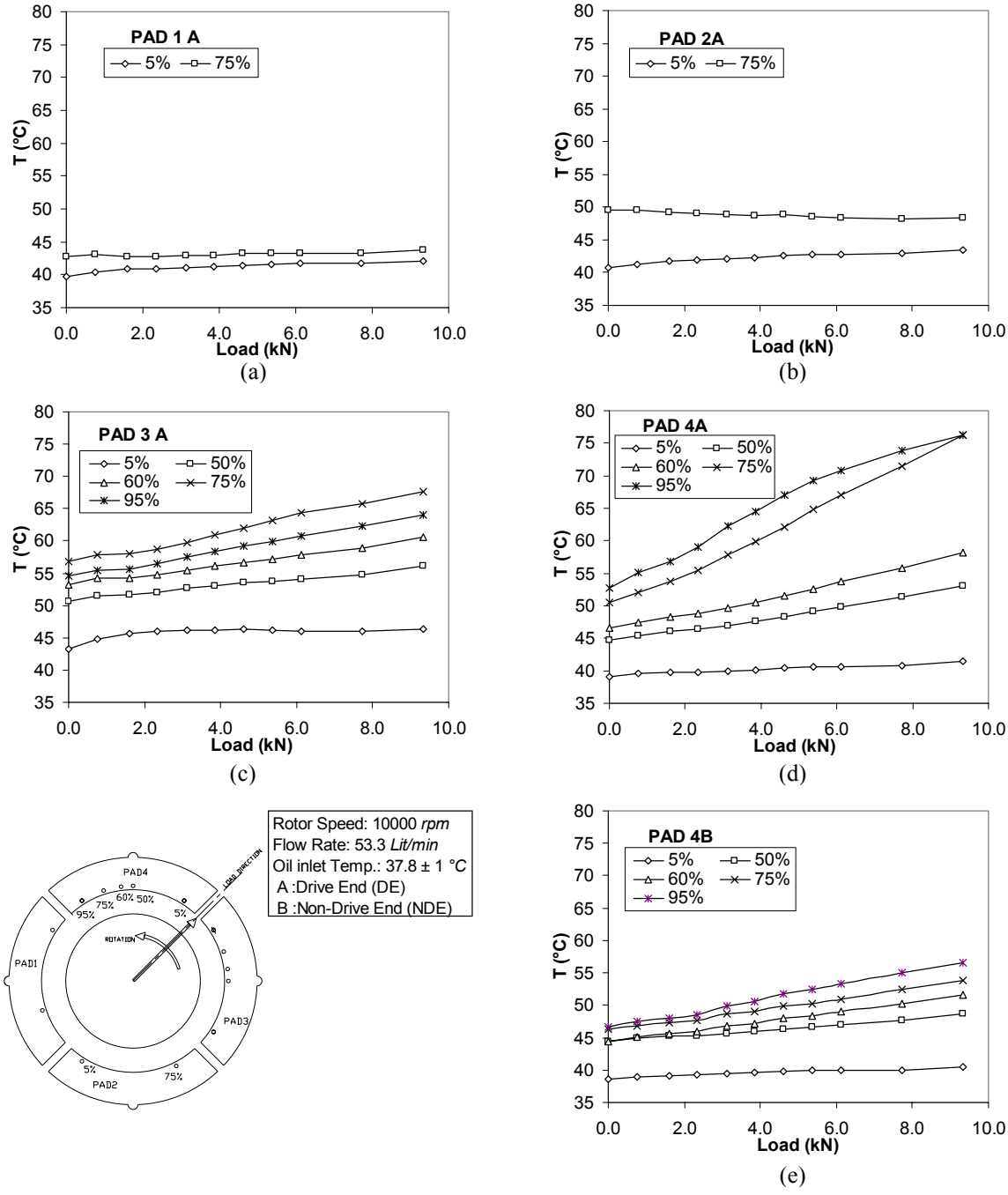

Figure 29. Pads temperatures versus applied static load at 10000 rpm for different thermocouple locations: (a) pad 1A, (b) pad 2A, (c) pad 3A, (d) pad 4A, and (e) pad 4B

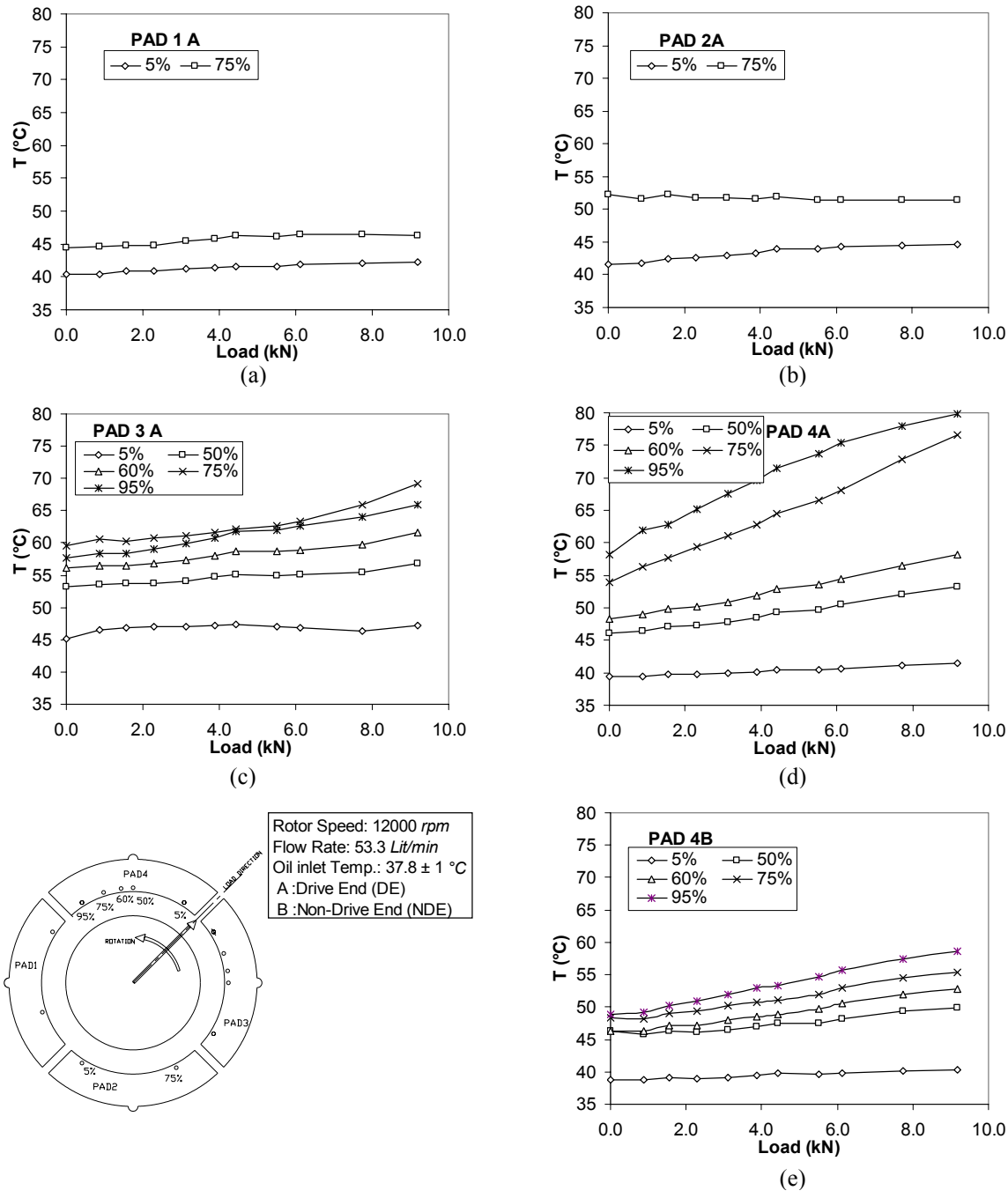

Figure 30. Pads temperatures versus applied static load at 12000 rpm for different thermocouple locations: (a) pad 1A, (b) pad 2A, (c) pad 3A, (d) pad 4A, and (e) pad 4B

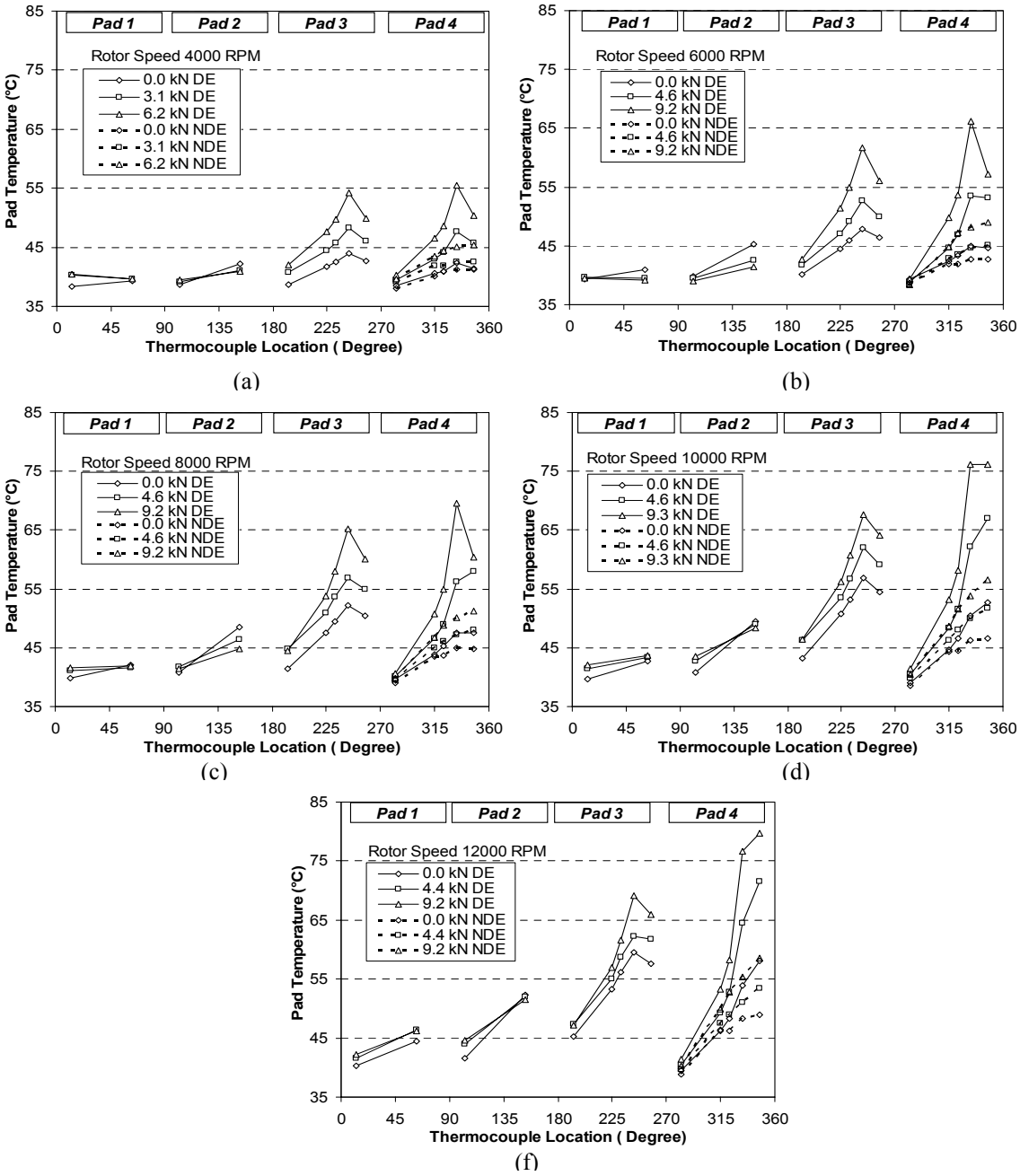

Figure 31. Pads circumferential temperature profiles for different applied static loads at: (a) 4000 rpm, (b) 6000 rpm, (c) 8000 rpm, (d) 10000 rpm, and (e) 12000 rpm

If we imagine cutting the bearing from the positive *x*-axis and unwrapping it, we will have the four pads next to each other starting from pad #1. This will facilitate seeing the maximum temperature, hot oil carry over and the trend of pads temperatures for different operating conditions discussed earlier. Figure 31(a, b, c, d and e) and Figure 32(a, b, c, d, e and

f) show the pads circumferential temperature profiles for different applied static loads and rotor speeds. The variation in pad temperatures due to the increase in rotor speed is higher (almost twice as high to around $15\,C^o$) than the variation due to the increase in the applied static load (around $8\,C^o$).

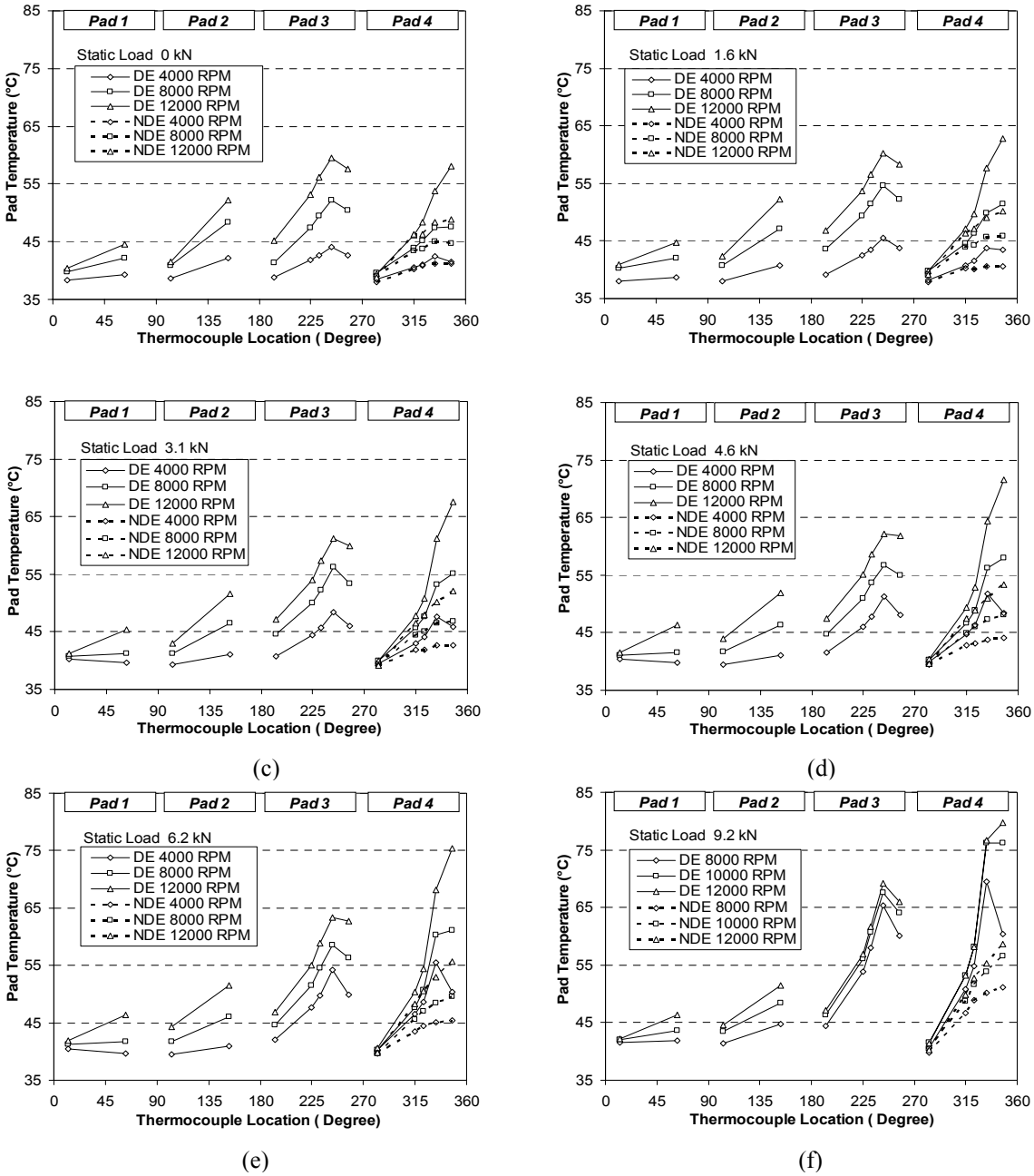

Figure 32. Pads circumferential temperature profiles for speeds for different rotor speeds at: (a) 0 kN, (b) 1.6 kN, (c) 3.1 kN, (d) 4.6 kN, (e) 6.2 kN, and (f) 9.2 kN

Dynamic Results

In this section, the experimental and theoretical rotordynamic coefficients and their uncertainties were identified using curve fitting for the experimental and theoretical dynamic stiffnesses, respectively. The base line dynamic stiffnesses will be discussed, and a comparison will be carried out between the experimental and theoretical dynamic stiffnesses. The experimental rotordynamic coefficients will be discussed and compared to predictions. Then, the stability characteristics will be studied through examining the whirl frequency ratio. Table 11-Table 15 in the Appendix contain the identified rotordynamic coefficients.

Identifying Rotordynamic Coefficients

To estimate the variability of dynamic data, 10 consecutive tests were conducted at each operating condition. The average of these 10 tests H_{ij} was used for calculating the rotordynamic-coefficients and their uncertainties. The uncertainty in H_{ij} is *two times the standard deviation* ($2S_{ij}^{y}$).

$$H_{ij} = \frac{\sum_{l=1}^{10} h_{ijl}}{10} \tag{21}$$

$$S_{ij}^{y} = \sqrt{\frac{\sum_{l=1}^{10} (h_{ijl} - H_{ij})^2}{9}} \quad , \tag{22}$$

where, h_{ij} is a vector representing the dynamic stiffness of one test, and S_{ij}^{y} is a vector representing the standard deviation for the 10 tests. The subscripts *i* and *j* represent *x* and *y*. Equation (21) can be written in a matrix form given by Eq. (23). Once again by solving Eq. (13), the rotordynamic coefficients can be extracted from the frequency response function *H*, by performing a straight line regression using the least-squares method for parameter estimation on each element of the real and the imaginary parts of Eq. (23).

$$\begin{bmatrix} H_{xx} & H_{xy} \\ H_{yx} & H_{yy} \end{bmatrix} = \begin{bmatrix} \mathrm{Re}(H_{xx}) & \mathrm{Re}(H_{xy}) \\ \mathrm{Re}(H_{yx}) & \mathrm{Re}(H_{yy}) \end{bmatrix} + \boldsymbol{j}. \begin{bmatrix} \mathrm{Im}(H_{xx}) & \mathrm{Im}(H_{xy}) \\ \mathrm{Im}(H_{yx}) & \mathrm{Im}(H_{yy}) \end{bmatrix} \tag{23}$$

The real and the imaginary parts take the forms of $K_{ij} - M_{ij}\Omega^2$ and $C_{ij}\Omega$, respectively.

Stiffness and Added Mass Coefficients

By performing a least-square fit on each element of the real and imaginary parts in Eq. (23), the predicted real and imaginary frequency response will be in the form:

$$\mathrm{Re}(\hat{H}_{ij}) = A_{ij} + B_{ij}\Omega^2 \tag{24}$$

$$\mathrm{Im}(\hat{H}_{ij}) = A_{ij} + B_{ij}\Omega \tag{25}$$

where A and B are the intercept and slope coefficients, respectively. Using the least-squares method, A and B are given by

$$B_{ij} = \frac{\sum_{l=1}^{n} \chi_l \,\mathrm{Re}(H_{ij})_l - n\bar{\chi}\,\mathrm{Re}(\bar{H}_{ij})}{\sum_{l=1}^{n} \chi_l^2 - n\bar{\chi}^2} \tag{26}$$

$$A_{ij} = \mathrm{Re}(\bar{H}_{ij}) - B_{ij}\bar{\chi}\,, \tag{27}$$

where $\mathrm{Re}(\bar{H}_{ij}) = \dfrac{\sum_{l=1}^{n}\mathrm{Re}(H_{ij})_l}{n}$, $\bar{\chi} = \dfrac{\sum_{l=1}^{n}\chi_l}{n}$, n is the number of data points, and $\chi = \Omega^2$ is the independent variable (square of excitation frequency). Comparing Eq. (24) with the real part of Eq. (12) yields the following equations.

$$K_{ij} = A_{ij} \quad \text{(Intercept)}$$

$$M_{ij} = -B_{ij} \quad \text{(Negative of the slope)} \tag{28}$$

Damping Coefficients

The least-square fitting used to obtain the stiffness and added mass term will be followed, using the imaginary part ($\mathrm{Im}(H_{ij})$) and replacing $\chi = \Omega^2$ with $\chi = \Omega$ in Eq. (26). Comparing Eq. (25) with the imaginary part of Eq. (12), yield the following.

$$C_{ij} = B_{ij} \quad \text{(Slope)} \tag{29}$$

Uncertainty Calculations

The uncertainty of the rotordynamic coefficients can be found utilizing what is called the confidence interval for that particular coefficient. For example, a 95% confidence interval for stiffness means that the probability of having the stiffness bounded by that interval is 95%. The confidence interval for the intercept and the slope coefficients are $A_{ij} \pm \Delta A_{ij}$ and $B_{ij} \pm \Delta B_{ij}$, respectively. ΔA_{ij} and ΔB_{ij} are given by

$$\Delta A_{ij} = t_{0.025}\, \hat{\sigma}_{ij} \sqrt{\frac{1}{n} + \frac{\overline{\chi}^2}{\sum_{l=1}^{n} \chi_l^2 - n\,\overline{\chi}^2}}, \tag{30}$$

$$\Delta B_{ij} = \frac{t_{0.025}\, \hat{\sigma}_{ij}}{\sqrt{\sum_{l=1}^{n} \chi_l^2 - n\,\overline{\chi}^2}}, \tag{31}$$

where, $\hat{\sigma}_{ij} = \sqrt{\frac{\sum_{l=1}^{n} (H_{ijl} - \hat{H}_{ijl})^2}{n-2}}$, (32)

and $t_{0.025} = 1.96$ is a value taken from the Normal Distribution table for 95% confidence interval. Eqs. (24, 30, 31, 32) are used to calculate the uncertainty in stiffness and added mass coefficients with $\chi = \Omega^2$ and $H_{ij} = \mathrm{Re}(H_{ij})$.For calculating the uncertainty in damping coefficients Eqs. (25, 31, 32) are used with $\chi = \Omega$ and $H_{ij} = \mathrm{Im}(H_{ij})$.

The predicted dynamic stiffnesses using the XLTFPBrg software were treated the same way as the experimental dynamic stiffnesses in obtaining the rotordynamic coefficients and their uncertainties. It is worth mentioning that the stiffness coefficients are equal to the real part of the dynamic stiffnesses at zero frequency. In addition, the damping coefficients are equal to zero at zero frequency. Therefore the stiffness can be predicted at very small frequency (zero frequency), and the damping can be predicted by fitting the imaginary part of the dynamic stiffness to a straight line passing through zero (this is the ideal case). However, the experimental dynamic stiffnesses were measured at frequencies starting from 20 Hz. To have an equivalent comparison between the experiment and the predicted coefficients, the same method discussed above was used for obtaining the rotordynamic coefficients. Figure 33 and Figure 34 show a

sample of the experimental and prediction dynamic stiffnesses and their fitted curves, respectively, at 12000 rpm and 1.4 kPa bearing unit loading.

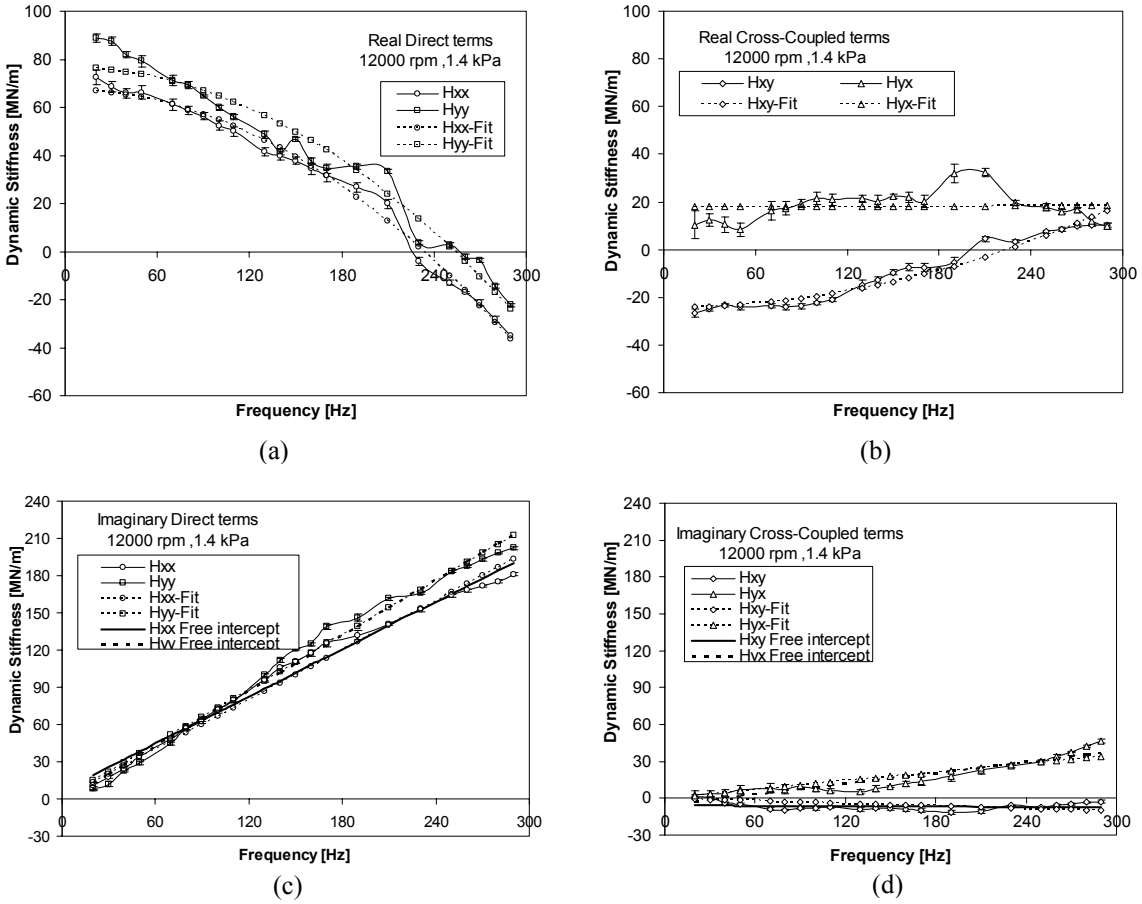

Figure 33. Experimental dynamic stiffnesses and their fit versus the excitation frequency at 12000 rpm and 1.4 kPa bearing unit loading

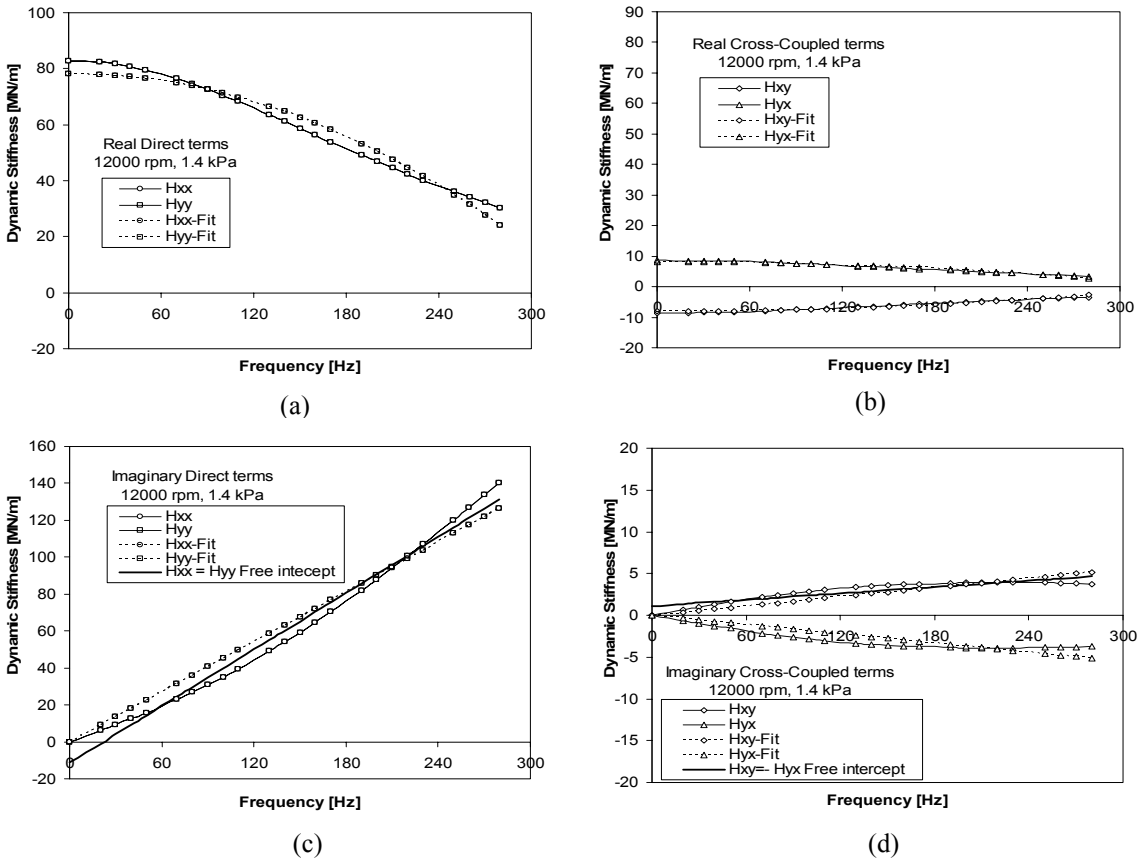

Figure 34. Predicted dynamic stiffnesses and their fit versus the excitation frequency at 12000 rpm and 1.4 kPa bearing unit loading

Baseline Dynamic Stiffness

The dynamic tests aims to measure rotordynamic coefficients of the flexure-pivot bearing (FPB). However, the measurement procedure will also measure stiffness and damping arising from the structure of the test rig that holds or feeds the existing FPB. This includes anything not coming from the bearing, like the hose connections, pitch stabilizers, etc. To account for these additional elements, 'base-line' tests were conducted with 'dry shakes' at zero rotor speed without oil in the bearing. The baseline dynamic stiffnesses have been subtracted from the average dynamic stiffnesses obtained for each test condition, and the rotordynamic coefficients are obtained from the corrected dynamic stiffness result.

Figures 35 and 36 show the real and imaginary parts of the baseline dynamic stiffness, respectively. Using the procedure for reducing the rotordynamic coefficients shown previously, the direct mass coefficients (M_{xx}, M_{yy}) were found to be almost equal, at 18.1± 1.1 kg (40 lbm).

From weighting, the actual mass of the stator is 19.1 kg (42.1 lbm). The direct stiffness coefficients (K_{xx}, K_{yy}) were found to be almost equal at 1.5± 1.8 MN/m. The large uncertainty in stiffness comes from the fact that this is a multi-degree of freedom system which has more than one natural frequency. Figures 35 (a) shows the first natural frequency around 65 Hz.

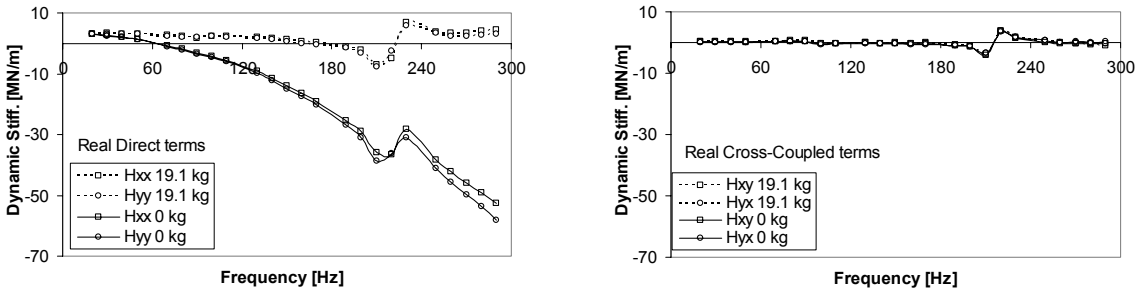

(a) (b)

Figure 35. Baseline real dynamic stiffness parts versus excitation frequency for different stator mass: (a) direct, and (b) cross-coupled

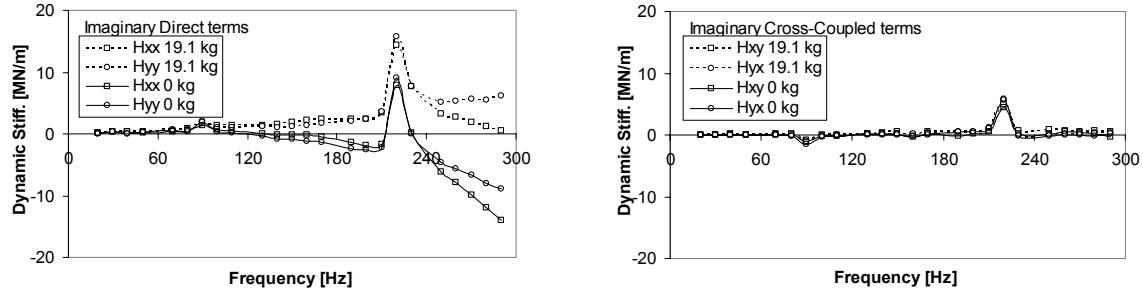

(a) (b)

Figure 36. Baseline imaginary dynamic stiffness parts versus excitation frequency for different stator mass: (a) direct, and (b) cross-coupled

The effects of the stator mass on the real direct dynamic stiffness parts (H_{xx}, H_{yy}) can be seen in figure 35(a). Accounting for the stator mass flattens the curvature to a constant value of 3.1 MN/m (using the average of the first 4 dynamic stiffnesses), and that mainly comes from the pitch stabilizers stiffness which is about 2.6 MN/m in the *x* and *y* directions. Figure 36 shows the imaginary part of the dynamic stiffnesses. Each of the direct and the cross-coupled imaginary dynamic stiffnesses can be fitted with the excitation frequency as the independent variable by a straight line. The slopes of these lines are the corresponding direct and cross-coupled damping. Direct damping coefficients are very small, in the order of (1.95 ± 0.45) kN.s/m. The cross coupled stiffness and damping coefficients are almost zero as expected with no shaft rotation.

Dynamic Stiffness Comparison

This section compares a sample of the experimental dynamic stiffnesses with the theoretical dynamic stiffnesses resulting from the bulk-flow model equations and the Reynolds equation at the lowest applied static load and the highest rotor speed combinations.

Figure 37 presents the experimental and theoretical dynamic stiffnesses at 4000 rpm and 1.4 kPa bearing unit loading and shows that the experimental and theoretical dynamic stiffnesses agree well at low frequencies. As the excitation frequency increases, the real direct dynamic stiffness shown in Figure 37(a) decrease quadraticaly. In addition, the difference between theoretical and experimental dynamic stiffnesses increases with excitation frequency.

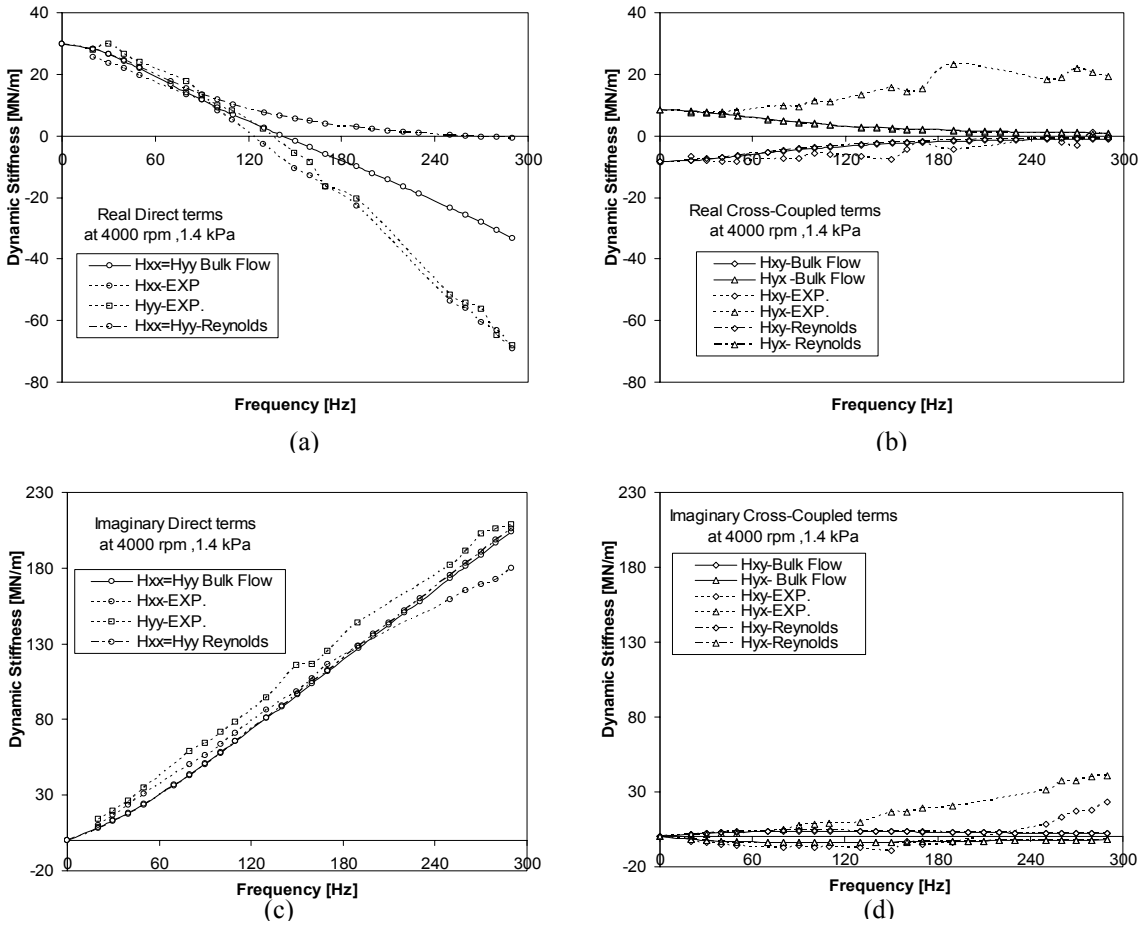

Figure 37. Experimental and theoretical dynamic stiffnesses versus the excitation frequency at 4000 rpm and 1.4 kPa bearing unit loading

The theoretical dynamic stiffness predicted using the Reynolds-equation model show the least frequency dependency compared with the bulk-flow and the experimental results. In

addition, if we look at the frequency dependency as an added mass term as in $K_{ij} - M_{ij}\,\Omega^2$, the added mass term using the Reynolds equation will be the smallest. Figure 37 (b) shows the experimental and the theoretical real cross-coupled dynamic stiffness terms. The experimental and theoretical real dynamic stiffnesses Re(H_{yx}) and Re(H_{xy}) increase and decrease, respectively, with increasing excitation frequency. The experimental and theoretical imaginary direct dynamic stiffness terms shown in Figure 37(c) increases linearly with increasing excitation frequency Ω. The experimental imaginary dynamic stiffnesses Im(H_{yx}) and Im(H_{xy}) increase with increasing Ω. The theoretical imaginary dynamic stiffnesses Im(H_{yx}) and Im(H_{xy}) terms increase then slightly decrease with increasing Ω.

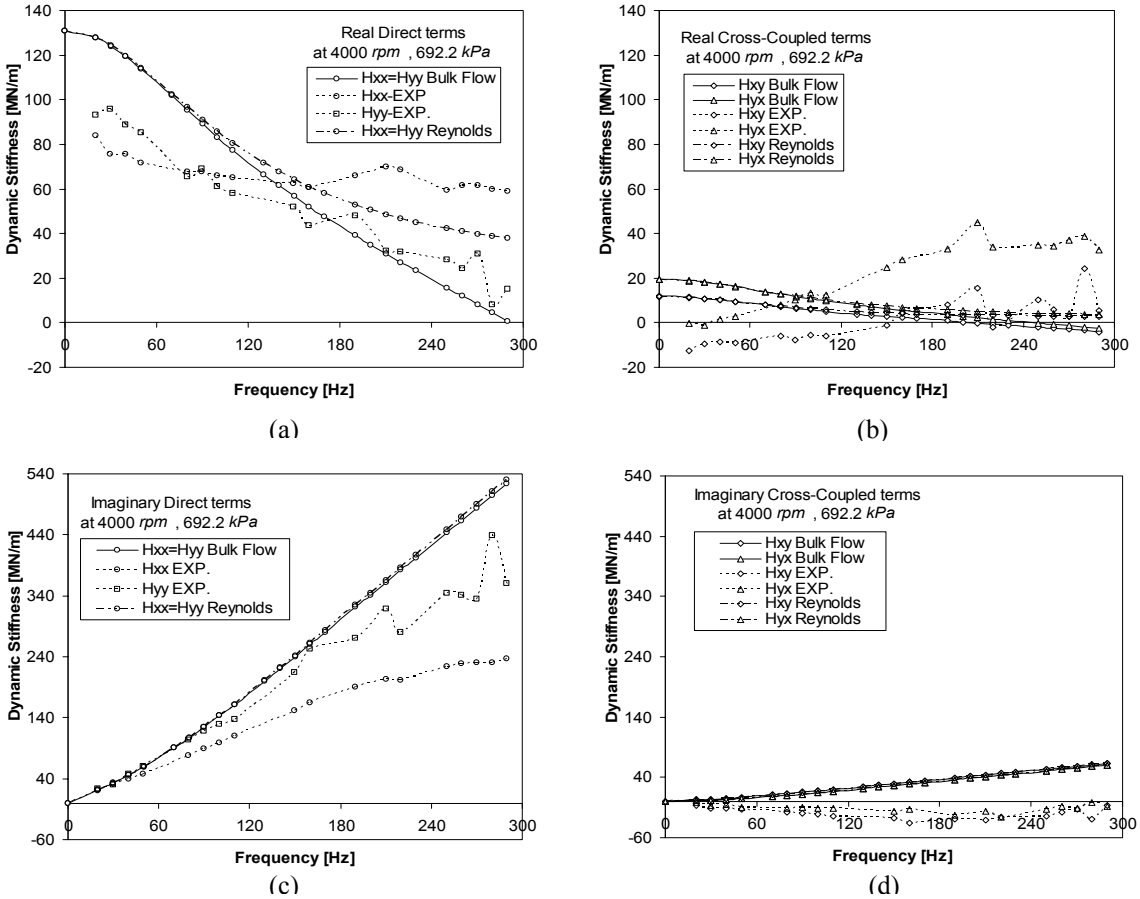

Figure 38. Experimental and theoretical dynamic stiffnesses versus the excitation frequency at 4000 rpm and 692.2 kPa bearing unit loading

As seen in Figure 37 (a and b), the Reynolds-equation model over predicts the real direct dynamic stiffness terms and under predicts the real cross-coupling dynamic stiffness terms.

Neglecting fluid inertia from the dynamic stiffness analysis has a very small effect on the imaginary dynamic stiffness parts; consequently, the stability is over predicted. Figure 38 shows the experimental and theoretical dynamic stiffnesses at 4000 rpm and 692.2 kPa bearing unit loading. The same trends in Figure 37 are seen except that, the experimental imaginary dynamic stiffnesses Im(H_{yx}) and Im(H_{xy}) decrease then slightly increase with increasing Ω. The theoretical imaginary dynamic stiffnesses Im(H_{yx}) and Im(H_{xy}) increase with increasing Ω. In addition, the theoretical real dynamic stiffnesses Re(H_{yx}) and Re(H_{xy}) terms have the same sign.

Figures 39 and 40 show additional dynamic stiffness samples at 12000 rpm with 1.4 kPa and 1038.2 kPa bearing unit loading, respectively. The general trends are the same as discussed in Figure 37 and 38.

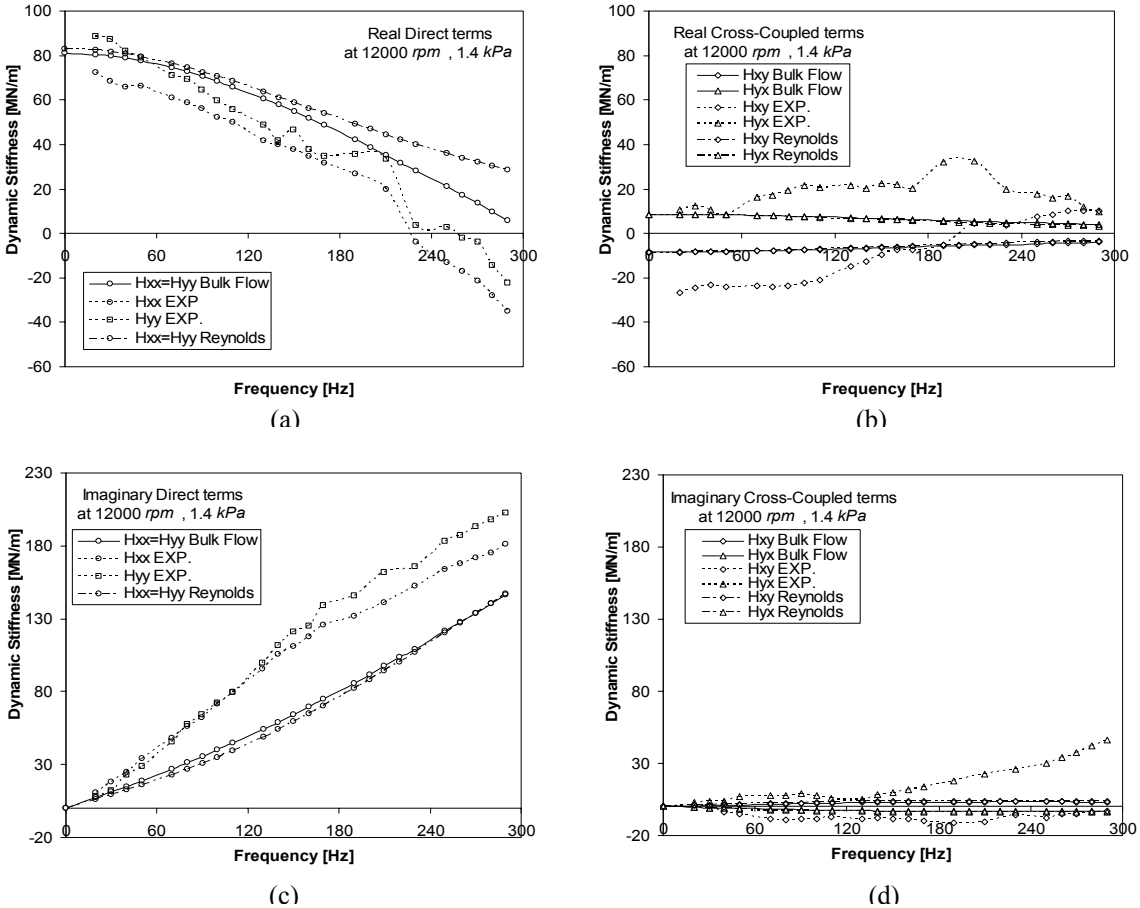

Figure 39. Experimental and theoretical dynamic stiffnesses versus the excitation frequency at 12000 rpm and 1.4 kPa bearing unit loading

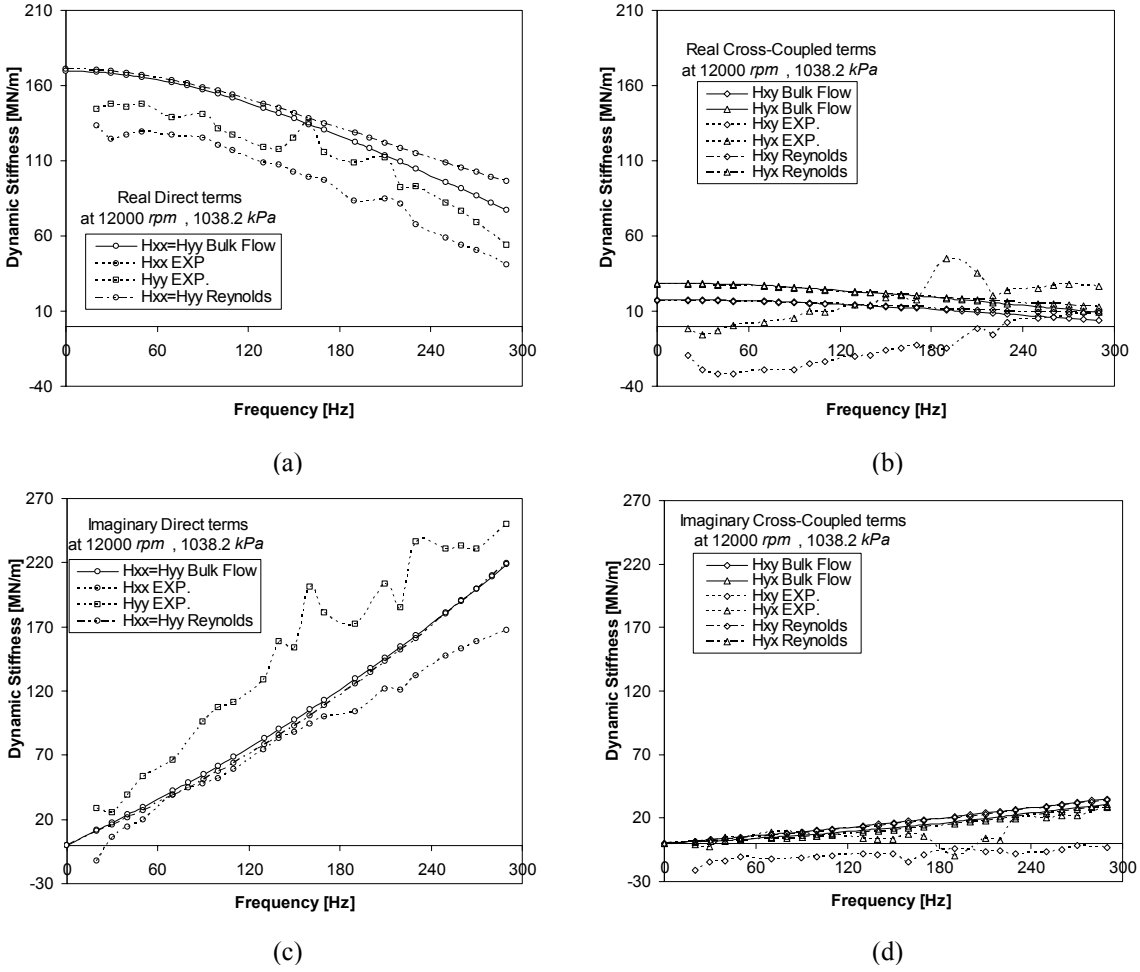

Figure 40. Experimental and theoretical dynamic stiffnesses versus the excitation frequency at 12000 rpm and 1038.2 kPa bearing unit loading

Results

Stiffness Coefficients

As stated earlier, rotordynamic coefficients are very important in designing any turbomachine. To understand this importance and to facilitate studying the results in hand, we need to understand each term in the model of the flexure-pivot bearing shown in Eq (1). The direct stiffness coefficients K_{xx} and K_{yy} support the weight of the rotating shaft and are a major factor in determining the critical speeds of the rotor. In general, stiff bearings are required, to support high loads and to elevate the critical speeds of the rotor. Cross-coupling stiffness coefficients K_{xy} and K_{yx} are present in all rotating machinery operating in fluid film "fixed geometry" bearings. The cross-couplings coefficients for tilting-pad bearings are zero (theoretically) when loaded on or between pads. Providing that the pad's inertia and pivot friction are neglected Zeidan [7].

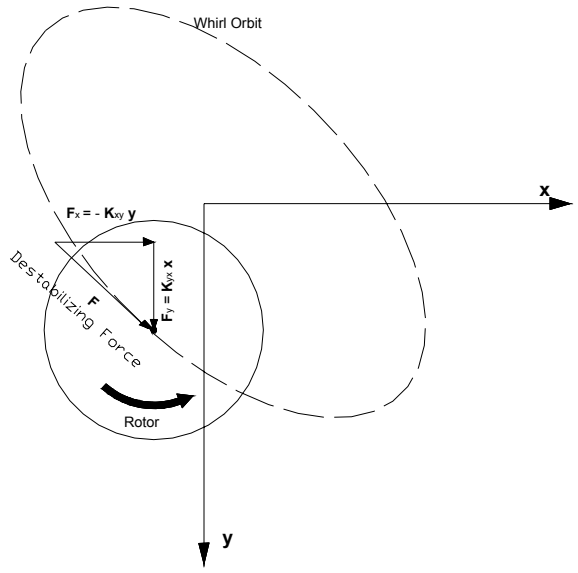

Figure 41. Schematic representation of the cross-coupled force after Zeidan [7]

Figure 41 shows the schematic representation of the cross-coupled force that is considered as the source of "forward whirl" instability in rotating machinery. The cross-coupled force destabilizes the dynamic system by adding energy to the system. This added energy is calculated by integrating the destabilizing force over the whirl orbit and is given by Zeidan [7],

$$Destablizing\ Energy = Area_{whirl\ orbit}(K_{yx} - K_{xy}) \tag{33}$$

Therefore, a positive K_{yx} and a negative K_{xy} will maximize the destabilizing energy. Alternatively, when K_{yx} and K_{xy} have the same sign, the destabilizing energy will be minimum. The direct damping coefficients C_{xx} and C_{yy} counteract the effects of K_{yx} and K_{xy} by dissipating energy and therefore stabilizing the dynamic system. The cross-coupled damping coefficients C_{xy} and C_{yx} and the direct added mass coefficients M_{xx} and M_{yy} arise mainly from fluid inertial effects. The Reynolds-equation analysis predicts zero added-mass terms, because the fluid acceleration terms are neglected in their derivation.

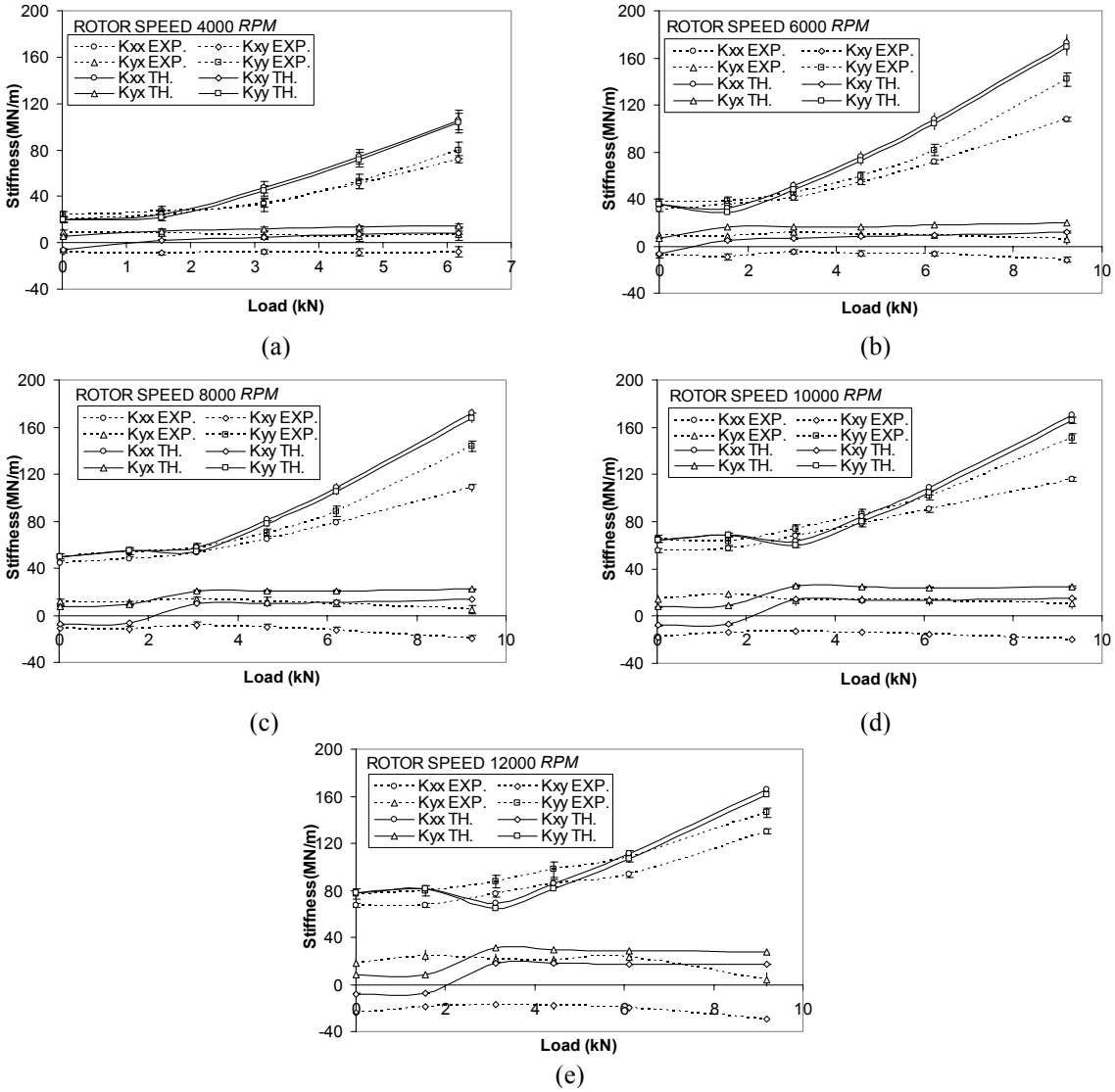

Figure 42. Stiffness coefficients in [MN/m] vs. static loads in [kN] for different rotor speeds: (a) 4000 rpm, (b) 6000 rpm, (c) 8000 rpm, (d) 10000 rpm, and (e) 12000 rpm

Figure 42 shows experimental and theoretical stiffness coefficients versus the applied static load for different rotor speed. The direct stiffness K_{yy} was found to be higher than K_{xx} for all running speeds and applied loads. The direct stiffness coefficients are almost constant (increase slightly) up to 3 kN load, then increase linearly with increasing load. The minimum direct stiffness coefficient was around 20 MN/m (at 4000 rpm speed and zero load). The maximum direct stiffness coefficient was around 150 MN/m (at 12000 rpm speed and 9.2 kN load). The maximum percent increase in direct stiffness with increasing load from 0 to 9.2 kN is about 200%. The cross-coupled stiffness coefficients K_{yx} and K_{xy} remain positive and negative, respectively, for all operating condition. Therefore, the difference between K_{yx} and K_{xy} are always positive and constant for all loads at a give running speed. Consequently, they are adding energy to the system (destabilizing). Even though the difference between K_{yx} and K_{xy} is constant for all loads, increasing the load will increase stability for the following reasons:

(a) The direct stiffness increases with load; therefore, the area of whirl orbit will decrease with increasing applied load.
(b) The direct damping also increases with increasing load as shown in Figure 46 later.

Figure 43 shows the experimental and theoretical stiffness coefficients versus rotor speed for different bearing unit loading. The direct stiffness increases linearly with increasing rotor speed at low bearing unit loading as seen in Figure 43(a). As seen in Figure 43(e), increasing the bearing unit loading causes the direct stiffness coefficients to become less sensitive to increases in rotor speed. When increasing the load further to the maximum loading (9.2 kN), Figure 43(e and f) shows that the direct stiffness coefficients increase with increasing rotor speed up to 10000 rpm and then decrease for speeds above 10000 rpm. The cross-coupling stiffness coefficients increase uniformly with increasing rotor speed, the maximum and minimum increase of cross-coupling stiffness coefficients are seen at the lowest load in Figure 43(a) and at the maximum load in Figure 43(f), respectively. The theory (bulk-flow model) captures the general trends of experimental stiffness coefficients while over predicting the direct stiffness K_{yy} by a maximum of 25% at the highest applied static load and under predicting the cross-coupling stiffness coefficient difference by almost 50%. The agreement between experiment and prediction improves with increasing rotor speed and decreasing applied static load.

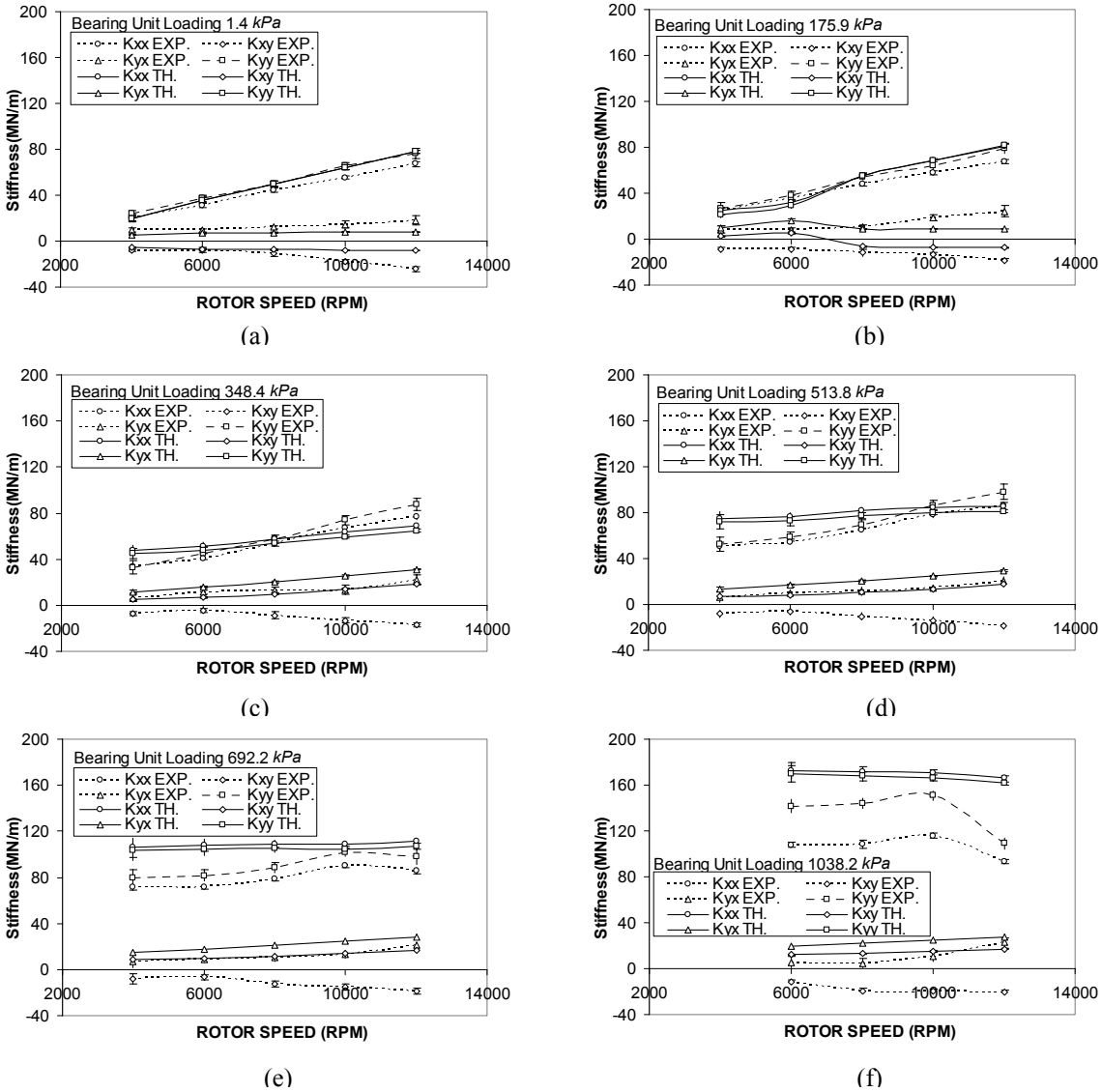

Figure 43. Stiffness coefficients versus rotor speeds for different bearing unit loading: (a) 1.4 kPa, (b) 175.9 kPa, (c) 348.4 kPa, (d) 513.8 kPa, (e) 692.2 kPa, and (f) 1038.2 kPa

Hydrodynamic bearings modeled by the Reynolds-equation can be characterized by one design curve utilizing the Sommerfeld number. Figure 44 presents the dimensionless stiffness coefficients ($k_{ij} = K_{ij} C_p / W$) versus Sommerfeld number. In general, the dimensionless stiffness coefficients increase with increasing Sommerfeld number, agreeing with Zeidan et al. [4] for the range of Sommerfeld number in hand. Figure 45 demonstrates the effect of eccentricity ratio on the dimensionless stiffness coefficients. The dimensionless stiffness coefficients decrease with increasing eccentricity ratio.

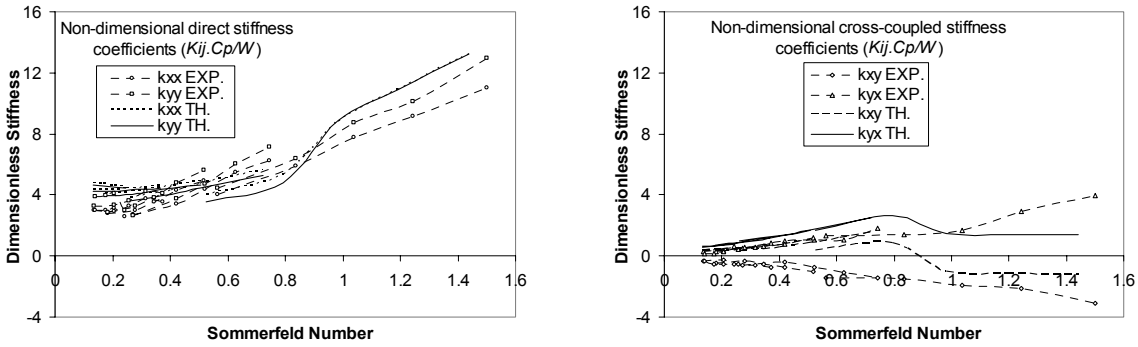

(a) (b)

Figure 44. Non-dimensional stiffness coefficients versus Sommerfeld number: (a) direct, and (b) cross-coupled

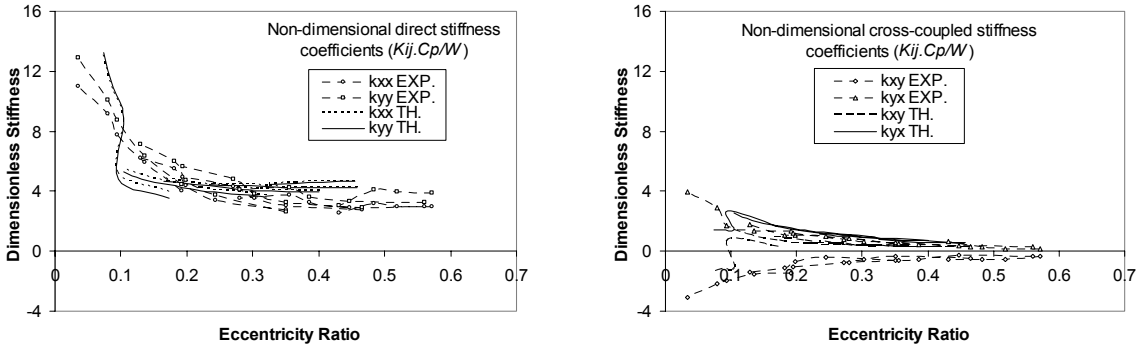

(a) (b)

Figure 45. Non-dimensional stiffness coefficients versus eccentricity ratio: (a) direct, and (b) cross-coupled

Damping Coefficients

The damping coefficients depend mainly on oil viscosity and bearing clearance. Changing the applied static load and/or the rotor running speed will affect these parameters, eventually, affecting the damping coefficients. Figure 46 shows the variation of damping coefficients with applied static load for different rotor speeds. As we can see from Figure 46(a, b, c, d and e) that the direct damping coefficient in the direction of load C_{yy} and the cross–coupled damping coefficient C_{yx} are always higher than C_{xx} and C_{xy} , respectively, for all operating conditions, because the clearance in the *y*-direction is smaller than in the *x*-direction (bearing crush discussed earlier). In addition, the cross-coupled damping coefficients are about 15% of the

direct damping coefficients. The direct damping coefficients C_{yy} and C_{xx} increase with increasing static load. Conversely, the cross-coupled damping coefficients C_{yx} and C_{xy} decrease with increasing applied static load. Figure 47 shows the damping coefficients versus rotor speed for different applied loads. Figure 47(a and b) clearly show that the direct damping coefficients decrease with increasing rotor speed up to 8000 rpm. Then, they start increasing again for higher speeds. In the other hand, the cross-coupling damping coefficients behave the opposite of direct damping; they increase then decrease with increasing rotor speed.

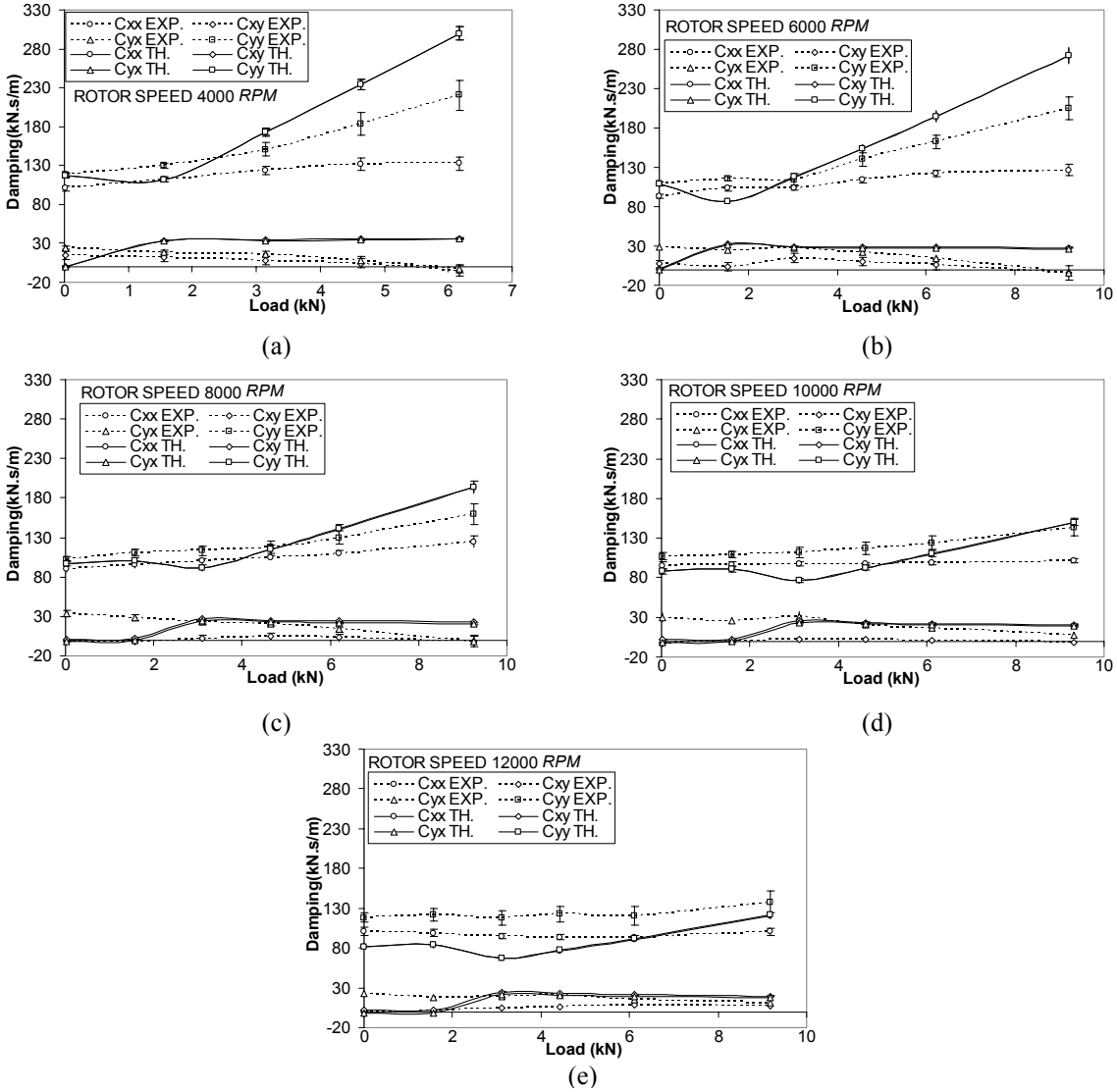

Figure 46. Damping coefficients in kN.s/m versus static loads in kN for different rotor speeds: (a) 4000 rpm, (b) 6000 rpm, (c) 8000 rpm, (d) 10000 rpm, and (e) 12000 rpm

Figure 47 (c, d, e and f) shows that the direct and cross-coupling damping coefficients are decreasing and increasing, respectively, with increasing rotor speed. The minimum and maximum drop in direct damping coefficients is about 10% and 50% as seen in Figure 47(a and f), respectively. The dimensionless damping coefficients ($c_{ij} = C_{ij} C_p \omega / W$) versus Sommerfeld number and eccentricity ratio are shown in figures 48 and 49, respectively. The dimensionless direct damping coefficients and the dimensionless cross-coupling damping c_{yx}, increases with increasing Sommerfeld number and decreases with increasing ε_0 the eccentricity ratio. The dimensionless cross-coupling damping coefficient c_{xy} is nearly constant.

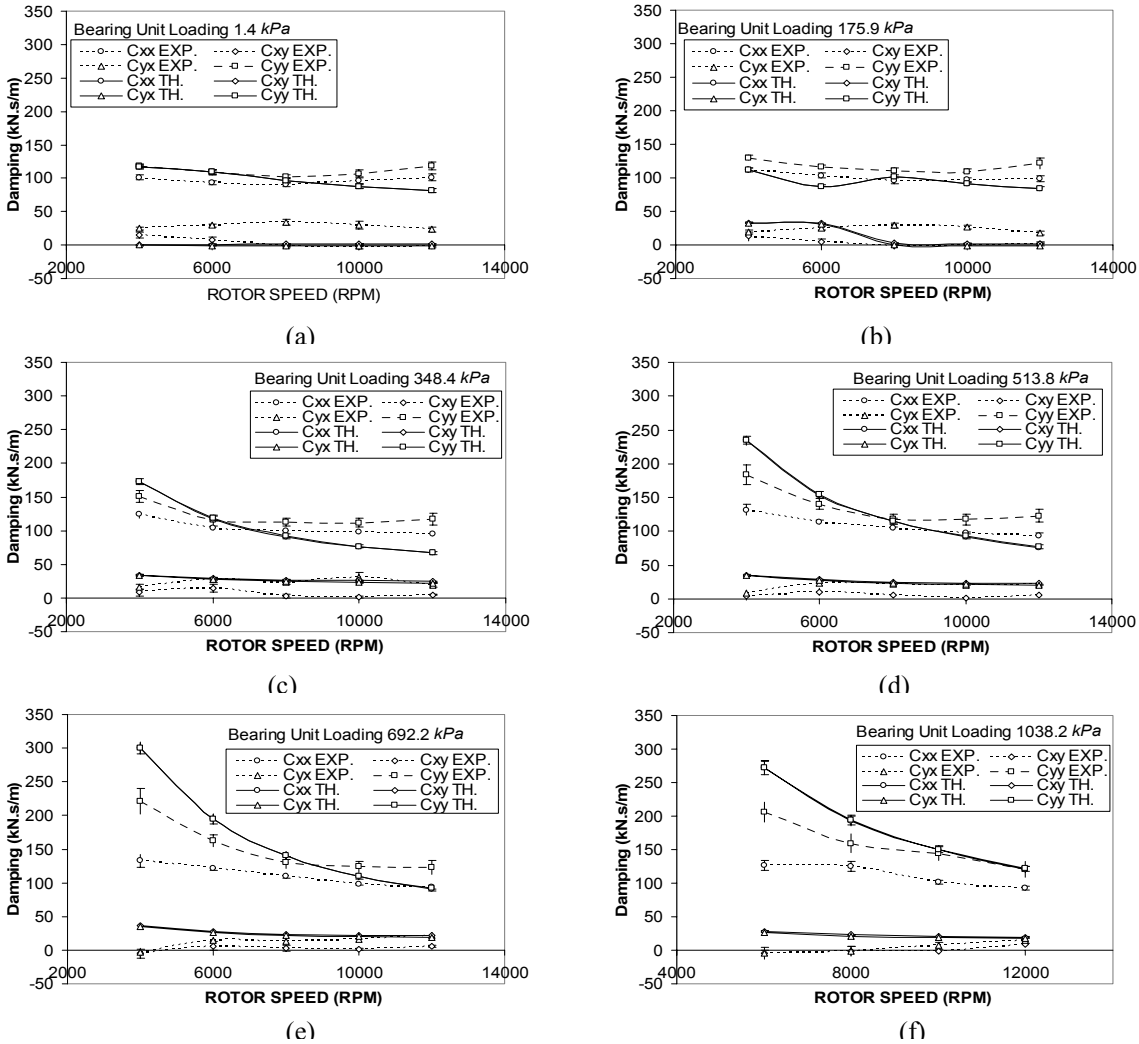

Figure 47. Damping coefficients versus rotor speeds for different bearing unit loading: (a) 1.4 kPa, (b) 175.9 kPa, (c) 348.4 kPa, (d) 513.8 kPa, (e) 692.2 kPa, and (f) 1038.2 kPa

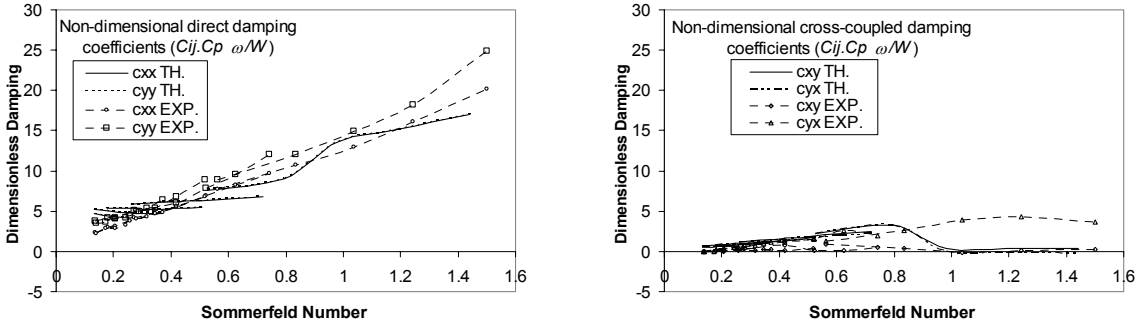

(a) (b)

Figure 48. Non-dimensional damping coefficients versus Sommerfeld number: (a) direct, and (b) cross-coupled

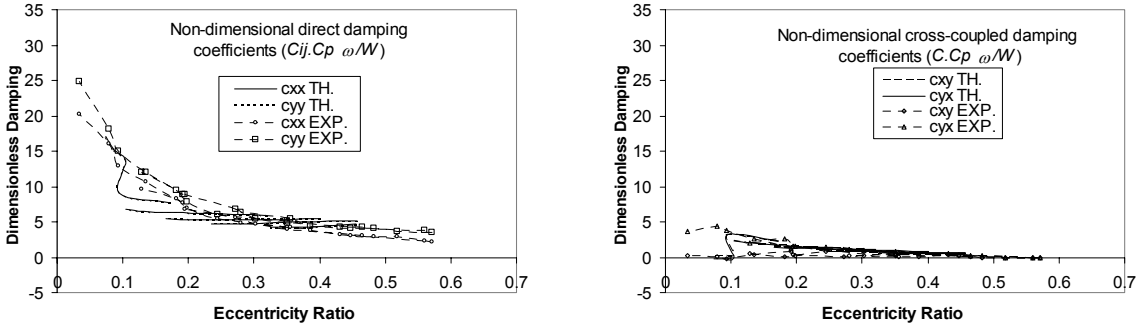

(a) (b)

Figure 49. Non-dimensional damping coefficients versus eccentricity ratio: (a) direct, and (b) cross-coupled

Added-Mass Coefficients

Figure 50 presents the added mass coefficients versus applied loads for different rotor speeds. The direct added mass M_{yy} is larger than M_{xx} for all cases. The difference between the direct added mass coefficients is very small for low applied static loads and/or for high rotor speeds. As seen in Figure 50(a, b and c) the direct added-mass coefficient M_{yy} is almost constant about (32 kg) for all applied static loads. The direct added mass coefficient M_{xx} decreases with increasing applied load, particularly at low rotor speeds. The cross-coupled added mass coefficients are negative in most cases and about 15% of the direct mass coefficients at low loads. For high loads they increase to 30% of the direct added mass coefficients. These negative values of cross-coupled added mass come from the approach used to fit the dynamic stiffnesses to a specific model K_{ij} - M_{ij} Ω^2. In fact the real cross-coupled dynamic stiffnesses show a

frequency dependency that does not follow this model. But, the cross-coupled terms were very small compared to the direct coefficients, and to maintain a consistency in presenting the data we kept these coefficients unmodified, even if the coefficient of determination (R^2) is very small for that line fit.

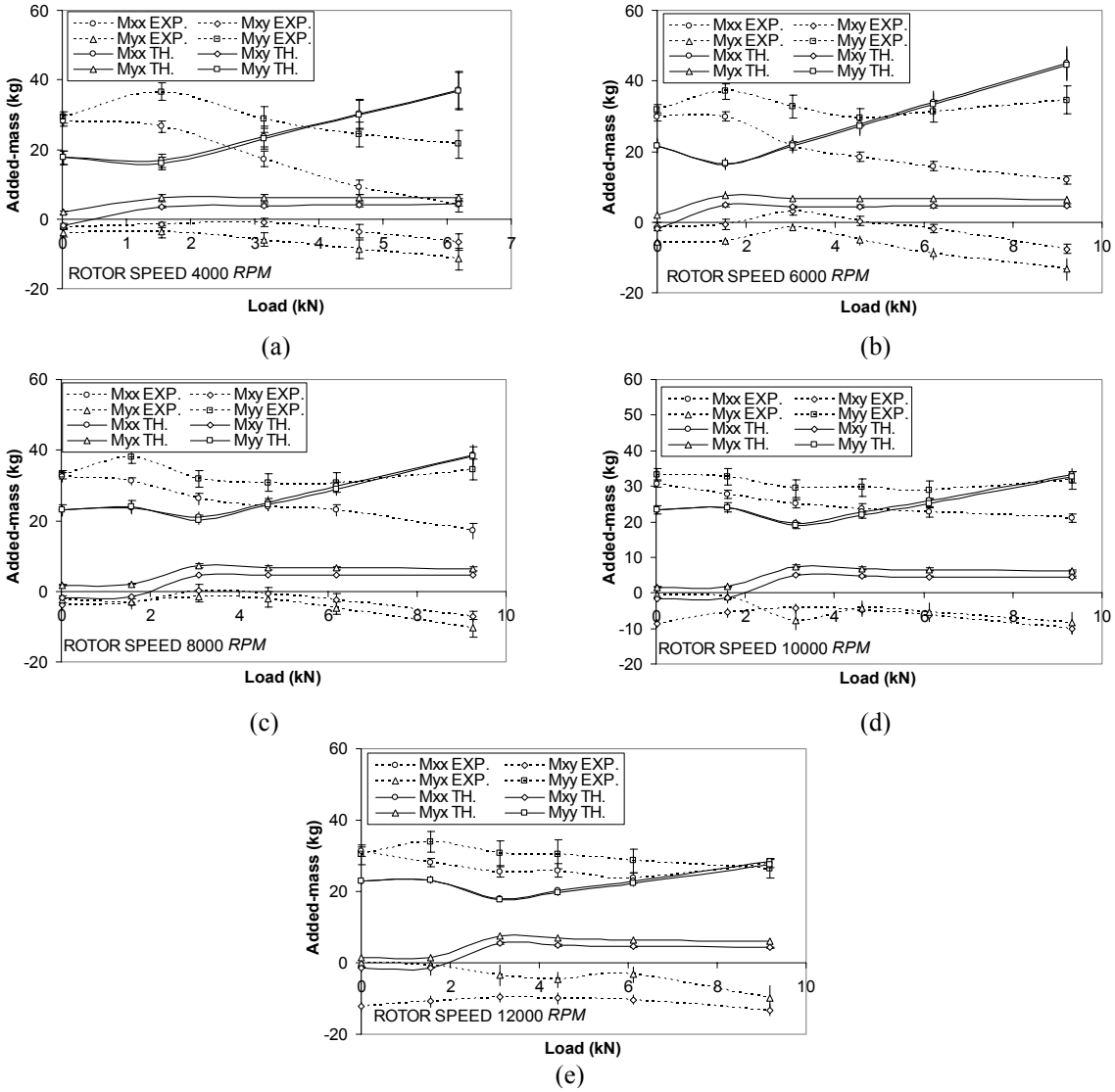

Figure 50. Added-mass coefficients in [kg] versus static loads in [kN] for different rotor speeds: (a) 4000 rpm, (b) 6000 rpm, (c) 8000 rpm, (d) 10000 rpm, and (e) 12000 rpm

Figure 51 demonstrates the effect of rotor speed on the added-mass coefficients for different bearing unit loading. M_{yy} slightly increases (is nearly constant), and M_{xx} increases with

increasing rotor speeds for all bearing unit loading. As seen in Figure 51(a) M_{xx} approaches M_{yy} at high speeds and/or at low bearing unit loading. The cross-coupled added mass coefficients M_{yx} and M_{xy} increase and decrease, respectively, with increasing rotor speed.

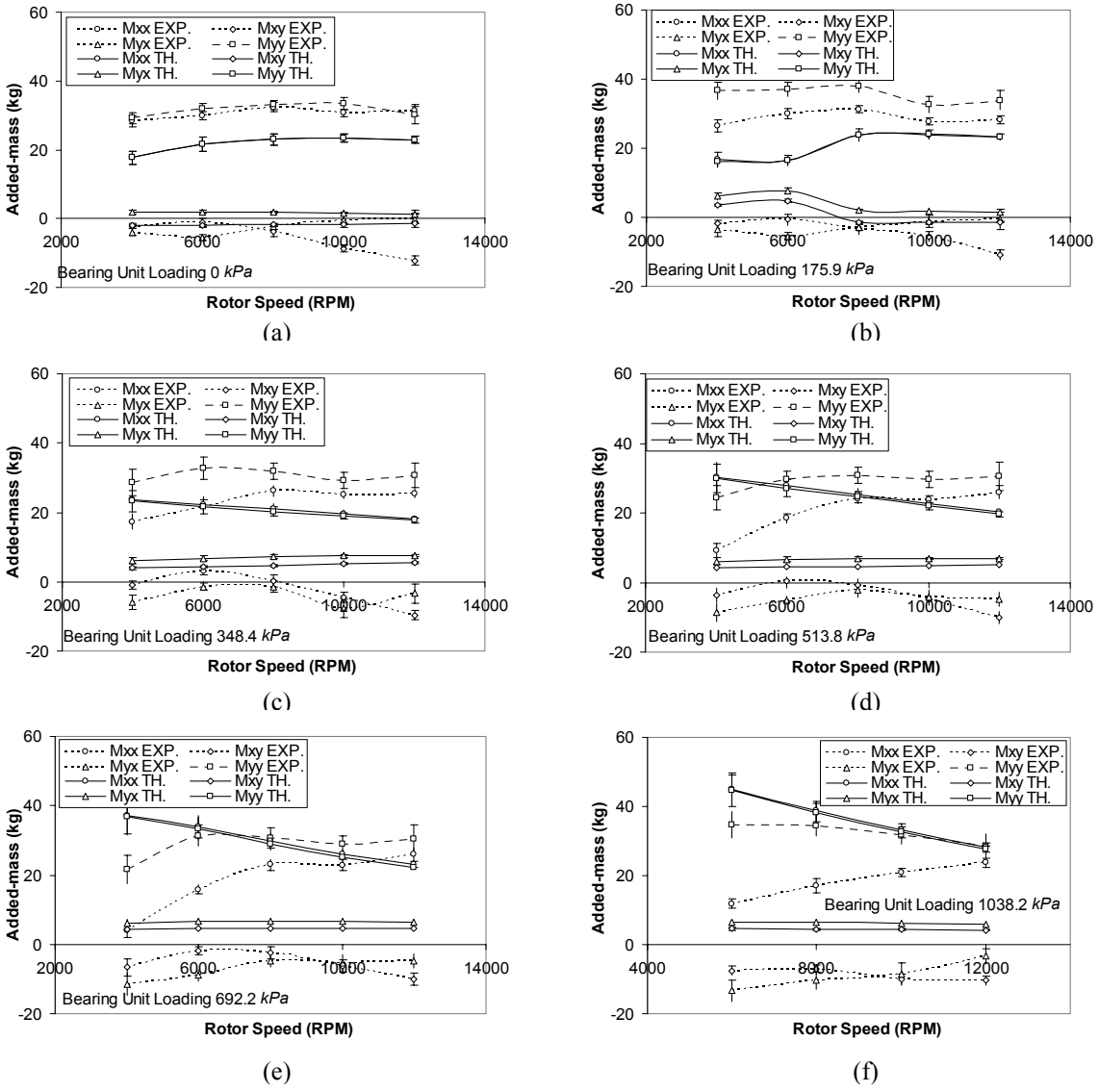

Figure 51. Added-mass coefficients versus rotor speeds for different bearing unit loading: (a) 1.4 kPa, (b) 175.9 kPa, (c) 348.4 kPa, (d) 513.8 kPa, (e) 692.2 kPa, and (f) 1038.2 kPa

The dimensionless added-mass coefficients ($m_{ij} = M_{ij} C_p \omega^2 / W$) versus Sommerfeld number and eccentricity ratio are presented in Figure 52 and Figure 53, respectively. The

coefficients m_{xx} and m_{yy} increase with increasing Sommerfeld number and decrease with increasing eccentricity ratio. On the other hand, m_{yx} is nearly constant, while m_{xy} decreases with increasing Sommerfeld number and increases with increasing ε_0 .

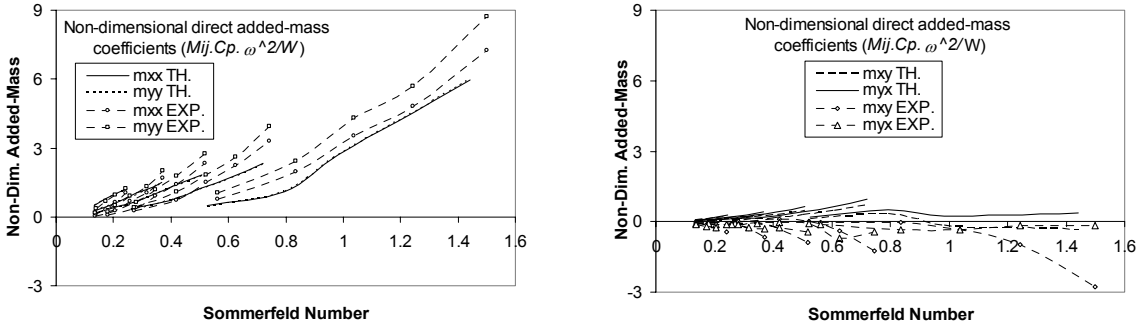

(a) (b)

Figure 52. Non-dimensional added-mass coefficients versus Sommerfeld number: (a) direct, and (b) cross-coupled

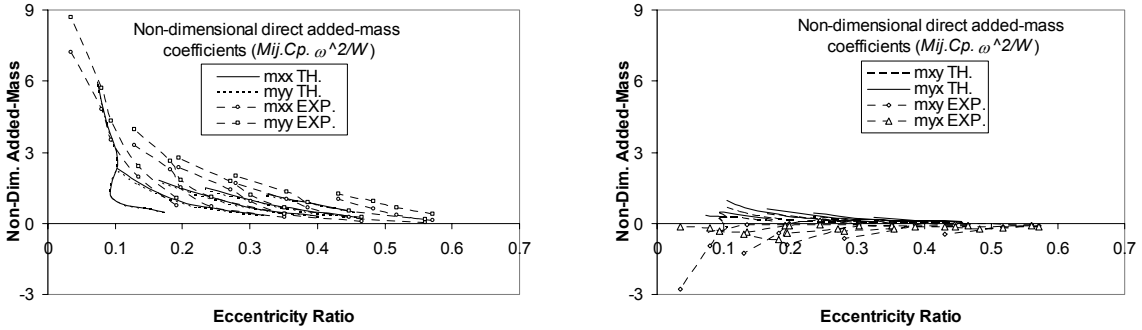

(a) (b)

Figure 53. Non-dimensional added-mass coefficients versus eccentricity ratio: (a) direct, and (b) cross-coupled

The theory under predicts the direct add mass coefficients at low bearing unit loading and over predicts it at high bearing unit loading for almost all cases. Good agreement is shown between the theory and the experimental direct added mass terms at high rotor speeds in figures 50(e) and 51(f). The maximum difference between theory and experiment for the direct added mass was about 75%. Regarding the cross-coupled added mass coefficients, the theory predicts the same order of magnitude as the experimental results but with an opposite sign.

Whirl Frequency Ratio (WFR)

WFR is defined as the ratio between the precession frequency of the rotor and the onset speed of instability (ω_s). The stability analysis of a rigid rotor supported by a flexure-pivot bearing is similar to the analysis carried for a rigid rotor supported by a plain journal bearing. Lund [17] discusses how to calculate the WFR for a rigid shaft supported by two identical plain journal bearings ignoring the fluid inertia and the result is given by

$$WFR^2 = \left(\frac{\Omega}{\omega_s}\right)^2 = \frac{(K_{eq} - k_{xx})(K_{eq} - k_{yy}) - k_{xy}k_{yx}}{c_{xx}c_{yy} - c_{xy}c_{yx}} \tag{34}$$

where,

$K_{eq} = \dfrac{c_{xx}k_{yy} + c_{yy}k_{xx} - c_{yx}k_{xy} - c_{xy}k_{yx}}{c_{xx} + c_{yy}}$, $k_{ij}\Big|_{i,j=x,y} = \dfrac{C_p}{W}K_{ij}$ is the dimensionless stiffness and $c_{ij}\Big|_{i,j=x,y} = \dfrac{C_p\omega}{W}C_{ij}$ is the dimensionless damping. To account for the effects of fluid inertia on the WFR a similar analysis following San Andres [31] is carried out. After lengthy equations manipulations, we have the following 4th order WFR equation, given by

$$a + b(WFR)^2 + c(WFR)^4 = 0 \tag{35}$$

Where,

$$a = k_{xx}k_{yy} - k_{xy}k_{yx} + K_{eq}^2 - (k_{xx} + k_{yy})K_{eq}$$

$$b = (k_{xx} + k_{yy})K_{eqm} + (m_{xx} + m_{yy})K_{eq} - 2K_{eq}K_{eqm} - Term$$

$$Term = k_{xx}m_{yy} + k_{yy}m_{xx} + c_{xx}c_{yy} - k_{xy}m_{yx} - k_{yx}m_{xy} - c_{xy}c_{yx}$$

$$c = K_{eqm}^2 + (m_{xx}m_{yy} - m_{xy}m_{yx}) - (m_{xx} + m_{yy})K_{eqm}$$

$$m_{ij}\Big|_{i,j=x,y} = \frac{C_p\omega^2}{W}M_{ij}$$

$$K_{eqm} = \frac{c_{yy}m_{xx} + c_{xx}m_{yy} - c_{xy}m_{yx} - c_{yx}m_{xy}}{c_{yy} + c_{xx}}$$

After obtaining the coefficients *a*, *b* and *c*, Equation (35) can be solved for the WFR using any software available. For example using *Matlab* with command, *roots ([c 0 b 0 a])*, will solve for the 4 roots of that equation. The WFR is a real positive number or pure imaginary number (indication of permanent stability), and in that case the WFR will equal to zero.

For plain journal bearings the WFR is equal to 0.5. This result means that the maximum attainable stable rotational speed will be twice the natural frequency of the rotor. From this perspective comes the importance of tilting-bad bearing, in which the cross-coupling stiffnesses are zero ($K_{xy} = K_{yx} = 0$). If the bearing are exactly similar in both directions then ($K_{xx} = K_{yy}$), therefore from Eq. (34) the $WFR = 0$ which means total stability. As mentioned earlier, the characteristics of the flexure-pivot bearing (FPB) lie between fixed-geometry bearings (such as plain journal bearings) and tilting-pad bearings, depending on the rotational stiffness of the pad. If the pad rotational stiffness is high then the FPB will act as a plain journal bearing. If the rotational stiffness is very small, the FPB will act like a tilting-pad bearing. Zeidan et al. [3] discuss in detail the effects of the flexure-pivot rotational stiffness on stability. The FPB should have a WFR between 0 and 0.5. Figure 54 , 55 and 56) show the WFR for the FPB and is about 0.15. To appreciate this results consider a rotor is supported by a plain journal bearings with an onset speed of instability at 9000 rpm. Replacing the plain journal bearing with this FPB will elevate the onset speed of instability to about 30000 rpm.

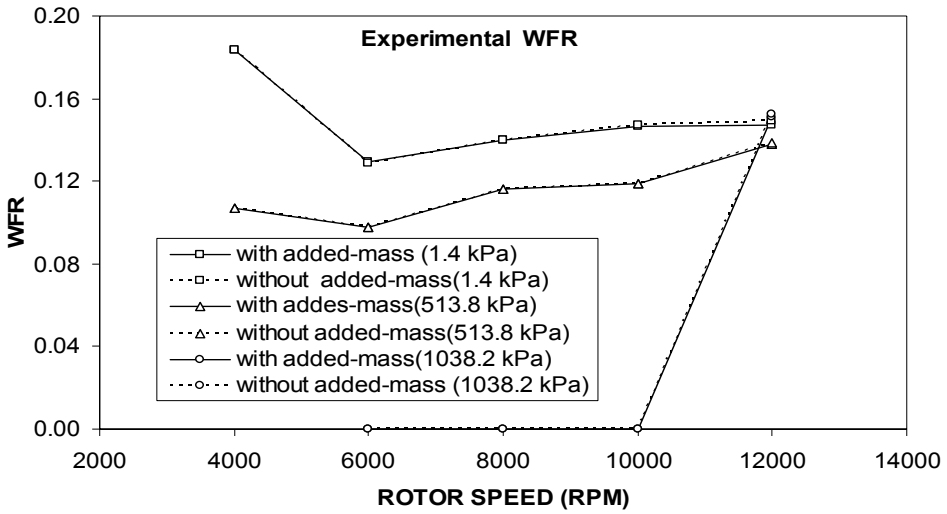

Figure 54. Experimental WFR versus rotor speed for different bearing unit loading, with and without fluid inertial effects

Figure 54 shows the effect of including the measured fluid inertia coefficients on the WFR. The fluid inertia has no effect on the WFR at low running speed and high applied static loads. The effects of inertia appear at low applied static loads and high speeds. Although the

increase in the WFR is very small (about 1% at 12000 rpm and 1.4 kPa) the effect of inertia may produce a dramatic increase in WFR at low loads and high speed.

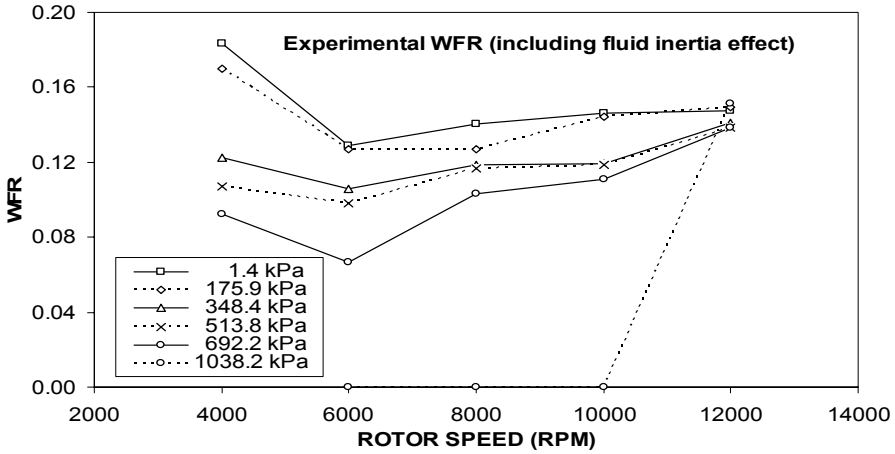

Figure 55. Experimental WFR versus rotor speed for different bearing unit loading, with fluid inertial effects

Figure 55 show the effects of applied loads and rotor speeds on the WFR. Increasing the load will decrease the WFR by almost 50% at 4000 rpm. On the other hand, an optimum value of the WFR is seen at 6000 rpm; increasing the rotor speed above 6000 rpm will increase the WFR to 0.15. Figure 56 shows the experimental and theoretical WFRs at low loads for different rotor speeds. The theory predicts a zero WFR for loads above 175.9 kPa. In addition, the theory fails to predict the general trend of WFR with increasing rotor speed.

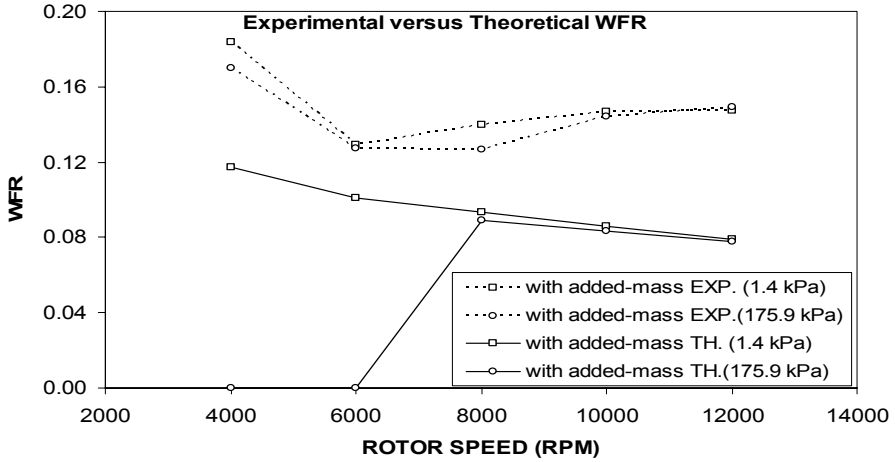

Figure 56. Experimental and theoretical WFR versus rotor speed at 1.4 kPa and 175.9 kPa bearing units loading

SUMMARY AND CONCLUSION

The importance of the experimental performed results comes from validating the analytical analysis through comparison and providing a tool for predicting a correct model. This outcome will increase the confidence in using these analyses for future design of tilting-pad bearings.

The discussion of the results in previous sections answers the question stated earlier which is: *Are the rotordynamic coefficients of a FPB frequency dependent or not*?
But, because of the importance of this question the following highlight the answer specifically. The results of the dynamic stiffness coefficients were found strongly dependent on frequency. The frequency dependency of the stiffness and damping coefficients depends on the mathematical model of the flexure-pivot bearing. Previous analyses were carried out either ignoring the fluid inertia from the analysis and/or neglecting the added-mass coefficients from the bearing model. Ignoring the fluid inertia from the analysis will under predict the influence of excitation frequency on the dynamic stiffness coefficients (Reynolds-equation model). On the other hand, neglecting the added-mass coefficients from the bearing model will result in a frequency-dependent stiffness and damping coefficients.

By introducing an added-mass coefficients in the flexure-pivot bearing model, the stiffness and damping coefficients were found to be *frequency-independent* (constant). The constant value of the rotordynamic coefficients will facilitate the designing process of the FPB for any turbomachine. Therefore, the *Reynolds-equation model is not adequate*, and the bulk-flow Navier-Stokes model should be used instead. In addition, *the added-mass coefficients should be included in the modeling stage*.

The following points summarize and conclude the additional results that were presented in this thesis.

- The main static performance advantage of the flexure-pivot bearings characterized by small attitude angle in the order of 10 degrees at medium to high loads for all rotor running speeds is confirmed.
- The frictional power losses mainly depend on rotor speed and increase quadraticly (almost linearly) with increasing speed.
- In most cases, the maximum pads temperature was measured at 75% of the pads arc length. For pad #4 at high rotor speeds and high applied static loads, the maximum

temperature was measured at 95%. In addition, the pads temperatures increase in the circumferential direction with load and speed. They increase more with increasing speed than load.

- The oil outlets temperatures mainly depend on speed and increase almost quadraticly. In addition, the oil outlets temperatures increase slightly with increasing load (the maximum increase is about 3 C^o).
- The greatest effect of the oil-heat carry-over phenomenon on pads temperatures was seen on pad #3, and the lowest effect was seen on pad #4.
- Two approaches were used to present the rotordynamic coefficients. First, the frequency-dependent dynamic stiffnesses were shown. Second, each element of the dynamic stiffness matrix H was fitted to $K - M\Omega^2 + \boldsymbol{j}C\Omega$, and then the frequency-independent rotordynamic coefficients were obtained. A goodness of fit (Coefficient of determination R^2) was calculated for each dynamic stiffness fit. The goodness of fit was found to be excellent for the direct coefficients and poor for the cross-coupled coefficients. Therefore the cross-coupled dynamic stiffness terms show a frequency dependency that cannot be fitted to $K - M\Omega^2 + \boldsymbol{j}C\Omega$.
- At the centered position, the direct stiffness and damping coefficients in orthogonal planes should be equal for these bearings. In this experiment, the direct stiffness and damping coefficients in the y direction were larger than in the x direction.
- The direct stiffness coefficients increase with load and increase with speed at low loads. The direct damping coefficients increase with increasing load and decrease with increasing speed, with the maximum decrease at high loads.
- The direct added mass coefficients are almost equal ($M_{xx} \cong M_{yy}$) and on the order of (32 kg). They are almost constant with load, but increase with speed.
- The *WFR* of the flexure-pivot bearing (FPB) was calculated and found to be approximately 0.15. The WFR decreases with increasing load and increases with increasing speed with minimum value around 6000 rpm. The added mass coefficients have very little influence on the WFR, with about 1% increase at the highest speed and lowest load.
- The Reynolds equation model over predicts the direct real dynamic stiffness terms and under predicts the cross-coupled real dynamic stiffness terms as compared to the bulk-

flow model prediction. Therefore, the bulk-flow model shows better agreement with the experimental dynamic stiffnesses than the Reynolds-equation model. The Reynolds-equation is not adequate for modeling flexible tilting-pad bearing and the bulk-flow model should be used instead.

- The theory (bulk-flow model) does a good job in most cases, especially in predicting the direct terms and agrees poorly with the measured cross-coupled terms. In addition, it over-predicts the stability of the FPB (under-predicts the WFR).

REFERENCES

[1] Rotech Engineering Services, 2003, "Tilting Pad Journal Bearings: Principles of Operation," http://www.rotechconsulting.com/bearings_sub2.htm , Web Site accessed October 2003, Delmont, PA.

[2] Reynolds, O.,1886, "On the Theory of Lubrication and Its Application to Mr. Beauchamp Tower's Experiments Including an Experimental Determination of the Viscosity of Olive Oil," Phil. Trans., Roy. Soc. London, **177**, pp. 157-234.

[3] Zeidan, F. Y., and Paquette, D. J., 1994, "Application of High Speed and High Performance Fluid Film Bearings in Rotating Machinery," *Proceedings of the 23th Turbomachinery Symposium*, Dallas, pp. 209-234.

[4] Nicholas, J., 1994, "Tilt Pad Bearing Design," *Proceeding of the 23rd Turbomachinery Symposium*, Houston, pp. 179-194.

[5] Armentrout, R. D., and Paquette, D. J., 1993, "Rotordynamic Characteristics of Flexure-Pivot Tilting-Pad Journal Bearings," Tribology Transactions, **36**, pp. 443-451.

[6] Kepple, W. E., Read, D. W., Zeidan, F.Y., Paraskevakos, C., and Dawson, M. P., 1998, "Experience in the Use of Flexure Pivot Tilt Pad Bearings in Boiler Feed Water Pumps," *Proceedings of the 15th International Pump Users Symposium*, Houston, pp. 77-84.

[7] Zeidan, F. Y., 1992, "Developments in Fluid Film Bearing Technology," Turbomachinery International, **9**, pp. 24-31.

[8] Chen, W. J., Zeidan, F. Y., and Jain, D., 1994, "Design, Analysis, and Testing of High Performance Bearings in a High Speed Integrally Geared Compressor," *Proceedings of the 23rd Turbomachinery Symposium*, Dallas, pp. 31-42.

[9] DeChoudhury, P., Hill, M. R., and Paquette, D. J., 1992, "A Flexible Pad Bearing System for High Speed Centrifugal Compressor," *Proceeding of 21st Turbomachinery Symposium*, Dallas, pp. 57-64.

[10] Fu, W. B., and Parkins, D. W., 1992, "Mathematical Analysis of the Performance of a tilting-Pad Journal Bearing Under Static Load," J. Phys. D: Appl. Phys., **25**, pp. A108-A115.

[11] Walton, N. V., and San Andrés, L. A., 1997, "Measurements of the Static Loading Versus Eccentricity in a Flexure-Pivot Tilting-Pad Bearing," ASME Journal of Tribology, **119** , pp. 297-305.

[12] San Andrés, L. A., and Jackson, M. C., 1998, "Measurements of the Static Load (On Pad) Performance and Pad Temperatures in a Flexure-Pivot Tilting-Pad Bearing," Tribology Transactions, **41**, pp. 225-232.

[13] DeChoudhury, P., and Barth, E. W., 1981, "A Comparison of Film Temperature and Oil Discharge Temperature for a Tilting-Pad Journal Bearing," Journal of lubrication Technology, **102**, pp. 115-119.

[14] Edney, S., and Mellinger, F., "Advances in Tilting Pad Journal Bearing Design," Dresser-Rand, Wellsville, N.Y., USA.

[15] Harangozo, A. V., Stolarski, T. A., and Gozdawa, R. J., 1991, "The Effects of Different Lubrication Methods on the Performance of a Tilting-Pad Journal Bearing," Tribology Transactions, **34**, 4, pp. 529-536.

[16] Lund, J., 1964, "Spring and Damping Coefficients for the Tilting Pad Journal Bearing," ASLE Transactions, **7**, pp. 342-352.

[17] Lund, J., 1965, "The Stability of an Elastic Rotor in Journal Bearings with Flexible Damped Supports," ASME Journal of Applied Mechanics, pp. 911-920.

[18] Nicholas, J. C., Gunter, E. J., and Allaire, P. E., 1977, "Stiffness and Damping Coefficients for the Five-Pad Tilting-Pad bearing," ASLE Transactions, **22** pp. 113-124.

[19] Rough, K. E., 1983, "Dynamics of Pivoted-Pad Journal Bearings, Including Pad Translation and Rotation Effects," ASLE Transactions, **26**, 1, pp. 102-109.

[20] Brockwell, K., Kleinbub, D., and Dmochowski, W., 1990, "Measurement and Calculation of the Dynamic Operating Characteristics of the Five Shoe, Tilting Pad Journal Bearing," STLE Tribology Transactions, **33**, 4, pp. 481-492.

[21] Parkins, D., and Horner, D., 1993, "Tilt Pad Journal Bearings - Measured and Predicted Stiffness Coefficients," Tribology Transactions, **36**, 3, pp. 359-366.

[22] Chen, W. J., 1995, "Bearing Dynamic Coefficients of Flexible-Pad Journal Bearings," STLE Tribology Transactions, **38**, 2, pp. 253-260.

[23] Reinhardt, E., and Lund, J., 1975, "The Influence of Fluid Inertia on the Dynamic Properties of Journal Bearings," ASME Journal of Lubrication Technology, **97**, pp. 159-167.

[24] San Andrés, L. A., 1996, "Turbulent Flow, Flexure-Pivot Hybrid Bearings for Cryogenic Applications," Transactions of the ASME, **118**, pp. 190-200.

[25] Parsell, J. K., Allaire, P. E., and Barrett, L. E., 1982, " Frequency Effects in Tilting-Pad Journal Bearing Dynamic Coefficients," ASLE Transactions, **26**, pp. 222-227.

[26] Barret, L., Allaire, P., and Wilson, B., 1987, "The Eigenvalue Dependence of Reduced Tilting Pad Bearing Stiffness and Damping Coefficients," Tribology Transactions, **31**, pp. 411-419.

[27] Ha, H. C., and Yang, S. H., 1999, "Excitation Frequency Effects on the Stiffness and Damping Coefficients of a Five-Pad Tilting Pad Journal Bearing," ASME Journal of Tribology, **121**, pp. 517-522.

[28] Kaul, Anmol, 1999, "Design and Development of a Test Setup for the Experimental Determination of the Rotordynamic and Leakage Characteristics of Annular Bushing Oil Seals," M.Sc. Thesis. Texas A&M University, College Station, Texas.

[29] Childs, D. W., and Hale, K., 1994, "A Test Apparatus and Facility to Identify the Rotordynamic Coefficients of High-Speed Hydrostatic Bearings," ASME Journal of Tribology, **116**, pp. 337-344.

[30] San Andrés, L. A., 1995, "Bulk-Flow Analysis of Flexure and Tilting Pad Fluid Film Bearings," TRC-B&C-3-95. Turbomachinery Laboratory, Texas A&M University, College Station, Texas

[31] San Andrés, L. A., 1991, "Effect of Eccentricity on the Force Response of a Hybrid Bearing," STLE Tribology Transactions, **34**, 4, pp. 537- 544.

APPENDIX

This Appendix contains the experimental data and results previously discussed in this thesis. This consists of the static measurements, dynamic stiffnesses and the corresponding coefficients and results.

Tables 8-10 list all static measurements and static results.

Tables 11-15 list the rotordynamic coefficients, uncertainties and the goodness of fit.

Tables 16-44 list the experimental dynamic stiffnesses and their uncertainties in MN/m.

The dynamic stiffnesses at subsynchronous (0.5X), synchronous (1X) and super-synchronous (2X) frequencies; in addition, at 220 Hz were ignored in most cases when reducing the rotordynamic coefficients.

Table 8. Static performance parameters and measurement data

ω [rpm]	W [kN]	p [kPa]	e_{xNDE} [μm]	e_{yNDE} [μm]	e_{xDE} [μm]	e_{yDE} [μm]	e_x [μm]	e_y [μm]	T_{in} [C°]	T_{oDE} [C°]	T_{oNDE} [C°]	T_o [C°]	$\dot{Q}$ [lit / min]	ε	Φ [degree]	S	P [kW]
12000	0.01	0.9	-9.9	-12.7	-1.8	-12.1	-5.8	-12.4	36.8	46.1	41.6	43.9	53.5	0.05	25.3	0.00	14.10
12000	0.88	98.8	-6.9	-2.0	1.3	-0.5	-2.8	-1.3	36.8	46.4	41.8	44.1	53.3	0.01	65.5	2.71	14.63
12000	1.56	175.5	-2.6	6.1	9.6	10.1	3.5	8.1	37.1	46.8	43.1	44.9	53.3	0.03	23.3	1.50	15.52
12000	2.30	258.3	1.5	18.3	10.9	19.9	6.2	19.1	37.3	46.9	43.2	45.1	53.3	0.08	18.0	1.02	15.54
12000	3.12	350.3	3.1	30.4	15.5	32.6	9.3	31.5	37.2	47.4	43.5	45.5	53.3	0.13	16.4	0.74	16.38
12000	3.88	435.4	5.1	41.1	16.8	43.6	10.9	42.4	37.3	47.7	43.9	45.8	53.3	0.17	14.5	0.60	16.82
12000	4.43	497.4	4.2	45.0	17.1	51.3	10.6	48.2	37.5	47.8	43.9	45.9	53.3	0.19	12.5	0.52	16.64
12000	5.51	619.2	5.5	60.6	18.5	62.1	12.0	61.4	37.5	48.3	44.3	46.3	53.3	0.25	11.0	0.41	17.51
12000	6.12	687.0	8.0	68.2	19.2	71.2	13.6	69.7	37.5	48.4	44.4	46.4	53.3	0.28	11.0	0.37	17.62
12000	7.73	868.0	8.4	85.7	20.8	89.1	14.6	87.4	37.7	49.1	45.3	47.2	53.2	0.35	9.5	0.29	18.89
12000	9.19	1032.4	9.0	108.9	17.7	108.3	13.4	108.6	38.1	49.1	46.0	47.6	53.3	0.43	7.0	0.24	18.94
10000	0.01	1.6	-9.5	-7.2	2.3	1.0	-3.6	-3.1	36.8	44.2	40.0	42.1	53.3	0.02	49.4	0.00	10.49
10000	0.76	85.9	-7.2	0.8	5.4	11.0	-0.9	5.9	37.2	44.8	40.8	42.8	53.5	0.02	-8.7	2.63	11.18
10000	1.60	179.7	-2.0	12.3	15.3	25.9	6.7	19.1	37.3	45.3	41.9	43.6	53.3	0.08	19.3	1.24	12.59
10000	2.34	263.2	-0.1	23.3	17.1	36.8	8.5	30.1	37.3	45.7	42.2	43.9	53.3	0.12	15.8	0.84	13.11
10000	3.13	351.0	4.2	39.5	18.4	49.9	11.3	44.7	37.7	46.2	42.2	44.2	53.4	0.18	14.2	0.63	12.96
10000	3.85	432.9	4.3	47.4	18.6	61.5	11.5	54.5	37.6	46.2	42.2	44.2	53.3	0.22	11.9	0.51	13.20
10000	4.61	517.9	7.0	62.3	19.5	73.0	13.2	67.7	37.9	46.7	42.7	44.7	53.3	0.27	11.1	0.42	13.67
10000	5.38	603.8	8.3	72.8	19.9	81.8	14.1	77.3	37.7	46.4	42.8	44.6	53.4	0.31	10.3	0.36	13.68
10000	6.12	686.9	11.7	86.4	19.1	91.4	15.4	88.9	38.0	46.4	43.2	44.8	53.3	0.36	9.9	0.32	13.50
10000	7.71	866.2	14.0	105.3	18.2	105.0	16.1	105.2	37.9	46.5	43.2	44.8	53.4	0.42	8.7	0.25	13.91
10000	9.32	1046.8	15.4	121.1	17.2	122.3	16.3	121.7	38.2	47.2	43.7	45.5	53.3	0.48	7.6	0.20	14.58
8000	0.02	2.5	-4.6	-7.7	5.1	-3.5	0.2	-5.6	37.2	42.7	39.2	41.0	53.3	0.02	-2.4	0.00	7.51
8000	0.74	83.0	-2.6	1.1	7.6	9.8	2.5	5.5	37.3	43.1	39.7	41.4	53.3	0.02	24.5	2.22	8.12
8000	1.58	177.0	-2.4	16.5	11.7	30.4	4.7	23.5	37.5	43.4	39.8	41.6	53.3	0.09	11.2	1.04	8.27
8000	2.27	255.3	4.3	22.9	19.8	36.7	12.0	29.8	37.3	43.7	40.4	42.0	53.4	0.13	22.0	0.72	9.46
8000	3.09	346.9	6.7	41.6	21.5	55.0	14.1	48.3	37.5	44.2	40.8	42.5	53.3	0.20	16.3	0.52	9.86
8000	3.83	430.5	9.5	55.6	22.4	66.0	15.9	60.8	37.6	44.0	40.8	42.4	53.3	0.25	14.7	0.42	9.42

Table 8. Continued

ω [rpm]	W [kN]	p [kPa]	e_{xNDE} [μm]	e_{yNDE} [μm]	e_{xDE} [μm]	e_{yDE} [μm]	e_x [μm]	e_y [μm]	T_{in} [C^o]	T_{oDE} [C^o]	T_{oNDE} [C^o]	T_o [C^o]	$\dot{Q}$ [lit / min]	ε	Φ [degree]	S	P [kW]
8000	4.65	521.7	12.0	69.6	24.1	79.5	18.1	74.5	37.6	44.1	40.9	42.5	53.3	0.30	13.6	0.35	9.70
8000	5.44	610.6	13.0	82.0	23.4	89.4	18.2	85.7	37.6	44.0	41.1	42.5	53.5	0.34	12.0	0.30	9.79
8000	6.19	695.8	14.8	92.8	23.4	99.8	19.1	96.3	37.7	44.4	41.0	42.7	53.3	0.39	11.2	0.26	10.03
8000	7.67	860.9	15.2	114.4	21.5	117.0	18.4	115.7	37.6	43.8	41.1	42.4	53.4	0.46	9.0	0.21	9.64
8000	9.25	1038.4	14.4	130.9	15.6	130.7	15.0	130.8	37.4	43.8	41.4	42.6	53.2	0.52	6.5	0.17	10.21
6000	0.01	0.9	2.8	0.1	10.3	0.9	6.6	0.5	37.0	41.1	38.5	39.8	53.2	0.03	85.8	0.00	5.43
6000	0.75	84.8	2.5	11.6	14.0	15.0	8.2	13.3	36.8	41.0	38.4	39.7	53.3	0.06	31.8	1.69	5.78
6000	1.54	172.7	7.1	29.0	18.6	34.8	12.9	31.9	36.5	41.0	38.0	39.5	53.3	0.14	21.9	0.84	6.05
6000	2.30	258.2	12.6	44.2	20.9	50.6	16.8	47.4	36.5	41.2	38.0	39.6	53.4	0.20	19.5	0.56	6.08
6000	3.04	341.0	19.1	53.0	30.3	60.6	24.7	56.8	36.3	41.9	38.3	40.1	53.3	0.24	23.5	0.42	7.54
6000	3.83	430.6	20.4	66.7	29.9	73.9	25.2	70.3	36.3	41.8	38.3	40.0	53.3	0.29	19.7	0.33	7.39
6000	4.56	512.1	21.8	83.2	29.3	87.9	25.5	85.5	36.4	41.6	38.5	40.0	53.5	0.35	16.6	0.28	7.27
6000	5.35	601.2	21.7	98.1	27.6	102.9	24.6	100.5	36.4	41.6	38.5	40.0	53.2	0.41	13.8	0.24	7.21
6000	6.22	698.1	23.0	109.9	26.4	111.7	24.7	110.8	36.2	41.4	38.4	39.9	53.4	0.45	12.6	0.21	7.50
6000	7.70	865.3	22.8	130.3	24.1	127.5	23.4	128.9	36.3	41.6	39.0	40.3	53.4	0.52	10.3	0.17	7.94
6000	9.21	1035.0	20.0	141.5	22.4	145.6	21.2	143.6	36.3	41.4	38.9	40.2	53.3	0.57	8.4	0.14	7.61
4000	0.01	0.9	7.0	2.3	12.5	4.6	9.7	3.5	37.2	40.3	38.3	39.3	53.5	0.04	70.4	0.00	4.13
4000	0.77	86.2	10.0	17.1	16.2	22.1	13.1	19.6	36.1	39.3	37.5	38.4	53.3	0.09	33.8	1.14	4.56
4000	1.55	174.6	14.7	42.4	22.6	47.6	18.6	45.0	36.0	39.4	37.5	38.4	53.3	0.19	22.5	0.56	4.83
4000	2.30	258.5	18.3	63.5	26.1	68.2	22.2	65.9	36.9	40.3	38.0	39.1	53.3	0.27	18.6	0.37	4.39
4000	3.14	353.1	20.8	82.3	28.7	89.0	24.7	85.6	37.3	40.2	38.0	39.1	53.2	0.35	16.1	0.27	3.71
4000	3.85	432.9	23.0	100.1	27.9	103.8	25.4	101.9	37.3	40.5	38.2	39.3	53.3	0.41	14.0	0.22	4.12
4000	4.63	520.0	23.1	112.5	28.7	118.3	25.9	115.4	37.6	40.8	38.4	39.6	53.3	0.47	12.6	0.18	4.10
4000	5.38	604.4	23.6	127.5	28.7	127.1	26.2	127.3	37.6	40.8	38.3	39.6	53.3	0.51	11.6	0.16	3.87
4000	6.17	693.3	22.2	138.7	28.5	141.4	25.3	140.1	37.6	40.9	38.5	39.7	53.3	0.56	10.2	0.14	4.18

Table 9. Pads temperatures

ω [rpm]	W [kN]	T_1 (C^o)	T_2 (C^o)	T_3 (C^o)	T_4 (C^o)	T_5 (C^o)	T_6 (C^o)	T_7 (C^o)	T_8 (C^o)	T_9 (C^o)	T_{10} (C^o)	T_{11} (C^o)	T_{12} (C^o)	T_{13} (C^o)	T_{14} (C^o)	T_{15} (C^o)	T_{16} (C^o)	T_{17} (C^o)	T_{18} (C^o)	T_{19} (C^o)
12000	0.01	40.3	44.5	41.5	52.2	45.2	53.2	56.1	59.6	57.6	39.5	46.1	48.3	53.8	58.1	38.8	46.3	46.3	48.4	48.9
12000	0.88	40.5	44.6	41.7	51.6	46.5	53.5	56.5	60.6	58.3	39.4	46.4	48.9	56.4	62.0	38.7	45.8	46.2	48.2	49.3
12000	1.56	40.9	44.8	42.4	52.2	46.9	53.7	56.5	60.3	58.3	39.8	47.1	49.8	57.6	62.8	39.1	46.4	47.1	49.0	50.3
12000	2.3	40.9	44.8	42.5	51.8	47.0	53.7	56.7	60.7	59.1	39.7	47.3	50.1	59.3	65.2	38.9	46.1	47.2	49.3	50.8
12000	3.12	41.2	45.4	42.9	51.7	47.1	54.1	57.3	61.1	60.0	39.9	47.8	50.8	61.1	67.5	39.1	46.5	48.0	50.1	52.0
12000	3.88	41.5	45.8	43.3	51.6	47.2	54.7	58.0	61.6	60.8	40.2	48.5	51.8	62.8	69.5	39.4	47.0	48.6	50.7	53.0
12000	4.43	41.6	46.4	44.0	51.9	47.4	55.1	58.7	62.2	61.8	40.4	49.3	52.8	64.4	71.5	39.7	47.5	48.9	51.0	53.4
12000	5.51	41.5	46.1	43.9	51.5	47.1	55.0	58.7	62.7	62.0	40.4	49.7	53.5	66.5	73.6	39.7	47.5	49.7	51.9	54.6
12000	6.12	41.8	46.4	44.3	51.5	46.8	55.1	58.9	63.4	62.7	40.6	50.4	54.4	68.1	75.4	39.8	48.2	50.6	52.9	55.6
12000	7.73	42.1	46.5	44.5	51.3	46.4	55.4	59.7	65.9	64.1	41.1	52.0	56.4	72.8	78.0	40.2	49.3	51.9	54.5	57.4
12000	9.19	42.2	46.3	44.6	51.5	47.2	56.9	61.6	69.2	65.9	41.4	53.2	58.2	76.7	79.8	40.3	49.8	52.8	55.3	58.6
10000	0.01	39.7	42.8	40.8	49.5	43.3	50.7	53.2	56.9	54.5	39.1	44.7	46.6	50.4	52.7	38.5	44.3	44.5	46.3	46.6
10000	0.76	40.3	43.1	41.2	49.5	44.8	51.6	54.2	57.9	55.4	39.6	45.5	47.5	52.1	55.1	39.0	44.9	45.1	46.8	47.5
10000	1.6	40.8	42.8	41.8	49.3	45.6	51.6	54.2	58.0	55.6	39.7	46.1	48.3	53.8	56.8	39.1	45.2	45.6	47.4	47.9
10000	2.34	41.0	42.8	41.9	49.0	45.9	52.0	54.7	58.7	56.4	39.8	46.4	48.8	55.5	59.1	39.3	45.3	46.0	47.7	48.6
10000	3.13	41.1	42.9	42.2	48.9	46.2	52.6	55.5	59.8	57.5	40.0	46.9	49.6	57.8	62.2	39.4	45.5	46.7	48.6	49.9
10000	3.85	41.2	43.0	42.3	48.7	46.1	53.0	56.1	60.9	58.3	40.2	47.5	50.5	59.9	64.5	39.5	45.9	47.2	49.0	50.6
10000	4.61	41.4	43.3	42.7	48.9	46.3	53.5	56.7	61.9	59.2	40.4	48.3	51.5	62.1	67.0	39.8	46.3	48.1	50.0	51.7
10000	5.38	41.5	43.3	42.8	48.6	46.2	53.7	57.1	63.1	59.9	40.6	49.2	52.6	64.8	69.3	40.0	46.7	48.4	50.3	52.4
10000	6.12	41.7	43.3	42.8	48.4	46.0	54.1	57.8	64.4	60.7	40.7	49.8	53.7	67.1	70.8	40.0	47.0	49.1	50.9	53.3
10000	7.71	41.7	43.3	43.0	48.2	46.0	54.8	58.9	65.7	62.2	40.8	51.3	55.8	71.4	73.9	40.0	47.7	50.2	52.4	54.9
10000	9.32	42.0	43.7	43.5	48.4	46.4	56.2	60.7	67.7	64.0	41.5	53.1	58.2	76.2	76.2	40.5	48.7	51.6	53.8	56.6
8000	0.02	39.8	42.1	40.8	48.4	41.4	47.5	49.5	52.1	50.5	39.6	43.9	45.2	47.5	47.6	39.0	43.5	43.7	45.0	44.8
8000	0.74	40.0	42.1	40.8	47.7	42.3	48.4	50.5	53.2	51.3	39.7	44.2	45.7	48.4	49.1	39.1	43.7	43.9	45.2	45.3
8000	1.58	40.2	42.1	40.8	47.1	43.6	49.3	51.4	54.6	52.2	39.8	44.6	46.3	49.9	51.4	39.2	44.0	44.2	45.7	45.9
8000	2.27	40.6	41.4	41.1	46.7	43.9	49.2	51.3	54.7	52.1	39.7	45.0	46.8	51.1	52.4	39.1	44.1	44.3	45.7	45.8
8000	3.09	40.7	41.3	41.3	46.4	44.6	50.0	52.3	56.2	53.3	39.9	45.6	47.6	53.1	55.0	39.3	44.3	45.1	46.4	46.8
8000	3.83	40.9	41.3	41.4	46.2	44.9	50.6	53.0	57.3	54.2	40.0	46.1	48.4	55.0	57.1	39.4	44.6	45.4	46.7	47.4
8000	4.65	41.1	41.5	41.7	46.3	44.8	51.0	53.6	56.8	54.9	40.2	46.6	48.9	56.2	58.0	39.5	44.9	46.0	47.3	48.1
8000	5.44	41.2	41.7	41.9	46.3	44.6	51.1	54.0	57.3	55.5	40.3	47.1	49.8	58.2	59.9	39.7	45.3	46.5	47.8	48.8

Table 9. Continued

ω [rpm]	W [kN]	T_1 (C^o)	T_2 (C^o)	T_3 (C^o)	T_4 (C^o)	T_5 (C^o)	T_6 (C^o)	T_7 (C^o)	T_8 (C^o)	T_9 (C^o)	T_{10} (C^o)	T_{11} (C^o)	T_{12} (C^o)	T_{13} (C^o)	T_{14} (C^o)	T_{15} (C^o)	T_{16} (C^o)	T_{17} (C^o)	T_{18} (C^o)	T_{19} (C^o)
8000	6.19	41.2	41.8	41.8	46.1	44.6	51.6	54.6	58.6	56.3	40.3	47.7	50.6	60.4	61.1	39.7	45.5	47.0	48.5	49.5
8000	7.67	41.5	41.9	41.7	45.5	44.5	52.5	56.0	61.4	58.0	40.5	49.1	52.6	64.8	63.8	39.9	46.2	47.9	49.3	50.3
8000	9.25	41.6	41.9	41.5	44.8	44.4	53.8	58.0	65.3	60.1	40.6	50.8	54.9	69.6	60.4	39.8	46.7	48.8	50.1	51.2
6000	0	39.3	40.9	39.8	45.2	40.2	44.4	45.9	47.9	46.4	39.3	42.3	43.3	45.0	44.6	38.7	41.9	42.0	42.8	42.6
6000	0.75	39.2	40.7	39.5	44.5	40.5	44.9	46.4	48.6	46.8	39.1	42.4	43.4	45.6	45.3	38.6	41.9	42.0	42.9	42.8
6000	1.54	38.9	40.3	39.2	43.7	41.0	45.6	47.2	49.7	47.6	38.9	42.7	44.0	46.7	47.1	38.4	42.0	42.2	43.2	43.2
6000	2.3	38.9	40.1	39.1	43.1	41.4	46.1	47.8	50.9	48.4	38.7	43.1	44.6	48.5	49.4	38.2	42.1	42.3	43.4	43.7
6000	3.04	39.5	39.4	39.4	42.9	41.6	46.2	47.9	50.8	48.3	38.8	43.6	45.3	49.8	50.0	38.2	42.3	42.8	43.6	43.9
6000	3.83	39.6	39.4	39.4	42.7	41.8	46.7	48.6	51.5	49.3	38.9	44.2	46.1	51.7	51.8	38.3	42.6	43.0	43.9	44.4
6000	4.56	39.7	39.5	39.4	42.6	41.8	47.1	49.2	52.6	50.0	38.9	44.7	46.9	53.5	53.2	38.3	42.9	43.6	44.6	45.1
6000	5.35	39.6	39.4	39.3	42.1	41.9	47.8	50.2	54.0	51.1	39.0	45.5	47.9	55.8	54.8	38.4	43.1	44.2	45.3	45.7
6000	6.22	39.4	39.3	39.2	41.9	41.9	48.5	51.1	55.6	52.2	39.0	46.4	49.1	58.3	56.7	38.3	43.4	44.7	46.0	46.5
6000	7.7	39.7	39.4	39.1	41.8	42.3	50.0	53.1	58.9	54.3	39.2	48.1	51.4	62.5	53.0	38.4	44.1	46.0	47.1	47.8
6000	9.21	39.5	39.2	39.1	41.5	42.8	51.4	55.0	61.6	56.1	39.4	49.8	53.6	66.1	57.1	38.4	44.8	47.2	48.2	49.0
4000	0	38.3	39.3	38.6	42.2	38.8	41.8	42.6	44.0	42.7	38.5	40.6	41.0	42.4	41.5	38.1	40.2	40.9	41.2	41.2
4000	0.77	37.9	38.8	38.2	41.2	38.7	41.7	42.7	44.3	42.9	38.2	40.3	40.9	42.5	41.9	37.8	39.9	39.7	40.2	40.1
4000	1.55	38.1	38.7	38.1	40.7	39.2	42.4	43.5	45.5	43.7	38.2	40.7	41.6	43.8	43.5	37.8	40.2	40.1	40.5	40.7
4000	2.3	39.2	39.6	39.1	41.3	40.5	43.9	45.1	47.5	45.3	39.3	42.2	43.2	46.2	46.1	39.0	41.4	41.4	42.1	42.1
4000	3.14	40.3	39.6	39.2	41.0	40.7	44.4	45.7	48.3	46.0	39.5	43.0	44.1	47.7	45.8	39.1	41.8	41.9	42.6	42.6
4000	3.85	40.4	39.6	39.3	40.9	41.0	45.0	46.5	49.5	46.9	39.7	43.6	45.1	49.5	46.9	39.2	42.1	42.5	43.0	43.3
4000	4.63	40.5	39.8	39.5	41.0	41.5	46.1	47.8	51.3	48.1	40.0	44.7	46.4	51.8	48.5	39.4	42.8	43.1	43.8	44.2
4000	5.38	40.3	39.7	39.5	41.0	41.7	46.9	48.8	52.7	49.1	40.0	45.6	47.5	53.7	49.9	39.4	43.1	43.6	44.4	44.7
4000	6.17	40.4	39.7	39.5	40.9	42.1	47.7	49.8	54.2	50.0	40.3	46.5	48.6	55.5	50.4	39.6	43.6	44.5	45.0	45.5

Table 10. Thermocouples number and location on each pad

Pad No.(Side)	Pad 1(DE)		Pad 2(DE)		Pad 3(DE)					Pad 4(DE)					Pad 4(NDE)				
Thermocouple	T_1	T_2	T_3	T_4	T_5	T_6	T_7	T_8	T_9	T_{10}	T_{11}	T_{12}	T_{13}	T_{14}	T_{15}	T_{16}	T_{17}	T_{18}	T_{19}
% From Pad Arc Length	5	75	5	75	5	50	60	75	95	5	50	60	75	95	5	50	60	75	95
Θ *(degree)*	12.6	63	103	153	193	225	232	243	257	283	315	322	333	347	283	315	322	333	347

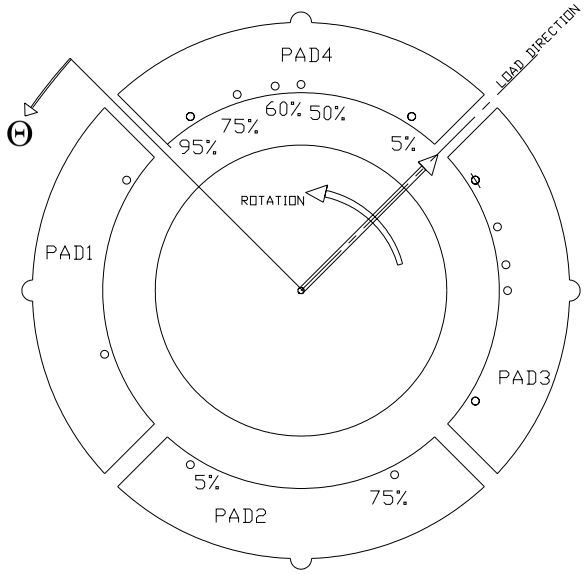

Figure 57. Thermocouples location on each pad, drive end (DE) side

Table 11. Experimental stiffness coefficients and their uncertainties, and the coefficient of determination (R^2) value

ω	W	Experiment								Coefficient of Determination			
		K_{xx}	K_{xy}	K_{yx}	K_{yy}	ΔK_{xx}	ΔK_{xy}	ΔK_{yx}	ΔK_{yy}				
[rpm]	[kN]	[MN/m]	[MN/m]	[MN/m]	[MN/m]	[MN/m]	[MN/m]	[MN/m]	[MN/m]	R^2_{xx}	R^2_{xy}	R^2_{yx}	R^2_{yy}
4000	0.01	20.05	-7.65	9.44	23.97	2.49	0.86	1.73	2.64	0.9881	0.8271	0.7722	0.9875
4000	1.55	24.56	-8.88	8.34	27.10	3.02	1.37	3.21	4.51	0.9812	0.4883	0.4703	0.9781
4000	3.14	33.81	-7.56	6.45	32.84	3.49	1.84	3.19	5.89	0.9322	0.1403	0.6576	0.9297
4000	4.63	50.64	-8.39	5.90	52.58	3.75	3.42	4.43	6.12	0.8096	0.4395	0.7338	0.919
4000	6.17	71.97	-8.01	6.97	79.26	3.35	4.25	5.41	7.06	0.509	0.6349	0.7597	0.8684
6000	0.01	31.53	-7.69	9.45	37.00	2.08	2.01	1.28	2.64	0.9908	0.1676	0.9058	0.9871
6000	1.54	35.79	-9.20	8.37	38.59	2.26	2.45	1.72	3.31	0.9898	0.0418	0.8483	0.9857
6000	3.04	40.68	-4.77	11.58	44.89	1.95	1.84	1.61	5.36	0.9866	0.6471	0.3136	0.9574
6000	4.56	54.24	-6.33	10.20	58.92	2.22	2.35	2.04	4.14	0.9765	0.0129	0.7944	0.9685
6000	6.22	71.37	-6.74	8.85	81.55	1.92	1.96	2.46	4.71	0.9712	0.3101	0.8668	0.9565
6000	9.21	107.98	-11.51	5.75	141.60	1.83	2.04	4.70	5.91	0.9547	0.8734	0.7982	0.9447
8000	0.02	44.39	-10.90	12.13	49.96	2.09	2.63	1.61	2.11	0.9923	0.5263	0.5294	0.9925
8000	1.58	48.28	-11.94	10.60	54.19	1.67	3.02	1.41	2.71	0.9948	0.3762	0.7026	0.9907
8000	3.09	53.57	-8.73	13.19	57.73	2.46	2.87	2.49	3.56	0.9843	0.0018	0.1596	0.978
8000	4.65	64.95	-10.33	11.67	69.70	2.16	2.79	3.40	3.78	0.9847	0.0393	0.1775	0.9719
8000	6.19	78.97	-12.67	10.06	88.25	2.42	2.71	2.75	4.30	0.9789	0.3076	0.6051	0.9634
8000	9.25	108.33	-19.35	4.76	143.86	3.27	2.12	3.81	4.54	0.9324	0.85	0.791	0.9668
10000	0.01	55.53	-17.93	14.64	65.40	1.73	1.82	3.29	2.93	0.994	0.9222	0.0111	0.9854
10000	1.6	57.56	-13.56	18.36	63.66	1.71	2.19	2.77	3.69	0.993	0.7771	0.0763	0.977
10000	3.13	67.37	-13.27	13.28	73.83	1.84	2.13	4.06	3.69	0.9902	0.7001	0.6602	0.9715
10000	4.61	78.13	-13.83	13.94	86.56	2.20	2.92	3.31	4.04	0.9858	0.6143	0.4876	0.97
10000	6.12	90.41	-15.11	13.06	101.78	2.23	2.58	3.77	3.67	0.9811	0.7461	0.5094	0.9689
10000	9.32	115.94	-19.59	10.86	150.69	1.89	2.26	4.83	3.79	0.984	0.9087	0.6069	0.9721
12000	0.01	67.17	-24.29	17.99	76.72	2.01	2.02	3.99	4.45	0.9916	0.9475	0.0006	0.9579
12000	1.56	67.58	-19.10	24.33	79.50	1.79	2.46	4.75	4.47	0.9919	0.9044	0.0081	0.9659
12000	3.12	76.60	-17.31	21.95	87.53	2.02	1.86	4.27	5.28	0.9871	0.9286	0.2374	0.9423
12000	4.43	85.86	-18.42	20.75	97.96	2.99	2.76	3.30	6.55	0.9737	0.8658	0.5062	0.914
12000	6.12	93.25	-20.18	23.12	109.00	1.96	1.95	3.30	5.02	0.9852	0.9269	0.3136	0.936
12000	9.19	129.87	-29.34	4.11	146.16	2.18	2.29	5.67	4.01	0.9875	0.9415	0.5994	0.9541

Table 12. Theoretical stiffness coefficients and the coefficient of determination (R^2) value

ω	W	Theory (bulk-flow)				Coefficient of Determination			
		K_{xx}	K_{xy}	K_{yx}	K_{yy}				
[rpm]	[kN]	[MN/m]	[MN/m]	[MN/m]	[MN/m]	R^2_{xx}	R^2_{xy}	R^2_{yx}	R^2_{yy}
4000	0.01	19.71	-5.70	5.69	19.71	0.935	0.705	0.705	0.935
4000	1.55	24.62	2.35	10.19	21.76	0.928	0.960	0.883	0.934
4000	3.14	47.62	4.82	11.78	44.98	0.914	0.923	0.881	0.915
4000	4.63	74.32	6.88	13.36	71.80	0.903	0.906	0.879	0.903
4000	6.17	105.77	8.60	14.73	103.37	0.893	0.892	0.873	0.893
6000	0.01	35.81	-6.87	6.88	35.81	0.951	0.831	0.831	0.951
6000	1.54	32.19	4.98	16.12	28.90	0.954	0.963	0.924	0.956
6000	3.04	51.42	6.65	15.87	47.91	0.952	0.962	0.931	0.954
6000	4.56	76.27	8.06	16.64	72.87	0.950	0.956	0.934	0.951
6000	6.22	107.58	9.60	17.69	104.29	0.948	0.951	0.935	0.948
6000	9.21	172.65	12.06	19.59	169.52	0.943	0.946	0.936	0.943
8000	0.02	50.09	-7.53	7.54	50.09	0.971	0.904	0.904	0.971
8000	1.58	54.75	-6.33	8.90	54.97	0.971	0.847	0.929	0.970
8000	3.09	57.67	9.86	20.42	53.70	0.973	0.978	0.959	0.975
8000	4.65	81.51	10.36	20.28	77.53	0.974	0.977	0.963	0.975
8000	6.19	109.00	11.24	20.69	105.07	0.974	0.977	0.965	0.975
8000	9.25	171.54	13.21	22.01	167.78	0.972	0.974	0.967	0.972
10000	0.01	64.38	-7.89	7.89	64.38	0.983	0.945	0.945	0.983
10000	1.60	68.51	-7.06	8.88	68.65	0.983	0.918	0.958	0.983
10000	3.13	63.61	14.12	25.57	59.45	0.985	0.986	0.976	0.986
10000	4.61	84.55	13.61	24.51	80.22	0.986	0.987	0.977	0.987
10000	6.12	109.14	13.76	24.24	104.79	0.986	0.987	0.979	0.987
10000	9.32	170.47	14.93	24.73	166.17	0.986	0.987	0.981	0.986
12000	0.01	77.79	-8.07	8.07	77.79	0.991	0.968	0.968	0.991
12000	1.56	81.24	-7.51	8.77	81.34	0.991	0.957	0.974	0.991
12000	3.12	68.66	18.39	30.98	64.84	0.991	0.992	0.987	0.992
12000	4.43	85.67	17.71	29.29	81.22	0.992	0.992	0.986	0.992
12000	6.12	111.21	17.06	28.20	106.60	0.992	0.992	0.987	0.993
12000	9.19	166.05	17.16	27.74	161.36	0.992	0.993	0.989	0.993

Table 13. Experimental damping coefficients and their uncertainties and the coefficient of determination (R^2) value

ω	W	Experiment								Coefficient of Determination			
		C_{xx}	C_{xy}	C_{yx}	C_{yy}	ΔC_{xx}	ΔC_{xy}	ΔC_{yx}	ΔC_{yy}				
[rpm]	[kN]	kN.s/m	kN.s/m	kN.s/m	kN.s/m	kN.s/m	kN.s/m	kN.s/m	kN.s/m	R^2_{xx}	R^2_{xy}	R^2_{yx}	R^2_{yy}
4000	0.01	100.99	14.93	24.57	118.32	3.30	5.07	2.07	2.23	0.9956	0.6755	0.9713	0.9985
4000	1.55	111.97	12.56	19.12	129.91	3.28	6.53	2.73	3.52	0.9962	0.4552	0.9175	0.9968
4000	3.14	124.19	8.11	16.34	150.60	5.16	5.47	3.65	8.85	0.9924	0.3315	0.819	0.9849
4000	4.63	131.60	4.56	8.49	183.74	8.00	6.19	4.76	14.26	0.9848	0.1154	0.4329	0.9755
4000	6.17	132.52	-4.85	-3.01	220.62	9.10	6.79	5.09	19.31	0.9807	0.1091	0.0773	0.9691
6000	0.01	93.52	7.01	29.32	109.02	2.81	4.73	2.57	2.92	0.9953	0.2973	0.9614	0.9963
6000	1.54	103.48	3.84	24.95	116.03	3.21	5.20	3.19	2.78	0.9958	0.1099	0.9325	0.9975
6000	3.04	104.06	14.60	27.10	114.86	2.62	5.88	3.35	7.55	0.997	0.5685	0.933	0.9802
6000	4.56	113.75	10.35	22.75	140.00	3.27	5.41	3.27	8.20	0.9961	0.4386	0.9116	0.9842
6000	6.22	121.67	6.06	14.22	162.39	3.81	6.86	3.15	8.33	0.9954	0.1425	0.813	0.9878
6000	9.21	126.59	-4.10	-4.48	205.28	7.04	9.23	4.49	14.60	0.9857	0.0404	0.1752	0.9768
8000	0.02	90.28	-1.25	33.64	102.10	3.49	2.83	4.37	3.22	0.9923	0.0362	0.9192	0.9948
8000	1.58	95.67	-1.16	28.71	111.01	4.07	4.22	4.16	4.38	0.9916	0.016	0.9103	0.9927
8000	3.09	99.95	2.45	23.31	113.14	2.74	3.17	3.62	5.97	0.9967	0.1184	0.9038	0.9878
8000	4.65	104.03	4.82	21.20	117.51	2.68	3.76	2.88	7.41	0.9969	0.2598	0.9205	0.9817
8000	6.19	110.21	3.01	13.52	130.07	3.19	4.36	3.62	8.32	0.9961	0.0922	0.7489	0.9812
8000	9.25	124.84	-1.35	-1.06	159.54	7.75	7.29	6.60	13.70	0.9821	0.0067	0.0054	0.9647
10000	0.01	95.39	-3.39	30.13	107.04	4.93	2.23	6.07	4.77	0.9863	0.3076	0.8256	0.9898
10000	1.60	96.77	0.55	26.25	109.32	3.54	1.34	3.42	3.93	0.9941	0.0375	0.9302	0.9943
10000	3.13	97.54	1.64	30.70	111.52	2.50	1.11	7.39	6.56	0.9971	0.3305	0.7958	0.9849
10000	4.61	97.32	1.67	19.89	117.25	1.83	1.42	3.11	7.92	0.9983	0.2269	0.8972	0.9791
10000	6.12	98.62	1.10	16.58	123.94	1.74	1.47	2.54	8.22	0.9985	0.1065	0.9009	0.9798
10000	9.32	101.53	-1.67	7.85	143.59	2.67	2.69	3.44	10.43	0.9968	0.0758	0.5258	0.9759
12000	0.01	100.96	-0.92	23.21	118.39	5.36	2.60	4.10	5.70	0.9855	0.0234	0.8604	0.9881
12000	1.56	98.76	0.97	17.73	121.55	4.67	3.45	2.83	7.66	0.9885	0.015	0.8832	0.9797
12000	3.12	94.74	4.87	19.30	117.46	3.13	1.38	2.79	9.05	0.9949	0.726	0.9111	0.973
12000	4.43	93.50	5.69	21.76	122.85	3.46	2.11	2.98	9.88	0.9929	0.5819	0.9111	0.9674
12000	6.12	92.75	9.13	14.63	120.48	2.59	1.34	2.73	11.38	0.9962	0.9033	0.8533	0.9578
12000	9.19	100.38	7.23	11.18	137.87	3.96	2.01	6.08	13.98	0.9924	0.7226	0.4059	0.9516

Table 14. Theoretical damping coefficients and the coefficient of determination (R^2) value

ω	W	Theory (bulk-flow)				Coefficient of Determination			
		C_{xx}	C_{xy}	C_{yx}	C_{yy}				
[rpm]	[kN]	kN.s/m	kN.s/m	kN.s/m	kN.s/m	R^2_{xx}	R^2_{xy}	R^2_{yx}	R^2_{yy}
4000	0.01	116.58	-0.10	0.10	116.58	0.997	0.004	0.004	0.997
4000	1.55	111.78	32.97	32.80	111.84	0.996	0.999	0.991	0.997
4000	3.14	172.87	34.20	33.72	173.13	0.996	0.998	0.991	0.996
4000	4.63	234.23	35.30	34.72	234.57	0.996	0.997	0.991	0.996
4000	6.17	299.57	36.09	35.47	299.92	0.995	0.997	0.991	0.996
6000	0.01	108.93	0.74	-0.74	108.93	0.994	0.185	0.184	0.994
6000	1.54	87.15	32.00	30.78	86.93	0.995	0.997	0.984	0.994
6000	3.04	117.47	29.29	28.04	117.80	0.993	0.997	0.985	0.994
6000	4.56	153.21	28.41	27.09	153.66	0.993	0.996	0.985	0.993
6000	6.22	194.45	28.09	26.74	194.91	0.992	0.995	0.984	0.993
6000	9.21	271.78	27.91	26.56	272.33	0.992	0.994	0.984	0.993
8000	0.02	96.26	1.29	-1.29	96.26	0.992	0.499	0.501	0.992
8000	1.58	101.19	2.39	-0.12	101.21	0.992	0.783	0.007	0.992
8000	3.09	91.10	26.62	24.75	91.62	0.992	0.996	0.982	0.993
8000	4.65	114.83	24.88	23.02	115.45	0.992	0.996	0.982	0.993
8000	6.19	140.33	23.95	22.11	140.94	0.992	0.995	0.982	0.992
8000	9.25	193.24	22.96	21.16	193.92	0.992	0.994	0.981	0.992
10000	0.01	87.92	1.57	-1.57	87.92	0.991	0.706	0.705	0.991
10000	1.60	91.13	2.15	-0.98	91.12	0.992	0.803	0.471	0.991
10000	3.13	76.03	25.57	23.30	76.64	0.992	0.996	0.983	0.993
10000	4.61	91.92	23.50	21.29	92.61	0.992	0.996	0.983	0.993
10000	6.12	109.43	22.20	20.06	110.19	0.992	0.996	0.983	0.993
10000	9.32	149.63	20.68	18.61	150.42	0.993	0.995	0.982	0.993
12000	0.01	81.38	1.68	-1.67	81.38	0.993	0.823	0.821	0.993
12000	1.56	83.48	2.01	-1.35	83.46	0.993	0.854	0.753	0.993
12000	3.12	66.71	24.61	22.21	66.58	0.993	0.996	0.985	0.994
12000	4.43	76.25	22.95	20.56	76.97	0.993	0.996	0.985	0.994
12000	6.12	91.10	21.26	18.95	91.90	0.994	0.996	0.985	0.994
12000	9.19	120.54	19.44	17.21	121.39	0.994	0.996	0.985	0.995

Table 15. Experimental and theoretical added-mass coefficients and experimental uncertainties

		Experiment								Theory (bulk-flow)			
ω [rpm]	W [kN]	M_{xx} kg	M_{xy} kg	M_{yx} kg	M_{yy} kg	ΔM_{xx} kg	ΔM_{xy} kg	ΔM_{yx} kg	ΔM_{yy} kg	M_{xx} kg	M_{xy} kg	M_{yx} kg	M_{yy} kg
4000	0.01	28.31	-2.35	-3.97	29.22	1.52	0.53	1.06	1.61	17.71	-1.90	1.90	17.71
4000	1.55	26.55	-1.63	-3.67	36.64	1.75	0.79	1.85	2.61	16.74	3.52	6.04	16.05
4000	3.14	17.28	-1.00	-5.91	28.66	2.22	1.17	2.03	3.75	23.77	3.93	6.04	23.25
4000	4.63	9.14	-3.58	-8.69	24.38	2.17	1.98	2.57	3.55	30.33	4.20	6.10	29.92
4000	6.17	4.05	-6.66	-11.43	21.53	1.95	2.47	3.15	4.11	37.09	4.40	6.16	36.77
6000	0.01	29.84	-1.25	-5.51	31.88	1.26	1.22	0.78	1.60	21.52	-1.95	1.95	21.52
6000	1.54	29.95	-0.69	-5.48	37.01	1.44	1.57	1.10	2.12	16.46	4.78	7.66	16.51
6000	3.04	21.62	3.22	-1.41	32.84	1.16	1.10	0.96	3.20	22.32	4.33	6.81	21.57
6000	4.56	18.52	0.35	-5.19	29.64	1.33	1.40	1.22	2.47	27.80	4.38	6.60	27.13
6000	6.22	15.84	-1.86	-8.89	31.35	1.26	1.28	1.61	3.09	33.89	4.52	6.54	33.31
6000	9.21	11.90	-7.61	-13.27	34.64	1.20	1.34	3.08	3.87	45.03	4.66	6.46	44.57
8000	0.02	32.35	-3.78	-2.33	33.03	1.25	1.57	0.96	1.26	22.97	-1.80	1.79	22.97
8000	1.58	31.25	-3.17	-2.93	37.96	1.04	1.89	0.88	1.70	23.73	-1.59	2.09	23.86
8000	3.09	26.22	0.16	-1.46	31.80	1.57	1.83	1.59	2.27	21.03	4.74	7.18	20.26
8000	4.65	24.09	-0.78	-2.20	30.84	1.39	1.79	2.18	2.42	25.27	4.54	6.75	24.54
8000	6.19	22.96	-2.52	-4.75	30.76	1.56	1.75	1.77	2.77	29.71	4.50	6.54	29.03
8000	9.25	17.13	-7.16	-10.41	34.44	2.12	1.37	2.47	2.95	38.75	4.53	6.33	38.18
10000	0.01	30.70	-8.64	-0.48	33.29	1.05	1.10	1.99	1.78	23.38	-1.58	1.58	23.38
10000	1.6	27.73	-5.56	-1.09	32.70	1.11	1.42	1.80	2.39	23.91	-1.51	1.72	23.99
10000	3.13	25.20	-4.42	-7.70	29.32	1.19	1.38	2.63	2.39	19.69	5.15	7.43	19.00
10000	4.61	23.70	-4.76	-4.16	29.62	1.31	1.74	1.97	2.41	22.70	4.75	6.86	21.97
10000	6.12	22.75	-6.24	-5.44	28.99	1.46	1.68	2.47	2.40	25.92	4.54	6.52	25.21
10000	9.32	20.97	-10.06	-8.49	31.67	1.23	1.47	3.16	2.48	33.20	4.38	6.15	32.55
12000	0.01	31.24	-12.23	-0.14	30.29	1.26	1.26	2.50	2.78	22.93	-1.36	1.36	22.93
12000	1.56	28.17	-10.81	-0.61	33.90	1.12	1.54	2.97	2.79	23.28	-1.35	1.43	23.32
12000	3.12	25.50	-9.64	-3.44	30.75	1.34	1.24	2.84	3.51	18.06	5.48	7.48	17.66
12000	4.43	25.93	-10.00	-4.76	30.47	1.87	1.73	2.06	4.10	20.23	4.97	6.91	19.58
12000	6.12	23.77	-10.34	-3.33	28.61	1.31	1.30	2.22	3.36	22.96	4.60	6.44	22.28
12000	9.19	27.94	-13.21	-9.98	26.26	1.41	1.48	3.67	2.59	28.29	4.26	5.94	27.62

Table 16. Experimental dynamic stiffnesses at 4000 rpm and 1.4 kPa bearing unit loading

Ω	Ω/ω	Experiment															
		Dynamic stiffness								Uncertainty							
Hz		$Re(H_{xx})$	$Im(H_{xx})$	$Re(H_{xy})$	$Im(H_{xy})$	$Re(H_{yx})$	$Im(H_{yx})$	$Re(H_{yy})$	$Im(H_{yy})$	$Re(U_{xx})$	$Im(U_{xx})$	$Re(U_{xy})$	$Im(U_{xy})$	$Re(U_{yx})$	$Im(U_{yx})$	$Re(U_{yy})$	$Im(U_{yy})$
20	0.30	25.5	10.4	-6.7	-2.9	7.4	1.6	27.7	14.4	0.31	0.61	0.12	0.21	0.37	0.39	0.26	0.63
30	0.45	23.4	16.7	-7.9	-4.0	7.7	1.8	29.8	19.4	0.36	0.55	0.18	0.14	0.35	0.33	0.14	0.60
40	0.60	21.8	23.2	-8.2	-5.2	7.9	2.6	26.5	25.9	0.27	0.76	0.13	0.15	0.26	0.33	0.38	0.67
50	0.75	19.6	30.7	-8.5	-5.6	8.1	2.4	23.9	34.5	0.48	0.90	0.25	0.19	0.75	0.88	0.42	0.99
70	1.05	12.8	39.3	-8.8	-4.7	18.8	-2.9	17.1	47.3	0.77	1.90	0.50	0.43	2.57	2.20	0.76	0.77
80	1.20	13.5	50.3	-7.4	-7.3	9.9	5.2	17.5	59.1	0.47	1.37	0.21	0.33	0.63	1.01	0.35	1.56
90	1.35	11.8	56.4	-7.3	-6.1	9.5	7.9	13.1	63.9	0.24	1.43	0.23	0.29	0.48	0.69	0.57	1.45
100	1.50	8.1	63.8	-5.8	-7.0	11.4	8.1	9.9	71.5	0.32	1.43	0.28	0.32	0.58	0.40	0.56	1.95
110	1.65	5.3	70.9	-6.1	-6.7	11.2	9.1	8.0	78.1	0.39	1.77	0.32	0.30	0.34	0.81	0.47	1.95
130	1.95	-2.9	86.5	-6.6	-7.4	13.2	10.0	2.1	94.2	1.06	3.96	1.34	1.13	1.37	2.28	1.46	3.49
140	2.10	-6.7	92.7	-2.8	-9.6	13.9	13.4	-7.2	104.2	1.42	1.97	0.67	1.67	1.95	1.83	0.81	1.94
150	2.25	-10.6	98.1	-7.7	-9.3	15.7	16.2	-5.8	115.7	0.83	2.65	0.75	0.78	0.81	1.26	0.53	3.11
160	2.40	-12.8	107.0	-4.4	-2.8	14.3	16.2	-8.5	116.2	1.35	3.07	0.77	1.25	1.60	0.99	0.56	3.19
170	2.55	-16.6	116.5	-2.2	-5.2	15.5	19.4	-16.5	124.8	1.77	4.28	1.88	1.43	2.05	2.39	1.48	3.88
190	2.85	-22.8	128.6	-4.3	-3.6	23.1	20.8	-20.6	143.9	2.40	3.04	1.81	1.55	2.16	1.74	1.89	3.74
200	3.00	-24.1	134.8	-0.3	3.3	20.2	19.3	-20.8	144.2	1.46	4.82	1.36	2.38	4.04	2.16	2.64	3.80
210	3.15	-25.5	134.8	3.2	-4.0	24.4	27.3	-28.9	160.9	1.06	3.38	1.54	0.83	1.50	0.92	1.44	4.28
220	3.30	-32.6	133.8	-9.7	0.5	19.8	18.6	-28.5	150.3	1.18	3.54	1.06	1.10	1.41	0.56	1.29	4.39
230	3.45	-47.2	144.7	-1.7	7.1	18.4	28.0	-46.6	160.9	1.00	3.94	0.87	1.07	0.90	0.72	1.21	4.83
250	3.75	-53.7	159.5	-0.6	8.6	18.2	31.6	-51.9	181.9	0.89	4.25	1.08	0.76	0.90	0.91	1.21	4.42
260	3.90	-55.9	165.0	-2.0	13.2	19.1	37.3	-54.4	191.4	1.17	4.91	1.40	1.83	1.13	2.13	2.27	6.01
270	4.05	-60.6	169.1	-3.1	16.9	22.0	37.6	-56.2	202.4	2.80	4.90	6.60	6.23	2.76	1.75	9.59	7.35
280	4.20	-63.3	172.7	1.2	17.5	20.5	40.3	-65.0	206.0	1.28	4.94	1.48	0.99	1.21	1.28	1.82	4.51
290	4.35	-69.1	180.0	-0.4	23.5	19.3	40.5	-68.1	208.9	0.73	5.23	1.62	1.09	1.26	1.32	0.85	4.51

Table 17. Experimental dynamic stiffnesses at 4000 rpm and 175.9 kPa bearing unit loading

Ω	Ω/ω	Experiment															
		Dynamic stiffness								Uncertainty							
Hz		$Re(H_{xx})$	$Im(H_{xx})$	$Re(H_{xy})$	$Im(H_{xy})$	$Re(H_{yx})$	$Im(H_{yx})$	$Re(H_{yy})$	$Im(H_{yy})$	$Re(U_{xx})$	$Im(U_{xx})$	$Re(U_{xy})$	$Im(U_{xy})$	$Re(U_{yx})$	$Im(U_{yx})$	$Re(U_{yy})$	$Im(U_{yy})$
20	0.3	30.1	12.6	-9.0	-3.7	4.9	0.6	33.0	11.7	0.32	0.46	0.15	0.26	0.25	0.22	0.17	0.31
30	0.45	28.0	19.2	-10.0	-5.3	4.9	0.4	32.2	18.2	0.60	0.45	0.22	0.22	0.25	0.33	0.19	0.15
40	0.6	26.5	26.4	-10.4	-6.5	4.9	0.8	28.2	26.7	0.14	0.35	0.17	0.20	0.22	0.40	0.18	0.17
50	0.75	24.5	34.7	-10.6	-7.0	5.4	0.4	25.3	35.1	0.49	0.41	0.28	0.27	0.94	0.84	0.25	0.35
70	1.05	16.2	43.2	-10.7	-6.4	17.2	-1.4	16.9	49.3	0.58	0.32	0.35	0.21	0.83	0.91	0.50	0.57
80	1.2	18.2	55.8	-9.0	-10.3	8.7	2.9	26.9	71.1	0.28	0.49	0.23	0.20	0.61	0.62	0.67	0.64
90	1.35	16.3	63.3	-9.3	-8.8	7.7	4.0	14.0	67.9	0.27	0.41	0.21	0.23	0.37	0.71	0.45	0.32
100	1.5	13.1	71.7	-7.8	-10.6	9.6	3.5	9.8	76.2	0.54	0.39	0.28	0.29	0.41	0.50	0.36	0.46
110	1.65	10.1	78.8	-8.3	-10.7	8.9	4.6	6.0	81.5	0.47	0.59	0.29	0.30	0.39	0.55	0.26	0.22
130	1.95	3.4	98.4	-6.8	-14.0	10.2	3.7	-3.0	99.4	0.88	1.30	0.96	1.25	1.25	0.79	1.09	0.99
140	2.1	-1.4	105.6	-5.3	-12.8	14.1	8.1	-14.9	110.0	1.04	1.54	0.98	0.89	1.13	1.09	1.16	0.75
150	2.25	-4.1	110.2	-7.6	-12.1	15.7	9.8	-11.8	118.9	0.97	0.70	0.52	0.68	1.02	1.01	0.58	0.43
160	2.4	-6.2	119.0	-5.3	-11.9	14.3	11.7	-5.0	132.2	1.17	1.31	0.85	1.27	0.88	0.94	0.96	1.37
170	2.55	-9.2	127.8	-6.3	-10.4	16.4	11.6	-20.9	138.3	2.14	2.65	2.34	1.99	2.08	2.33	2.30	1.45
190	2.85	-16.9	141.7	-5.9	-9.0	21.3	12.3	-21.8	152.0	2.87	2.98	1.71	2.15	2.29	3.74	1.98	1.23
200	3	-18.0	147.6	-4.4	-5.5	17.4	12.3	-31.6	146.2	2.67	4.70	2.51	1.46	4.79	3.61	2.51	2.52
210	3.15	-19.5	151.6	-1.4	-6.5	24.7	19.5	-40.5	167.3	1.36	0.80	1.01	1.19	1.60	1.02	1.54	1.28
220	3.3	-24.6	150.8	-15.0	4.6	17.0	11.8	-79.2	147.2	1.31	1.14	1.52	1.22	1.83	1.70	2.04	3.63
230	3.45	-39.1	161.1	-3.0	-0.6	19.8	21.1	-49.9	184.5	0.78	0.83	0.80	1.07	1.18	1.56	0.93	0.69
250	3.75	-44.6	177.0	-4.3	4.0	18.2	21.7	-59.2	192.9	0.96	1.40	0.49	0.94	0.80	2.00	1.19	1.19
260	3.9	-47.9	183.3	-3.8	7.0	17.8	24.9	-72.3	206.9	0.91	1.00	1.12	0.86	1.26	1.66	1.48	1.62
270	4.05	-50.2	188.8	-7.3	10.0	15.1	28.1	-64.1	218.1	1.90	2.26	4.46	7.82	2.44	3.29	6.41	9.13
280	4.2	-52.5	193.3	-7.1	14.1	14.5	31.9	-79.7	216.1	1.36	1.71	1.57	1.10	1.43	1.28	2.01	3.13
290	4.35	-56.4	199.7	-4.2	27.0	14.1	33.9	-107.6	237.9	1.33	1.44	1.45	2.16	1.88	1.07	4.63	2.50

Table 18. Experimental dynamic stiffnesses at 4000 rpm and 348.4 kPa bearing unit loading

Ω	Ω/ω	Experiment															
		Dynamic stiffness								Uncertainty							
Hz		$Re(H_{xx})$	$Im(H_{xx})$	$Re(H_{xy})$	$Im(H_{xy})$	$Re(H_{yx})$	$Im(H_{yx})$	$Re(H_{yy})$	$Im(H_{yy})$	$Re(U_{xx})$	$Im(U_{xx})$	$Re(U_{xy})$	$Im(U_{xy})$	$Re(U_{yx})$	$Im(U_{yx})$	$Re(U_{yy})$	$Im(U_{yy})$
20	0.3	44.7	14.7	-8.7	-0.3	6.8	1.3	39.9	12.9	11.05	9.04	3.20	3.05	6.18	6.05	2.67	1.41
30	0.45	38.2	24.6	-7.8	-6.6	3.5	-2.4	43.2	20.1	2.29	3.20	0.52	1.14	1.70	1.15	0.60	0.59
40	0.6	36.7	29.2	-8.7	-6.4	3.6	-1.3	38.8	30.4	1.21	1.40	0.79	0.36	0.90	1.36	0.73	0.63
50	0.75	33.6	37.7	-8.6	-7.3	3.7	-2.1	35.5	40.1	1.97	1.52	0.99	0.85	1.81	1.54	1.05	0.91
70	1.05	25.5	47.9	-9.3	-6.0	16.7	-6.6	26.6	55.2	1.46	1.38	0.87	0.88	2.16	1.84	0.87	1.60
80	1.2	27.5	61.2	-4.0	-8.1	6.7	-1.5	-0.4	101.9	0.97	0.74	1.03	1.16	1.31	2.35	2.72	1.30
90	1.35	26.6	69.3	-8.1	-8.7	5.9	1.5	23.9	76.9	1.13	0.77	0.51	0.73	1.59	1.40	0.74	1.36
100	1.5	23.9	79.9	-7.4	-10.7	9.0	0.9	18.5	85.9	1.06	1.62	1.07	0.96	1.17	0.95	1.05	1.08
110	1.65	22.3	88.0	-7.8	-10.9	8.1	1.7	14.4	91.4	0.68	1.44	0.84	0.61	1.08	0.89	1.46	1.31
130	1.95	19.5	118.4	-5.4	-15.6	7.1	-5.3	6.3	112.0	3.23	4.42	3.22	2.73	2.78	3.06	3.03	1.25
140	2.1	11.9	114.6	-6.4	-10.9	14.0	7.0	-7.5	128.8	1.82	1.65	1.25	1.24	1.84	1.37	1.60	1.19
150	2.25	12.4	122.4	-6.6	-12.1	16.0	5.9	5.1	141.4	2.21	1.21	0.93	1.19	1.02	1.19	1.22	1.63
160	2.4	11.6	132.8	-6.3	-12.8	13.4	9.7	2.5	154.2	1.24	1.95	1.74	1.90	1.92	1.13	1.52	2.33
170	2.55	11.0	141.9	-5.5	-8.4	14.3	6.7	-13.6	161.3	2.06	1.57	1.37	1.83	1.91	1.45	2.64	1.70
190	2.85	6.8	158.6	-4.0	-8.9	23.8	7.6	-3.3	177.8	2.26	2.60	2.56	1.91	1.86	1.07	2.59	2.25
200	3	5.1	165.8	-7.1	-4.2	18.0	10.4	-22.0	172.3	2.43	3.13	1.99	2.62	3.59	1.52	4.51	3.17
210	3.15	7.3	167.2	-0.5	-5.0	27.8	16.6	-21.1	206.9	1.13	2.34	1.27	1.80	1.58	2.33	1.80	2.57
220	3.3	2.4	167.6	-16.2	-2.0	19.7	5.2	-23.8	174.7	1.59	2.48	1.39	0.94	2.40	2.20	1.09	1.23
230	3.45	-8.9	179.8	-2.4	-1.8	20.7	17.7	-39.1	222.2	2.33	1.57	1.71	1.78	0.93	2.46	2.97	1.79
250	3.75	-10.4	197.4	-4.0	4.1	18.5	17.2	-43.9	229.4	2.45	2.29	1.91	1.93	2.13	2.63	3.13	4.91
260	3.9	-11.2	203.4	-7.1	6.4	20.1	23.4	-40.2	229.2	3.64	3.00	1.98	2.22	2.84	2.13	1.67	4.75
270	4.05	-13.9	208.0	-12.1	12.6	20.6	18.7	-40.1	221.9	2.83	2.12	2.21	1.50	1.90	1.60	2.77	2.08
280	4.2	-11.1	211.2	-2.5	5.8	17.8	27.8	-41.4	273.4	2.04	2.76	2.14	1.90	2.35	3.10	2.84	2.78
290	4.35	-15.9	217.0	-15.7	28.5	13.7	22.6	-82.8	212.2	2.09	2.11	2.06	1.73	2.39	2.04	4.38	2.58

Table 19. Experimental dynamic stiffnesses at 4000 rpm and 513.8 kPa bearing unit loading

Ω	Ω/ω	Experiment															
		Dynamic stiffness								Uncertainty							
Hz		$Re(H_{xx})$	$Im(H_{xx})$	$Re(H_{xy})$	$Im(H_{xy})$	$Re(H_{yx})$	$Im(H_{yx})$	$Re(H_{yy})$	$Im(H_{yy})$	$Re(U_{xx})$	$Im(U_{xx})$	$Re(U_{xy})$	$Im(U_{xy})$	$Re(U_{yx})$	$Im(U_{yx})$	$Re(U_{yy})$	$Im(U_{yy})$
20	0.3	61.2	14.0	-12.6	-5.9	4.8	1.0	63.3	15.3	5.17	5.47	3.05	2.45	3.08	3.69	1.61	1.22
30	0.45	57.8	27.1	-8.7	-8.2	1.6	-3.7	66.6	23.4	1.46	2.65	0.95	0.96	2.34	1.39	0.49	1.01
40	0.6	54.6	33.1	-9.3	-9.3	3.3	-3.6	60.5	37.2	2.08	1.78	0.75	0.79	0.68	0.83	0.66	0.89
50	0.75	52.8	42.0	-9.2	-9.7	2.1	-6.2	57.3	49.7	3.29	2.52	1.45	1.10	1.74	2.79	0.79	1.16
70	1.05	37.8	55.6	-9.3	-9.2	22.6	-19.4	45.8	66.1	1.14	1.89	0.71	1.10	3.14	2.34	1.09	1.00
80	1.2	45.5	69.8	-7.4	-11.5	7.9	-6.0	27.5	82.3	1.15	1.50	0.47	0.90	1.02	1.27	1.00	0.86
90	1.35	44.5	78.7	-8.1	-13.9	7.2	-4.9	42.8	95.2	1.37	1.07	0.69	0.87	1.06	1.74	0.92	0.70
100	1.5	42.2	90.6	-7.6	-16.4	9.4	-5.8	36.0	105.0	0.93	0.96	0.54	0.48	1.56	0.76	0.85	1.57
110	1.65	41.5	99.8	-7.7	-17.2	9.4	-3.6	32.3	111.9	0.99	0.80	0.61	0.84	1.17	1.28	0.63	1.41
130	1.95	42.3	134.5	-6.0	-23.3	4.8	-13.6	25.7	137.4	4.12	3.37	2.96	2.36	2.52	2.31	2.57	2.41
140	2.1	36.6	133.9	-4.2	-17.6	16.9	-5.2	4.5	161.7	1.37	1.53	1.19	1.06	2.50	2.74	0.75	1.69
150	2.25	34.3	140.1	-3.6	-17.2	20.4	-3.1	24.1	176.7	1.61	1.37	1.21	0.85	1.65	1.40	1.82	1.16
160	2.4	33.9	150.4	-2.0	-21.6	18.1	0.9	20.1	198.2	2.41	1.11	1.71	1.13	2.08	2.47	1.97	1.07
170	2.55	35.2	162.3	-2.9	-15.4	21.3	-3.9	-1.4	202.7	2.13	3.90	2.52	2.02	3.40	3.67	4.37	3.09
190	2.85	33.2	179.1	1.8	-18.9	26.8	-5.5	16.6	221.2	2.95	2.71	3.24	2.34	3.93	2.90	3.57	3.38
200	3	38.7	191.3	1.6	-9.4	34.2	-2.2	-3.5	215.5	9.11	21.83	19.03	9.69	30.15	6.07	18.06	21.83
210	3.15	37.6	189.4	8.7	-13.0	37.7	3.5	-0.7	262.8	1.21	1.40	1.89	1.55	1.50	2.02	1.37	1.25
220	3.3	33.9	188.8	-7.8	-12.3	27.0	-8.0	0.4	227.6	1.57	0.96	1.87	1.44	1.14	1.47	1.29	1.42
230	3.45	22.7	199.2	6.3	-13.4	29.3	3.2	-22.0	282.5	0.97	1.36	1.21	1.42	1.36	1.75	3.04	3.20
250	3.75	25.3	216.0	3.2	-8.5	25.4	4.9	-12.1	289.0	1.92	1.67	1.35	1.52	1.76	1.44	2.05	2.90
260	3.9	25.8	222.0	2.4	-6.1	26.1	9.5	-13.2	294.1	1.42	2.72	2.21	1.49	3.28	1.95	2.98	2.75
270	4.05	26.9	224.4	-3.8	0.5	29.8	6.4	-6.4	281.3	1.79	1.64	2.97	2.71	1.81	2.39	4.48	3.95
280	4.2	25.7	226.1	8.9	-9.3	30.0	14.8	-16.0	350.0	1.60	1.44	1.35	2.04	1.69	1.69	4.10	2.31
290	4.35	23.6	233.1	-5.4	8.2	26.2	11.5	-23.1	293.4	0.86	1.46	1.28	1.18	1.08	2.10	1.83	1.93

Table 20. Experimental dynamic stiffnesses at 4000 rpm and 692.2 kPa bearing unit loading

Ω	Ω/ω	Experiment															
		Dynamic stiffness								Uncertainty							
Hz		$Re(H_{xx})$	$Im(H_{xx})$	$Re(H_{xy})$	$Im(H_{xy})$	$Re(H_{yx})$	$Im(H_{yx})$	$Re(H_{yy})$	$Im(H_{yy})$	$Re(U_{xx})$	$Im(U_{xx})$	$Re(U_{xy})$	$Im(U_{xy})$	$Re(U_{yx})$	$Im(U_{yx})$	$Re(U_{yy})$	$Im(U_{yy})$
20	0.3	84.1	21.0	-12.6	-6.9	-0.4	-1.2	93.2	23.9	6.48	10.00	4.38	2.84	5.18	3.12	2.81	1.79
30	0.45	75.3	30.9	-9.3	-10.6	-0.9	-5.8	95.9	29.9	4.21	4.82	1.05	1.60	2.63	2.49	1.21	1.16
40	0.6	75.3	39.2	-8.5	-11.2	1.7	-4.4	88.7	47.8	2.83	2.36	1.60	1.55	1.28	1.43	0.60	0.75
50	0.75	71.6	48.0	-8.9	-13.3	2.9	-9.8	85.3	60.4	1.36	2.93	0.92	1.12	1.97	2.51	1.43	1.09
70	1.05	55.7	66.1	-9.1	-11.6	24.1	-28.3	68.9	79.8	0.95	1.21	0.67	0.80	3.38	4.05	1.07	1.53
80	1.2	67.6	78.6	-6.0	-17.1	8.1	-12.0	65.4	103.2	1.66	1.02	0.61	0.54	1.76	1.53	1.36	0.76
90	1.35	67.9	88.6	-7.7	-19.3	10.0	-10.5	68.9	117.4	1.17	0.46	0.85	0.82	1.46	1.79	0.76	1.26
100	1.5	66.0	99.5	-5.6	-21.7	13.4	-11.6	61.1	129.8	1.20	0.82	0.70	0.95	1.26	2.04	0.98	1.53
110	1.65	65.2	110.4	-6.0	-23.6	12.6	-10.8	58.0	137.4	1.28	1.16	0.67	0.66	1.80	2.10	1.25	1.15
130	1.95	83.3	148.4	-8.4	-35.9	-2.0	-22.0	54.0	174.0	6.96	7.24	6.00	12.75	5.95	6.63	4.04	9.28
140	2.1	61.5	143.6	-0.9	-23.5	25.9	-15.2	29.0	199.5	1.54	1.73	2.17	1.51	2.62	3.20	2.09	2.48
150	2.25	62.4	152.5	-1.0	-26.9	24.6	-15.6	51.9	214.2	1.87	1.11	1.17	1.51	1.73	2.52	2.13	1.93
160	2.4	60.8	164.2	4.5	-35.2	28.0	-12.2	43.4	253.4	1.42	2.06	2.16	2.09	3.02	3.23	3.53	2.93
170	2.55	63.8	173.4	7.1	-24.4	27.5	-15.9	26.2	249.2	3.69	2.51	3.72	3.55	6.70	2.73	4.37	5.33
190	2.85	65.8	190.5	8.2	-28.9	33.0	-22.7	48.0	270.3	4.02	2.81	3.92	3.64	4.93	4.73	5.81	5.89
200	3	68.9	198.9	6.2	-24.1	34.3	-17.0	17.1	273.5	1.80	2.38	1.97	3.89	4.06	4.07	5.62	4.59
210	3.15	70.0	202.4	15.7	-30.1	45.0	-16.7	32.3	319.0	1.71	1.12	1.58	2.20	5.04	2.18	2.58	3.82
220	3.3	68.6	201.3	-1.9	-25.8	33.8	-26.0	31.6	280.3	1.88	2.04	1.99	1.53	2.62	1.71	1.72	3.25
230	3.45	57.6	211.2	16.0	-30.1	38.2	-13.6	6.6	345.9	1.52	1.41	2.36	2.67	2.17	2.98	2.23	2.46
250	3.75	59.2	224.4	10.4	-24.2	34.8	-12.4	28.1	343.6	1.68	0.72	1.74	1.31	2.13	2.19	3.45	2.40
260	3.9	61.7	228.5	5.9	-17.9	34.4	-8.7	24.4	340.9	2.75	2.61	2.97	3.62	4.85	4.13	5.60	6.70
270	4.05	61.4	230.7	2.7	-12.4	37.0	-11.7	31.0	334.5	1.03	0.82	1.46	3.28	2.49	1.55	3.11	4.06
280	4.2	60.0	230.6	24.1	-29.4	38.6	-2.0	8.3	438.4	1.33	1.55	2.59	1.76	1.62	2.20	3.36	5.25
290	4.35	58.9	236.8	5.2	-6.0	32.6	-7.3	15.0	359.9	1.13	2.20	1.83	2.21	2.13	1.53	3.14	3.13

Table 21. Experimental dynamic stiffnesses at 6000 rpm and 1.4 kPa bearing unit loading

Ω	Ω/ω	Experiment															
		Dynamic stiffness								Uncertainty							
Hz		$Re(H_{xx})$	$Im(H_{xx})$	$Re(H_{xy})$	$Im(H_{xy})$	$Re(H_{yx})$	$Im(H_{yx})$	$Re(H_{yy})$	$Im(H_{yy})$	$Re(U_{xx})$	$Im(U_{xx})$	$Re(U_{xy})$	$Im(U_{xy})$	$Re(U_{yx})$	$Im(U_{yx})$	$Re(U_{yy})$	$Im(U_{yy})$
20	0.2	35.1	10.5	-8.0	-3.3	9.6	2.1	38.8	15.3	0.93	0.30	0.17	0.26	0.47	0.65	0.22	0.29
30	0.3	33.7	16.3	-9.2	-4.3	10.1	2.5	42.4	18.7	0.59	0.50	0.22	0.17	0.34	0.63	0.27	0.36
40	0.4	31.9	22.6	-9.2	-6.3	10.3	3.1	39.0	24.8	0.30	0.41	0.15	0.14	0.61	0.49	0.37	0.41
50	0.5	29.7	29.7	-10.0	-7.6	10.3	2.8	36.8	32.3	0.52	0.45	0.24	0.30	1.16	1.05	0.62	0.60
70	0.7	25.7	42.8	-10.6	-7.5	11.0	4.8	31.6	44.7	0.69	0.74	0.36	0.40	1.49	1.22	0.55	0.64
80	0.8	24.5	50.1	-9.9	-9.2	10.1	5.5	30.5	55.4	0.38	0.59	0.26	0.20	0.74	0.85	0.62	0.61
90	0.9	23.0	55.4	-9.5	-7.6	10.6	8.5	25.5	60.8	0.28	0.47	0.27	0.29	0.40	0.71	0.37	0.42
100	1	19.6	51.0	-10.3	-5.4	37.5	2.5	17.0	64.0	13.50	7.45	3.78	4.13	20.43	26.55	8.48	8.16
110	1.1	17.5	68.1	-7.5	-8.7	12.6	9.9	20.4	74.0	0.46	0.45	0.39	0.42	0.37	0.83	0.39	0.53
130	1.3	9.6	81.4	-5.9	-8.7	12.9	11.2	14.9	86.8	0.53	0.39	0.36	0.34	0.77	0.59	0.79	0.36
140	1.4	5.9	86.8	-3.1	-11.0	13.0	13.8	7.7	96.9	0.74	0.57	0.41	0.43	0.62	0.79	0.35	0.67
150	1.5	1.6	92.7	-5.4	-11.3	13.2	17.3	7.9	105.6	0.72	0.43	0.63	0.54	0.82	0.80	0.51	0.71
160	1.6	-1.6	99.5	-2.6	-8.0	11.0	19.3	3.0	106.9	0.81	1.22	0.74	0.90	0.93	0.95	0.57	0.69
170	1.7	-3.6	108.9	-1.0	-10.7	13.9	23.1	-4.6	115.3	1.60	2.53	1.56	1.39	1.91	1.48	1.08	1.68
190	1.9	-13.5	120.9	-2.1	-11.4	20.2	28.5	-11.9	132.3	1.92	1.51	1.86	1.50	1.66	2.30	2.17	1.53
200	2	-0.7	137.5	5.3	-10.9	7.9	15.7	-20.6	135.7	23.79	59.86	27.89	13.21	17.43	54.92	23.13	13.43
210	2.1	-16.9	127.8	1.8	-11.9	24.4	34.9	-19.9	148.9	1.30	1.48	1.30	0.97	1.04	1.56	1.04	0.89
220	2.2	-24.1	125.1	-10.1	-10.3	20.3	28.4	-22.3	138.5	0.99	1.22	0.89	1.02	1.18	1.07	0.97	0.91
230	2.3	-38.8	136.3	-5.2	-3.5	20.0	38.0	-40.0	151.1	0.63	0.82	0.96	0.80	1.06	0.65	1.03	1.10
250	2.5	-46.0	150.4	-5.0	-0.5	23.2	41.0	-45.1	171.6	0.46	1.06	0.66	0.70	0.78	0.71	0.68	0.72
260	2.6	-48.4	155.1	-5.9	3.7	24.8	44.2	-46.5	178.9	0.95	1.06	0.93	0.90	1.07	1.14	0.97	1.12
270	2.7	-52.9	159.3	-7.1	5.6	28.0	45.3	-51.0	188.6	0.96	1.19	1.14	0.51	0.81	0.80	1.24	1.54
280	2.8	-56.6	162.1	-3.8	8.9	24.9	45.8	-58.0	191.8	0.78	1.09	1.02	0.76	0.93	0.95	1.06	1.41
290	2.9	-63.0	168.3	-5.7	13.3	25.0	45.5	-62.7	195.1	1.13	1.66	1.26	0.69	1.35	1.20	1.05	1.80

Table 22. Experimental dynamic stiffnesses at 6000 rpm and 175.9 kPa bearing unit loading

Ω	Ω/ω	Experiment															
		Dynamic stiffness								Uncertainty							
Hz		$Re(H_{xx})$	$Im(H_{xx})$	$Re(H_{xy})$	$Im(H_{xy})$	$Re(H_{yx})$	$Im(H_{yx})$	$Re(H_{yy})$	$Im(H_{yy})$	$Re(U_{xx})$	$Im(U_{xx})$	$Re(U_{xy})$	$Im(U_{xy})$	$Re(U_{yx})$	$Im(U_{yx})$	$Re(U_{yy})$	$Im(U_{yy})$
20	0.2	38.9	11.8	-10.9	-3.1	7.4	1.5	44.4	10.8	0.88	0.53	0.27	0.20	0.67	0.47	0.38	0.24
30	0.3	37.0	18.6	-11.3	-4.8	7.6	1.3	43.8	16.4	0.50	0.54	0.15	0.34	0.44	0.62	0.24	0.34
40	0.4	35.6	25.2	-11.6	-6.4	7.6	2.0	39.9	25.1	0.35	0.34	0.16	0.21	0.48	0.58	0.30	0.37
50	0.5	34.1	33.4	-12.2	-7.8	7.3	1.5	37.7	32.1	0.61	0.66	0.22	0.35	1.18	0.89	0.40	0.54
70	0.7	30.8	46.2	-12.5	-8.2	9.1	3.1	30.7	45.9	0.72	0.58	0.32	0.42	1.53	1.01	0.65	0.71
80	0.8	29.4	53.8	-11.1	-10.3	9.7	5.0	40.7	66.6	0.54	0.30	0.30	0.30	0.76	0.95	0.48	0.54
90	0.9	27.1	58.9	-11.3	-8.1	10.1	5.9	26.3	63.3	0.60	0.40	0.36	0.31	0.68	0.79	0.42	0.42
100	1	19.2	57.6	-12.5	-8.3	29.1	-0.2	21.4	67.5	0.91	0.40	0.46	0.43	1.01	1.27	0.82	0.60
110	1.1	21.8	73.0	-9.3	-10.2	12.1	6.7	20.2	75.7	0.56	0.58	0.37	0.29	0.71	0.62	0.45	0.34
130	1.3	13.6	87.9	-7.6	-11.3	12.1	7.4	13.0	88.6	0.52	0.47	0.40	0.38	0.51	0.64	0.40	0.45
140	1.4	9.8	95.1	-5.3	-11.8	12.7	9.7	3.0	98.4	0.76	0.75	0.32	0.48	0.90	0.80	0.69	0.69
150	1.5	7.5	100.7	-6.2	-12.5	12.9	11.4	1.8	103.9	1.00	0.84	0.60	0.65	0.97	0.78	0.59	0.66
160	1.6	4.1	108.0	-4.0	-14.0	11.5	16.5	9.5	117.5	0.94	1.49	0.80	0.84	1.26	0.85	0.99	0.66
170	1.7	1.2	115.5	-4.1	-14.8	11.7	16.7	-6.8	121.4	2.19	2.04	1.20	1.69	2.28	1.52	1.36	1.48
190	1.9	-9.5	129.8	-4.7	-15.2	18.7	21.3	-15.2	134.0	2.44	2.67	1.80	2.06	2.40	2.71	1.63	1.99
200	2	-15.8	141.6	-0.8	-11.8	19.9	19.2	-26.2	132.5	3.19	4.13	1.78	2.52	2.24	3.48	1.80	1.87
210	2.1	-13.9	138.7	-3.5	-12.1	23.3	29.3	-30.8	148.3	1.43	0.97	0.78	0.85	1.08	1.27	0.95	1.35
220	2.2	-18.7	137.8	-15.2	-1.0	16.9	22.8	-72.3	137.7	1.34	1.33	1.46	0.89	1.74	0.77	3.41	3.10
230	2.3	-33.7	147.6	-7.1	-7.7	22.1	33.5	-40.5	166.6	1.13	0.96	0.71	0.78	0.80	1.17	1.06	0.97
250	2.5	-40.0	162.9	-8.8	-1.6	22.5	33.9	-52.4	175.2	0.95	0.71	0.56	0.63	0.74	0.93	0.74	1.38
260	2.6	-44.3	168.5	-8.1	2.2	24.9	33.8	-63.9	190.0	1.16	0.94	0.52	1.07	1.04	1.21	1.48	1.49
270	2.7	-46.7	173.7	-11.8	2.2	20.0	38.5	-61.0	197.2	1.17	0.69	1.12	0.78	1.28	1.43	1.10	0.52
280	2.8	-50.4	177.4	-12.2	8.1	20.9	39.1	-67.4	194.8	0.97	0.91	1.09	0.70	0.91	1.00	1.41	1.59
290	2.9	-55.5	183.8	-8.2	18.5	20.3	42.5	-89.7	221.2	1.50	1.41	1.22	1.74	1.92	1.62	2.67	1.93

Table 23. Experimental dynamic stiffnesses at 6000 rpm and 348.4 kPa bearing unit loading

Ω	Ω/ω	Experiment															
		Dynamic stiffness								Uncertainty							
Hz		$Re(H_{xx})$	$Im(H_{xx})$	$Re(H_{xy})$	$Im(H_{xy})$	$Re(H_{yx})$	$Im(H_{yx})$	$Re(H_{yy})$	$Im(H_{yy})$	$Re(U_{xx})$	$Im(U_{xx})$	$Re(U_{xy})$	$Im(U_{xy})$	$Re(U_{yx})$	$Im(U_{yx})$	$Re(U_{yy})$	$Im(U_{yy})$
20	0.2	43.3	12.6	-5.8	-2.1	12.1	2.5	45.6	10.5	0.73	1.08	0.20	0.26	1.14	1.23	0.51	0.45
30	0.3	42.3	19.9	-6.2	-4.1	10.9	1.9	47.4	16.0	0.54	0.56	0.28	0.33	0.94	0.73	0.24	0.24
40	0.4	41.5	25.7	-7.2	-4.2	11.3	3.0	43.5	25.5	0.38	0.43	0.20	0.28	0.75	0.61	0.28	0.32
50	0.5	39.9	33.6	-7.6	-4.8	10.2	1.7	41.5	33.1	0.92	0.82	0.25	0.35	1.26	1.06	0.45	0.55
70	0.7	38.4	44.3	-8.7	-4.1	13.3	3.6	34.9	46.7	0.99	0.83	0.35	0.35	1.68	1.32	0.45	0.65
80	0.8	37.1	53.1	-3.6	-4.3	9.1	4.0	16.7	98.1	0.45	0.50	0.46	0.49	1.16	0.73	1.47	0.80
90	0.9	34.7	58.9	-7.6	-3.1	11.7	5.7	33.5	66.1	0.53	0.50	0.26	0.31	0.59	0.79	0.40	0.39
100	1	27.3	58.5	-12.6	-8.7	28.8	-0.9	38.7	65.7	5.82	19.49	5.72	10.43	34.33	9.35	19.12	9.03
110	1.1	30.0	74.0	-6.5	-4.6	11.7	7.1	27.5	76.9	0.65	0.64	0.34	0.35	0.79	1.10	0.53	0.47
130	1.3	23.6	88.8	-6.6	-4.5	11.9	7.9	21.4	88.5	0.60	0.55	0.47	0.64	0.75	0.56	0.31	0.32
140	1.4	19.8	96.6	-4.4	-3.4	13.2	12.8	11.1	103.2	1.12	0.96	0.72	0.84	0.82	0.88	0.98	0.77
150	1.5	18.7	101.5	-5.3	-5.5	13.4	13.7	16.1	108.3	1.05	0.78	0.74	0.55	1.04	0.66	0.74	0.65
160	1.6	16.8	110.7	-4.7	-6.2	10.5	18.1	19.7	124.3	1.39	1.50	1.09	1.06	1.22	1.38	0.62	1.11
170	1.7	15.9	118.6	-4.4	-4.7	10.0	17.6	4.0	125.9	2.05	2.40	1.28	2.51	2.29	1.74	1.36	1.58
190	1.9	8.2	131.3	-6.9	-4.9	16.0	22.3	1.8	138.2	2.50	2.97	1.13	1.96	1.85	2.29	1.46	2.02
200	2	-38.9	139.0	-20.7	-4.1	44.0	22.9	-1.9	139.1	80.45	81.34	59.23	45.22	53.28	53.87	39.09	30.48
210	2.1	5.8	140.7	-6.5	-1.5	20.1	32.0	-12.6	157.6	1.53	1.07	1.43	1.03	1.36	1.50	1.37	1.02
220	2.2	0.2	140.4	-20.2	2.6	14.4	21.3	-22.9	135.5	1.30	0.78	0.67	0.95	1.31	0.96	0.85	0.86
230	2.3	-11.3	151.7	-11.2	3.5	15.2	35.8	-25.6	174.5	1.01	0.77	1.01	0.72	1.43	1.34	1.11	0.57
250	2.5	-15.2	166.9	-12.5	9.5	15.4	36.9	-33.1	184.9	0.96	1.15	0.83	0.89	1.27	1.73	1.16	1.27
260	2.6	-16.3	171.5	-15.0	15.2	15.6	40.8	-39.3	186.0	0.87	1.19	0.85	0.72	1.13	1.31	1.32	1.32
270	2.7	-20.3	176.5	-18.6	19.7	18.7	37.5	-44.2	181.2	1.12	0.64	0.98	0.79	0.98	0.90	1.06	0.76
280	2.8	-21.9	178.6	-12.2	16.3	15.3	47.3	-39.5	216.3	1.08	1.07	0.65	1.06	1.23	1.16	1.01	1.03
290	2.9	-28.8	187.3	-19.3	32.4	10.9	38.6	-88.7	179.7	1.29	0.93	1.03	0.87	1.52	0.86	1.11	1.76

Table 24. Experimental dynamic stiffnesses at 6000 rpm and 513.8 kPa bearing unit loading

Ω	Ω/ω	Experiment															
		Dynamic stiffness								Uncertainty							
Hz		$Re(H_{xx})$	$Im(H_{xx})$	$Re(H_{xy})$	$Im(H_{xy})$	$Re(H_{yx})$	$Im(H_{yx})$	$Re(H_{yy})$	$Im(H_{yy})$	$Re(U_{xx})$	$Im(U_{xx})$	$Re(U_{xy})$	$Im(U_{xy})$	$Re(U_{yx})$	$Im(U_{yx})$	$Re(U_{yy})$	$Im(U_{yy})$
20	0.2	57.8	12.2	-8.7	-2.8	9.0	1.6	62.1	13.1	1.64	1.69	0.55	0.51	1.86	2.14	0.79	0.91
30	0.3	56.1	20.2	-8.3	-4.7	9.8	0.9	64.7	18.0	1.22	1.48	0.50	0.54	0.78	1.57	0.46	0.74
40	0.4	55.0	29.1	-8.7	-5.3	8.3	1.3	60.4	30.2	0.89	1.37	0.49	0.61	0.46	1.20	0.50	0.60
50	0.5	55.4	36.9	-9.3	-6.2	9.0	0.8	58.6	39.9	1.07	1.06	0.47	0.58	0.84	0.75	0.36	0.63
70	0.7	52.8	50.0	-9.4	-6.2	12.5	2.6	52.0	54.0	0.52	0.66	0.36	0.25	0.86	0.70	0.27	0.48
80	0.8	51.5	57.8	-6.9	-4.2	9.4	1.7	31.7	69.3	0.65	0.74	0.25	0.21	0.57	0.62	0.61	0.46
90	0.9	49.1	63.8	-8.3	-5.5	12.0	3.7	49.8	77.7	0.41	0.31	0.41	0.32	0.41	0.52	0.57	0.46
100	1	35.8	63.5	-11.7	-4.1	35.7	-14.1	44.2	77.8	1.07	1.31	0.69	1.04	2.25	2.46	1.68	1.42
110	1.1	43.9	79.6	-7.0	-7.5	12.9	3.5	43.5	88.8	0.46	0.50	0.34	0.30	0.71	0.86	0.48	0.62
130	1.3	38.4	97.3	-6.5	-8.0	12.2	3.4	38.6	102.8	0.51	0.70	0.59	0.37	0.76	0.51	0.59	0.55
140	1.4	35.8	105.2	-4.0	-6.1	14.7	6.9	23.7	122.1	0.88	0.60	0.60	0.48	0.87	1.17	0.85	0.99
150	1.5	34.1	112.4	-3.0	-8.2	14.9	10.2	33.7	128.0	0.48	0.69	0.77	0.72	0.94	0.93	0.41	0.67
160	1.6	33.0	120.1	-2.0	-11.9	13.1	13.9	38.6	149.8	0.69	1.08	0.91	0.96	1.67	0.86	0.92	1.05
170	1.7	33.2	130.7	-1.5	-7.5	15.7	12.7	15.8	148.8	1.06	1.44	1.15	1.62	1.92	1.42	1.52	1.13
190	1.9	25.2	144.5	-3.9	-10.3	20.7	17.3	17.2	162.3	1.44	1.89	1.17	1.32	1.13	1.97	1.48	1.99
200	2	19.5	171.0	0.2	-10.2	22.5	4.3	-3.7	166.6	6.77	6.27	4.14	7.12	3.82	4.54	3.63	4.44
210	2.1	26.2	155.6	-2.2	-6.4	29.0	24.1	2.5	190.9	1.61	1.09	1.31	1.86	0.78	1.50	0.62	1.50
220	2.2	20.4	154.9	-15.9	-3.8	21.8	14.7	-3.0	166.5	1.16	1.11	1.06	1.01	1.29	0.57	1.42	1.19
230	2.3	8.8	166.0	-6.6	-2.3	22.7	28.5	-12.9	208.6	0.75	0.63	1.08	0.84	1.14	0.69	0.73	1.01
250	2.5	6.0	182.4	-8.3	6.1	22.5	28.7	-18.8	214.0	0.38	0.79	0.83	0.98	1.24	1.27	1.06	1.33
260	2.6	5.2	187.6	-10.0	9.3	23.6	32.2	-20.8	220.1	0.98	1.24	1.13	0.67	1.04	1.46	0.72	1.04
270	2.7	2.5	191.8	-11.9	13.0	27.4	30.3	-21.2	218.7	0.70	0.78	0.99	0.90	1.20	1.33	1.10	1.30
280	2.8	0.9	194.7	-2.8	9.0	23.3	40.0	-23.1	265.9	0.86	0.65	1.46	1.15	1.18	1.08	1.39	1.42
290	2.9	-4.1	203.3	-13.1	20.3	22.5	33.1	-37.7	227.6	1.36	1.06	0.83	0.61	1.08	1.25	1.39	1.23

Table 25. Experimental dynamic stiffnesses at 6000 rpm and 692.2 kPa bearing unit loading

Ω	Ω/ω	Experiment															
		Dynamic stiffness								Uncertainty							
Hz		$Re(H_{xx})$	$Im(H_{xx})$	$Re(H_{xy})$	$Im(H_{xy})$	$Re(H_{yx})$	$Im(H_{yx})$	$Re(H_{yy})$	$Im(H_{yy})$	$Re(U_{xx})$	$Im(U_{xx})$	$Re(U_{xy})$	$Im(U_{xy})$	$Re(U_{yx})$	$Im(U_{yx})$	$Re(U_{yy})$	$Im(U_{yy})$
20	0.2	72.9	15.8	-8.5	-3.9	6.8	0.5	85.8	17.6	4.01	3.27	1.16	0.99	1.54	2.13	1.07	0.87
30	0.3	73.0	25.9	-8.5	-5.9	6.3	-1.2	89.5	22.1	2.16	1.76	1.05	1.44	1.46	1.86	1.31	0.71
40	0.4	72.2	33.3	-8.7	-7.2	6.0	-0.7	84.1	37.1	1.03	1.48	0.69	0.51	1.02	1.26	1.16	0.86
50	0.5	73.1	41.4	-9.8	-8.9	7.0	-0.7	82.8	47.7	1.81	1.43	0.71	0.71	1.71	2.02	0.96	1.38
70	0.7	70.3	55.3	-9.6	-9.7	10.9	-1.0	75.3	64.5	1.59	0.99	0.63	0.57	2.41	1.80	1.65	1.02
80	0.8	68.6	63.4	-6.8	-9.4	10.3	-3.3	67.9	82.8	1.02	0.84	0.45	0.50	1.33	1.15	0.98	0.96
90	0.9	67.8	70.9	-8.0	-10.0	12.6	-0.1	73.7	92.9	1.11	0.59	0.36	0.78	1.32	0.63	0.81	1.03
100	1	47.9	65.2	-10.5	-1.4	50.3	-25.6	55.3	87.5	4.38	14.32	6.44	16.62	19.90	16.62	30.11	15.55
110	1.1	62.2	88.1	-6.4	-13.0	13.3	-2.0	65.6	105.0	0.97	0.99	0.55	0.52	0.83	1.18	0.78	1.00
130	1.3	57.5	106.7	-4.9	-14.1	14.1	-2.8	58.1	124.6	1.24	0.65	0.91	0.74	0.76	0.93	1.38	0.84
140	1.4	54.7	115.9	-2.2	-13.1	18.4	-0.7	44.8	145.1	1.37	1.29	0.73	0.84	1.53	1.03	1.33	1.06
150	1.5	53.8	123.0	-2.1	-15.1	17.6	1.5	55.4	150.7	0.87	1.41	0.95	0.88	0.57	1.22	0.79	1.02
160	1.6	53.4	131.9	0.7	-21.4	18.5	6.4	60.1	185.3	1.56	0.98	1.20	1.47	1.06	2.38	1.58	1.90
170	1.7	51.9	142.2	0.2	-16.6	18.8	5.8	33.7	178.3	2.19	2.82	2.10	1.64	3.25	2.41	2.48	2.09
190	1.9	48.1	156.6	-2.1	-18.0	24.7	6.2	35.7	192.4	2.98	2.21	2.04	2.46	2.51	2.33	3.44	1.90
200	2	55.1	165.2	-3.7	8.2	20.9	11.3	17.6	180.4	40.01	45.04	50.96	38.83	27.37	34.48	34.51	30.21
210	2.1	47.5	169.4	1.3	-14.0	35.1	12.6	23.7	225.1	1.80	1.26	1.87	0.74	1.62	2.36	2.01	3.24
220	2.2	43.3	168.6	-11.9	-9.7	28.4	3.9	17.0	201.3	1.21	1.32	1.36	1.03	1.28	1.15	1.85	2.48
230	2.3	32.6	179.4	-1.7	-10.8	31.1	16.9	2.8	252.1	1.28	1.20	1.30	0.59	0.99	1.52	1.39	2.37
250	2.5	30.1	196.1	-3.6	-2.6	30.8	15.9	2.5	254.9	1.16	1.19	1.37	1.09	1.67	1.04	1.45	2.70
260	2.6	30.5	202.0	-4.8	4.3	31.2	19.3	-2.9	256.7	1.32	0.97	1.10	1.60	1.82	1.66	1.01	2.51
270	2.7	27.9	206.1	-4.6	7.7	33.9	16.5	0.3	259.5	1.34	0.85	1.46	1.08	1.24	1.58	1.18	2.52
280	2.8	27.2	208.8	9.5	-1.2	32.1	28.3	-8.7	331.9	1.26	1.34	1.67	1.51	0.90	1.83	1.72	3.98
290	2.9	23.0	215.8	-2.6	12.4	29.9	22.3	-13.7	279.6	1.57	1.07	1.37	1.21	1.88	1.80	2.26	1.97

Table 26. Experimental dynamic stiffnesses at 6000 rpm and 1038.2 kPa bearing unit loading

Ω	Ω/ω	Experiment															
		Dynamic stiffness								Uncertainty							
Hz		$Re(H_{xx})$	$Im(H_{xx})$	$Re(H_{xy})$	$Im(H_{xy})$	$Re(H_{yx})$	$Im(H_{yx})$	$Re(H_{yy})$	$Im(H_{yy})$	$Re(U_{xx})$	$Im(U_{xx})$	$Re(U_{xy})$	$Im(U_{xy})$	$Re(U_{yx})$	$Im(U_{yx})$	$Re(U_{yy})$	$Im(U_{yy})$
20	0.2	106.7	13.5	-13.1	-8.0	-1.1	-1.6	143.5	29.4	8.98	8.86	4.86	2.99	4.23	6.32	2.42	2.05
30	0.3	105.0	27.5	-12.7	-7.4	-2.1	-3.8	152.0	32.9	4.59	3.41	2.28	1.26	3.40	3.03	2.09	1.37
40	0.4	107.7	37.8	-13.4	-11.6	0.2	-3.6	146.3	52.8	2.53	1.30	1.07	1.42	2.83	2.51	2.03	2.26
50	0.5	107.7	46.6	-13.2	-12.9	-3.8	-7.4	145.8	66.5	4.19	2.28	1.45	2.20	6.78	5.31	3.34	3.80
70	0.7	108.2	62.6	-12.1	-16.8	10.8	-7.2	135.9	86.1	2.90	3.79	1.72	0.97	6.31	7.23	3.96	2.63
80	0.8	106.5	73.8	-9.6	-21.4	6.6	-7.9	136.4	126.7	1.71	0.91	1.27	1.06	4.61	2.13	2.51	3.26
90	0.9	101.9	80.3	-10.1	-18.9	12.1	-14.6	132.7	122.2	2.27	1.59	1.21	0.88	4.74	4.90	2.56	2.59
100	1	75.3	83.9	-14.0	-7.4	51.0	-55.2	107.3	112.0	3.90	7.65	3.42	2.23	13.10	10.31	5.82	5.25
110	1.1	101.3	99.9	-9.2	-23.5	14.9	-13.7	123.1	137.4	1.49	0.76	1.37	0.86	2.87	1.54	1.06	1.41
130	1.3	99.2	118.8	-7.0	-24.9	15.9	-13.7	109.5	158.9	0.95	0.98	1.15	1.11	1.39	1.65	1.53	1.83
140	1.4	96.9	128.8	-2.1	-27.9	19.8	-16.8	100.8	191.5	2.03	1.30	1.14	1.40	2.69	2.13	1.54	2.01
150	1.5	96.7	135.2	-3.4	-29.7	23.5	-13.9	112.6	195.0	1.05	1.05	1.12	1.18	1.91	1.75	1.15	1.58
160	1.6	96.2	142.6	5.9	-40.4	27.3	-8.4	101.7	259.4	1.17	1.49	1.08	1.29	1.68	2.37	4.08	3.48
170	1.7	96.5	153.8	2.3	-34.8	27.2	-15.8	90.4	234.2	1.63	1.35	2.16	1.68	2.87	2.79	4.35	2.71
190	1.9	96.5	180.3	-2.6	-39.8	27.2	-25.1	94.9	252.0	4.84	10.60	5.52	4.02	3.92	9.49	3.72	5.35
200	2	96.4	201.6	3.3	-32.0	30.6	-34.5	67.3	257.5	15.75	15.00	12.57	19.55	12.33	10.37	10.94	16.85
210	2.1	92.7	183.0	1.2	-33.1	43.8	-18.7	84.1	286.1	2.29	3.28	1.65	2.39	2.01	3.67	3.25	4.39
220	2.2	90.0	181.3	-11.4	-24.9	34.8	-23.6	72.6	255.7	1.61	1.66	1.14	1.02	2.72	1.35	2.60	2.92
230	2.3	77.5	190.3	6.4	-31.9	40.3	-10.8	50.4	336.0	1.28	0.87	1.56	1.51	1.69	1.54	2.58	3.20
250	2.5	74.5	206.1	6.0	-18.0	38.1	-13.5	47.6	326.7	1.09	1.04	1.03	1.67	2.05	2.43	2.15	3.14
260	2.6	75.9	211.6	6.8	-12.1	37.0	-9.7	50.4	330.9	1.38	1.19	0.96	1.79	1.60	1.67	2.11	3.83
270	2.7	74.4	215.4	7.9	-9.9	39.1	-11.7	53.3	331.2	1.27	1.60	1.40	1.09	1.34	1.92	3.30	3.13
280	2.8	73.3	215.8	40.7	-24.3	36.2	2.3	-4.9	467.4	1.18	1.02	1.68	1.82	1.41	1.96	6.87	6.82
290	2.9	69.8	224.3	13.0	-6.6	37.0	-5.7	40.8	360.9	1.92	1.40	1.48	1.54	1.65	2.98	4.78	3.09

Table 27. Experimental dynamic stiffnesses at 8000 rpm and 1.4 kPa bearing unit loading

Ω	Ω/ω	Experiment															
		Dynamic stiffness								Uncertainty							
Hz		$Re(H_{xx})$	$Im(H_{xx})$	$Re(H_{xy})$	$Im(H_{xy})$	$Re(H_{yx})$	$Im(H_{yx})$	$Re(H_{yy})$	$Im(H_{yy})$	$Re(U_{xx})$	$Im(U_{xx})$	$Re(U_{xy})$	$Im(U_{xy})$	$Re(U_{yx})$	$Im(U_{yx})$	$Re(U_{yy})$	$Im(U_{yy})$
20	0.15	45.9	10.6	-11.3	-3.0	11.1	2.1	52.2	12.5	0.63	1.49	0.41	0.27	0.54	0.63	0.37	0.34
30	0.23	43.6	16.7	-11.9	-4.2	12.5	1.4	52.0	17.7	0.83	0.59	0.35	0.31	0.68	1.21	0.50	0.42
40	0.30	42.2	22.8	-11.6	-6.8	12.6	2.8	49.7	24.9	0.71	0.54	0.17	0.27	0.70	0.63	0.47	0.35
50	0.38	40.3	30.6	-12.6	-8.6	12.3	2.1	47.9	32.1	0.90	0.82	0.30	0.42	1.72	2.05	0.58	0.58
70	0.53	34.9	43.9	-13.5	-9.3	13.3	3.0	43.7	44.9	0.83	0.74	0.56	0.41	1.62	1.56	1.02	0.85
80	0.60	33.4	52.1	-13.6	-10.9	11.8	2.8	41.2	53.9	0.46	0.62	0.23	0.28	0.80	0.84	0.67	0.35
90	0.68	33.0	58.9	-13.1	-9.4	11.5	5.7	36.8	59.1	0.74	0.75	0.26	0.36	0.49	0.77	0.40	0.66
100	0.75	30.2	66.0	-10.8	-10.2	13.1	6.4	34.2	67.3	0.55	0.74	0.23	0.46	0.99	0.53	0.41	0.42
110	0.83	28.8	71.3	-10.4	-9.4	12.6	8.7	30.5	73.0	0.45	0.61	0.32	0.33	0.44	0.97	0.46	0.28
130	0.98	22.7	71.6	-12.8	-10.5	38.2	5.6	23.8	79.3	0.84	1.17	0.52	0.53	2.38	0.98	0.58	0.64
140	1.05	21.2	80.4	-8.3	-12.7	35.4	13.4	19.3	92.3	0.89	1.95	0.88	0.51	3.65	0.97	0.49	0.95
150	1.13	15.6	94.2	-7.0	-13.0	18.9	15.6	19.5	101.6	0.46	0.77	0.63	0.58	0.50	1.19	0.60	0.51
160	1.20	14.5	101.4	-2.7	-11.3	16.3	16.4	15.7	107.1	1.31	1.07	0.71	0.92	1.16	1.27	0.73	0.73
170	1.28	10.0	110.0	-2.6	-14.2	15.9	19.6	10.2	114.1	2.09	2.50	1.49	1.49	2.06	2.15	1.57	1.26
190	1.43	-0.3	117.5	-1.3	-13.4	15.4	22.0	4.6	127.1	2.41	2.21	1.54	1.54	2.15	1.80	1.19	1.41
200	1.50	-2.9	123.3	1.8	-12.4	15.9	25.4	0.6	130.0	1.34	1.27	0.76	1.17	1.14	1.24	0.87	1.07
210	1.58	-5.7	125.2	4.6	-15.1	17.9	30.4	-2.9	138.3	1.51	1.02	0.56	0.64	0.83	1.11	0.68	0.44
220	1.65	-13.6	122.6	-5.6	-14.9	12.4	26.3	-8.7	128.0	0.91	1.12	0.82	0.61	1.04	1.10	0.52	0.63
230	1.73	-28.5	132.7	-0.1	-10.4	12.4	37.6	-27.5	142.1	0.90	0.79	0.60	0.38	0.93	0.88	0.72	0.58
250	1.88	-39.0	145.2	-0.3	-11.9	14.7	44.2	-34.4	160.3	0.64	0.91	0.74	0.53	1.04	0.61	0.83	0.68
260	1.95	-44.1	150.5	-0.7	-8.8	17.4	49.9	-39.8	168.2	1.31	1.29	1.01	0.91	1.78	1.02	1.16	1.09
270	2.03	-55.1	157.5	-0.2	-5.6	25.1	51.4	-46.7	174.7	1.97	2.41	2.91	1.58	2.37	1.90	3.08	1.87
280	2.10	-54.3	159.2	-4.2	-6.5	19.9	55.5	-50.7	183.0	1.43	1.16	0.54	0.95	1.51	0.96	0.94	0.73
290	2.18	-59.9	165.9	-6.5	-2.8	19.7	57.7	-55.8	188.4	0.97	1.07	0.81	0.78	0.82	1.12	0.62	0.83

Table 28. Experimental dynamic stiffnesses at 8000 rpm and 175.9 kPa bearing unit loading

Ω	Ω/ω	Experiment															
		Dynamic stiffness								Uncertainty							
Hz		$Re(H_{xx})$	$Im(H_{xx})$	$Re(H_{xy})$	$Im(H_{xy})$	$Re(H_{yx})$	$Im(H_{yx})$	$Re(H_{yy})$	$Im(H_{yy})$	$Re(U_{xx})$	$Im(U_{xx})$	$Re(U_{xy})$	$Im(U_{xy})$	$Re(U_{yx})$	$Im(U_{yx})$	$Re(U_{yy})$	$Im(U_{yy})$
20	0.15	48.5	11.0	-14.9	0.0	8.5	2.5	57.7	9.0	1.00	0.59	0.52	0.45	0.77	0.60	0.51	0.50
30	0.23	47.3	18.0	-14.2	-2.5	9.3	1.2	57.7	14.0	0.82	0.76	0.31	0.37	0.62	0.73	0.43	0.44
40	0.30	45.4	25.2	-14.1	-5.2	9.5	2.3	52.9	23.9	0.48	0.36	0.25	0.20	0.89	1.03	0.38	0.49
50	0.38	44.6	33.1	-14.5	-7.2	9.6	1.2	50.4	30.7	0.74	0.72	0.39	0.43	1.85	1.29	0.69	0.72
70	0.53	39.9	47.0	-15.3	-8.8	10.3	3.1	43.4	44.0	0.95	1.00	0.46	0.43	1.51	1.66	0.80	0.85
80	0.60	38.9	55.2	-14.6	-11.0	10.1	4.4	55.4	65.9	0.48	0.72	0.31	0.36	1.20	0.90	0.95	0.43
90	0.68	38.1	60.8	-14.4	-8.8	10.3	6.1	38.8	62.7	0.62	0.43	0.19	0.37	1.04	0.76	0.58	0.55
100	0.75	35.3	68.2	-12.3	-9.2	11.8	5.5	36.7	70.9	0.72	0.40	0.30	0.44	0.76	0.69	0.46	0.52
110	0.83	33.6	74.6	-11.8	-10.0	11.5	7.5	33.4	75.8	0.75	0.96	0.41	0.43	0.73	0.59	0.28	0.45
130	0.98	23.7	72.9	-15.7	-12.4	37.5	1.7	28.3	81.4	2.49	1.01	1.14	1.63	1.60	3.82	2.24	1.03
140	1.05	23.4	94.2	-7.4	-11.2	17.1	12.3	16.3	100.0	1.08	1.21	0.51	0.69	1.80	1.06	0.51	1.15
150	1.13	19.0	100.7	-7.0	-12.5	16.2	13.2	17.2	105.6	1.08	1.01	0.59	0.63	0.75	0.95	0.56	1.19
160	1.20	17.7	107.6	-4.9	-14.4	15.8	14.8	25.1	118.0	1.17	1.39	0.96	0.74	1.05	1.28	0.87	0.82
170	1.28	15.4	115.8	-3.8	-14.3	16.3	15.1	13.8	121.9	2.60	1.96	1.49	1.59	2.26	2.33	1.41	1.15
190	1.43	5.6	125.8	-2.4	-13.4	15.9	17.6	4.1	128.3	2.22	2.69	1.70	2.00	1.81	2.73	1.75	1.64
200	1.50	2.4	130.6	-1.6	-12.2	14.5	20.4	-5.8	127.4	1.19	1.31	0.99	0.83	1.56	1.52	0.76	1.76
210	1.58	0.2	132.8	2.7	-12.5	18.5	25.7	-12.3	139.1	1.57	1.03	0.71	0.57	1.70	1.44	0.74	1.50
220	1.65	-8.0	130.3	-7.5	-7.4	10.6	20.6	-49.9	127.4	0.61	1.19	0.78	1.20	1.62	1.51	1.54	2.77
230	1.73	-22.1	139.9	-0.6	-13.3	13.2	34.8	-26.3	154.8	1.08	0.90	0.79	0.59	0.80	1.41	1.05	0.83
250	1.88	-32.1	153.2	-3.0	-10.6	15.8	40.1	-40.5	165.5	1.01	1.12	1.05	0.87	1.12	1.19	1.28	1.73
260	1.95	-52.4	159.1	4.7	-6.7	31.0	44.8	-59.8	172.9	7.48	4.11	5.29	4.72	6.26	3.15	4.26	3.30
270	2.03	-43.0	164.4	-5.5	-8.4	17.5	44.5	-54.2	187.0	2.14	1.38	1.73	1.37	1.48	1.20	1.76	0.86
280	2.10	-48.4	167.4	-9.9	-2.3	21.0	48.3	-59.9	186.1	1.61	1.01	0.68	0.89	1.31	0.90	1.22	1.82
290	2.18	-54.7	173.8	-7.7	3.5	19.5	48.0	-75.4	209.1	1.23	1.12	1.23	1.23	1.77	1.33	2.75	1.66

Table 29. Experimental dynamic stiffnesses at 8000 rpm and 348.4 kPa bearing unit loading

Ω	Ω/ω	Experiment															
		Dynamic stiffness								Uncertainty							
Hz		$Re(H_{xx})$	$Im(H_{xx})$	$Re(H_{xy})$	$Im(H_{xy})$	$Re(H_{yx})$	$Im(H_{yx})$	$Re(H_{yy})$	$Im(H_{yy})$	$Re(U_{xx})$	$Im(U_{xx})$	$Re(U_{xy})$	$Im(U_{xy})$	$Re(U_{yx})$	$Im(U_{yx})$	$Re(U_{yy})$	$Im(U_{yy})$
20	0.15	52.9	11.7	-10.6	-1.7	12.2	3.4	61.2	7.6	0.38	0.47	0.35	0.23	1.30	1.67	1.00	0.65
30	0.23	51.5	18.9	-10.1	-3.4	12.6	2.8	60.9	13.2	0.63	0.78	0.22	0.37	0.65	0.88	0.51	0.56
40	0.30	50.3	25.9	-10.4	-4.8	12.9	1.1	56.4	24.0	0.73	0.40	0.16	0.31	0.87	0.88	0.46	0.63
50	0.38	49.4	34.2	-11.2	-6.1	10.1	0.7	55.2	32.3	1.18	0.96	0.52	0.34	1.91	1.51	0.81	0.50
70	0.53	48.6	47.5	-12.7	-5.5	10.5	3.5	47.6	44.2	0.94	1.21	0.32	0.46	2.03	1.27	0.50	0.75
80	0.60	47.7	54.3	-8.3	-5.9	7.4	6.3	27.0	94.5	0.77	0.44	0.38	0.49	0.86	1.44	2.39	1.38
90	0.68	46.1	58.9	-12.2	-3.8	12.6	8.2	44.2	63.7	0.64	0.80	0.25	0.45	0.87	0.64	0.37	0.75
100	0.75	43.7	66.2	-9.9	-4.4	14.3	7.7	40.6	71.8	0.63	0.59	0.28	0.43	0.69	0.85	0.53	0.68
110	0.83	41.7	71.4	-10.2	-4.7	16.0	8.5	37.6	76.1	0.49	0.71	0.46	0.37	0.62	0.99	0.50	0.42
130	0.98	31.4	72.2	-14.1	-5.6	39.2	1.7	33.7	82.6	1.07	0.80	0.59	0.64	1.60	1.14	0.56	0.82
140	1.05	31.8	82.5	-8.1	-5.1	33.9	11.5	23.9	101.5	1.00	2.26	0.39	0.49	4.10	1.04	0.44	0.74
150	1.13	28.6	97.4	-5.7	-6.1	20.9	11.3	30.2	108.6	0.82	0.63	0.52	0.47	1.01	1.25	0.62	0.87
160	1.20	26.2	106.7	-4.6	-7.5	16.7	14.8	35.8	125.5	1.12	1.61	0.90	0.97	1.03	1.75	1.13	0.89
170	1.28	25.3	114.5	-5.2	-6.6	16.7	13.3	19.8	126.5	1.97	2.49	1.24	1.37	2.72	1.85	1.27	1.77
190	1.43	17.6	127.5	-4.6	-8.3	17.6	15.5	17.3	131.5	2.83	1.47	1.22	1.30	1.91	1.85	0.83	1.66
200	1.50	15.2	132.4	-3.9	-5.7	14.0	18.2	5.5	131.5	1.14	1.08	0.76	0.82	0.96	1.61	0.94	0.94
210	1.58	15.4	134.9	-0.2	-6.7	18.2	23.9	4.5	147.6	1.29	1.07	1.03	0.67	1.52	0.94	0.57	0.78
220	1.65	8.2	133.8	-13.0	-5.6	11.0	16.5	-11.9	125.7	1.06	0.87	0.93	0.53	1.02	0.96	0.79	0.90
230	1.73	-4.7	144.2	-6.1	-6.6	11.5	31.2	-13.6	164.9	0.77	0.83	0.60	0.44	1.14	0.89	0.68	1.00
250	1.88	-11.7	158.7	-10.1	-4.5	11.5	34.1	-24.1	176.5	0.99	0.42	0.71	0.58	0.91	1.08	0.95	1.19
260	1.95	-18.0	165.7	-12.2	1.0	16.7	35.3	-31.3	176.8	1.93	1.56	1.50	1.27	1.56	1.37	1.67	1.83
270	2.03	-31.0	171.1	-15.6	7.3	25.3	32.8	-39.2	171.9	4.29	3.11	3.26	2.47	3.23	2.77	1.97	2.33
280	2.10	-21.3	171.1	-14.1	2.7	13.2	43.9	-29.6	203.9	1.53	0.96	0.73	0.99	0.88	1.13	1.14	1.02
290	2.18	-27.0	178.2	-18.4	18.1	10.8	37.6	-78.1	179.2	1.02	1.27	0.84	1.45	0.87	1.46	1.30	3.16

Table 30. Experimental dynamic stiffnesses at 8000 rpm and 513.8 kPa bearing unit loading

Ω	Ω/ω	Experiment															
		Dynamic stiffness								Uncertainty							
Hz		$Re(H_{xx})$	$Im(H_{xx})$	$Re(H_{xy})$	$Im(H_{xy})$	$Re(H_{yx})$	$Im(H_{yx})$	$Re(H_{yy})$	$Im(H_{yy})$	$Re(U_{xx})$	$Im(U_{xx})$	$Re(U_{xy})$	$Im(U_{xy})$	$Re(U_{yx})$	$Im(U_{yx})$	$Re(U_{yy})$	$Im(U_{yy})$
20	0.15	63.6	14.8	-11.2	-2.3	8.2	-8.3	65.5	13.2	0.68	0.86	0.32	0.38	1.85	2.64	0.71	1.73
30	0.23	62.7	21.5	-11.2	-4.6	5.9	-3.0	73.8	17.8	0.75	0.78	0.21	0.16	2.22	1.40	1.01	1.35
40	0.30	64.0	28.2	-12.2	-5.7	5.6	1.6	70.4	27.2	0.64	0.85	0.29	0.31	1.71	1.60	0.51	0.88
50	0.38	62.9	35.7	-13.1	-7.0	6.6	1.2	69.1	35.0	1.48	1.20	0.52	0.85	2.66	1.89	0.87	1.45
70	0.53	61.2	47.1	-14.6	-6.1	10.9	3.1	61.0	46.7	1.37	1.29	0.78	0.67	1.85	2.69	1.18	0.73
80	0.60	61.1	54.2	-12.3	-4.2	8.4	3.8	39.5	62.5	0.61	0.95	0.47	0.30	0.97	1.05	0.91	1.45
90	0.68	59.9	59.4	-14.1	-4.4	11.4	7.4	58.2	69.6	0.97	0.59	0.49	0.45	1.30	0.89	0.66	0.82
100	0.75	56.0	65.8	-12.2	-4.9	14.8	5.0	53.5	77.1	0.63	0.53	0.45	0.35	0.99	0.91	0.58	1.12
110	0.83	53.4	71.1	-11.3	-5.2	15.1	6.0	51.6	81.6	0.99	0.65	0.53	0.37	1.30	1.16	0.48	0.63
130	0.98	38.8	73.6	-16.9	-6.0	41.9	-12.9	50.2	85.5	1.35	1.03	0.88	0.82	2.06	4.27	2.01	1.38
140	1.05	43.6	89.8	-9.2	-5.1	26.8	6.9	35.2	112.4	0.54	3.61	1.25	0.89	7.43	1.03	0.87	2.21
150	1.13	40.8	100.6	-6.4	-6.5	19.1	7.8	45.4	119.0	0.77	1.31	0.73	0.46	1.33	1.09	0.73	1.19
160	1.20	39.3	110.2	-6.2	-10.4	17.0	11.8	53.0	139.9	1.14	1.36	0.79	0.96	1.83	1.25	1.07	0.95
170	1.28	38.1	117.9	-4.3	-6.7	15.8	10.9	33.1	138.5	2.76	2.48	1.69	1.69	2.70	2.09	1.87	1.79
190	1.43	32.4	130.0	-4.6	-7.4	16.3	10.8	33.5	144.4	2.35	2.42	1.60	2.11	2.84	2.77	1.68	1.28
200	1.50	29.6	136.9	-5.7	-5.7	15.6	15.4	16.9	145.9	1.88	1.45	1.02	0.89	1.55	1.15	1.11	1.69
210	1.58	29.7	139.6	-0.9	-7.0	19.6	19.0	19.6	164.3	1.83	1.53	0.73	0.70	1.47	1.81	1.31	1.60
220	1.65	23.9	137.3	-13.7	-6.9	11.5	12.3	6.3	141.3	1.54	1.39	0.71	0.92	0.98	1.68	1.24	1.35
230	1.73	11.3	149.0	-6.0	-6.5	11.9	26.1	2.3	182.6	0.95	0.76	0.96	0.68	0.76	1.09	1.35	1.53
250	1.88	5.4	163.3	-9.1	-0.5	11.8	29.4	-12.2	187.2	1.15	1.09	0.67	0.72	1.24	1.19	1.96	3.91
260	1.95	-6.4	176.5	-6.9	0.7	19.1	26.5	-15.1	191.6	5.76	6.89	4.59	1.44	1.99	4.62	3.49	2.22
270	2.03	-7.2	179.9	-11.7	6.5	20.8	26.6	-16.8	191.3	3.81	3.13	1.77	1.94	2.30	4.93	1.82	2.39
280	2.10	-3.5	176.6	-8.6	1.8	13.8	41.3	-10.4	227.6	0.93	1.34	1.09	0.97	1.93	1.18	2.25	1.58
290	2.18	-9.1	184.5	-17.2	11.4	12.7	36.1	-30.6	196.9	1.58	1.60	0.95	0.97	1.44	1.45	0.97	1.76

Table 31. Experimental dynamic stiffnesses at 8000 rpm and 692.2 kPa bearing unit loading

Ω	Ω/ω	Experiment															
		Dynamic stiffness								Uncertainty							
Hz		$Re(H_{xx})$	$Im(H_{xx})$	$Re(H_{xy})$	$Im(H_{xy})$	$Re(H_{yx})$	$Im(H_{yx})$	$Re(H_{yy})$	$Im(H_{yy})$	$Re(U_{xx})$	$Im(U_{xx})$	$Re(U_{xy})$	$Im(U_{xy})$	$Re(U_{yx})$	$Im(U_{yx})$	$Re(U_{yy})$	$Im(U_{yy})$
20	0.15	76.9	13.4	-14.3	-4.6	7.0	2.0	87.8	15.2	1.63	0.93	0.74	0.50	4.65	5.24	1.39	2.32
30	0.23	76.0	21.2	-13.6	-5.4	7.6	1.3	92.2	19.1	0.53	0.91	0.81	0.61	1.68	2.23	1.52	1.41
40	0.30	75.3	28.4	-14.8	-6.1	6.9	0.2	85.9	31.0	1.54	1.18	0.33	0.48	1.62	1.43	1.00	0.59
50	0.38	75.4	37.7	-14.5	-7.0	5.0	-0.8	86.3	43.2	1.30	1.34	0.70	0.56	3.52	3.64	1.62	0.88
70	0.53	75.1	51.5	-15.6	-8.1	9.5	1.7	79.1	53.8	2.65	2.08	0.76	0.98	4.33	3.81	0.88	1.05
80	0.60	74.9	57.9	-14.4	-6.7	8.9	2.4	69.9	72.2	1.74	1.18	0.81	0.44	1.73	2.47	1.07	1.38
90	0.68	74.0	62.7	-14.8	-7.0	11.7	4.2	77.4	80.7	0.96	1.06	0.50	0.61	1.91	1.74	0.66	0.89
100	0.75	70.5	69.8	-13.3	-7.9	14.6	1.3	71.4	88.6	0.74	0.95	0.57	0.37	1.60	1.02	0.55	1.23
110	0.83	68.2	76.0	-12.7	-8.2	13.9	2.0	69.8	92.5	1.06	0.70	0.49	0.61	1.53	1.55	1.15	0.86
130	0.98	49.1	77.9	-19.1	-6.3	48.3	-21.3	64.0	94.6	1.18	1.96	1.42	0.85	4.42	1.11	1.02	2.35
140	1.05	56.3	91.8	-11.6	-7.1	35.4	-1.5	52.2	124.4	1.02	3.72	1.62	0.53	6.69	1.97	1.67	2.35
150	1.13	56.8	104.8	-7.4	-10.2	22.3	2.6	65.8	131.7	0.90	1.50	0.75	0.42	1.52	1.77	1.90	0.99
160	1.20	55.6	114.7	-6.5	-15.7	20.4	7.8	74.6	161.4	1.26	1.84	1.13	0.96	1.83	2.48	2.09	1.47
170	1.28	54.1	122.9	-4.5	-9.8	18.2	5.9	53.3	157.1	2.22	2.71	1.53	1.61	3.92	1.52	1.60	2.74
190	1.43	48.6	135.9	-4.8	-11.3	19.3	4.6	52.6	161.0	2.55	2.05	2.32	1.67	3.22	2.82	1.75	2.68
200	1.50	46.0	142.7	-4.5	-9.8	19.1	9.5	33.7	164.2	1.69	1.57	0.75	1.50	1.97	1.97	1.83	1.65
210	1.58	45.8	146.4	0.6	-11.4	23.6	11.6	39.6	182.9	1.08	1.40	1.35	1.45	1.53	2.43	1.51	1.29
220	1.65	40.6	144.9	-11.2	-10.2	14.2	5.3	25.4	160.6	0.84	0.54	0.60	0.67	1.49	1.36	2.06	0.75
230	1.73	28.2	155.7	-3.6	-11.2	16.5	19.6	19.3	204.9	1.13	0.72	0.89	1.00	0.61	1.71	1.22	1.54
250	1.88	22.1	171.5	-7.0	-7.1	17.0	21.7	9.7	206.3	1.63	1.21	0.59	0.79	1.38	1.81	0.63	1.38
260	1.95	11.3	187.8	-8.1	2.0	23.0	16.3	-3.4	207.0	10.06	6.03	1.96	2.80	6.16	5.31	2.36	2.39
270	2.03	5.4	195.1	-9.4	5.2	27.8	13.3	1.2	211.9	5.16	5.06	2.13	3.30	3.32	4.62	2.42	1.70
280	2.10	14.9	186.2	-1.6	-5.9	18.7	35.6	4.8	269.7	1.59	1.40	1.42	1.11	1.90	1.78	1.97	1.12
290	2.18	9.9	192.4	-12.3	5.5	18.6	30.7	-10.4	227.8	1.22	0.89	1.12	1.13	1.66	1.59	0.98	1.16

Table 32. Experimental dynamic stiffnesses at 8000 rpm and 1038.2 kPa bearing unit loading

Ω	Ω/ω	Experiment															
		Dynamic stiffness								Uncertainty							
Hz		$Re(H_{xx})$	$Im(H_{xx})$	$Re(H_{xy})$	$Im(H_{xy})$	$Re(H_{yx})$	$Im(H_{yx})$	$Re(H_{yy})$	$Im(H_{yy})$	$Re(U_{xx})$	$Im(U_{xx})$	$Re(U_{xy})$	$Im(U_{xy})$	$Re(U_{yx})$	$Im(U_{yx})$	$Re(U_{yy})$	$Im(U_{yy})$
20	0.15	100.7	5.1	-19.6	-1.5	-1.0	4.0	137.5	22.0	8.13	10.63	4.29	5.87	5.48	5.34	3.93	4.16
30	0.23	102.3	20.7	-18.9	-6.8	-2.4	0.6	147.0	27.6	2.57	3.02	1.52	1.94	3.57	4.97	1.78	1.89
40	0.30	105.7	30.0	-22.0	-10.0	1.4	0.2	141.1	43.9	3.26	2.95	1.69	1.44	2.57	4.02	2.75	1.58
50	0.38	102.5	37.9	-20.1	-8.9	-3.7	-9.1	141.7	60.0	3.28	2.29	1.50	1.68	6.14	7.19	2.04	3.65
70	0.53	107.7	57.0	-21.8	-13.7	13.1	-4.4	131.9	71.9	3.07	4.69	1.81	2.45	5.43	9.08	3.98	4.05
80	0.60	106.4	67.6	-17.9	-16.5	4.6	-1.0	137.0	112.5	2.53	1.71	1.04	1.28	4.29	1.97	3.03	1.98
90	0.68	105.3	71.7	-19.6	-14.4	5.6	-5.7	133.4	106.3	1.82	0.49	1.09	1.12	4.10	1.59	2.47	1.67
100	0.75	103.1	81.1	-17.4	-15.0	8.8	-7.1	126.0	116.5	0.89	1.67	0.97	1.50	2.03	2.58	1.28	2.07
110	0.83	102.7	87.4	-17.6	-16.3	11.2	-5.6	124.7	119.2	0.55	1.09	0.80	0.97	2.75	1.93	1.10	1.65
130	0.98	72.1	92.9	-27.1	-4.9	52.3	-47.0	100.3	105.3	1.72	2.18	1.53	1.32	3.91	3.53	2.55	2.38
140	1.05	90.9	109.5	-12.4	-17.0	25.5	-15.2	108.3	163.1	1.98	1.72	1.01	2.04	6.46	4.27	2.41	2.60
150	1.13	93.7	119.2	-10.9	-21.2	22.1	-11.6	121.5	165.9	1.12	1.30	1.30	0.94	2.03	2.68	1.75	1.09
160	1.20	93.0	127.9	-5.9	-29.1	21.0	-5.1	118.2	222.2	1.28	1.98	1.71	1.42	3.34	2.41	2.72	2.59
170	1.28	93.3	136.4	-8.1	-22.9	20.5	-12.9	107.0	199.3	1.70	2.17	2.35	1.55	4.05	2.61	3.32	2.16
190	1.43	89.1	151.4	-8.7	-24.1	20.3	-12.1	105.0	203.3	2.76	1.22	2.37	1.68	3.46	3.26	2.38	3.14
200	1.50	87.8	156.9	-6.4	-22.0	23.0	-7.3	84.8	206.7	1.65	1.13	1.74	0.75	1.98	2.70	2.05	1.52
210	1.58	87.1	163.4	-2.4	-24.6	28.5	-6.2	95.5	226.8	0.94	1.54	1.12	1.20	2.47	2.12	1.04	2.02
220	1.65	82.5	160.6	-12.8	-18.9	19.4	-11.6	78.1	200.8	1.72	1.23	0.71	0.73	1.55	2.19	2.01	1.28
230	1.73	70.1	169.8	-0.7	-24.5	25.0	3.5	67.5	269.0	0.93	1.03	0.89	1.64	1.67	1.75	1.41	2.23
250	1.88	63.0	189.3	-5.1	-14.0	26.5	3.3	50.7	254.0	2.24	1.60	1.29	1.19	1.73	1.22	1.50	1.83
260	1.95	51.5	234.0	2.5	4.3	30.3	-24.5	39.9	255.5	8.17	10.99	5.56	7.80	6.60	8.67	5.97	5.81
270	2.03	57.2	207.6	-0.8	-5.1	34.2	-1.8	45.7	267.4	2.68	3.66	3.15	4.08	1.47	3.95	3.08	3.66
280	2.10	58.2	202.3	19.5	-17.9	29.8	17.8	19.9	373.2	0.79	1.24	2.82	2.14	2.51	2.31	3.51	2.01
290	2.18	53.8	209.0	-2.2	-3.7	33.5	9.2	36.3	291.6	1.45	0.96	0.73	0.76	1.03	2.10	1.74	1.56

Table 33. Experimental dynamic stiffnesses at 10000 rpm and 1.4 kPa bearing unit loading

Ω	Ω/ω	Experiment															
		Dynamic stiffness								Uncertainty							
Hz		$Re(H_{xx})$	$Im(H_{xx})$	$Re(H_{xy})$	$Im(H_{xy})$	$Re(H_{yx})$	$Im(H_{yx})$	$Re(H_{yy})$	$Im(H_{yy})$	$Re(U_{xx})$	$Im(U_{xx})$	$Re(U_{xy})$	$Im(U_{xy})$	$Re(U_{yx})$	$Im(U_{yx})$	$Re(U_{yy})$	$Im(U_{yy})$
20	0.12	58.0	11.1	-18.7	-0.6	10.8	6.0	69.2	10.2	1.87	0.98	0.63	0.54	2.89	4.40	1.42	1.58
30	0.18	56.6	17.4	-17.5	-1.6	6.7	5.2	69.2	15.0	1.30	1.34	0.65	0.93	4.31	3.53	1.14	1.40
40	0.24	54.0	24.1	-17.9	-5.1	11.3	2.2	65.7	25.5	0.58	1.14	0.31	0.46	1.38	1.19	0.74	0.65
50	0.30	51.2	32.7	-18.0	-7.1	8.9	2.3	62.7	32.0	1.52	0.86	0.54	0.67	3.08	2.28	1.73	1.30
70	0.42	48.5	47.2	-18.5	-9.2	14.2	3.9	58.4	47.3	1.62	1.17	0.60	0.83	1.94	2.45	1.10	0.75
80	0.48	45.8	56.0	-18.7	-9.7	12.8	4.9	55.3	58.5	1.25	0.96	0.93	0.49	1.86	2.33	1.17	0.98
90	0.54	43.3	62.6	-17.3	-9.2	14.9	5.4	50.5	65.5	1.22	1.17	0.83	0.64	1.58	1.21	0.82	1.23
100	0.60	41.0	71.4	-15.8	-9.9	13.5	2.4	47.5	73.5	1.61	1.33	0.82	0.57	1.90	3.06	0.98	1.37
110	0.66	40.1	79.6	-15.0	-10.1	16.3	3.9	45.1	80.0	0.92	0.73	0.68	0.75	3.03	2.34	1.01	0.91
130	0.78	33.1	93.6	-11.2	-10.6	16.1	9.1	39.7	93.9	1.08	0.92	0.79	0.40	1.65	2.40	1.64	0.96
140	0.84	30.4	100.3	-9.6	-11.7	19.9	12.1	33.3	106.2	1.36	1.51	0.92	0.61	3.02	2.76	1.15	0.85
150	0.90	29.0	103.4	-8.6	-12.1	23.8	15.5	36.0	111.7	1.14	1.91	1.07	0.62	2.55	1.90	1.15	1.42
160	0.96	28.4	91.1	-10.1	-11.1	48.2	15.1	26.2	110.6	1.32	3.05	0.82	0.91	3.77	2.63	1.28	0.86
170	1.02	22.1	87.3	-12.7	-15.1	69.3	8.0	24.2	117.2	1.46	2.73	1.83	1.30	7.08	7.21	3.11	3.94
190	1.14	14.5	129.6	-1.4	-13.2	25.1	16.5	23.1	138.6	1.95	2.76	1.97	1.64	4.23	3.71	1.67	2.25
200	1.20	11.0	134.9	-0.2	-13.6	21.0	20.9	15.9	142.8	1.24	1.70	1.39	1.28	1.28	5.49	1.60	1.77
210	1.26	7.7	138.5	3.4	-13.0	26.1	24.3	18.2	153.2	1.22	0.89	0.73	0.83	2.12	5.27	0.99	0.97
220	1.32	2.1	134.8	-3.6	-13.8	16.2	18.2	8.4	137.8	0.66	1.05	0.84	0.71	3.61	4.34	1.58	1.40
230	1.38	-13.2	145.4	1.8	-9.6	15.1	29.8	-11.1	152.5	0.95	0.85	0.68	0.59	1.88	2.92	1.13	1.14
250	1.50	-22.4	156.4	5.5	-10.1	13.4	36.9	-17.2	168.7	0.94	1.18	0.44	0.35	2.67	3.86	1.32	1.50
260	1.56	-27.6	160.2	6.4	-9.5	13.9	43.2	-23.8	174.5	1.15	0.91	0.87	0.80	3.22	4.79	1.15	1.82
270	1.62	-32.9	163.4	6.0	-9.6	11.5	48.1	-29.0	181.9	0.62	0.86	0.84	0.90	2.31	5.32	1.34	1.73
280	1.68	-39.8	166.2	5.9	-8.4	11.7	54.6	-39.9	187.6	1.08	0.89	0.83	0.63	2.52	6.40	1.20	2.20
290	1.74	-48.0	173.5	4.7	-8.9	12.1	61.1	-48.4	193.4	1.14	1.12	0.96	1.04	3.49	3.92	1.48	1.55

Table 34. Experimental dynamic stiffnesses at 10000 rpm and 175.9 kPa bearing unit loading

Ω	Ω/ω	Experiment															
		Dynamic stiffness								Uncertainty							
Hz		$Re(H_{xx})$	$Im(H_{xx})$	$Re(H_{xy})$	$Im(H_{xy})$	$Re(H_{yx})$	$Im(H_{yx})$	$Re(H_{yy})$	$Im(H_{yy})$	$Re(U_{xx})$	$Im(U_{xx})$	$Re(U_{xy})$	$Im(U_{xy})$	$Re(U_{yx})$	$Im(U_{yx})$	$Re(U_{yy})$	$Im(U_{yy})$
20	0.12	58.9	10.9	-15.7	-0.2	14.1	5.3	72.9	5.1	0.75	1.41	0.54	0.38	2.59	3.29	0.68	1.48
30	0.18	57.6	16.4	-13.9	-1.4	16.8	4.9	69.9	9.8	0.83	0.96	0.59	0.37	2.65	4.99	1.17	1.13
40	0.24	55.0	24.1	-13.7	-3.0	16.1	3.5	63.9	20.3	0.80	1.04	0.53	0.36	1.97	1.82	0.87	1.10
50	0.30	52.8	30.9	-13.1	-3.7	15.4	1.3	61.6	27.8	1.86	1.83	0.64	0.60	4.53	2.53	1.62	1.24
70	0.42	49.5	46.9	-14.4	-6.2	17.9	6.1	54.2	41.1	1.57	1.47	0.63	0.61	3.77	2.57	1.49	1.41
80	0.48	48.4	54.9	-14.3	-6.4	14.7	8.1	66.7	64.5	1.02	0.78	0.76	0.55	2.77	2.45	1.66	1.31
90	0.54	48.4	60.6	-14.7	-3.9	17.0	8.9	49.2	60.7	0.62	0.88	0.47	0.63	1.96	1.81	0.58	1.21
100	0.60	45.8	68.2	-13.0	-3.9	17.6	7.2	48.2	67.9	0.87	0.64	0.39	0.42	2.14	2.63	0.75	1.97
110	0.66	44.5	75.9	-12.2	-4.1	16.4	10.6	44.6	73.6	1.63	1.18	0.58	0.46	1.79	1.48	0.75	1.41
130	0.78	38.3	88.6	-9.0	-3.5	21.2	10.3	36.0	88.4	0.75	0.97	0.75	0.54	2.24	1.86	1.44	1.55
140	0.84	36.1	93.0	-8.2	-3.1	23.1	12.8	27.8	100.3	1.18	1.31	0.65	0.70	3.19	2.14	0.85	2.63
150	0.90	35.1	97.4	-6.8	-3.4	24.1	15.2	29.4	105.0	1.34	1.25	0.82	0.63	2.44	1.80	0.95	1.51
160	0.96	30.5	84.1	-9.4	-6.1	58.8	4.1	35.2	110.4	1.66	2.26	1.02	1.08	4.92	2.53	1.46	2.96
170	1.02	28.1	85.7	-11.3	-6.7	68.1	-0.3	31.1	111.4	2.29	2.38	1.38	1.43	3.76	3.74	1.88	4.58
190	1.14	19.9	124.3	-1.7	-4.2	27.3	24.1	24.1	131.3	1.56	1.73	1.29	1.14	2.59	2.97	1.29	1.49
200	1.20	17.2	129.3	-1.5	-4.8	23.7	23.5	12.7	133.5	1.08	1.08	1.05	1.03	1.62	2.06	0.94	1.78
210	1.26	14.9	132.9	2.0	-1.5	29.4	25.3	11.4	143.1	1.02	1.40	1.12	0.41	3.21	2.22	1.18	1.69
220	1.32	7.8	130.7	-3.7	3.0	18.8	19.3	-28.3	130.5	0.93	0.92	1.63	1.20	2.56	1.21	2.59	2.74
230	1.38	-5.9	141.6	0.8	-3.3	19.3	32.8	0.2	156.2	0.75	0.81	0.79	0.72	2.35	0.60	0.88	0.92
250	1.50	-13.0	154.8	1.1	-2.2	18.7	39.3	-13.3	162.3	1.11	1.16	0.58	0.66	1.18	2.78	1.27	1.43
260	1.56	-18.5	158.2	3.5	-1.7	19.7	41.0	-28.4	169.1	1.23	1.15	0.41	0.93	1.39	2.92	1.74	1.09
270	1.62	-20.9	164.4	-1.2	-3.2	16.5	42.0	-31.4	177.3	0.90	0.85	0.70	0.68	3.23	3.84	1.74	1.94
280	1.68	-28.0	168.2	-4.4	0.2	18.2	45.8	-38.2	183.8	0.74	1.01	0.89	0.62	2.84	2.28	1.76	1.46
290	1.74	-34.6	173.3	-1.2	5.5	14.4	46.1	-61.4	210.9	1.05	1.60	1.49	1.86	3.42	2.75	4.57	1.72

Table 35. Experimental dynamic stiffnesses at 10000 rpm and 348.4 kPa bearing unit loading

Ω	Ω/ω	Experiment															
		Dynamic stiffness								Uncertainty							
Hz		$Re(H_{xx})$	$Im(H_{xx})$	$Re(H_{xy})$	$Im(H_{xy})$	$Re(H_{yx})$	$Im(H_{yx})$	$Re(H_{yy})$	$Im(H_{yy})$	$Re(U_{xx})$	$Im(U_{xx})$	$Re(U_{xy})$	$Im(U_{xy})$	$Re(U_{yx})$	$Im(U_{yx})$	$Re(U_{yy})$	$Im(U_{yy})$
20	0.12	66.2	12.5	-14.0	-1.7	18.8	14.1	79.4	7.9	1.43	1.39	0.47	0.34	3.95	5.29	1.42	1.72
30	0.18	65.0	20.0	-13.2	-2.4	2.5	9.7	79.7	8.5	0.86	1.07	0.38	0.37	4.79	5.21	1.19	1.48
40	0.24	64.1	26.2	-13.5	-3.6	12.8	3.4	73.1	21.0	0.57	0.78	0.34	0.40	2.63	2.84	1.00	1.46
50	0.30	62.4	34.6	-14.0	-4.3	10.9	0.7	72.4	32.4	1.08	1.12	0.46	0.50	3.82	2.84	1.61	1.43
70	0.42	60.9	48.1	-14.7	-5.0	10.9	4.8	66.3	45.0	1.29	1.56	0.59	0.38	3.10	2.57	1.14	0.95
80	0.48	60.7	56.2	-10.9	-6.0	5.2	6.2	45.3	101.5	1.09	0.98	0.76	0.54	2.08	3.37	2.67	1.95
90	0.54	60.9	61.9	-15.1	-2.8	16.7	11.3	61.7	63.5	1.10	0.72	0.66	0.50	3.16	1.50	1.61	1.78
100	0.60	57.7	69.4	-13.2	-3.0	11.7	-0.4	59.3	72.9	0.90	0.70	0.48	0.48	3.34	2.31	1.54	1.11
110	0.66	56.9	75.2	-12.5	-2.6	19.5	8.1	55.3	78.1	1.42	1.39	0.58	0.48	2.24	1.32	1.49	2.04
130	0.78	51.2	88.1	-9.9	-1.8	20.3	9.7	49.2	91.2	0.90	0.92	0.56	0.67	2.35	2.03	0.99	1.63
140	0.84	48.9	94.5	-8.3	-1.8	26.1	7.4	39.7	110.0	1.23	0.75	0.42	0.68	2.92	4.17	0.99	1.36
150	0.90	46.8	97.2	-7.5	-3.1	22.7	11.5	48.8	110.2	0.86	1.31	0.76	0.50	2.12	3.97	1.44	1.12
160	0.96	41.6	88.5	-10.1	-3.5	56.9	3.7	49.5	122.7	2.20	3.16	0.75	0.77	8.16	3.99	1.97	2.49
170	1.02	29.5	80.6	-13.0	-7.0	79.9	-37.9	57.5	121.5	3.08	1.69	1.44	2.06	7.65	19.21	9.29	5.07
190	1.14	32.6	123.7	-3.4	-3.3	29.3	23.8	39.3	135.2	2.09	2.26	1.39	1.58	3.13	5.41	1.28	1.83
200	1.20	31.5	130.7	-2.8	-2.5	28.0	29.1	25.9	138.2	1.16	1.02	0.86	0.61	3.17	6.29	1.80	2.10
210	1.26	29.4	134.4	0.6	-1.4	39.3	25.4	30.9	149.1	1.82	1.61	0.89	0.65	5.13	5.55	2.27	1.93
220	1.32	22.5	132.4	-8.5	-0.3	18.2	19.5	9.6	126.6	1.07	1.39	0.70	0.74	3.37	3.67	1.65	1.84
230	1.38	9.3	143.4	-0.7	-1.8	23.6	37.9	15.8	165.6	0.68	0.96	0.66	0.58	3.38	4.02	1.89	2.04
250	1.50	1.5	158.3	0.1	-2.5	22.4	47.8	4.2	172.7	1.32	1.18	0.61	0.75	3.43	7.55	1.69	1.74
260	1.56	-2.0	163.1	-2.6	0.0	31.2	54.4	-8.1	171.7	1.14	1.29	0.95	0.74	5.89	8.61	2.14	2.17
270	1.62	-5.8	168.2	-6.8	2.2	39.3	50.8	-18.1	167.1	0.72	0.93	1.42	0.68	5.88	7.20	1.77	1.68
280	1.68	-8.5	171.6	-4.0	-2.2	34.5	51.8	-13.1	198.7	0.76	0.83	0.81	0.50	10.27	7.11	2.31	1.95
290	1.74	-14.7	179.5	-10.3	10.7	38.7	49.3	-56.9	174.5	0.70	1.45	1.20	1.00	7.98	5.01	2.97	4.14

Table 36. Experimental dynamic stiffnesses at 10000 rpm and 513.8 kPa bearing unit loading

Ω	Ω/ω	Experiment															
		Dynamic stiffness								Uncertainty							
Hz		$Re(H_{xx})$	$Im(H_{xx})$	$Re(H_{xy})$	$Im(H_{xy})$	$Re(H_{yx})$	$Im(H_{yx})$	$Re(H_{yy})$	$Im(H_{yy})$	$Re(U_{xx})$	$Im(U_{xx})$	$Re(U_{xy})$	$Im(U_{xy})$	$Re(U_{yx})$	$Im(U_{yx})$	$Re(U_{yy})$	$Im(U_{yy})$
20	0.12	74.6	14.8	-14.6	-2.2	11.3	5.9	93.4	9.3	0.79	1.03	0.55	0.43	3.55	10.69	1.36	2.45
30	0.18	74.4	21.6	-14.2	-2.9	7.6	0.7	91.3	12.1	1.39	1.18	0.41	0.50	11.05	7.23	1.17	2.03
40	0.24	73.7	28.4	-14.7	-3.9	12.4	1.6	86.3	25.1	0.89	0.80	0.42	0.57	4.63	2.66	1.03	1.07
50	0.30	73.8	36.2	-15.3	-4.9	10.6	-0.7	84.5	34.2	1.69	2.33	1.04	0.93	5.84	5.05	2.43	1.84
70	0.42	72.2	50.5	-16.0	-5.3	12.7	2.3	77.6	49.2	1.94	2.84	1.15	0.64	4.31	5.71	2.11	1.27
80	0.48	71.9	57.8	-12.9	-3.2	8.7	2.9	53.4	64.9	1.31	1.49	0.89	0.52	4.50	3.43	1.66	1.59
90	0.54	72.9	63.2	-15.9	-3.5	13.9	7.5	75.1	70.3	0.97	1.28	0.79	0.46	2.49	2.19	1.59	1.40
100	0.60	71.1	70.1	-14.3	-3.3	11.9	4.6	71.2	77.0	0.83	0.84	0.72	0.67	5.98	5.28	1.87	1.24
110	0.66	69.3	75.4	-13.6	-3.5	16.6	5.3	67.5	82.4	1.15	0.85	0.53	0.76	5.12	5.92	0.89	1.13
130	0.78	63.5	88.2	-10.2	-2.9	17.1	7.0	62.9	98.3	0.73	0.74	1.05	0.48	0.97	1.60	2.33	1.00
140	0.84	62.8	95.3	-8.9	-1.7	20.9	6.6	51.7	117.3	1.50	1.08	0.73	1.12	4.46	5.88	0.88	1.50
150	0.90	58.5	98.1	-7.6	-2.0	25.4	10.0	61.4	118.8	0.76	1.45	0.73	0.95	2.60	2.78	0.59	1.08
160	0.96	48.1	86.4	-11.4	-4.3	61.5	-13.1	67.6	133.4	4.85	5.96	0.87	0.93	11.34	21.87	3.26	10.69
170	1.02	37.8	84.6	-15.4	-6.0	77.8	-26.8	58.1	127.7	4.85	2.78	1.79	2.28	3.53	7.44	2.88	6.29
190	1.14	46.3	124.0	-2.7	-4.1	26.5	13.6	53.8	143.9	2.16	1.91	1.07	1.36	2.08	2.17	2.67	2.20
200	1.20	44.4	131.1	-2.1	-2.9	27.0	16.9	38.2	148.5	1.03	1.87	0.77	1.38	5.02	3.16	1.62	1.93
210	1.26	43.0	135.4	3.4	-2.2	32.5	18.4	44.5	161.8	1.02	1.48	1.02	1.16	6.99	4.65	1.86	3.37
220	1.32	35.1	133.0	-6.2	-2.0	19.9	10.3	27.2	137.4	0.91	1.30	0.70	0.82	1.07	1.19	5.43	0.71
230	1.38	22.2	143.9	0.7	-4.1	22.6	24.7	26.9	180.6	1.26	0.74	0.66	0.78	4.06	1.06	2.50	2.26
250	1.50	14.5	159.6	3.2	-1.9	23.3	27.6	7.6	190.1	1.17	1.01	0.69	0.95	3.47	2.80	5.53	3.24
260	1.56	11.8	165.5	-1.0	-1.5	22.2	29.5	6.5	182.7	1.18	1.14	0.94	1.02	4.66	2.66	2.68	1.86
270	1.62	9.4	171.1	-3.8	0.2	25.1	27.8	-0.8	180.9	1.14	1.09	1.08	0.71	7.99	2.86	2.21	0.92
280	1.68	6.1	174.4	0.1	-4.9	23.2	37.7	4.5	221.0	1.12	1.04	1.14	1.04	9.71	3.87	2.82	1.69
290	1.74	1.4	181.8	-9.4	3.6	20.7	31.3	-18.6	191.8	1.35	1.23	1.12	1.07	9.20	1.57	6.91	5.20

Table 37. Experimental dynamic stiffnesses at 10000 rpm and 692.2 kPa bearing unit loading

Ω	Ω/ω	Experiment															
		Dynamic stiffness								Uncertainty							
Hz		$Re(H_{xx})$	$Im(H_{xx})$	$Re(H_{xy})$	$Im(H_{xy})$	$Re(H_{yx})$	$Im(H_{yx})$	$Re(H_{yy})$	$Im(H_{yy})$	$Re(U_{xx})$	$Im(U_{xx})$	$Re(U_{xy})$	$Im(U_{xy})$	$Re(U_{yx})$	$Im(U_{yx})$	$Re(U_{yy})$	$Im(U_{yy})$
20	0.12	86.1	15.4	-15.6	-2.6	12.4	0.2	107.0	11.4	1.23	1.24	0.29	0.56	2.45	4.23	1.55	2.56
30	0.18	85.7	23.8	-15.3	-3.9	12.0	-4.8	106.3	13.4	1.67	1.40	0.41	0.54	2.75	2.98	2.29	1.17
40	0.24	85.7	30.1	-16.0	-4.3	9.7	-4.9	102.4	29.1	0.86	1.21	0.40	0.59	2.81	2.57	1.51	1.08
50	0.30	85.2	39.6	-16.0	-5.6	4.3	-3.1	102.1	39.4	1.58	2.34	0.62	0.63	2.63	3.21	1.68	1.13
70	0.42	85.8	51.3	-17.1	-6.0	10.1	-1.0	94.4	53.8	1.94	2.02	0.82	0.66	2.82	4.22	0.45	1.28
80	0.48	85.8	59.6	-14.4	-5.6	8.5	0.2	85.8	70.5	0.98	1.00	0.40	0.67	1.56	1.24	1.79	1.33
90	0.54	86.4	63.5	-16.4	-5.0	12.6	7.7	92.9	78.7	0.81	0.97	0.72	0.44	2.15	1.78	1.09	1.53
100	0.60	83.9	71.0	-14.5	-4.8	14.3	4.6	87.5	86.7	0.79	0.94	0.59	0.91	1.34	1.54	1.29	1.04
110	0.66	83.1	76.5	-13.9	-4.5	17.1	5.3	83.7	90.5	1.08	1.07	0.59	0.83	1.77	1.98	1.11	1.72
130	0.78	76.1	90.0	-10.4	-4.5	18.5	4.0	76.5	112.4	1.16	0.88	0.68	0.62	1.42	1.25	0.87	0.92
140	0.84	74.6	95.1	-8.7	-3.2	23.2	5.4	68.6	128.9	1.46	0.62	0.83	0.76	0.78	1.71	0.89	1.62
150	0.90	71.6	98.4	-7.4	-3.4	30.9	4.7	78.9	128.7	0.97	1.10	0.79	0.88	1.48	2.02	1.42	1.75
160	0.96	52.6	85.7	-13.0	-4.4	75.8	-28.5	84.6	151.5	4.21	2.67	1.58	0.98	8.52	11.07	2.22	1.80
170	1.02	47.7	88.7	-16.9	-4.5	78.1	-36.3	73.1	139.4	3.02	1.78	2.32	1.67	5.40	8.77	4.51	2.60
190	1.14	60.1	127.3	-3.0	-6.4	28.4	7.4	70.0	158.6	2.01	2.02	1.28	1.95	1.88	2.93	1.12	1.50
200	1.20	58.0	132.0	-0.3	-5.1	26.5	10.8	54.4	162.1	1.12	1.15	1.13	1.20	1.16	1.42	1.82	1.24
210	1.26	57.2	137.2	4.7	-5.9	31.6	10.2	62.2	176.5	0.76	0.68	0.81	0.94	1.91	1.30	1.62	1.18
220	1.32	50.7	135.2	-4.1	-4.6	20.7	5.1	44.1	152.8	1.00	1.23	0.81	0.63	1.35	1.55	1.66	1.16
230	1.38	36.6	146.0	2.8	-7.0	24.4	18.9	43.9	199.6	0.87	1.07	0.63	0.96	1.18	1.01	1.07	1.30
250	1.50	29.5	163.5	2.0	-3.6	24.1	20.2	26.9	196.5	1.25	0.94	1.18	0.58	1.72	1.32	0.61	1.24
260	1.56	27.1	169.3	1.5	-2.7	25.3	23.2	23.8	201.1	0.76	1.08	1.08	0.75	1.23	1.32	0.96	1.06
270	1.62	24.5	173.6	-0.3	-2.0	26.0	22.0	19.2	198.6	0.79	0.84	1.15	0.81	0.92	1.20	0.58	1.93
280	1.68	21.0	176.6	6.9	-8.0	23.7	32.7	23.2	252.8	1.32	1.36	1.12	1.09	2.67	1.33	0.85	1.55
290	1.74	17.1	184.6	-4.3	1.0	22.7	25.4	1.5	211.7	0.58	0.78	0.91	0.78	1.21	1.85	1.14	1.55

Table 38: Experimental dynamic stiffnesses at 10000 rpm and 1038.2 kPa bearing unit loading

Ω	Ω/ω	Experiment															
		dynamic stiffness								Uncertainty							
Hz		Re(Hxx	Im(Hxx	Re(Hxy	Im(Hxy	Re(Hyx	Im(Hyx	Re(Hyy	Im(Hyy	Re(Uxx	Im(Uxx	Re(Uxy	Im(Uxy	Re(Uyx	Im(Uyx	Re(Uyy	Im(Uyy
20	0.12	111.6	14.7	-18.8	-5.6	8.7	-7.9	148.5	22.2	2.47	2.23	0.80	0.81	10.42	8.55	4.94	5.28
30	0.18	111.5	22.8	-19.2	-6.9	6.4	-5.4	153.8	24.4	3.29	2.40	0.93	1.19	5.77	6.17	2.37	3.22
40	0.24	111.2	33.0	-20.3	-8.1	2.3	-5.0	150.1	41.3	1.53	1.41	0.77	0.75	4.76	2.45	1.50	2.07
50	0.30	113.4	40.6	-20.0	-9.4	1.8	-1.9	152.0	52.3	1.88	3.68	1.26	2.11	6.71	8.00	3.16	4.37
70	0.42	110.7	54.0	-21.3	-10.6	9.9	-1.5	141.7	68.1	2.73	2.70	0.91	0.97	9.28	6.63	2.92	2.60
80	0.48	110.9	61.9	-18.0	-12.9	6.9	-4.3	146.9	104.6	1.97	1.45	1.01	0.99	3.63	4.47	1.76	3.75
90	0.54	112.0	67.2	-20.5	-10.4	13.1	0.1	140.3	98.3	1.49	1.51	0.98	0.68	3.36	3.35	2.50	1.54
100	0.60	110.2	75.1	-17.4	-10.3	14.0	-2.3	135.4	108.1	1.24	1.62	1.17	0.48	3.19	2.38	1.61	1.77
110	0.66	109.4	79.7	-16.4	-10.0	15.3	-1.0	130.7	110.4	1.43	0.99	0.57	0.67	2.90	2.07	1.01	1.68
130	0.78	103.5	94.7	-11.7	-8.8	19.7	-3.6	120.0	129.6	1.14	1.44	0.74	0.92	2.14	1.85	1.25	1.31
140	0.84	101.9	100.7	-9.7	-10.1	27.5	-4.0	117.6	156.8	1.20	1.30	0.98	0.67	4.37	1.92	1.90	2.38
150	0.90	96.8	104.3	-8.3	-10.4	33.9	-7.1	125.4	154.1	1.19	1.08	1.31	1.01	2.95	2.80	1.54	1.19
160	0.96	79.1	98.3	-11.7	-9.4	73.7	-31.4	114.5	187.5	5.09	1.99	3.23	1.66	10.53	9.75	4.14	4.54
170	1.02	55.1	100.9	-22.5	-6.2	87.1	-75.4	108.1	147.7	3.18	1.91	2.40	2.42	5.12	6.63	4.05	3.93
190	1.14	87.9	131.8	-2.0	-15.5	28.9	-7.7	115.8	189.1	2.20	3.10	1.99	2.45	4.99	5.06	5.34	2.92
200	1.20	86.2	139.2	0.3	-13.9	33.7	-2.5	98.8	195.3	1.61	1.84	1.51	1.57	2.42	2.44	3.06	2.31
210	1.26	84.7	146.0	5.1	-16.6	36.8	-4.0	109.9	210.6	0.98	1.53	1.10	1.12	2.27	2.51	2.32	0.98
220	1.32	80.8	143.0	-2.7	-13.1	25.1	-9.2	89.4	186.0	1.51	1.26	0.95	0.71	1.07	0.97	1.75	1.23
230	1.38	67.5	152.3	7.2	-17.6	31.4	5.7	84.7	248.7	0.86	0.97	0.91	1.35	1.55	1.38	1.50	1.96
250	1.50	60.4	168.7	4.3	-10.5	28.4	5.1	66.6	233.1	1.57	0.91	1.03	0.54	1.16	1.57	1.58	1.70
260	1.56	58.6	173.9	6.1	-8.9	29.3	8.3	63.9	237.2	1.12	0.93	0.93	1.01	1.02	1.04	1.18	1.57
270	1.62	55.2	178.2	6.6	-7.4	30.2	8.0	60.2	238.2	1.57	0.80	1.06	1.09	1.45	1.71	1.21	1.91
280	1.68	53.1	179.8	25.3	-16.7	26.2	20.5	44.9	339.9	1.17	1.31	1.45	0.96	1.90	1.68	2.01	4.43
290	1.74	47.0	187.3	6.9	-6.3	28.9	13.3	44.0	258.6	1.05	1.08	0.80	1.31	1.22	1.68	1.54	1.54

Table 39. Experimental dynamic stiffnesses at 12000 rpm and 1.4 kPa bearing unit loading

Ω	Ω/ω	Experiment															
		Dynamic stiffness								Uncertainty							
Hz		Re(Hxx)	Im(Hxx)	Re(Hxy)	Im(Hxy)	Re(Hyx)	Im(Hyx)	Re(Hyy)	Im(Hyy)	Re(Uxx)	Im(Uxx)	Re(Uxy)	Im(Uxy)	Re(Uyx)	Im(Uyx)	Re(Uyy)	Im(Uyy)
20	0.10	72.6	10.5	-26.7	1.2	10.4	3.1	88.8	8.4	3.01	2.82	1.66	1.15	6.04	3.17	1.63	1.91
30	0.15	68.4	17.9	-24.7	0.0	12.4	3.5	87.4	11.9	2.18	1.01	1.22	1.47	2.63	2.71	1.78	2.26
40	0.20	65.9	24.5	-23.3	-3.9	10.6	3.9	82.0	22.7	1.93	1.54	0.80	1.22	3.22	2.72	1.44	0.95
50	0.25	66.2	34.5	-24.1	-5.0	8.3	7.0	79.2	28.8	2.64	2.65	1.21	1.06	2.71	3.05	2.22	1.18
70	0.35	61.2	48.2	-23.4	-8.8	16.4	7.9	71.1	45.3	2.49	1.97	0.79	1.32	3.80	3.77	2.19	2.28
80	0.40	58.6	56.3	-24.2	-9.5	17.3	7.4	69.3	57.4	1.77	1.33	0.93	0.71	2.85	3.60	1.37	1.75
90	0.45	56.3	62.5	-23.6	-8.3	19.3	9.3	64.7	64.2	1.45	1.79	1.06	0.92	1.85	2.16	0.52	1.29
100	0.50	52.4	71.4	-22.4	-8.4	21.5	7.5	59.8	72.1	1.82	2.36	0.71	1.11	2.64	1.92	1.17	0.94
110	0.55	49.9	79.9	-21.1	-7.3	20.9	6.0	55.9	79.6	2.10	2.17	0.85	1.11	2.43	1.91	1.16	0.95
130	0.65	41.7	95.9	-14.7	-8.8	21.4	5.3	48.7	99.6	1.70	1.91	1.86	1.48	1.55	1.92	1.60	1.62
140	0.70	39.9	105.7	-12.8	-7.8	20.2	8.1	41.6	111.7	1.67	1.98	1.16	1.25	2.63	2.70	1.20	1.47
150	0.75	37.8	111.0	-9.5	-8.2	22.4	9.6	46.6	120.9	1.69	1.74	0.96	1.39	0.98	1.03	0.88	1.04
160	0.80	34.5	117.6	-7.3	-8.6	22.0	11.9	37.8	124.7	2.32	2.42	1.65	1.92	2.16	2.05	1.30	1.36
170	0.85	31.7	125.6	-7.4	-10.0	20.2	13.9	34.5	138.9	2.42	2.86	1.72	1.62	2.56	3.72	1.88	2.07
190	0.95	26.7	131.7	-5.2	-11.3	31.9	17.9	35.4	146.1	1.79	3.76	2.04	1.50	3.76	4.24	0.98	2.67
200	1.00	7.3	99.0	-15.2	-25.9	87.5	-10.3	37.9	127.7	2.80	2.71	1.96	1.97	3.04	5.03	3.19	1.97
210	1.05	19.8	141.2	4.5	-10.6	32.4	22.6	33.4	161.5	1.91	1.47	1.07	1.38	1.62	2.61	0.76	1.33
220	1.10	12.5	140.2	-0.5	-10.5	21.2	16.1	23.9	150.3	0.99	1.77	1.03	0.85	1.14	1.46	0.75	1.16
230	1.15	-3.9	152.4	3.4	-6.0	19.6	26.1	3.8	165.9	1.72	1.44	0.63	0.64	0.93	1.06	0.95	0.91
250	1.25	-12.9	163.8	7.4	-7.5	17.8	29.9	2.6	183.4	1.00	1.08	0.79	0.68	1.39	1.40	1.16	0.97
260	1.30	-16.9	168.1	8.5	-5.4	15.8	34.2	-2.2	187.5	0.55	1.16	1.00	0.67	0.87	1.29	1.19	1.17
270	1.35	-21.3	171.6	10.0	-5.0	16.6	37.7	-3.8	192.9	1.20	0.74	0.72	0.82	1.12	0.77	0.91	1.00
280	1.40	-28.1	175.3	10.2	-3.5	12.0	42.3	-14.3	198.0	1.29	1.26	0.58	0.79	1.18	1.11	0.79	0.42
290	1.45	-34.9	181.2	10.2	-2.9	9.9	46.5	-22.2	202.5	1.32	1.09	0.89	1.15	1.20	1.53	0.67	1.22

Table 40. Experimental dynamic stiffnesses at 12000 rpm and 175.9 kPa bearing unit loading

Ω	Ω/ω	Experiment															
		Dynamic stiffness								Uncertainty							
Hz		Re(Hxx)	Im(Hxx)	Re(Hxy)	Im(Hxy)	Re(Hyx)	Im(Hyx)	Re(Hyy)	Im(Hyy)	Re(Uxx)	Im(Uxx)	Re(Uxy)	Im(Uxy)	Re(Uyx)	Im(Uyx)	Re(Uyy)	Im(Uyy)
20	0.10	69.5	6.0	-27.3	11.4	16.6	10.9	93.1	-9.8	2.89	1.76	1.59	2.32	4.98	5.07	3.64	2.84
30	0.15	69.6	13.4	-22.2	5.7	18.6	9.2	89.2	-1.3	1.30	2.12	0.92	1.29	3.08	2.77	2.02	1.98
40	0.20	65.3	22.4	-18.7	2.6	18.0	10.9	79.0	12.9	0.93	1.42	0.70	0.82	2.77	1.27	1.34	1.24
50	0.25	63.8	34.1	-16.9	0.2	17.1	9.4	75.1	24.1	1.78	0.98	0.73	0.98	4.86	4.33	2.67	2.59
70	0.35	60.0	45.8	-17.1	-3.5	19.5	10.1	68.3	41.1	1.51	1.55	1.18	0.98	3.85	3.30	1.82	1.92
80	0.40	61.3	53.5	-17.6	-4.6	22.5	11.9	80.8	65.5	1.95	1.09	0.98	0.89	2.49	3.04	2.55	2.68
90	0.45	58.3	61.4	-17.7	-2.6	24.3	13.9	64.0	62.0	1.41	0.95	0.59	1.03	1.34	1.61	1.24	1.00
100	0.50	55.5	69.7	-17.0	-2.1	26.7	9.6	60.1	70.4	1.12	1.44	0.75	0.66	2.51	2.40	1.32	1.17
110	0.55	52.1	75.5	-16.8	-2.3	25.9	10.2	57.8	76.1	1.32	2.21	0.95	0.92	2.63	2.70	1.93	1.72
130	0.65	46.6	92.7	-12.2	0.3	26.1	9.2	48.0	91.8	1.56	1.89	0.86	1.67	1.57	1.60	1.97	2.28
140	0.70	41.9	98.9	-8.1	1.8	26.8	14.1	38.4	108.3	2.28	1.82	1.22	1.24	1.99	1.88	1.54	1.97
150	0.75	42.5	104.0	-2.7	0.4	27.4	16.0	41.5	112.9	1.91	1.48	0.86	1.32	1.62	1.57	1.41	2.07
160	0.80	40.1	110.1	-3.8	-4.1	29.9	20.8	47.7	128.9	1.85	2.39	1.68	1.39	2.80	1.83	1.96	2.20
170	0.85	36.7	117.7	-1.2	-1.4	30.4	21.2	40.3	134.4	2.26	2.43	2.50	1.89	3.73	2.54	3.49	2.84
190	0.95	32.0	121.1	-1.3	-5.2	44.2	19.9	36.0	137.1	3.48	3.23	2.34	1.75	4.59	3.70	2.43	2.66
200	1.00	13.6	97.7	-14.2	-19.0	79.9	-2.1	36.5	131.0	2.40	2.28	2.10	2.08	2.31	3.15	2.02	1.64
210	1.05	26.1	135.2	5.7	-0.3	41.1	24.5	25.9	150.8	0.93	1.12	1.24	1.42	2.34	1.49	1.25	2.02
220	1.10	17.8	135.5	2.0	4.5	25.8	16.4	-19.2	137.3	0.91	1.18	0.87	1.21	1.25	1.51	1.63	2.42
230	1.15	3.6	146.5	6.2	-1.1	30.0	28.5	13.1	167.0	0.88	0.92	1.23	1.11	1.25	1.31	0.75	1.35
250	1.25	-4.8	158.8	6.9	1.9	26.7	29.9	1.9	170.2	1.05	0.90	1.11	0.94	1.61	1.25	0.64	1.31
260	1.30	-8.2	162.8	11.1	3.5	26.3	33.1	-15.3	175.1	1.04	1.17	0.88	1.09	1.10	1.28	1.69	1.75
270	1.35	-12.5	167.5	11.1	2.5	19.3	32.8	-19.6	191.9	0.94	0.84	0.63	0.83	1.11	0.71	0.97	1.58
280	1.40	-18.3	169.9	8.0	8.4	21.0	38.9	-26.9	192.7	0.76	1.46	1.37	1.08	1.27	0.72	1.74	1.10
290	1.45	-26.9	175.8	12.5	6.6	12.8	39.6	-30.9	214.5	1.47	1.50	1.64	1.30	1.29	0.86	1.63	1.50

Table 41. Experimental dynamic stiffnesses at 12000 rpm and 348.4 kPa bearing unit loading

Ω	Ω/ω	Experiment															
		Dynamic stiffness								Uncertainty							
Hz		Re(Hxx)	Im(Hxx)	Re(Hxy)	Im(Hxy)	Re(Hyx)	Im(Hyx)	Re(Hyy)	Im(Hyy)	Re(Uxx)	Im(Uxx)	Re(Uxy)	Im(Uxy)	Re(Uyx)	Im(Uyx)	Re(Uyy)	Im(Uyy)
20	0.10	75.7	13.5	-17.9	-0.9	16.1	8.8	101.0	6.9	1.33	1.49	0.84	0.82	5.05	6.52	1.87	4.45
30	0.15	73.8	20.1	-17.4	-1.6	17.9	4.4	98.4	4.7	1.47	1.51	0.70	1.02	5.12	3.48	1.30	2.99
40	0.20	73.3	25.9	-17.1	-1.4	18.9	7.5	89.9	14.4	1.16	0.76	0.36	0.64	2.94	3.31	2.31	2.83
50	0.25	72.6	34.2	-17.9	-2.5	16.2	7.7	88.1	23.3	1.70	2.00	0.77	1.23	4.60	4.04	1.67	2.62
70	0.35	71.3	47.6	-16.7	-2.6	22.6	4.3	77.8	41.8	2.40	2.10	1.27	1.08	5.75	3.50	2.49	2.52
80	0.40	69.2	53.8	-12.6	-5.9	19.6	9.8	60.2	106.6	1.61	1.68	1.05	0.94	3.92	2.98	3.20	2.00
90	0.45	69.1	60.2	-17.0	-1.0	20.5	10.5	73.6	61.2	1.30	2.49	0.73	0.57	2.44	3.04	1.16	2.30
100	0.50	66.6	66.5	-16.4	-1.0	23.4	9.0	70.1	69.2	1.73	1.33	0.56	1.20	2.80	1.67	1.58	2.47
110	0.55	64.1	73.0	-15.1	-0.1	23.9	11.8	64.3	76.0	1.61	1.21	0.87	0.58	2.37	2.53	1.72	1.62
130	0.65	57.1	88.8	-10.9	2.8	20.6	11.6	55.6	90.8	1.73	1.44	0.88	0.86	2.00	2.18	1.87	2.10
140	0.70	56.5	93.7	-9.3	3.5	26.5	17.5	49.7	109.2	1.55	2.28	0.59	1.22	2.78	2.25	1.17	2.59
150	0.75	54.7	100.2	-4.6	4.0	28.0	18.9	53.7	112.8	1.53	1.77	0.94	0.91	2.01	1.61	2.23	2.63
160	0.80	52.7	105.9	-4.5	-0.9	29.5	23.3	61.8	133.5	1.61	2.49	1.11	1.07	2.54	2.68	1.86	2.18
170	0.85	52.7	113.9	-2.7	3.8	33.5	21.4	50.9	135.6	2.53	3.74	2.52	1.41	2.75	3.41	3.02	2.42
190	0.95	43.3	117.8	-2.5	1.8	41.7	18.4	50.2	136.4	1.87	2.96	2.66	1.75	6.08	2.46	2.39	2.05
200	1.00	21.1	95.0	-17.0	-14.2	79.5	-15.1	53.5	130.0	3.60	3.56	2.48	2.80	2.88	3.70	2.51	1.99
210	1.05	40.7	130.0	4.4	4.5	42.4	22.7	42.8	151.9	1.64	3.00	0.97	0.71	2.38	2.32	1.40	2.39
220	1.10	32.4	129.8	-1.7	6.0	26.0	15.1	17.4	131.3	1.29	1.91	0.86	1.07	1.65	1.15	1.08	1.87
230	1.15	18.7	140.4	5.5	4.8	29.6	28.8	24.8	169.9	0.68	1.55	1.17	0.67	1.34	1.64	1.13	2.27
250	1.25	10.4	154.6	7.9	4.6	26.9	29.5	14.2	174.2	0.77	2.54	0.89	0.79	1.23	1.13	1.66	2.40
260	1.30	6.2	159.1	8.1	4.9	26.3	33.5	3.8	173.3	0.95	1.53	1.04	0.56	1.06	1.25	0.90	1.93
270	1.35	1.7	164.4	4.9	7.4	26.5	32.2	-9.3	169.4	1.37	1.80	1.03	0.79	0.86	0.98	1.15	2.21
280	1.40	-1.2	167.4	9.2	2.9	25.0	40.6	-0.3	200.7	1.35	1.75	0.85	0.86	1.60	0.97	0.80	2.52
290	1.45	-7.7	175.0	4.4	15.2	21.3	36.0	-56.7	178.9	1.26	1.15	1.27	1.11	0.91	1.09	1.61	3.72

Table 42. Experimental dynamic stiffnesses at 12000 rpm and 513.8 kPa bearing unit loading

Ω	Ω/ω	Experiment															
		Dynamic stiffness								Uncertainty							
Hz		Re(Hxx)	Im(Hxx)	Re(Hxy)	Im(Hxy)	Re(Hyx)	Im(Hyx)	Re(Hyy)	Im(Hyy)	Re(Uxx)	Im(Uxx)	Re(Uxy)	Im(Uxy)	Re(Uyx)	Im(Uyx)	Re(Uyy)	Im(Uyy)
20	0.10	79.3	13.1	-16.5	-2.8	16.0	-1.7	118.6	4.5	0.06	0.08	0.03	0.04	0.03	0.02	0.02	0.01
30	0.15	80.6	20.0	-16.5	-1.8	21.1	-1.8	115.5	-0.8	0.18	0.08	0.04	0.04	0.02	0.04	0.04	0.01
40	0.20	81.8	22.6	-17.3	-3.0	22.3	2.9	103.5	7.6	0.05	0.11	0.04	0.08	0.03	0.03	0.04	0.02
50	0.25	78.1	31.4	-16.6	-3.0	12.8	-7.7	104.2	24.3	0.15	0.16	0.10	0.11	0.04	0.04	0.03	0.04
70	0.35	83.2	43.3	-19.6	-5.3	28.0	1.3	86.0	33.1	0.11	0.12	0.19	0.13	0.02	0.03	0.04	0.04
80	0.40	79.6	55.0	-16.2	-2.2	18.9	9.2	66.8	51.7	0.15	0.08	0.12	0.09	0.02	0.03	0.02	0.02
90	0.45	76.9	59.3	-18.7	-2.9	15.8	8.6	84.1	60.5	0.05	0.09	0.11	0.11	0.04	0.03	0.03	0.03
100	0.50	74.8	67.0	-18.1	-2.0	23.5	8.6	80.1	69.7	0.03	0.06	0.12	0.17	0.02	0.02	0.04	0.04
110	0.55	74.2	73.4	-16.9	-0.8	24.3	8.9	75.6	74.5	0.09	0.08	0.14	0.21	0.02	0.03	0.03	0.04
130	0.65	68.5	89.4	-13.5	1.5	20.2	13.0	72.2	92.8	0.10	0.08	0.10	0.19	0.01	0.02	0.02	0.03
140	0.70	65.8	91.2	-13.5	5.1	20.1	16.9	57.6	108.0	0.08	0.09	0.14	0.19	0.01	0.02	0.02	0.02
150	0.75	69.9	98.4	-6.4	3.2	29.1	20.7	66.4	118.2	0.11	0.18	0.34	0.30	0.01	0.01	0.03	0.03
160	0.80	62.6	106.2	-9.5	0.9	29.4	23.3	70.7	135.0	0.29	0.21	0.37	0.52	0.02	0.01	0.02	0.03
170	0.85	65.8	105.3	-5.3	7.2	30.4	15.7	63.0	140.4	0.37	0.61	0.71	0.57	0.03	0.02	0.05	0.04
190	0.95	54.2	119.1	-3.4	7.7	38.4	16.7	54.6	145.6	0.60	0.42	0.51	0.77	0.04	0.03	0.04	0.04
200	1.00	28.8	34.9	35.1	10.5	145.1	-17.0	18.9	179.3	0.18	0.16	0.24	0.17	0.02	0.01	0.02	0.02
210	1.05	50.3	122.3	8.8	6.6	39.9	21.6	52.1	158.0	0.18	0.21	0.14	0.17	0.02	0.05	0.02	0.02
220	1.10	40.9	123.6	0.4	7.8	26.8	14.8	30.9	137.0	0.23	0.19	0.19	0.33	0.07	0.11	0.11	0.15
230	1.15	26.9	132.6	7.9	6.4	31.3	27.9	37.1	176.0	0.11	0.12	0.09	0.11	0.03	0.02	0.02	0.04
250	1.25	15.7	150.7	11.6	5.4	30.0	26.2	22.3	182.8	0.10	0.12	0.10	0.09	0.02	0.02	0.02	0.03
260	1.30	12.1	156.6	10.9	4.3	31.5	30.6	17.1	178.8	0.10	0.10	0.14	0.12	0.03	0.02	0.03	0.02
270	1.35	7.3	161.0	7.4	3.0	32.9	28.6	11.6	178.8	0.21	0.16	0.15	0.15	0.03	0.03	0.03	0.03
280	1.40	7.2	168.4	13.6	1.2	34.7	38.5	14.7	216.1	0.20	0.21	0.24	0.34	0.04	0.03	0.04	0.03
290	1.45	0.1	178.1	2.7	5.4	29.9	31.1	-11.3	186.6	0.42	0.33	0.52	0.49	0.04	0.03	0.04	0.05

Table 43. Experimental dynamic stiffnesses at 12000 rpm and 692.2 kPa bearing unit loading

Ω	Ω/ω	Experiment															
		Dynamic stiffness								Uncertainty							
Hz		Re(Hxx)	Im(Hxx)	Re(Hxy)	Im(Hxy)	Re(Hyx)	Im(Hyx)	Re(Hyy)	Im(Hyy)	Re(Uxx)	Im(Uxx)	Re(Uxy)	Im(Uxy)	Re(Uyx)	Im(Uyx)	Re(Uyy)	Im(Uyy)
20	0.10	90.4	14.1	-16.8	-3.3	15.7	2.6	122.2	5.7	2.03	1.59	0.64	0.48	4.83	3.34	2.09	2.96
30	0.15	88.4	20.3	-17.7	-4.7	18.4	0.3	117.9	7.1	1.74	1.70	0.97	0.73	6.30	2.84	3.29	2.45
40	0.20	90.5	25.8	-18.4	-4.9	19.4	2.8	109.9	18.0	1.01	1.05	0.61	0.81	3.21	2.18	1.86	2.12
50	0.25	88.1	31.8	-19.7	-5.0	15.0	0.7	108.2	31.4	1.63	2.54	1.10	1.52	3.52	2.74	2.44	2.76
70	0.35	89.1	44.9	-19.0	-5.2	25.9	4.9	100.0	48.0	2.50	2.69	0.77	1.42	4.26	6.67	2.22	3.00
80	0.40	87.9	52.9	-18.9	-4.5	23.8	8.3	91.6	63.1	1.47	1.55	0.60	0.71	2.37	2.46	1.95	1.64
90	0.45	85.6	57.4	-19.6	-4.1	23.9	7.5	99.5	69.7	0.59	1.00	0.76	0.76	3.75	1.81	1.50	1.78
100	0.50	83.1	64.8	-18.6	-3.9	26.7	6.5	93.0	78.9	1.15	1.63	0.98	0.45	2.45	1.97	2.11	1.81
110	0.55	82.8	70.2	-18.7	-2.5	26.3	5.3	89.9	82.6	2.04	1.04	1.12	1.20	2.29	2.03	1.35	1.74
130	0.65	77.0	86.8	-15.5	1.0	25.5	4.5	77.7	101.8	1.48	1.62	1.07	0.81	2.71	2.38	2.30	1.90
140	0.70	75.1	91.5	-13.9	3.1	26.4	6.5	72.1	119.7	1.42	1.42	1.26	1.45	2.46	2.38	1.85	2.01
150	0.75	74.4	97.4	-10.7	3.6	30.6	8.7	81.1	123.6	1.54	1.78	0.93	0.98	2.50	2.08	2.75	2.82
160	0.80	72.8	103.5	-10.2	-0.1	31.6	14.4	93.1	153.5	2.14	1.49	1.12	1.53	2.77	4.17	3.16	2.47
170	0.85	70.8	108.3	-6.9	3.0	31.5	10.5	73.9	147.9	2.69	3.92	2.14	2.34	3.84	5.22	3.26	4.24
190	0.95	63.5	115.9	-4.5	3.4	36.8	7.1	73.8	148.5	2.12	2.70	3.08	2.42	4.96	3.61	2.72	3.25
200	1.00	30.3	97.6	-26.0	-10.6	80.4	-47.0	83.7	130.6	4.36	4.16	2.95	4.65	5.19	5.11	4.69	3.37
210	1.05	59.1	127.3	4.3	6.3	39.9	12.6	70.9	167.8	1.42	1.63	1.44	1.13	1.68	2.54	2.32	2.20
220	1.10	53.8	124.8	-1.4	6.8	26.1	7.5	50.0	146.4	0.87	1.42	1.06	0.57	1.25	1.47	1.97	1.13
230	1.15	38.9	134.8	5.5	5.6	30.4	19.4	52.5	186.1	1.12	0.88	1.60	1.25	1.78	1.31	1.15	1.58
250	1.25	31.3	150.5	7.7	8.0	28.4	21.0	36.1	182.5	0.49	1.00	1.40	1.11	0.98	1.28	0.66	1.07
260	1.30	27.0	155.7	9.5	7.3	29.1	24.4	32.9	185.8	1.06	1.22	1.08	0.90	1.08	1.16	0.89	1.23
270	1.35	23.8	160.4	8.6	8.2	29.7	24.3	27.0	185.0	0.90	1.15	1.10	0.62	1.08	0.81	1.11	1.19
280	1.40	20.2	164.4	15.3	1.1	28.3	34.5	34.6	235.4	0.61	1.34	1.19	0.92	1.85	0.96	0.95	1.53
290	1.45	14.3	171.9	6.6	7.8	26.7	28.4	10.2	197.7	0.64	1.13	1.19	0.92	1.39	1.48	0.62	1.57

Table 44. Experimental dynamic stiffnesses at 12000 rpm and 1038.2 kPa bearing unit loading

Ω	Ω/ω	Experiment															
		Dynamic stiffness								Uncertainty							
Hz		Re(Hxx)	Im(Hxx)	Re(Hxy)	Im(Hxy)	Re(Hyx)	Im(Hyx)	Re(Hyy)	Im(Hyy)	Re(Uxx)	Im(Uxx)	Re(Uxy)	Im(Uxy)	Re(Uyx)	Im(Uyx)	Re(Uyy)	Im(Uyy)
20	0.10	133.5	-12.7	-19.4	-21.2	-1.9	-0.5	144.3	28.3	10.27	8.95	5.31	5.26	4.84	5.16	2.10	3.18
30	0.15	124.7	6.1	-29.2	-14.5	-5.8	-2.2	147.9	25.3	8.16	6.18	4.63	4.51	5.09	5.57	2.88	2.47
40	0.20	127.3	13.9	-32.1	-13.9	-2.9	5.2	145.6	38.8	5.81	5.86	3.12	2.57	5.01	5.49	2.80	2.67
50	0.25	128.9	20.0	-31.8	-10.7	0.3	4.4	147.6	53.1	6.11	3.86	1.40	2.12	4.62	9.10	2.93	3.67
70	0.35	127.4	39.1	-29.1	-12.3	2.4	8.8	138.8	66.5	4.14	3.85	2.34	2.29	7.73	7.32	3.92	3.15
80	0.40	125.2	43.3	-27.6	-14.2	2.3	7.7	142.1	114.0	2.84	3.38	1.82	2.57	4.71	5.74	2.80	3.44
90	0.45	125.3	48.0	-28.8	-11.6	5.0	8.5	141.0	96.3	2.66	2.71	1.34	1.55	2.61	1.88	2.96	2.44
100	0.50	120.6	51.7	-25.1	-10.3	9.7	5.9	131.1	107.0	1.46	2.14	1.80	1.51	2.19	2.15	1.51	2.26
110	0.55	116.9	59.1	-23.7	-9.4	9.6	7.2	127.3	111.3	1.78	2.89	1.77	1.62	2.78	2.82	1.39	1.01
130	0.65	108.9	74.1	-20.2	-8.3	14.1	3.9	118.8	129.0	1.76	1.60	1.75	1.74	2.35	1.44	1.69	1.75
140	0.70	107.3	82.9	-19.2	-8.7	14.1	3.3	117.4	158.6	1.75	2.07	1.96	1.90	1.46	2.82	2.87	1.64
150	0.75	102.3	87.6	-15.8	-8.2	18.7	3.4	125.1	154.1	1.87	1.53	1.18	1.40	2.31	2.27	2.19	1.82
160	0.80	99.1	94.0	-14.6	-14.2	20.3	7.0	135.6	201.0	2.23	1.13	2.61	1.85	3.33	3.19	2.60	3.87
170	0.85	97.1	100.0	-12.5	-8.7	17.3	5.3	115.8	181.2	2.29	1.31	2.44	1.85	4.39	4.05	3.77	4.42
190	0.95	83.4	104.2	-14.8	-4.0	45.1	-10.1	108.5	172.2	3.00	1.26	2.37	1.60	4.45	3.88	2.92	4.49
200	1.00	57.1	102.4	-29.1	-4.5	72.0	-51.5	96.8	144.5	2.01	2.36	2.03	2.12	2.51	3.45	2.67	2.26
210	1.05	84.9	121.6	-1.7	-6.8	35.5	3.9	112.1	203.8	1.33	2.01	2.52	1.16	1.64	2.41	2.18	2.65
220	1.10	81.3	120.8	-5.7	-5.4	20.1	2.8	92.5	184.6	2.10	1.24	1.31	1.09	2.20	1.28	1.81	1.97
230	1.15	67.4	131.8	2.3	-8.2	23.8	19.2	93.1	236.7	0.64	1.68	1.41	1.40	1.07	1.89	2.08	2.38
250	1.25	58.8	147.3	5.4	-6.3	24.7	19.9	81.9	230.6	1.30	0.87	1.26	1.12	1.89	1.63	1.75	1.51
260	1.30	54.1	152.7	6.1	-4.7	26.8	21.9	76.7	233.3	1.06	1.25	1.14	0.86	1.73	1.64	2.14	1.74
270	1.35	50.7	158.1	8.2	-1.9	28.0	21.6	69.2	230.5	0.96	1.48	1.51	1.19	0.86	2.19	1.60	1.70
280	1.40	47.7	161.6	24.7	-12.4	23.3	37.8	67.0	330.4	0.90	0.98	1.67	1.42	1.38	3.66	3.32	3.58
290	1.45	41.2	167.7	10.2	-3.5	26.5	28.6	54.0	250.1	0.90	1.43	1.26	1.11	1.25	2.70	2.03	1.90

VITA

Adnan Mahmoud Al-Ghasem was born on October 3, 1973 in Iribid, Jordan. In September 1991 after finishing high school, he was admitted to Jordan University of Science and Technology (JUST). He graduated with a B.Sc. degree in mechanical engineering in June 1996. He continued his education and graduated in February 1999 with a M.Sc. degree in mechanical engineering. Adnan was distinguished through his undergraduate and graduate studies, graduating from both with the first rank. He worked as a full time lecturer in the Department of Mechanical Engineering at JUST from February 1999 to August 2001.

In September 2001, Adnan was admitted to Texas A&M University in the Department of Mechanical Engineering. He graduated with a M.S. degree in May 2004.

Adnan married in December 2000, and is blessed with two wonderful children: Mahmoud, born in May 2002 and Salma, born in August 2003.

Adnan Mahmoud Al-Ghasem
Email address: adnan_jaradat@hotmail.com
P.O.Box 2
Bushra 21144 – Irbid
Jordan